Evolution of reservoir properties in the Lower Triassic aquifer sandstones of the Thuringian Syncline in Central Germany

Dissertation

zur Erlangung des akademischen Grades doctor rerum naturalium

(Dr. rer. nat.)

vorgelegt dem Rat der Chemisch-Geowissenschaftlichen Fakultät der

Friedrich-Schiller-Universität Jena

von Dipl.-Geol. Daniel Beyer, geboren am 22.10.1983 in Suhl

Gutachter:

1) Prof. Dr. Reinhard Gaupp (Universität Jena)

2) Prof. Dr. Jonas Kley (Universität Göttingen)

Tag der Verteidigung: 04.02.2015

Abstract

The Buntsandstein (Lower Triassic) aquifer sandstones of the Thuringian Syncline are important for water supply, geothermal energy and storage wells. The properties of these aquifers reflect a combination of depositional characteristics, diagenetic evolution and burial history. It is necessary to understand the connection between these factors for a prediction of sandstone reservoir quality. The aim of this study was to analyse the control factors of the diagenetic and petrophysical properties of the Buntsandstein, and particularly the influence of varying depositional parameters, thermal history, subsidence and exhumation.

The Thuringian Buntsandstein records fluvial, sandflat, lacustrine and eolian environments. Petrophysical data imply a strong control of facies on porosity and permeability. Petrographic analysis has been used to estimate the mineralogical influence on the diagenesis and petrophysical aquifer evolution. The study reveals the importance of carbonate and sulphate cements for porosity loss due to cementation in the sandstones. The amount of cement is related to the original depositional environment: high carbonate (6 %) and low sulphate (1 %) cement content in the lacustrine sandstones; medium carbonate and sulphate cement (2 – 5 %) in the sandflat and fluvial sandstones; low carbonate (3 %) and high sulphate (7 %) cement content in the eolian sandstones. The presence of ooids is crucial for carbonate cementation whereas sulphate cementation is largely controlled by the size of detrital grains. The sandstones lost 8 % – 12 % porosity by cementation, but the dominant reason for porosity loss is mechanical compaction, which accounts for a decrease of 23 % – 27 %. Mechanical compaction is controlled by facies-dependent clay and mud availability and the amount of framework-stabilizing quartz cement. The permeabilities of the potential aquifers/reservoirs in the Buntsandstein in the centre of the Thuringian Syncline depend on their predominant depositional facies: fine grained lacustrine sandstones in the Lower Buntsandstein have low permeabilities (about 4 mD); conversely, Middle Buntsandstein sandflat, fluvial and eolian sandstones are moderately to highly permeable (27 – 108 mD).

Thermal maturity data of Carboniferous, Permian and Triassic sediments provide information about the maximum burial depth of the Buntsandstein rocks. Between 1800 m and 3800 m of overburden must have been eroded from the Thuringian Syncline. The youngest strata preserved in the Syncline are Lower Jurassic (minor remnants of Cretaceous sediments are present on the syncline margin). The thickness of the Zechstein to Lower Jurassic succession is insufficient to explain the level of thermal

maturity. A substantial cover of strata younger than Lower Jurassic must have been present over most of the Thuringian Syncline. The erosion of this cover must have occurred near the end of the Cretaceous period during a widespread inversion event. In detail, the reconstructed thickness of the eroded cover varies across the Thuringian Syncline, indicating the existence of a centrally located, elongated subsidence maximum in Jurassic and Cretaceous time. Documented extension structures in the Thuringian Syncline and a correlation with surrounding regions suggest that the subsiding area may have been a graben-like extensional structure, most likely of Late Jurassic to Early Cretaceous age, which became inverted in the contraction phase of Late Cretaceous age.

The pore space and the mineral surfaces exposed to the pore space of the four main facies types (lacustrine, sandflat, fluvial and eolian) were studied using digital image analysis on thin sections and BET measurements. Pore space distribution shows higher frequency of smaller pores in lacustrine and sandflat sandstones than in fluvial and eolian sandstones, caused predominantly by different grain sizes and cement contents. The abundance of large pores influences the permeability of a rock, as well as pore density and porosity. Mineral surfaces were analysed to estimate their individual reactivity in the sandstones. The majority of mineral surfaces in fluvial red sediments consist of iron oxide coatings, but detrital quartz and quartz cements are also common. In greyish bleached sandstones detrital quartz and quartz cements represent the most abundant mineral surfaces. Pore space in eolian sandstones is often filled with gypsum. Remaining pores are usually in contact with quartz, gypsum or radial/tangential illite. In lacustrine sandstones feldspar surface areas are more frequent than in the other sandstones. Many of the feldspars are corroded and therefore their mineral surface area is strongly increased. In the sandstones the mineral surface area depends on the depositional environment and the diagenesis. As a result of different types of mineral surfaces exposed to the pore space, the sandstones of the four facies types will exhibit distinctly different reactions upon contact with fluids. Especially the potential dissolution of sulphate cement can strongly improve the permeability in sandstones.

Kurzfassung

Die Sandsteine der Unteren Trias (Buntsandstein) stellen den wichtigsten Aquifer in der Thüringischen Senke dar. Diese Sandsteine könnten eine große Rolle in der Zukunft spielen, wenn poröse Sedimentgesteine für die Wasserversorgung, geothermale Energie oder Speicherung von Gasen im Untergrund genutzt werden. Die Entwicklung der Durchlässigkeit in diesen Sandsteinen ist eine Kombination aus Ablagerungsmilieu, Diagenese, Versenkungs- und Hebungsgeschichte. Für die Einschätzung der Reservoirqualität von Sandsteinen, ist es notwendig die beeinflussenden Faktoren zu verstehen. Ziel dieser Arbeit war es, die komplette Entstehungsgeschichte zu untersuchen und den Einfluss des Ablagerungsmilieus und der Diagenese während der Subsidenz und Hebung auf die Sandsteine und deren Charakteristika zu verstehen.

Die folgenden Ablagerungstypen wurden für die Sandsteine des Buntsandsteins in Thüringen unterschieden: lakustrin, fluviatil, äolisch und Sandebene. Petrophysikalische Ergebnisse zeigen einen deutlichen Zusammenhang zwischen dem ursprünglichen Ablagerungsraum und den heutigen petrophysikalischen Eigenschaften. Sandsteinproben aus Bohrungen und von Aufschlüssen zeigen einen Zusammenhang zwischen dem Ablagerungstyp und dessen Permeabilität. Petrographische Analysen zeigen, dass Karbonat- und Sulphatzemente die Porosität erheblich verringern und die Menge an vorkommendem Zement mit dessen Faziestyp korreliert: ein hoher Gehalt an Karbonatzement (6 %) und ein niedriger Gehalt an Sulphatzement (1 %) in den lakustrinen Sandsteinen; mittlere Gehalte an Karbonat- und Sulphatzement (2 % bis 5 %) in den Sandsteinen der Sandebene und in den fluviatilen Sandsteinen; ein geringer Karbonat- (3 %) und ein hoher Sulphatgehalt (7 %) in den äolischen Sandsteinen. Kommen Ooide im Gestein vor, so sind diese der Hauptgrund für eine karbonatische Zementierung, wohingegen die Menge an Sulphatzement an die Größe detritischer Körner gebunden ist. Die Sandsteine haben 8 % bis 12 % ihrer Porosität durch Zementation verloren, aber die Hauptursache für den Porositätsverlust (ca. 26 %) in den Sandsteinen ist die mechanische Kompaktion. Diese wird besonders intensiv durch den Gehalt an Ton und an gefügestützendem Quarzzement beeinflusst, was wiederum vom urspünglichem Ablagerungsmilieu abhängig ist. Auch die Permeabilität in den Formationen des Buntsandsteins im Zentrum der Thüringer Senke ist abhängig vom vorherrschenden Lithofaziestyp: feinsandige lakustrine Sandsteine des Unteren Buntsandsteins zeigen eine geringe Permeabilität (ca. 4 mD), während die Sandsteine des Mittleren Buntsandsteins (vom Faziestyp Sandebene, fluviatil und äolisch) moderate bis hohe Permeabilitäten (27 mD bis 108 mD) zeigen.

Nach der Ablagerung folgt die Phase der Subsidenz. Für eine Berechnung der maximalen Versenkungstiefe wurde die thermische Reife von organischen Bestandteilen genutzt. Dazu wurden Gesteine aus dem Karbon, Perm und der Trias gemessen. Es zeigt sich, dass eine Sedimentmächtigkeit von 1800 m bis 3800 m abgetragen wurde in Gebiet der Thüringischen Senke. Die jüngsten mesozoischen Ablagerungen im Thüringer Becken sind aus dem Jura. Die Mächtigkeit der heutigen Schichtenabfolge bis zum Unteren Jura ist nicht ausreichend, um die gemessene thermische Reife zu erklären. Es muss eine Überlagerung von Sedimenten aus der Jura oder Kreidezeit gegeben haben, die heute nicht mehr vorhanden ist. Eine Erosion dieser Sedimente am Ende der Kreidezeit während eines Hebungsereignisses ist anzunehmen. Die rekonstruierten Mächtigkeiten der abgetragenen Sedimente aus Jura- und Kreidezeit in der Thüringer Senke zeigen in deren Zentrum ein Maximum. Invertierte Strukturen in der Thüringer Senke und ihrem regionalem Umfeld lassen vermuten, dass es sich bei diesem Mächtigkeitsmaximum um einen Jura- bis Kreidezeitlichen Graben handeln könnte, der später invertiert wurde.

Für die Sandsteine der vier Ablagerungsmilieus wurden der Porenraum und die Mineraloberfläche im Gestein mit digitaler Bildanalyse und mit BET-Messungen untersucht. Porenraummessungen zeigen eine größere Häufigkeit von kleinen Poren in den lakustrinen Sandsteinen und in den Sandsteinen der Sandebene als in den fluviatilen oder äolischen Sandsteinen. Ursachen dafür sind die Unterschiede in der Korngröße und im Zementgehalt. Einen großen Einfluss auf die Permeabilität haben die großen Poren im Gestein. Auch die Porendichte und die Porosität sind hierbei ein wichtiger Faktor. Um die Reaktivität der Sandsteine abschätzen zu können, wurden auch die Mineraloberflächen untersucht. Die meisten Oberflächen innerhalb des Sandsteins bestehen aus Kornüberzügen, welche aus Eisenoxid und Tonmineralen zusammengesetzt sind (und welche auch die Ursache für die rote Färbung des Sandsteins sind). Aber auch Quarz und Quarzzement ist häufig, vor allem in den nicht roten Sandsteinen. Da in den äolischen Sandsteinen viele Poren mit Gipszement gefüllt sind, bilden diese in den äolischen Sandsteinen neben Quarz und Tonmineralen die häufigsten Oberflächen. In den lakustrinen Sandsteinen bestehen deutlich mehr Oberflächen aus Feldspat als in den anderen Sandsteinen. Viele der Feldspäte sind teilweise gelöst und haben dadurch eine höhere Oberfläche. Die Mineraloberflächen in einem Sandstein sind abhängig vom Ablagerungsmilieu und der Diagenese. In Folge unterschiedlicher Mineraloberflächen reagieren die Sandsteine auch unterschiedlich mit Fluiden. Besonders hervorzuheben ist hier die Lösung von Gips in äolischen Sandsteinen, die die Permeabilität des Sandsteins um ein vielfaches erhöhen kann.

Inhalt

1. Introduction

1.1. Motivation and aims of the work

When searching for usable sandstone reservoirs, e.g. for hydrocarbon exploration, underground gas storage, geothermal energy and groundwater supply, it is essential to understand the major factors that influence the reservoir quality. The evolution of the reservoir quality depends predominantly on the depositional environment and sedimentary facies (Giles 1997), the compaction (Ehrenberg 1989), the type and amount of authigenic cement and clay as well as on mineral dissolution (Wilson & Stanton 1994) and weathering (Bricker et al. 1994). Based on the sandstone lithology, structure and texture, the original depositional environment can be deduced (Walker 2006). The depositional environment influences the diagenesis in the following factors (Giles 1997): fine grained layers show preferentially quartz, feldspar cement and authigenic clay minerals, whereas carbonate and sulphate cements are concentrated on coarse grained layers (Füchtbauer 1979). Other studies describe the connection between the diagenesis of sandstones and their petrophysical properties (e.g., Knox et al. 1984, Giles et al. 1992, Morad et al. 2010 and Gaupp & Okkerman 2011). Often the important role of organic rich fluids in diagenetic evolution is highlighted (e.g. Surdam et al. 1984, Gaupp et al. 1993, Parnell 1994, Marchand et al. 2002, Schöner 2006, and Lippmann 2012).

In order to analyse the evolution of potential source rocks, modelling of the thermal history can provide information on organic maturity over time and therefore if hydrocarbons were available for migration and ascending into reservoir rocks (e.g. Schöner 2006, Senglaub et al. 2006, Yalcin et al. 1997).

Many articles discuss the influence of pore geometry on reservoir characteristics (e.g. Wardlaw & Taylor 1976, Bliefnick & Kaldi 1996). X-ray micro tomography is a new method providing 3D information about micro- and nano-scale porosity (Bai et al. 2013), but this method is inappropriate for studying a large quantity of sandstones with macro-scale pores. In contrast, thin section evaluations are a common, fast and economic method for quantitative pore data analysis. Investigations on thin sections based on digital image analysis in order to quantify the pore space were made, among others, by Cerepi et al. (2002) and Kayser (2006).

The relationship between depositional environment, burial history, petrography, diagenesis, pore space and reservoir quality for the Buntsandstein sandstones has not been determined quantitatively until now, even though these factors influence the present reservoir quality.

The aims of this work are: (1) To classify the depositional environment for the Buntsandstein sandstones in regard to diagenesis. (2) To determine the burial history and the maturity of underlying source rocks with respect to the migration of hydrocarbons. (3) To analyse the influence of the facies on diagenesis, pore space and finally on the petrophysical properties.

In the Thuringian Syncline, target horizons for potential underground gas storage are the sandstones of the Lower Triassic Buntsandstein Group (Huckriede & Zander 2010). Fundamental studies on Buntsandstein sandstones to define individual units, facies and stratigraphic order were performed e.g. by Hoppe (1957, 1968, 1976a, 1976b), Puff (1969, 1976), Seidel (1995), Radzinski (1995), Voigt & Gaupp (2000) and Puff & Langbein (2003). Petrographic information about Buntsandstein sandstones of the Thuringian Syncline is rare in published literature. Basic studies of Seidel (1972) and Langbein (1970, 1985) describe petrography, texture, evolution and other characteristics of the Buntsandstein, but petrophysical data are not available.

For the Buntsandstein sandstones of the Thuringian Syncline the digital image analysis can provide additional information concerning the influence of depositional environment on the evolution of pore space. Also the mineral surfaces, which are directly exposed to the open pore space, can be determined with digital image analysis. The intensity of dissolution and corrosion inside sandstones depends on their specific mineral surfaces in contact with formation water (Nesbitt et al. 1997). The pore size distribution and mineral surface quantification have not been applied before, for Buntsandstein lithologies in the Thuringian Syncline.

The burial history of the sedimentary rocks in the Thuringian Syncline is briefly described by Karnin et al. (1996), but the maximum burial depth of the rocks was not well constrained. On the major fault zones one extensional and a subsequent contractional phase has been determined (Martini 1940, Dolezalek 1955, Rauche & Franzke 1990, Malz & Kley 2012). The original normal offsets of the faults are poorly known due to the inversion phase and the associated reverse movements. Therefore the maximum depth attained by the Buntsandstein rocks is uncertain. Investigations on the

burial history and the maturity of organic matter are necessary for understanding the migration of hydrocarbons and its influence on the Buntsandstein rocks. Moreover, thermal evolution is important for the diagenetic processes in the sandstones.

For this purpose Buntsandstein sandstones have been analysed based on material from drill cores from the centre of the Thuringian Syncline and from surface outcrops along its margins in order to compare different facies types and the influence of diagenetic processes. At the syncline margins meteoric water and weathering affected the sandstone during the Tertiary and Quaternary, whereas in the centre only evolved formation water has been present. The following investigations were performed on the Buntsandstein sandstones: analysis of depositional environment (facies type), petrological and mineralogical investigations, and petrophysical measurements. Digital image analysis was applied in order to examine the size and distribution of the pore space and mineral surfaces in contact with open pores. Organic matter from Keuper and Zechstein sediments was used for vitrinite reflection analysis in order to constrain a model of the Thuringian Syncline`s burial history.

1.2. Reservoir properties of Buntsandstein sandstones in Germany

In Germany, the Buntsandstein (Lower Triassic) sandstones were targets of hydrocarbon exploration in the past. Especially in northern Germany many boreholes were drilled in order to explore the hydrocarbon potential (Lepper & Röhling 1998). Many studies were part of commercial, confidential exploration and are therefore not available for academic research. However, some scientific studies listed below provide information about porosity and permeability of Buntsandstein sandstones in Germany (Fig. 1).

In the area of the east Spessart, Harzer (2003) measured the following ranges of permeabilities on Buntsandstein sandstones: For the Lower Buntsandstein 0.3 mD to 4 mD, for the Middle Buntsandstein up to 6 mD and for the Upper Buntsandstein < 1 mD.

Udluft (1971) measured permeability on the Buntsandstein sandstones of the Rhön which gave the following values: For the Lower Buntsandstein 6 mD to 9 mD, for the Middle Buntsandstein up to 12 mD and for the Upper Buntsandstein < 1 mD. März (1977) described permeabilities of Buntsandstein sandstones also from the Rhön: For the

Middle Buntsandstein 0.004 mD to 5 mD and for the Upper Buntsandstein 2 mD to 240 mD.

Hessian Buntsandstein sandstones have been analysed by Bär (2012): fine grained sandstones are in a range of 6 % to 16 % porosity and permeabilities of 1 mD to 202 mD; medium grained sandstones show porosities of 12 % to 16 % and permeabilities of 27 mD to 442 mD, whereas coarse grained sandstones have porosities of about 15 % and permeabilities of 3 mD to 299 mD.
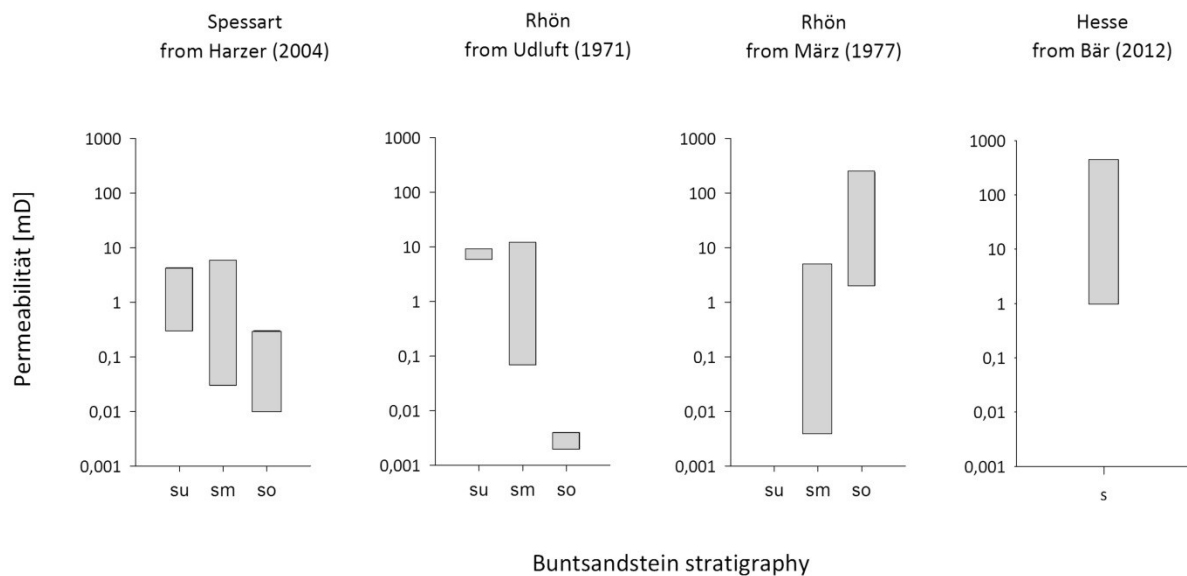
Fig. 1: Buntsandstein permeabilities (shown are min to max) in the region of the Spessart, Rhön and Hesse. su – Lower Buntsandstein; sm – Middle Buntsandstein; so – Upper Buntsandstein; s – Buntsandstein.

For Thuringia, Huckriede & Zander (2010) characterized the reservoir quality of the Buntsandstein sandstones as follows: sandstones of the Lower Buntsandstein have porosities between 1 % and 15 %. Sandstones of the Middle Buntsandstein show porosities between 12 % and 17 %, sometimes up to 22 %. Depositional environment discrimination has not been carried out by these authors.

For the rocks of the Lower Buntsandstein in east Thuringia, Rödiger (2005) measured high permeabilities around 2000 mD. For the rocks of the Middle Buntsandstein Rödiger (2005) measured up to 25000 mD. These values are extraordinarily high due to

the shallow reservoir depth of the measurement (low depth with abundant fracturing and advanced weathering of the rocks).

For a more detailed comparison between Buntsandstein sandstones from Middle Europe see chapter 7.3.

2. Geological setting

2.1. Tectonic and stratigraphic evolution of the Thuringian Syncline

The Thuringian Syncline (Fig. 2) is part of the North German Basin, which is a part of the Central European Basin System (e.g. Hoppe 1976a, van Wees et al. 2000, Geluk 2007, Bayer et al. 2008). The Central European Basin System extends from the southern North Sea to Poland and from Denmark to central Germany (Ziegler 1990). The Thuringian Syncline is a saucer-shaped, slightly elongated syncline with a northwest-southeast-trending fold axis (Fig. 1). The length of the major axis is about 150 km and the minor axis is about 70 km. Late Permian to Triassic sediments (with Keuper sediments on top) overlie a Paleozoic basement (Cambrian to early Carboniferous) and Upper Carboniferous to Lower Permian continental deposits. It is surrounded by the basement uplifts of the Harz Mountains to the north, and the Thüringer Wald/Thüringer Schiefergebirge to the south and east. The border to the west is marked by the Leinetal Graben.

After the Variscan orogeny (Latest Carboniferous and Early Permian Rotliegend time) the area was characterized by basin-and-range-type extension (Ménard and Molnar 1988). A phase of thermal subsidence caused deposition of thick evaporates and shale in the Upper Permian (Zechstein, e.g. Ziegler 1990). Subsidence and E-W directed extension with localized graben formation followed in Triassic times, concomitant with the deposition of clastic sediments, carbonates and evaporates (Kockel 2002). Regional extension from Late Jurassic until Early Cretaceous time created NW-SE-trending fault zones (Ziegler 1990). During the Late Cretaceous and the Early Paleogene, a regional compression event led to uplift and to reactivation and inversion of the fault zones (Ziegler 1978, Thomson & Zeh 2000, Senglaub et al. 2005, Kley & Voigt 2008). During this phase the present syncline structure was established and a substantial volume of Mesozoic strata was eroded due to basin inversion (Kästner et al. 2003) (Fig. 2).
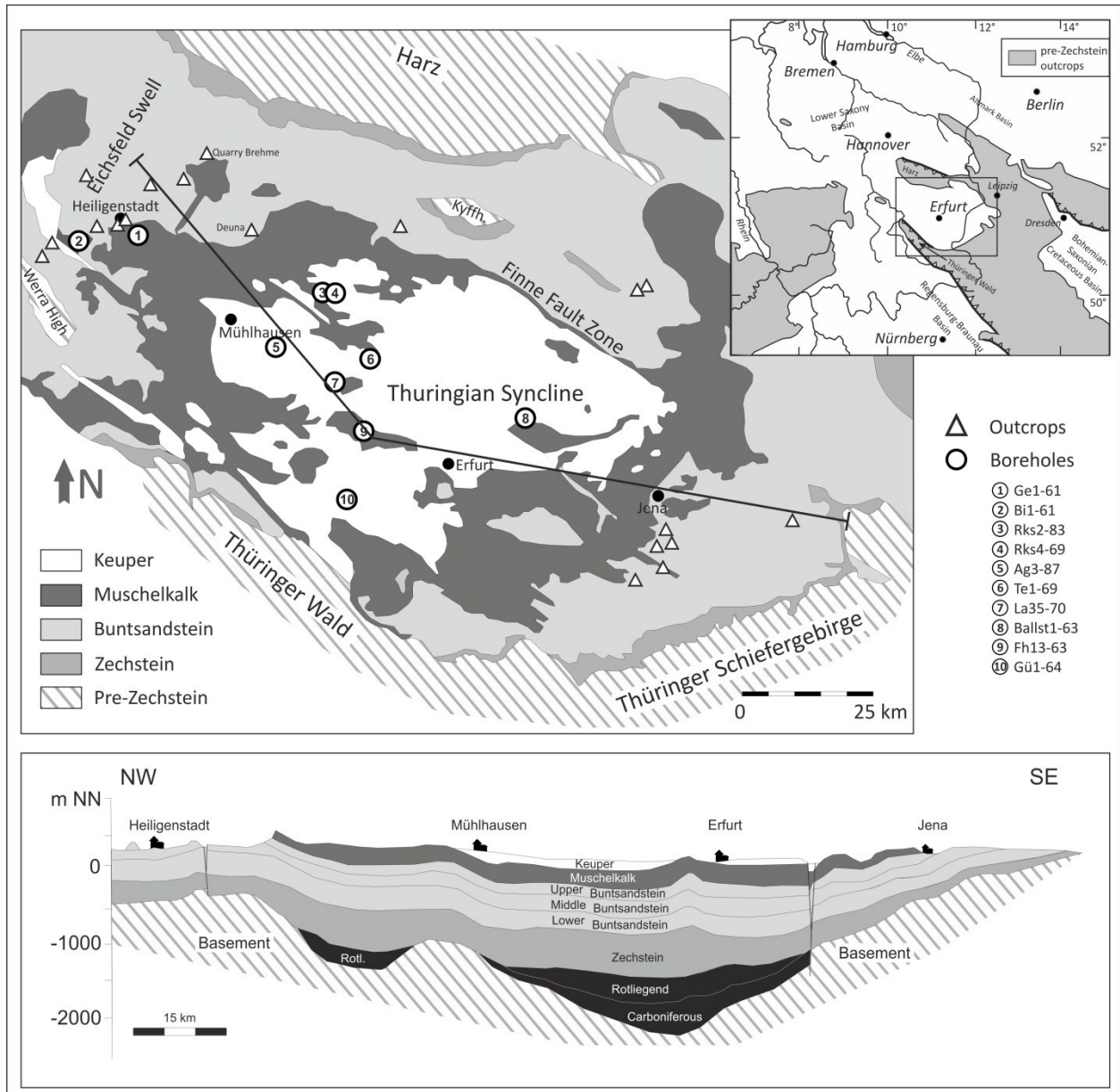
Fig. 2: Geological map and NW-SE cross section of the Thuringian Syncline (modified from Puff 1994, Seidel 2003). The basement map in the upper right is modified after Ziegler (1990). The cross section is approx. with 13x vertical exaggeration.

2.2. Stratigraphy of the Triassic Buntsandstein in Germany

The Lower Triassic Buntsandstein Group of Germany is subdivided into three subgroups comprising seven formations. The Lower Buntsandstein consists of the Calvörde (suC) and Bernburg (suB) formations, the Middle Buntsandstein is composed of the Volpriehausen (smV), Detfurth (smD), Hardegsen (smH) and Solling (smS) formations and the Upper Buntsandstein includes the Röt Formation. Rödiger (2005)

described the Buntsandstein formations of the eastern Thuringian Syncline as almost 100 % aquifers, except for the Röt and Calvörde formations (Fig. 3). To the northwest of the syncline, the sandstones of the Bernburg Formation grade laterally into fine grained claystones and shales and therefore represent an aquiclude.

The sediments of the Buntsandstein are mainly terrigeneous and were deposited under arid to semi-arid climate conditions with the main paleocurrent directions towards the north (Langbein 1985) (Fig. 4); only the Upper Buntsandstein shows a significant marine influence (Ziegler 1990, Paul 1999a, Voigt et al. 2011).

Super-group	Group	Subgroup		Formation	Aquifer type	Depositional environment
Germanic Triassic		M	Lower	Jena	Aquiclude	marine
	Buntsandstein		Upper	Röt	Aquiclude	marine
		Middle		Solling	Aquifer	fluvial
				Hardegsen	Aquifer	sandflat
				Detfurth	Aquifer	with eolian interbedding
				Volpriehausen	Aquifer	
		Lower		Bernburg	Aquifer	lacustrine/ floodplain
				Calvörde	Aquitard	
Permian	Zech-stein			Bröckelschiefer	Aquifer	

(Scale: 100 m / 0)

Fig. 3: German lithostratigraphy, description of aquifer type and predominant depositional environments of the Buntsandstein Group (stratigraphy and hydrogeology for the east of the Thuringian Syncline after Rödiger 2005).

The deposits of the Lower and Middle Thuringian Buntsandstein are characterized by a low morphological gradient and by the marginal location of the sedimentation area in the south-eastern part of the North German Basin (Gaupp et al. 1998). In the north a large lake covered the basin centre of the Central European Basin during this time

(Voigt & Gaupp 2000). In the Lower Buntsandstein ooliths associated with algal mats and stromatolitic structures were deposited predominantly in the centre of the Basin, but also sandstones enriched with single ooids are present in the southern marginal parts (Paul 1999b), where the centre of the present Thuringian Syncline was. These ooids were formed in a lagoonal or lacustrine depositional environment (Voigt & Gaupp 2000). Units of fluvial, floodplain and eolian sediments dominate the south-eastern margin of the Lower Buntsandstein deposits (Gaupp et al. 1998). The end of the Lower Buntsandstein is characterized by an unconformity caused by a rifting event (Lepper & Röhling 1998). The depositional environment in the Middle Buntsandstein is fluvial to lacustrine and the deposits are dominated by braided river sediments with a general material transport from south to north (Gaupp et al. 1998). Sediments of the Middle Buntsandstein were deposited under arid to semi-arid conditions with a fluctuating groundwater table (Roman 2004). Eolian sediments and pedogenic overprints are observable in the formations of the Middle Buntsandstein (Paul 1999a). A higher precipitation supported the formation of channels and associated flood plains with paleosols in the Solling Formation (Gaupp et al. 1998). From the Middle to the Upper Buntsandstein the marine influence increased (Beutler & Szulc 1999). In the Upper Buntsandstein a transgression of the saline "Röt-"sea formed deposits of evaporates, mudstones and thin intercalations of lime- and sandstones (Paul 1999a, Puff & Langbein 2003).
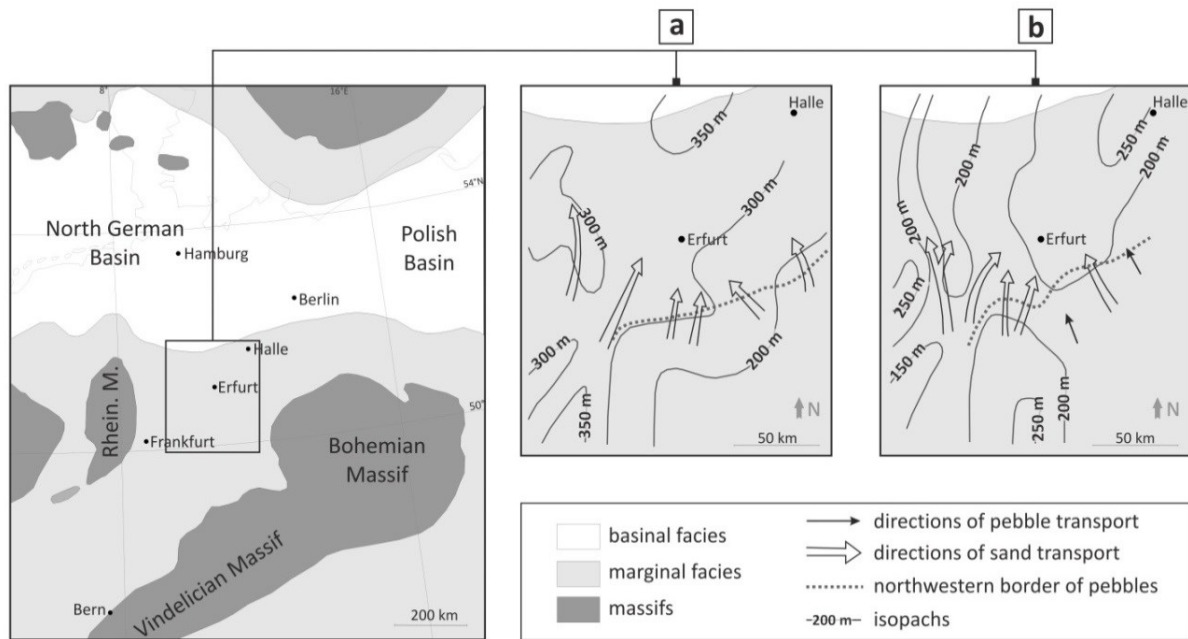
Fig. 4: Paleogeographic map of Central Europe in the Triassic showing paleocurrent directions in the Lower (a) and Middle (b) Buntsandstein. The paleogeographic map on the left is modified from Bachmann et al. (2009). Transport directions and isopachs on the right are after Langbein (1985).

2.3. Hydrocarbon reservoirs in the Thuringian Syncline

Natural gas was from the western part of the Thuringian Syncline in the 20th century (Kästner 2003, Brosin 2013). Oil and gas were found in carbonates (Staßfurtkarbonat) of the Zechstein Group (Fig. 5; Puff 1994, Niedersächsisches Landesamt für Bodenforschung 1991). The hydrocarbons migrated from lagoonal sediments stained with organic material to the overlying porous oncoid-limestones (Kästner 2003). In some cases gas also migrated through fault structures into the sediments of the Middle Buntsandstein (Fig. 5).
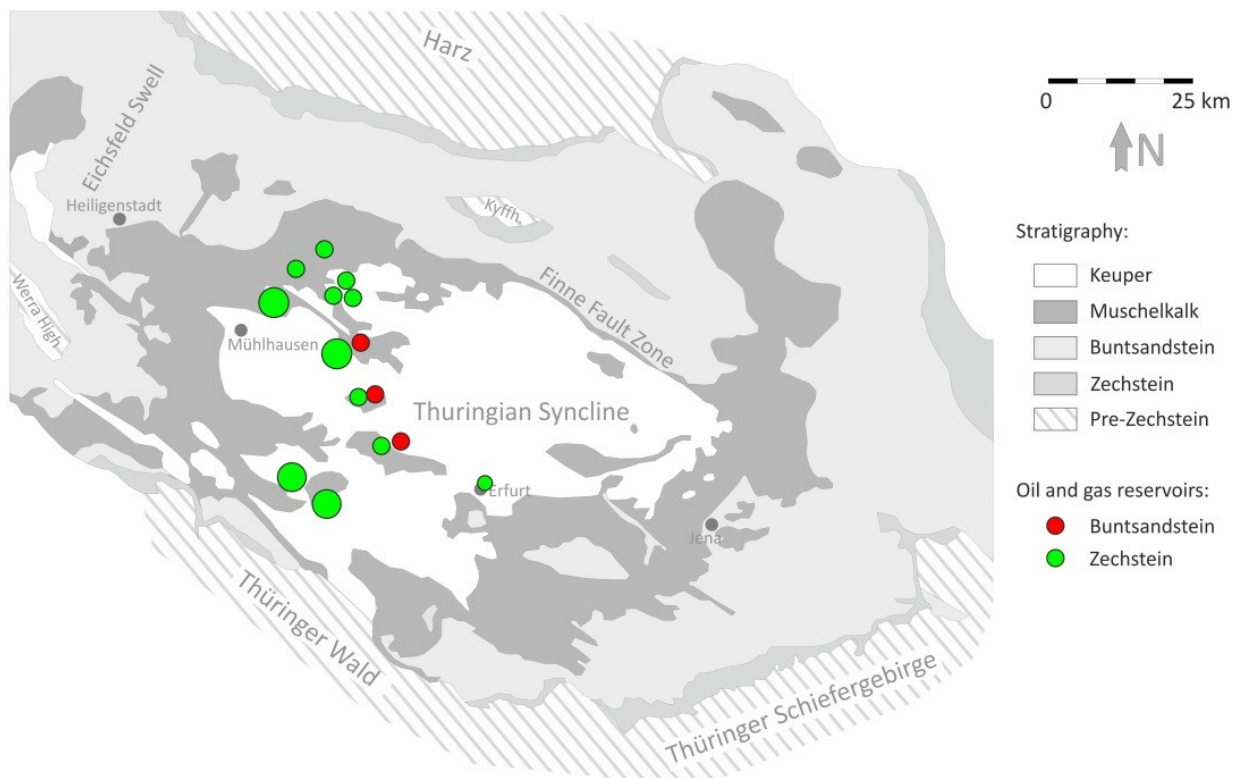
Fig. 5: Oil and gas reservoirs in the Thuringian Syncline (map after Puff 1994, reservoirs after Niedersächsisches Landesamt für Bodenforschung 1991). In the Buntsandstein sandstones hydrocarbons are exclusively natural gas reservoirs.

3. Material and Methods

3.1. Sedimentology, petrography and petrophysical properties

Drill core material from ten boreholes has been analysed; the borehole locations are shown in Fig. 2. Two cores from the syncline centre include a complete succession of the entire Buntsandstein Group. In two drillings from the northwest part of the syncline (close to Heiligenstadt), the Middle Buntsandstein was cored at relatively shallow depths from 15 m to 160 m. The samples from the centre of the Thuringian Syncline are from depths of 400 m to 1040 m. Facies interpretation was made by Kunkel (in prep.) and is based on field data from outcrops (Fig. 2) and the ten drill cores. All analysed material is from the Lower and Middle Buntsandstein.

Petrophysical data have been obtained from 250 core plugs with a diameter of 2.6 cm and a length of 3 cm, measured by G. Nover at the Steinmann Institute, University Bonn (Germany). Density and porosity were measured on vacuum-dried cylindrical plug samples to remove 'access-water' from the pore system. A Multivolume Gas-Pycnometer 1305 (Micromeritics) was used. The basis of this measurement is to record a pressure drop of He-gas between the sample chamber and calibrated reference chamber. The absolute error in density is $\pm$ 0.01 g/cm³. Density together with the sample volume allowed calculating the porosity with a percentage error of 2 %.

Gas permeabilities were determined on the same plug samples that were used for the density and porosity measurements. The permeability system consists of an autoclave with an appropriate rubber tube acting as a sample container. The confining pressure on the rubber-tube can be increased up to 10 MPa thus allowing measuring the pressure dependence of the permeability up to this pressure. The autoclave is connected on the inlet-side to a stabilized flow pressure (Argo-Gas) supply of about 1.5 bar and on the other side to the atmosphere or a second autoclave to measure flow conditions at higher pressure levels. These data are required to calculate Klinckenberg corrected permeabilities. The system can be considered as a modified Hassler-cell. Five flow-meters arranged in series but with different metering range (GFM Mass-Flow-Meter, Aalborg) record the gas-flow at the inlet-side of the autoclave, a pressure transducer records the actual inlet-pressure (Nover 2005, Zisser et al. 2007). The outlet pressure

was measured on the rear-side of the autoclave together with the actual temperature. Data were recorded continuously and were then used to calculate the permeability of the sample using the Darcy equation and the known geometry of the plug-sample. The flow meters are calibrated to resolve sample permeabilities ranging from $> 10^{-13}$ m² up to $< 10^{-17}$ m² (0.01 mD to 101 mD).

Plug sampling/measurement and thin section preparation of samples from boreholes Rks4-69, Te1-69, Fh13-63, La35-70 and Gü1-64 were carried out in the framework of the DFG-Project AD 315/1-1 ("Long-term impact of CO_2 on the stability of mineral assemblages in porous reservoir sandstones – Analogue study in natural CO_2 reservoirs from Central Europe") by Pudlo et al. (2010).

All petrographic and mineralogical investigations were made at the Institute of Geoscience, University of Jena (Germany). In total, 146 thin-sections of sandstone (24 from lacustrine facies, 83 from sandflat, 16 from fluvial and 23 from eolian sandstone) were point-counted with a polarising microscope (Axioplan 2 von Carl Zeiss). 300 points were counted for each sample with an automatic Point Counter (PRIOR, Type G). To avoid counting a grain two times, the distance between two counts was calibrated on grain size. The following detrital components were counted: Quartz (mono- and polyquartz, chert), feldspar (K-feldspar and plagioclase), lithic fragments (sedimentary and igneous), heavy minerals, opaque minerals, ooids, mica and detrital clay (clay coatings and clay matrix). Authigenic iron oxide and detrital clay coatings form together coatings around the grain; therefore they were summarized as clay coatings. The following authigenic minerals were counted: blocky cements (carbonate, gypsum, anhydrite, salt, quartz and feldspar), kaolinite and illite (cutans, radial overgrowth and meshwork). Porosity (intra- and intergranular porosity) was also counted. Grain size of the samples was measured quantitative, grain roundness and sorting of the sandstone were determined qualitative with an optical microscope. The sorting was described according to Folk (1968). The grain roundness was described according to Pettijohn et al. (1987). All point-counted thin-sections were taken from drill cores of the 8 boreholes located in the syncline centre. The petrography of samples (thin sections) from outcrops and the two shallow boreholes were analysed in a qualitative way.

Porosity and permeability values reported in this study were mainly determined from petrophysical measurements on core plugs. Porosity values from point-counting were

used for the estimation of intergranular volume and porosity loss by compaction or cementation.

The chemical composition of feldspars, micas, carbonate and sulphate cement, Ti-oxide, clay minerals and heavy minerals were determined with back-scattered electron imaging and energy-dispersive X-ray spectroscopy using a Jeol JXA-8230 microprobe University Jena. Quantitative measurements were made with an Electron Microprobe Analyser (wavelength dispersive X-ray spectroscopy; 15 kV and 15 nA) using a defocussed beam (10 µm). For element calibration the following minerals were used: Wollastonite (Ca), Periklase (Mg), Hematite (Fe), Rhodonite (Mn), Baryte (Ba), Celestine (Sr), Baryte (S) and Wollastonite (Si).

Surface attributes, such as grain surface area and mineral shape were obtained using a scanning electron microscope Zeiss ULTRA PLUS FE-SEM at the University Jena (secondary electron imaging mode).

Quartz and carbonate cements were also analysed with a hot-cathode luminescence microscope HC1-LM at the University Jena.

3.2. Digital image analysis

For studying the pore space (porosity, amount of pores, size and shape of pores, perimeter, pore density) the image analysing software Zeiss Axiovision© was used. The program identifies areas of the same colour in an image. Hence it was possible to examine the blue coloured pore space in an image of a thin section. The pore space was analysed in 24 lacustrine, 61 sandflat, 14 fluvial and 13 eolian sandstones (in total 112 samples). For one thin section 20 images (made with a microscope, normal light, 5x lens) were used for the measurement. These 20 images were chosen in a way that they represent the thin section well. The analysed area of a thin section was 52544556 μm^2 (area of 20 images). The program is not able to identify pore areas which are smaller than 1.8 μm^2. The measured pore areas in a thin section were classified into four categories (Fig. 6): small pores (1 – 1000 μm^2), medium pores (1000 – 10000 μm^2), large pores (10000 – 50000 μm^2) and very large pores (> 50000 μm^2).
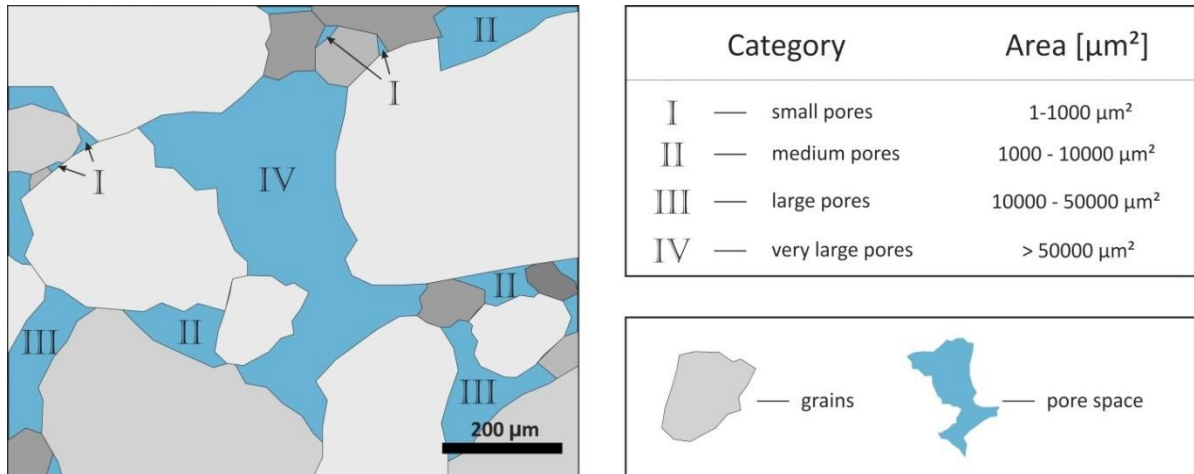
Fig. 6: Four defined pore size categories for an image of a thin section.

In order to measure the mineral surface areas, images of 24 thin sections (6 per facies type) were analysed with the program JMicroVision©. For one thin section approx. 30 images (made with a microscope, normal light and crossed nicols, 20x lens) were used for mineral surface quantification. Only surfaces exposed to the pore space are taken into account. Every measured line was referred to mineral grain type or authigenic cement (Fig. 7). Important for the measurement of surface area is the porosity of the sandstone. It was not possible to determine surface areas with this method for thin sections without blue stained pore space. The surface areas of the Ballst-samples were measured by Naumann (2013) during his diploma thesis.
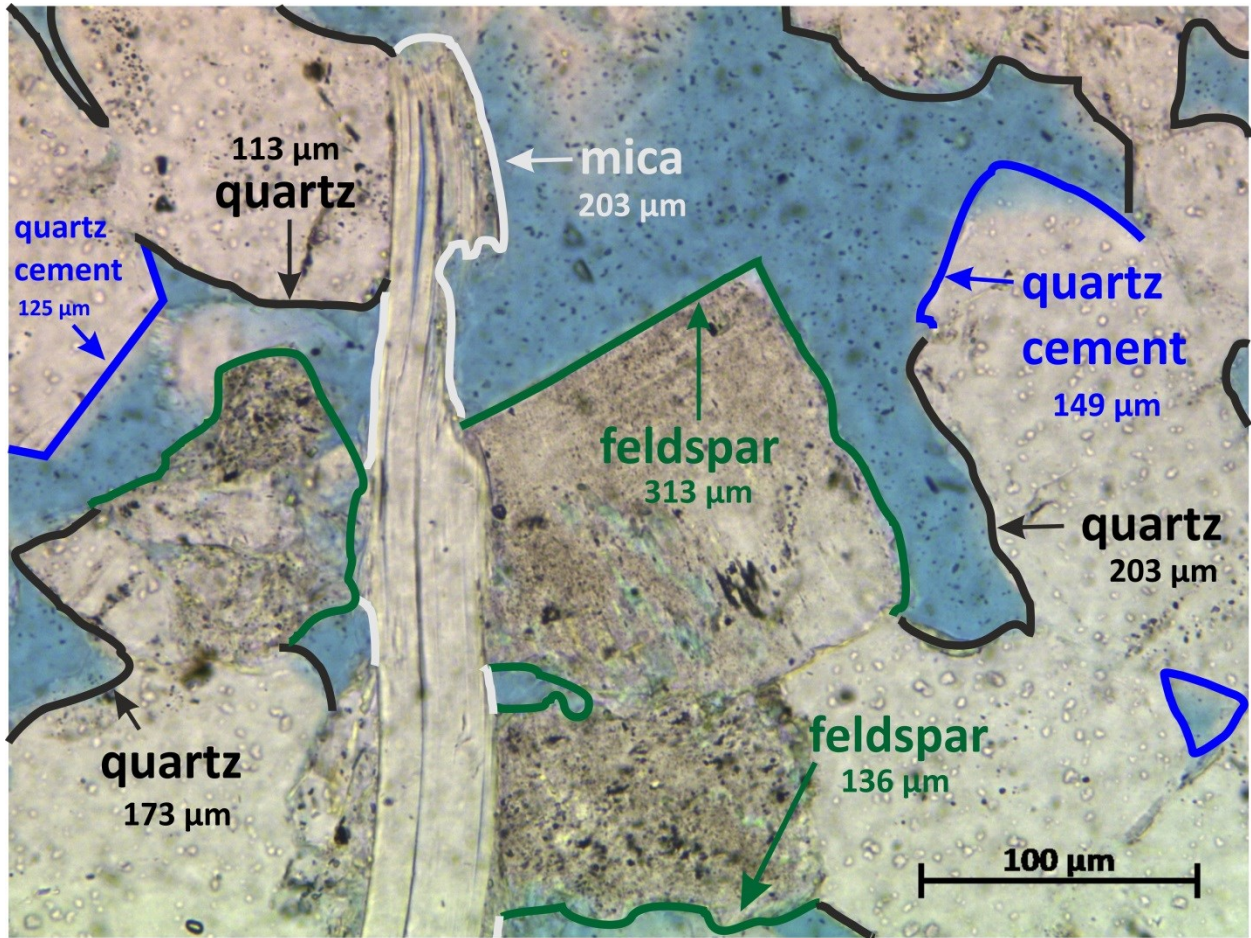
Fig. 7: Measurement of the mineral surface areas exposed to the pore space (sample Gü1-6, Solling Formation, fluvial facies type).

3.3. BET measurements

The surface area of 26 Bundsandstein sandstones were measured with BET (16 samples are from by D. Pudlo). The small sandstone fragments (< 5 mm in length or width) were measured at the TU München by Dr. K. Heister.

The BET theory was invented by S. Brunauer, P. H. Emmett, and E. Teller in 1938. The first letters of their names gives the method the name BET. The BET method based on the theory of adsorption of gas, first described by Brunauer et al. (1938). With this method, it is possible to measure the surface area (in m²/g) of pores inside sandstone. This surface area quantification by BET (Gregg & Sing 1982) uses adsorption of chemically inert gas nitrogen on the surface area. The concept of the theory is

adsorption of an inert gas by van-der-Waals-force as a monolayer on a solid surface area. The reaction depends on the relative pressure p/p0 (p: partial pressure of the gas, p0: equilibrium vapor pressure). With the adsorbed volume and the volume of the molecule (nitrogen: 0.16 nm^2) a calculation of the monolayer area is possible (Gregg & Sing 1982).

BET surface area = $(a * V_m * N)/(V * w_S)$

$\quad$ a: area of the gas monolayer (m^2)

$\quad$ V_m: volume of the gas (m^3); standard pressure and temperature

$\quad$ N: Avogadro constant $\quad$ V: molecular gas volume (m^3/mol)

$\quad$ w_S: density of the solid sample

3.4. Vitrinite reflectance and thermal modelling

For the analysis of the maturity of organic matter sedimentary rocks were taken from different stratigraphic units from boreholes and outcrops of different locations in the Thuringian Syncline (see Fig. 9 for sample locations and Table 3 for sample characteristics). In the Thuringian Syncline, sediments containing organic matter are rare and the amount of analysed samples is therefore limited. Twenty locations (5 wells and 15 outcrops) of the Erfurt Formation (Lower Keuper) have been sampled (Götze 2011). The samples are sandstones with a low content of coal or coaly particles. Eight locations (6 wells and 2 outcrops) of the Kupferschiefer Formation (Lower Zechstein) have been sampled as well (Peisker 2011). These samples are shales with relatively high content of bituminous organic matter. Moreover, two coal samples from the Carboniferous (Wettin Formation and Mansfeld Formation) and two sandstone samples from the Rotliegend Group (Netzkater Formation and Manebach Formation) have been used (Grobleben 2007). The samples were used in a framework of diploma thesis (Grobleben 2007, Götze 2011) and in a "Forschungsarbeit" (Peisker 2011) as well.

The degree of maturity/coalification yields information about the integral of temperature exposure over time attained by organic (vitrinitic) matter. Vitrinite is a constituent of coal (mazeral) whose reflectance is an indicator for thermal maturity and

directly linked to the temperature. Vitrinite reflectance is therefore one of the most important parameters to evaluate the burial history of sedimentary rocks (Hantschel & Kauerauf 2009). The grade of coalification VRr (reflectance of randomly orientated vitrinite grains) was measured with a microscope photometer. The measurement was done under oil immersion and with monochromatic light. A measurement of standard samples was used for the calibration. The program MPVGEOR with the method "Coal Random" was used. The samples were measured at the TU Freiberg by the working group of Prof. N. Volkmann and at RWTH Aachen by working group of Prof. R. Littke.

The reflectance of bituminite was measured, because no vitrinite is present in the Kupferschiefer-samples. These values can be converted into vitrinite reflectance values using the regression equation of Landis and Castaño (1995):

VRr = (Br + 0.41)/1.09   VRr: Vitrinite reflectance

                                Br: Bituminite reflectance

Vitrinite reflectance values were used as input data for the modelling software PetroMod 11 1DExpress from IES GmbH.

Burial history modelling

For the modelling the program PetroMod 11 1D Express was used. 13 models/virtual wells were generated. For every model the input data depends on the following parameters: stratigraphy, layer thickness, eroded stratigraphy, time of deposition, time of erosion and lithology; vitrinite reflectance was used as calibration data; boundary conditions were paleo-water-depth, sediment-water-interface (swi) temperature and heat flow.

In the simulation the program starts with the oldest layer and successively adds younger layers, taking compaction, temperature evolution and porosity loss into account. The calculation of the thermal history is based on the vitrinite value. The kinetic model of Sweeney and Burnham (1990) was used for the maturity modelling.

Since the forward-simulation of temperatures is an iterative process, the fit of the modelled data with the calibration data is necessary after each simulation step. The modelled results are fit to the measured calibration data by changing / adjusting the input simulation parameters until a "best-fit" scenario has been reached. Often several models are fulfilling the conditions. Alternative simulations and modelling problems are discussed in chapter 4.3. After the "best-fit" scenario has been reached, a model provides a maximum burial depth and a maximum temperature for the different layers.

4. Burial history simulation for the Thuringian Syncline

4.1. 1D simulations in the Thuringian Syncline

4.1.1. Conceptual model, input and calibration data

In order to improve the understanding of the burial and thermal history of the Buntsandstein sandstones a simulation of basin subsidence and uplift has been carried out. Therefore burial histories were modelled for 17 virtual wells in the Thuringian Syncline. The stratigraphic data of these wells were generated from two geological cross sections (Fig. 13). These cross sections are based on a large set of well data provided by the "Thüringer Landesanstalt für Umwelt und Geologie" (TLUG).

Lithological composition and physical rock properties assigned to the layers in the simulation were taken from the literature (Seidel 1992, see Table 1) and were implemented in the program by using the standard lithologies of Petromod (stratigraphic data of the models/virtual wells are shown in Table 2). The thicknesses of the preserved layers vary only slightly in the Thuringian Syncline. Therefore the thickness of the Zechstein to Upper Keuper strata is nearly the same in the different models. Local lithological and thickness information are taken from Seidel (1992). The heat flow over the geological history of the syncline is not well constrained. For Permian time, Seidel (2003) describes an extensional regime. After Allen and Allen (2005) it can be supposed that the heat flow for an extensional regime is in the range of 65 to 110 mW/m². In the models a heat flow of 90 mW/m² was used for the Lower Permian (Fig. 8). The heat flow decreases logarithmically to 60 mW/m² till the end of Permian times (Fig. 8), corresponding to a mean global heat flow (Allen and Allen 2005). The paleo water depth was estimated after facies type and paleo-geographic maps described by Ziegler (1990) (Fig. 8). The program considers the climate and the sediment-water-interface-temperature (SWIT) automatically (Fig. 8).

Table 1: Formation layer thickness for the centre of the Thuringian Syncline (northeast area of the Syncline, near Ballstedt) according to Seidel (1992).

formations	layer thickness	short description	assumed water depth
Upper Keuper	45 – 62 m	sandstone and claystone	0 m
Middle Keuper	410 – 554 m	evaporates, sandstone and marl	0 – 10 m
Lower Keuper	38 – 57 m	sandstone and marl	0 m
Upper Muschelkalk	77 m	limestone	up to 100 m
Middle Muschelkalk	117 m	dolomite and sulphates	up to 100 m
Lower Muschelkalk	105 m	limestone and marl	up to 100 m
Röt	182 m	evaporates and claystones	up to 50 m
Solling	18 m	sandstone	0 m
Hardegsen	48 m	sandstone	0 m
Detfurth	56 m	sandstone	0 m
Volpriehausen	236 m	sandstone	0 m
Bernburg	148 m	sand- and claystone	0 m
Calvörde (described as Nordhausen-Folge, Bröckelschiefer is not included)	161 m	sand- and claystone	0 m
Zechstein (Bröckelschiefer included)	637 m	evaporates and mudstones	up to 100 m

For Jurassic and Cretaceous time, depositional environments like in the Lower Saxony Basin or North German Basin were assumed: intracontinental marine deposition was established in the Jurassic, like in the Lower Saxony Basin (Betz et al. 1987) or in the North German Basin (Ziegler 1990). Marine conditions continued in the Lower Saxony Basin during the Cretaceous time (Betz et al. 1987) till a global eustatic sea level highstand was reached in the Late Cretaceous (Haq et al. 1987). Hence intracontinental marine conditions can be assumed for the Thuringian Syncline also in the Cretaceous. It is important for the burial history model to add Jurassic and Cretaceous sediments (which were later eroded), because without these layers the thickness of the other layers is not sufficient to match the measured vitrinite reflectance values. Compared with the stratigraphy of the Lower Saxony Basin or the North German Basin it is highly likely that sediments of Jurassic and Cretaceous age were present in the area of the Thuringian Syncline. Terrestrial clastic sediments were deposited in the Paleogene and Neogene (Steinmüller 2003).
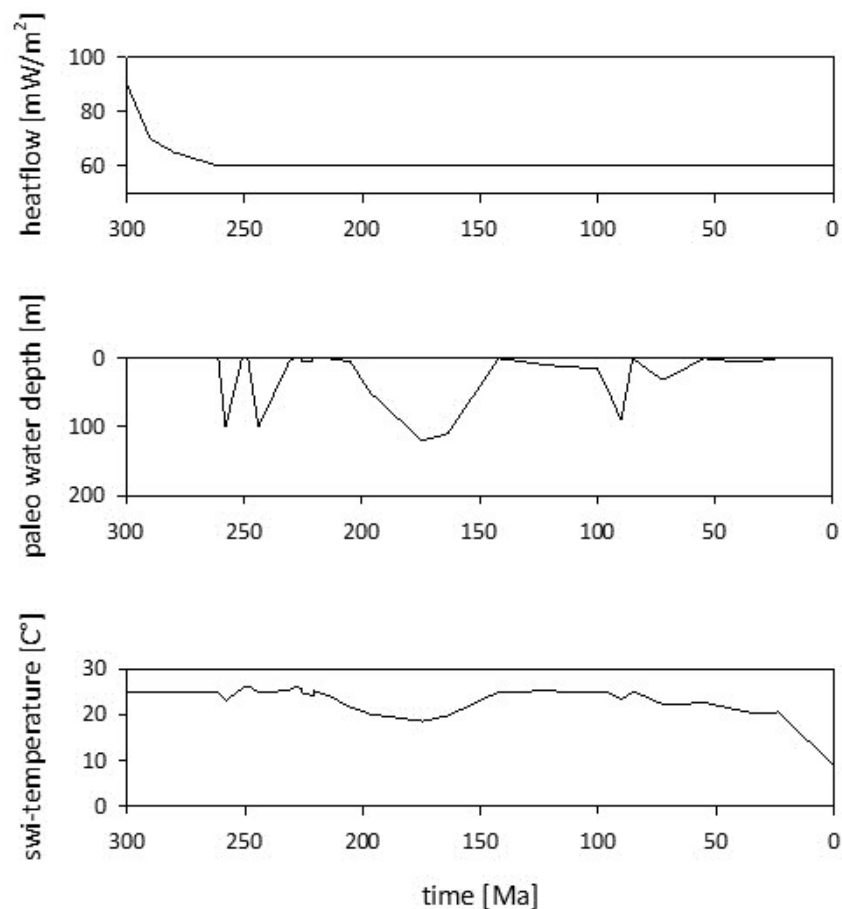
Fig. 8: Model boundary conditions: heat flow, paleo water depth and temperature at the sediment-water interface (swi) in the Thuringian Syncline through time. The heat flow is relatively high in Permian time and decrease logarithmically till Triassic time. The swi-temperature is calculated by PetroMod.

The following key hypotheses were made for the models:

– Steady marine and terrestrial deposition due to base level fluctuations from Zechstein until the Upper Cretaceous (end of Turonian).
– At the end of the Turonian a phase of uplift starts and lasts until the Campanian. In this time a great thickness of sediments was being eroded.
– In the early Paleogene deposition of sediments resumed, followed by a short erosional phase.
– Deposition took place under terrestrial or marine conditions with a maximum of 120 m water depth.
– Sediment-water interface temperature was between 20° and 25°C from Permian to Neogene time and decreased then to present day values.

– Heat flow was increased in Permian times to 90 mW/m², due to an extensional rifting regime. Later a logarithmically heat flow decrease to 60 mW/m² is assumed.

Table 2: Input data for the modelling with the software PetroMod© 1D. Thickness values depend on the location of the virtual well and are approximately constant for the models in the Thuringian Syncline. Thickness values of Jurassic and Cretaceous sediments differ from well to well, based on the maturity of organic matter. Thermal conductivity determined on the basis of Allen & Allen (2005).

Layer	Top [m]	Base [m]	Thickness [m]	Eroded [m]	Deposition from [Ma]	Deposition to [Ma]	Eroded from [Ma]	Eroded to [Ma]	Thermal conductivity [Wm-1K-1]	Lithologie
Tertiär	0	0	0	80	41	33	33	10	1.5-4.2	Sandcongl
Oberes Campan	0	0	0	0	73	41	x	x	x	none
höhere Oberkreide	0	0	0	0	89	73	x	x	x	none
tiefere Oberkreide (Turon)	0	0	0	65	93.5	89	87	86	2.0-3.4	LIMESTONE
tiefere Oberkreide (Cenoman)	0	0	0	35	99	93,5	86	85	2.0-3.4	LIMEmarly
höhere Unterkreide (Alb)	0	0	0	250	112.2	99	85	84	1.5-4.2	SANDSTONE
höhere Unterkreide (Apt)	0	0	0	150	121	112,2	84	83.5	1.5-4.2	SANDSTONE
tiefere Unterkreide	0	0	0	100	142	121	83.5	83.2	1.5-4.2	SANDSTONE
Oberer Jura (Malm)	0	0	0	400	154	142	83.2	82	2.0-3.4	LIMEmarly
Mittlerer Jura (Dogger)	0	0	0	400	177	154	82	81.5	1.2-3.4	SHALE&LIME
Unterer Jura (Lias)	0	0	0	200	200	177	81.5	80	1.2-3.0	MARL
Oberer Keuper (Exter)	0	0	0	53	207	200	80	79.8	1.5-4.2	SANDSTONE
Mittlerer Keuper (Arnstadt)	0	0	0	134	214	207	79.8	79.5	1.2-3.0	MARL
Mittlerer Keuper (Weser)	0	0	0	112	224.5	214	79.5	79	6.3	GYPSUM
Mittlerer Keuper (Stuttgart)	0	0	0	10	226	224,5	79	78	1.5-4.2	SANDSTONE
Mittlerer Keuper (Grabfeld)	0	27	27	111	232.5	226	78	74	6.3	GYPSUM
Unterer Keuper (Erfurt)	27	75	48	0	235	232,5	x	x	1.5-4.2	SANDSTONE
Oberer Muschelkalk	75	133	58	0	238.5	235	x	x	2.0-3.4	LIMEmarly
Mittlerer Muschelkalk	133	210	77	0	240	238,5	x	x	3.2-5.0	DOLOMITE
Unterer Muschelkalk	210	320	110	0	243	240	x	x	2.0-3.4	LIMEmarly
Oberer Buntsandstein (Röt)	320	480	160	0	244.5	243	x	x	2.0-3.4	LIME&EVAP
Solling	480	493	13	0	245	244,5	x	x	1.5-4.2	SANDshaly
Hardegsen	493	530	37	0	247	245	x	x	1.5-4.2	SANDshaly
Dethfurt	530	565	35	0	247.5	247	x	x	1.5-4.2	SANDshaly
Volpriehausen	565	658	93	0	248.5	247,5	x	x	1.5-4.2	SANDshaly
Bernburg	658	807	149	0	250	248,5	x	x	1.2-4.2	SAND&SHALE
Calvörde	807	955	148	0	251	250	x	x	1.2-4.2	SAND&SHALE
Zechstein	955	1400	445	x	258	251	x	x	5.4-7.2	EVAPORITE

4.1.2. Vitrinite reflectance

The results of vitrinite reflectance measurements are shown in Table 3 for the Keuper, Zechstein and Carboniferous/Rotliegend samples. The standard deviation SD (%) is a significant parameter for the usability of the sample: in a normally distributed sample 95 % of the values lie in an interval of their mean value plus/minus two times their standard deviation ($x_{arith} \pm 2*SD$). All samples listed in Table 3 fulfil this requirement.

Table 3: Vitrinite reflectance data of the Keuper, Rotliegend and Siles/Rotliegend samples; Coordinates are given in the Gauss- Krüger Coordinate System. Keuper samples from Götze (2011), Kupferschiefer samples from Peisker (2011) and Siles and Rotliegend samples from Grobleben (2007).

	Location	Depth [m]	Easting	Northing	Lithology	Stratigraphy	Bituminit Br (%)	Vitrinite VRr (%)	SD (%)	Measured points
Keuper samples	Reisdorf	surface	4468779	5662393	sandstone with coal	Keuper	x	0.54	0.06	112
	Eberstedt	surface	4470471	5659963	sandstone	Keuper	x	0.56	0.04	50
	Finnetunnel	surface	4461357	5667254	sandstone	Keuper	x	0.57	0.04	100
	Lauterbach	surface	4384429	5661055	sandstone	Keuper	x	0.62	0.05	13
	Freienbessingen	surface	4415120	5679720	sandstone	Keuper	x	0.81	0.04	5
	Hochstedt	surface	4439980	5649980	sandstone	Keuper	x	0.77	0.08	37
	Eischleben	surface	4429590	5640020	sandstone	Keuper	x	0.60	0.09	67
	Bad Langensalza	surface	4403819	5664763	sandstone	Keuper	x	0.65	0.07	10
	Magdala	surface	4460150	5643000	sandstone	Keuper	x	0.55	0.05	74
	Kb Schillingstedt	506 m	4445310	5679226	sandstone	Keuper	x	0.53	0.06	100
	Kleinvargula	surface	4415925	5667175	sandstone	Keuper	x	0.55	0.05	106
	Melchendorf	surface	4434570	5646210	sandstone	Keuper	x	0.68	0.14	36
	Tennstedt	surface	4415940	5669690	sandstone	Keuper	x	0.79	0.11	28
	Vogelsberg	surface	4446425	5666000	sandstone	Keuper	x	0.86	0.17	22
	Tröchtelborn	surface	4415625	5652025	sandstone	Keuper	x	0.53	0.04	8
	Kb Seebergen 1/64	402 m	4415660	5642437	sandstone	Keuper	x	0.64	0.05	97
	Hy Arnstadt 10/92	13.7 m	4424276	5634336	sandstone	Keuper	x	0.75	0.23	129
	Kb Apolda 1/65	250 m	4466436	5655896	sand-/siltstone	Keuper	x	0.57	0.04	100
	S4/Tb4-1 Kammerforst	20.5 m	4392925	5666035	claystone	Keuper	x	0.62	0.04	107
	Eisenach	surface	4379492	5653867	sandstone	Keuper	x	0.79	x	x
	Netragraben	surface	4363977	5665547	sandstone	Keuper	x	0.99	0.06	x
	Buchberg 106	surface	4360064	5658284	sandstone	Keuper	x	1.24	0.04	x
Kupferschiefer samples	Altengottern 1/58	1652 m	4399547	5671479	shale	Kupfer-schiefer	0.80	0.97	0.10	78
	Ettersburg 7/63	1279 m	4455209	5653473	shale	Kupfer-schiefer	0.93	1.16	0.12	55
	Erfurt 1/64	1085 m	4432285	5650445	shale	Kupfer-schiefer	0.75	0.89	0.14	56
	Hainich Berka 101/63	1215 m	4387742	5656034	shale	Kupfer-schiefer	0.81	0.98	0.08	81
	Gera Märzenberg	Surface	4503730	5640407	shale	Kupfer-schiefer	0.75	0.90	0.12	41
	GTB Kamsdorf	Surface	4463413	5612070	shale	Kupfer-schiefer	0.71	0.83	0.09	34
	Mansfeld Fortschritt SF	542 m	4470043	5712978	shale	Kupfer-schiefer	1.04	1.32	0.10	97
	Wettelrode Röhrigschacht	162 m	4450741	5709725	shale	Kupfer-schiefer	0.91	1.14	0.10	52
Siles and Rotliegend	Querfurt 1/64	2500	4482915	5697205	coal	Wettin F.	x	2.40	x	x
	Querfurt 1/64	3000	4482915	5697205	coal	Mansfeld F.	x	2.80	x	x
	Ilfeld	1200	4419905	5717220	sandstone	Netzkater F.	x	1.45	x	x
	Thuringian Forest	0	4415693	5618306	sandstone	Manebach F.	x	1.80	x	x

Values of the vitrinite reflectance of the Keuper samples are high in the centre of the syncline: a NW-SE directed swath of higher VRr values between 0.77 % and 0.86 % is

observable in area 1 of Fig. 9. The vitrinite reflectance values calculated from bituminite reflectance in the Kupferschiefer samples are lower in the south and southwest (between 0.89 % and 0.98 %) than in the centre and north/northeast of the syncline (values between 1.14 % and 1.32 %) (area 2 in Fig. 9). The VRr values of the Upper Carboniferous/Lower Permian samples (Fig. 9) are lower in the north (1.45 % and 1.80 %) than in the northeast (2.40 % and 2.80 %).
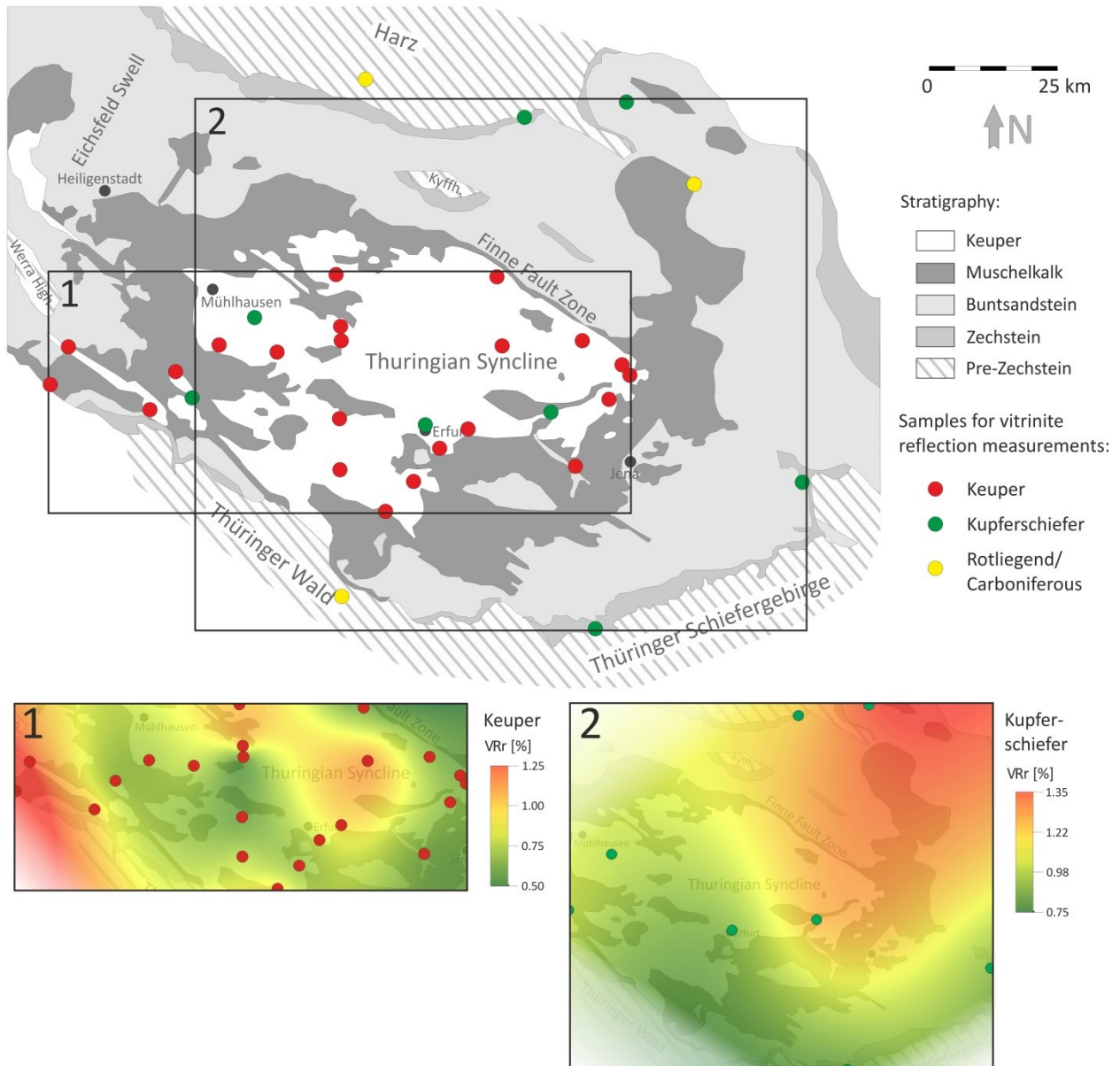
Fig. 9: Sampling locations for Carboniferous, Permian and Triassic sediments from drill cores and outcrops for vitrinite reflection measurements in the Thuringian Syncline and adjacent areas (map modified after Puff 1994). The coloured maps show spline-interpolations of the measured vitrinite VRr values for the Keuper and Kupferschiefer samples.

4.1.3. Burial history modelling

In order to create 2D models along the two cross section traces shown in Fig. 10, several virtual wells were created on these profiles in order to calculate 1D models. The positions of these virtual wells are also shown in Fig. 10. They correspond to 17 one-dimensional (1D) thermal models in the syncline and along the two profiles. The thermal models were calculated using the program PetroMod 1D. Taking into account that significant changes in the paleo-thickness of Mesozoic strata might be related to structural elements, the positions of the virtual wells were chosen such that wells are located on both sides of each major fault zone.
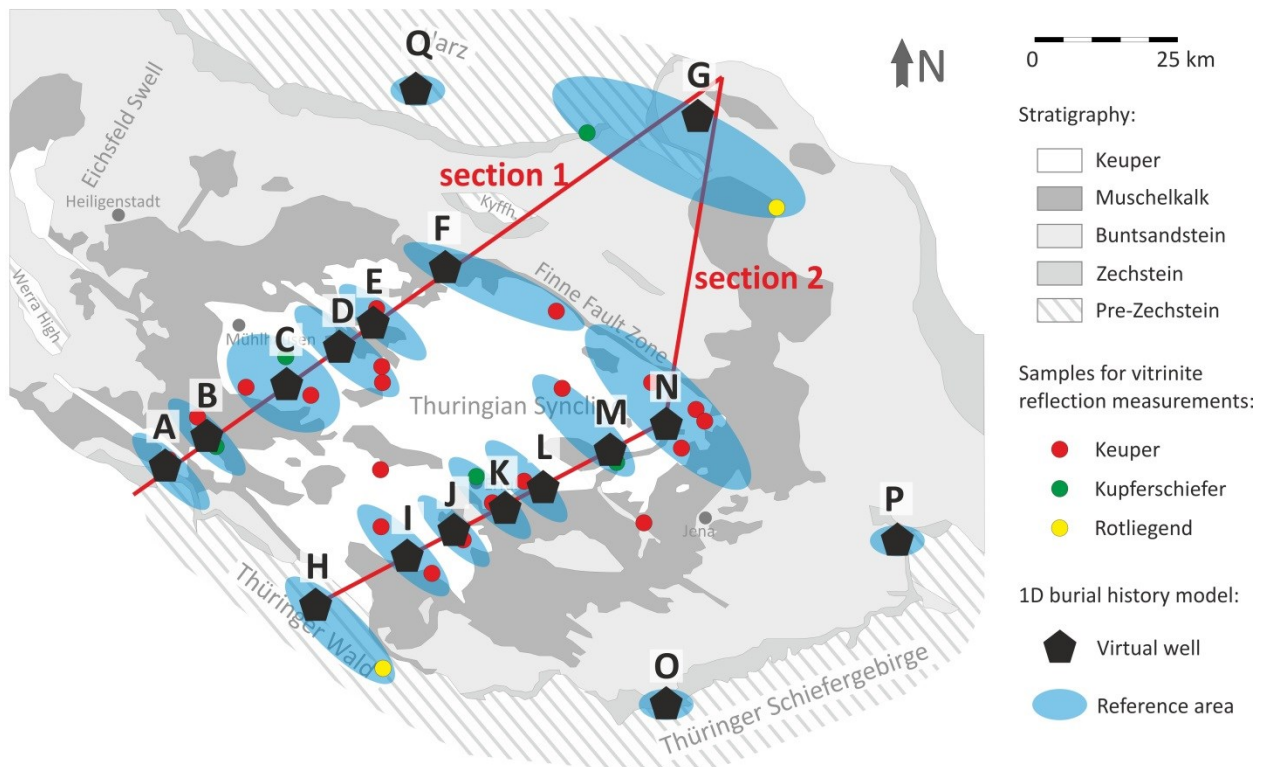
Fig. 10: The two sections and the locations of the virtual wells. The ellipses around the wells show which vitrinite reflectance values were taken into account in each virtual well (map modified after Puff 1994).

The calculation of the standard deviation (see Table 3) indicates the spread of the vitrinite reflectance measurements. Every burial history model is calibrated with its associated measured vitrinite reflectance data (Fig. 10). Therefore, it was necessary to analyse the potential error of this calibration. By means of the vitrinite reflection data it

was possible to calculate the thickness of eroded Jurassic and Cretaceous strata in a best fitting calibration. By using the standard deviations of the values, it was possible to calculate the boundary conditions (minimum and maximum). The calculated thickness for all models (incl. minimum and maximum) is shown in Table 4. The calibration for the model/virtual well C with the vitrinite values is displayed in Fig. 11.
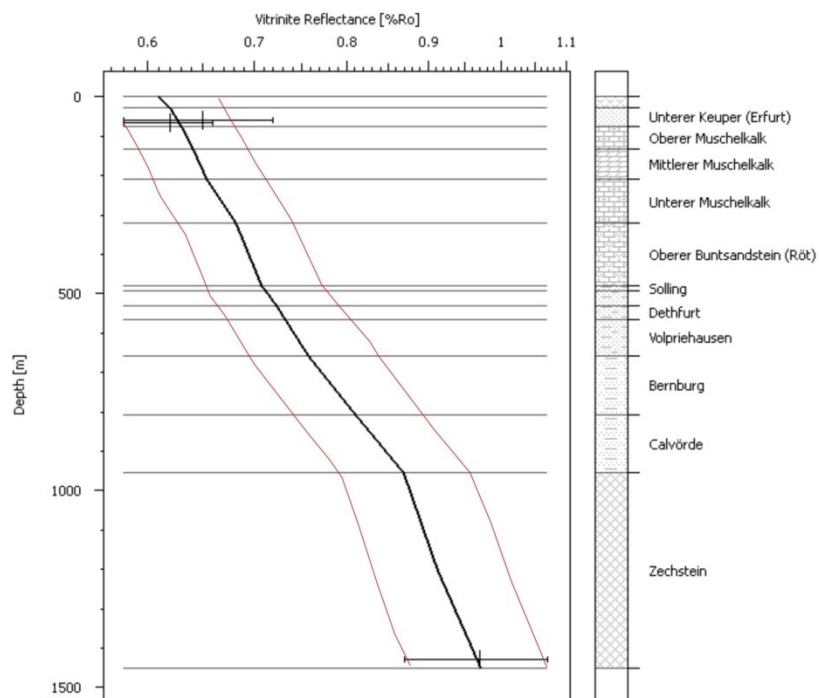
Fig. 11: Vitrinite reflectance calibration for model C. Three vitrinite values of reflection are marked with mean and min/max values. The black line is the used calibration for this model (best fit calibration). The red lines show the boundary calibrations (minimum and maximum) for these data, calculated by the standard deviation of the vitrinite reflection values.

Table 4: The calculated thicknesses (in a best/minimum/maximum fit model) of Jurassic and Cretaceous strata for the 17 virtual wells, based on the standard deviation of the used values. The calculation for model A and Q is based on values without standard deviation, therefore a calculation of minimum and maximum fit for these models was not possible.

model/ virtual well	thickness of Jurassic and Cretaceous strata (best fit model)	thickness of Jurassic and Cretaceous strata (minimum fit model)	thickness of Jurassic and Cretaceous strata (maximum fit model)
A	2300 m	x	x
B	1600 m	1550 m	1900 m
C	1600 m	1400 m	1700 m
D	2200 m	1900 m	2700 m
E	2300 m	2250 m	2450 m
F	1300 m	900 m	1400 m
G	2100 m	2000 m	2300 m
H	1000 m	900 m	1050 m
I	2000 m	1600 m	2500 m
J	1500 m	1250 m	1800 m
K	1600 m	1400 m	1800 m
L	2200 m	2000 m	2400 m
M	2100 m	1900 m	2150 m
N	1350 m	1250 m	1400 m
O	1450 m	1200 m	1700 m
P	1700 m	1400 m	1850 m
Q	1800 m	x	x

After applying the modelling software, it was possible to determine the burial history of every virtual well. The burial history reveals the maximum burial depth of the sedimentary rocks. Compared with the layer depth of today, the uplift of the rocks can be estimated. The Zechstein sediments at the margin of the Thuringian Syncline were uplifted 800 m relative to the sediments in the centre of the basin (Fig. 12). The uplift took place during the inversion phase in the Upper Cretaceous (Thomson & Zeh 2000, Kley & Voigt 2008).
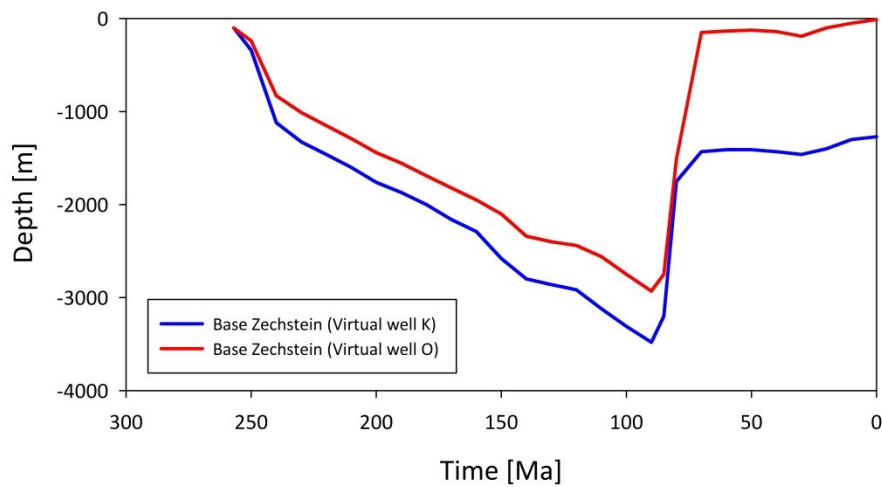
Fig. 12: The base of Zechstein in depth plots of two virtual wells over time. Well K is located in the syncline centre. Well O is located at the syncline margin, where the Zechstein is at the surface today. In accordance to apatite fission track data from Thuringian Forrest and Harz Mountains, the major uplift is assumed to have occurred between 85 Ma and 72 Ma (Thomson & Zeh 2000).

4.2. 2D interpretation of the 1D models in the Thuringian Syncline

4.2.1. Cross sections

Two cross sections across the Thuringian Syncline have been constructed from well data and geological maps of Thuringia (Malz, unpublished, Fig. 13). Most of the virtual wells are located on the traces of these cross sections.
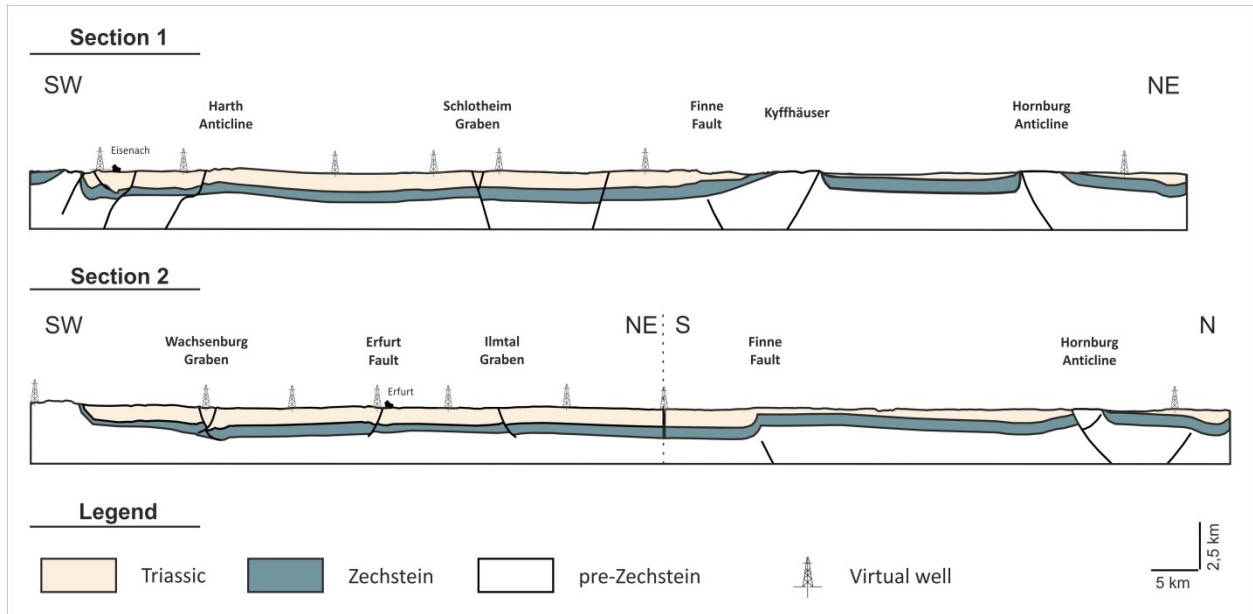
Fig. 13: Geological cross sections of the Thuringian Syncline (2x vertical exaggeration) (profiles redrawn after Malz, unpublished).

By means of the different maximum burial depths obtained from the virtual wells along the profiles it was possible to generate profiles for the geological situation near the end of the Cretaceous (Fig. 14). At this time, directly before the uplift phase, the sediments reached the deepest point in their burial history. The reconstructed thickness of the Jurassic and Cretaceous sediments varies around 2 km across the Thuringian Syncline (Fig. 14).
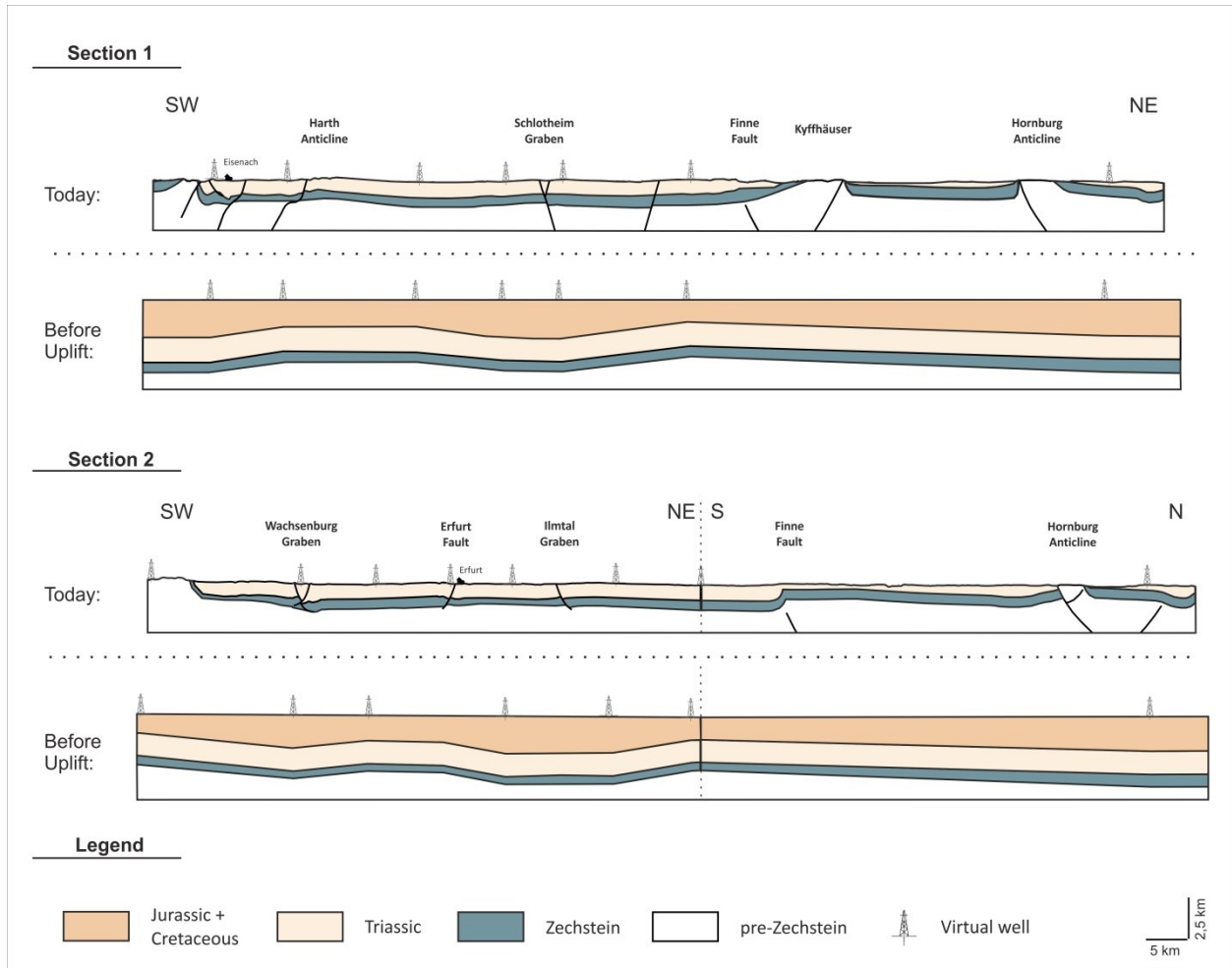
Fig. 14: Estimated original thickness of Jurassic and Cretaceous strata for cross sections 1 and 2, based on the modelled burial depths. Faults are not shown in the reconstructed versions (2x vertical exaggeration; present day cross sections after Malz, unpublished).

4.2.2. Explanation of the variations of the overburden thickness

Pronounced gradients in the reconstructed thickness of Jurassic and Cretaceous strata often correlate with present fault zones (Fig. 16). It is therefore suggested that these changes in thickness were caused by differential subsidence and tilting of fault-bounded blocks during the Jurassic and Cretaceous. An interpretation of the thickness changes of Jurassic and Cretaceous according to this hypothesis is shown in Fig. 15 and Fig. 16: Thickness variations of Jurassic and Cretaceous strata are explained by syndepositional movement of graben and halfgraben structures. The normal offsets of the faults attain values of about 700 m to about 1200 m in the area of maximum overburden.
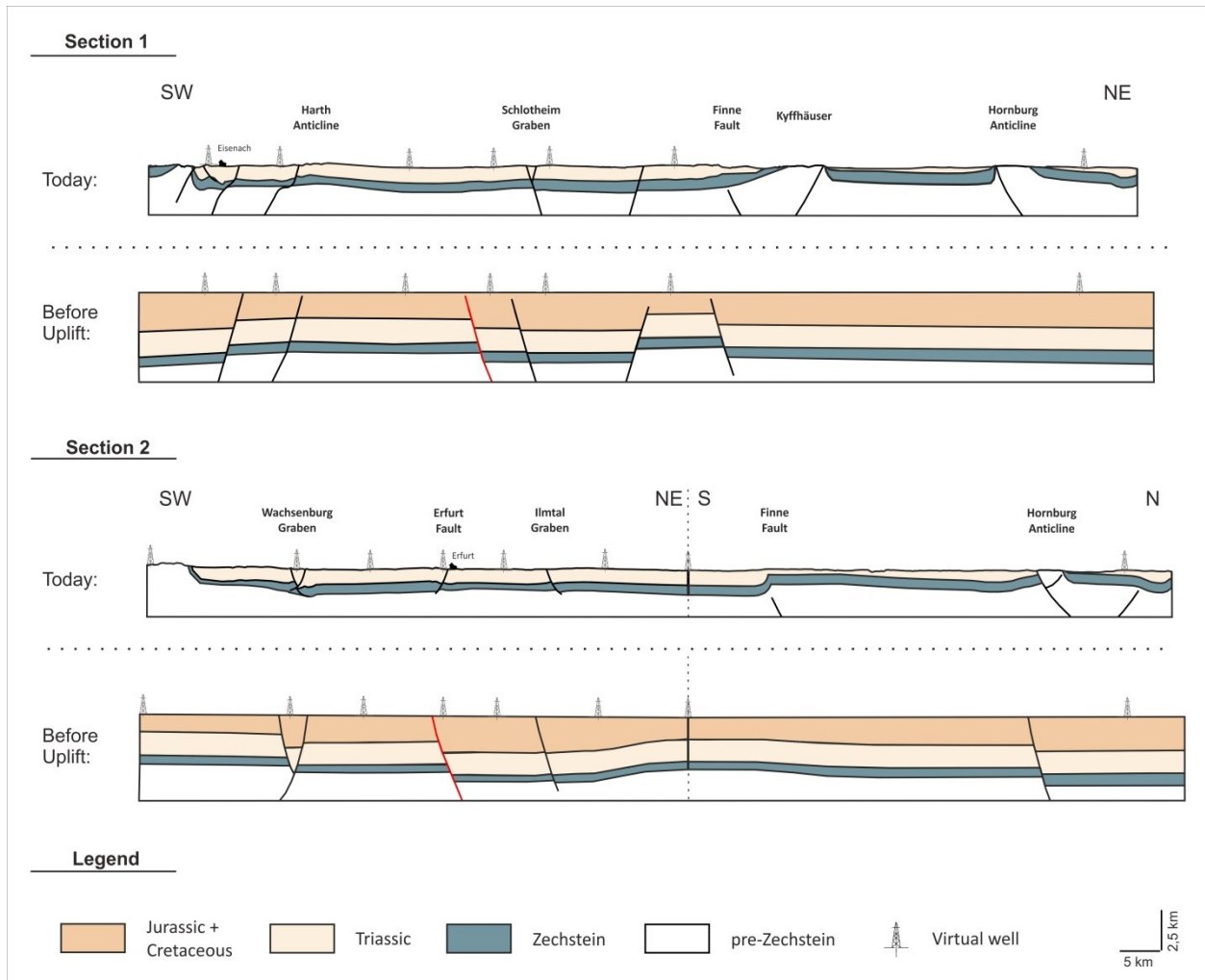
Fig. 15: Cross sections 1 and 2 in present-day and restored stages. Different from Fig. 14, the thickness variations of the reconstructed overburden are interpreted due to syndepositional normal faulting. Fault locations and dips match present-day fault zones, except the one which is marked in red (2x vertical exaggeration; present-day cross sections after Malz, unpublished).

The maps of the Thuringian Syncline in Fig. 16 show that in the centre of the syncline the thickness of Jurassic and Cretaceous strata and also the uplift of the sediments were higher than in the surrounding area.
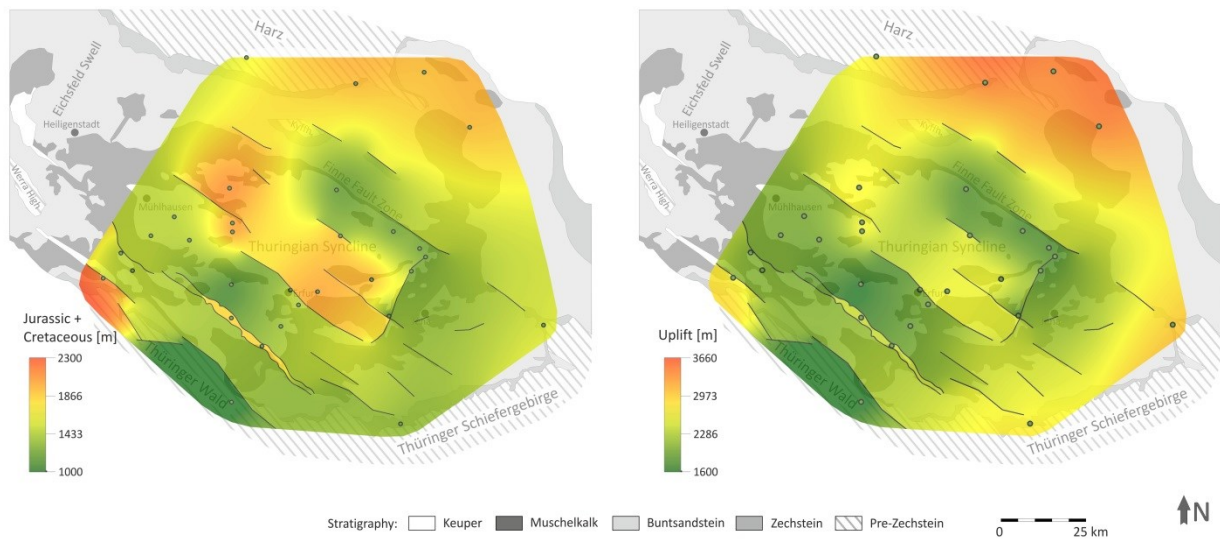
Fig. 16: Left map: spline interpolation of the thicknesses of Jurassic + Cretaceous strata. Right map: spline interpolation of the estimated magnitudes of uplift. Used values based on the calculated maximum burial depths for the models/virtual wells (spline interpolation with faults as barriers; compare with Fig. 15 for an interpolation across fault zones; maps in the background are modified after Puff 1994; faults after Franke 2014).

4.3. Discussion of the burial history model

4.3.1. Alternative heat flows

The calculation of the thickness of Jurassic and Cretaceous strata (as well as maximum burial depth and uplift) is depending, among other parameters, on the defined heat flow. The most expectable heat flow was 60 mW/m² during burial history (see chapter 4.1.1.), named as normal heat flow. Even if they are not so assumable, other heat flow scenarios are possible and described in the following text.

Lower or higher heat flow during the Mesozoic

A higher and a lower heat flow scenario were calculated for the models and virtual wells. The lower heat flow is assumed as 50 mW/m², the higher heat flow is assumed as 70 mW/m² during Mesozoic and Cenozoic time (Fig. 17).
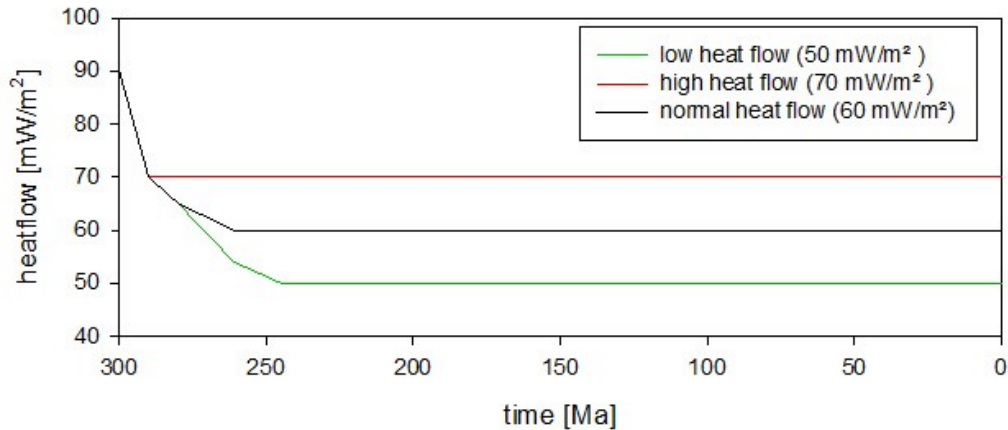
Fig. 17: Normal heat flow (60 mW/m²) and two alternative heat flow scenarios (high: 70 mW/m²; low: 50 mW/m²).

As shown in Fig. 18, the calculated thickness of Jurassic and Cretaceous sediments is different for each heat flow scenario. A heat flow increase of 10 mW/m² results in an approximately 500 m less thickness in Jurassic and Cretaceous sediments. The thickness difference between two virtual wells remains similar. Hence, also the assumed graben structures between two wells and their downthrown remain similar.

Local changes of the heat flow are also a possible reason for the vitrinite reflectance differences between two wells. As it can be seen in Fig. 18, for a constant Jurassic and Cretaceous thickness of e.g. 1500 m for all virtual wells, it would be necessary to vary the heat flow for every single virtual well. Nevertheless a change of heat flow over these short distances and without a structure element in between is unlikely.

The measured maturity of the organic matter cannot be created only by a high heat flow and without Jurassic and Cretaceous overburden. Without the overburden of Jurassic and Cretaceous strata is even a heat flow of 100 mW/m² through time not enough to generate the present vitrinite reflectance in the Thuringian Syncline centre.
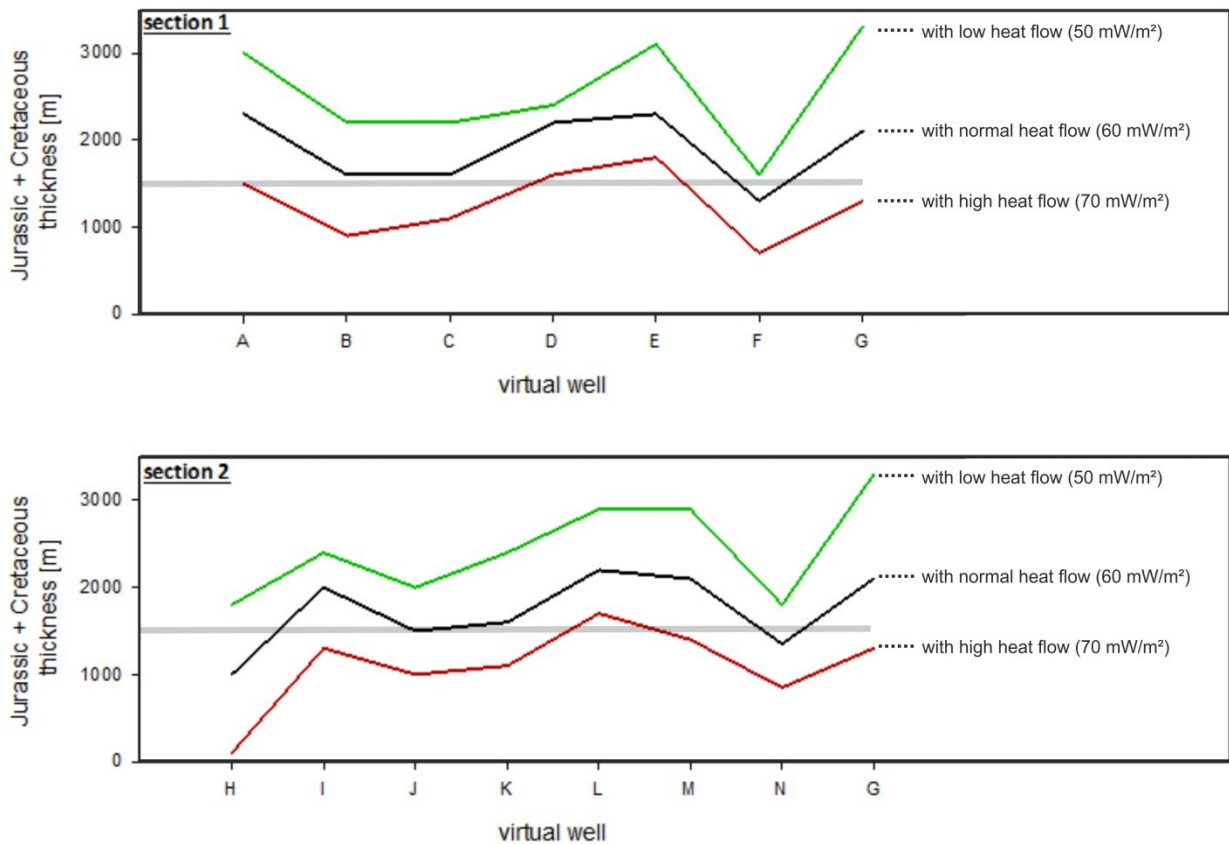
Fig. 18: Calculated thickness of Jurassic and Cretaceous sediments along the two sections with normal, high and low heat flow (60, 70 and 50 mW/m²). The different heat flow scenarios are shown in Fig. 17. The grey line marks a Jurassic and Cretaceous thickness of 1500 m.

Potential increase of the heat flow triggered by Jurassic/Cretaceous rifting

Evidence for an increased heat flow caused by active rift zones in the Thuringian Syncline is given by the assumed graben structures formed during Late Jurassic/ Early Cretaceous (Fig. 15). In rift zones, high heat flows are common. Typical non-volcanic rift margins show heat flows commonly ranging below 90 mW/m² (Allen & Allen 2005). By increasing the heat flow in the models to approximately 80 mW/m² in Jurassic and Cretaceous times (see Fig. 19), a lower maximum burial depth is required to reach the same maturity level as in the other scenario. Conclusively the thickness of Mesozoic strata is lower when Jurassic rifting associated with increased heat flow is taken into account.
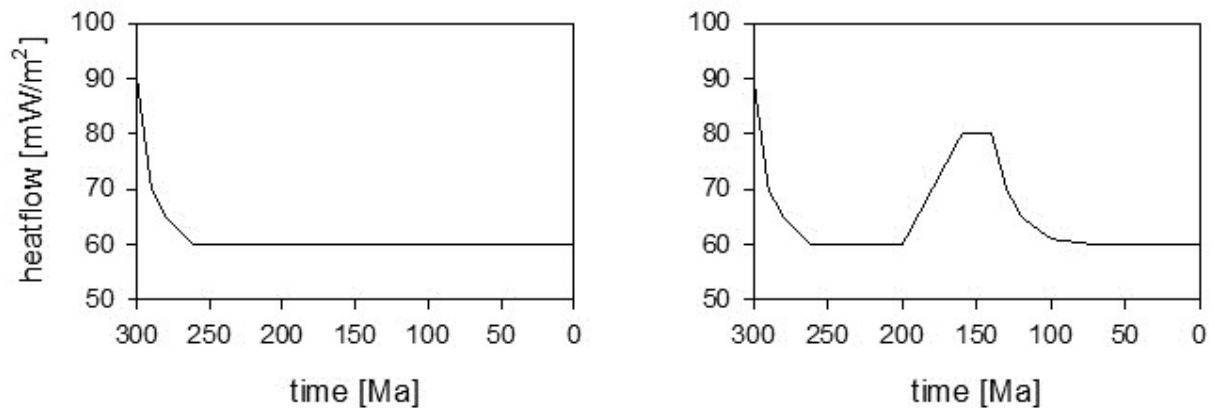
Fig. 19: Left: normal heat flow. Right: alternative heat flow scenario. The increased heat flow around 150 Ma is triggered by an assumed rifting process in Jurassic and Cretaceous times.

In the alternative scenario with heat flow anomaly, the reconstructed overburden is 200 m to 400 m thinner than in the scenario without heat flow anomaly (Fig. 20). In both scenarios the Mesozoic overburden thickness differs from one virtual well to another (Fig. 20). The absolute overburden thickness decreases with higher heat flow in Jurassic/Cretaceous times, but the relative differences of overburden between the wells remains similar, especially in the centre of the Thuringian Syncline.
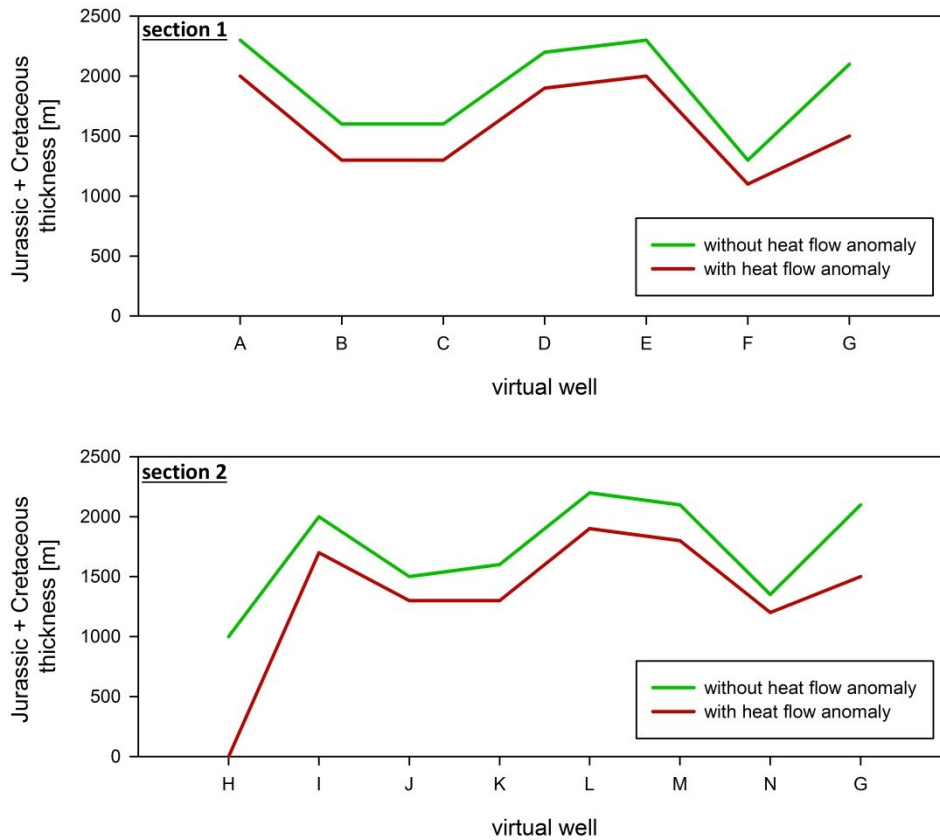
Fig. 20: Calculated thickness of Jurassic and Cretaceous sediments along the two sections with and without heat flow anomaly. The heat flow anomaly is an increase of heat flow from normally 60 mW/m² to 80 mW/m² during Jurassic/Cretaceous time as shown in Fig. 19.

4.3.2. Faults and graben structures in the 2D burial history model

The 2D burial history model suggests that present fault zones were also active during the Mesozoic. These graben structures developed in an extensional regime during the Jurassic and Cretaceous. Indicators for Jurassic and Cretaceous sedimentation in the Thuringian Syncline are Liassic sediments (up to 200 m) at the "Großer Seeberg locality" near Gotha from Jurassic and Cenomanian sediments (up to 55 m) in the area of the Ohmgebirge from Cretaceous (Kästner et al. 2003). Hence there is a contradiction between the present-day preserved thicknesses of approximal 255 m and the estimated thicknesses in the burial history models (up to 2300 m) for the Jurassic and Cretaceous sediments. One explanation could be an increased heat flow in the burial history models (see chapter 4.3.1.) and therefore a lower estimated thickness of Jurassic and

Cretaceous sediments. A more plausible solution without an increased heat flow scenario is a widespread erosion of Mesozoic sediment in the area of the Thuringian Syncline during the uplift event in the Late Cretaceous. Jurassic (Lias) marine claystones and limestones in the Thuringian Syncline (Ernst 2003) are an evidence for further sedimentation in the Jurassic. Moreover the rock sequence of the Cretaceous sediments (Ohmgebirge) begins with nearshore sandstones, then deep water clay- and marlstones and eventually marine limestones, indicating increasing water depth (Klaua 2003). A widening of the depositional area in Late Cretaceous time is therefore assumed (Klaua 2003). This trend suggests that larger volumes of sediments were deposited than those preserved today. In the Lower Saxony Basin the basin fill was also uplifted during Late Cretaceous inversion and subsequently an erosion of Cretaceous sedimentary rocks took place (Drozdzewski 2003, Senglaub et al. 2006). Another option is a sparse sedimentation and hence nearly no erosion, but the Jurassic and Cretaceous facies descriptions, the vitrinite reflectance of the sediments and the comparable situation of the Lower Saxony Basin are in conflict with this scenario.

The North German Basin provides evidence for much higher thicknesses of Jurassic (up to 2400 m) and Cretaceous (up to 6000 m) sediments (Walter 1992) than those calculated in the Thuringian Syncline. Also in the Lower Saxony Basin the thicknesses of Jurassic (3350 m) and Cretaceous (4300 m) sediments are very high (Kockel et al. 1994, Senglaub et al. 2006). Nevertheless the subsidence was lower in the marginal parts than in the centre of the basin (Fig. 21). In the marginal parts, like in the Polish Trough, the thickness of Jurassic and Cretaceous sediments is about 1000 m to 3000 m (Dadlez 2003). Accordingly, it is assumed that the thickness of Jurassic and Cretaceous sediments in the Thuringian Syncline is more similarly to the Polish Trough and not as high as in the North German Basin or the Lower Saxony Basin. Therefore a Jurassic and Cretaceous thickness about 2000 m in the Thuringian Syncline is plausible.
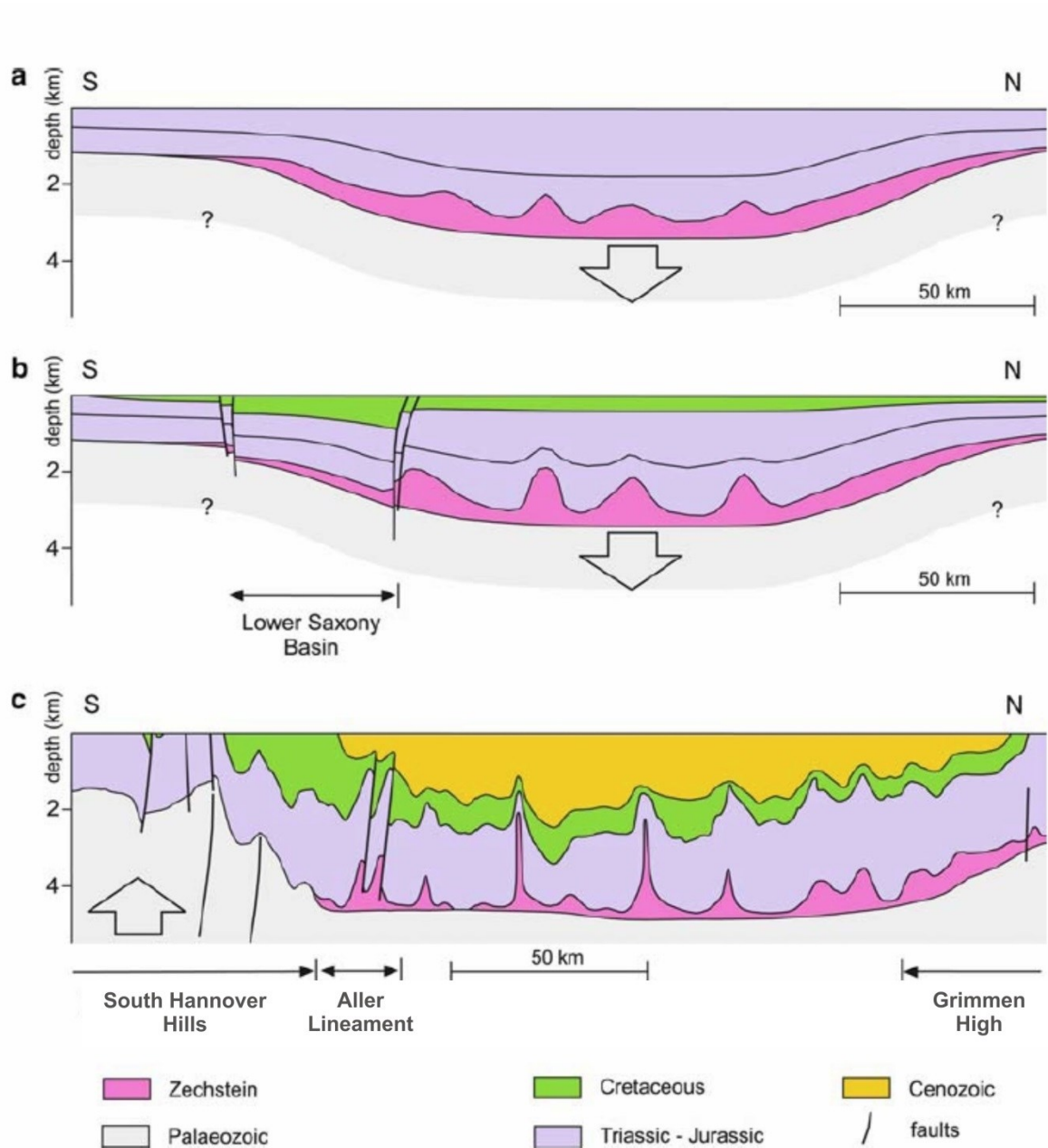
Fig. 21: In the tectonic evolution of the North German Basin after Mazur et al. (2005), the subsidence of the southern parts was not as high as in the centre of the basin during Triassic-Jurassic (a); high subsidence is visible in the area of the Lower Saxony Basin in the Early Cretaceous (b); an uplift event took place in the Late Cretaceous-Paleocene (c).

The area of increased Jurassic and Cretaceous thickness in the middle of the Thuringian Syncline (see map in Fig. 16) can be interpreted as a synsedimentary paleo-graben in the axis of the sedimentation area (Fig. 22). Today this paleo-graben is not evident on geological maps because of the inversion of the main faults in Thuringian Syncline in

the Late Cretaceous and the accompanying erosion of the basin fill. The majority of faults in the Thuringian Syncline have present-day offsets of less than 200 m. The higher offsets of the Mesozoic inferred here are not observable anymore.
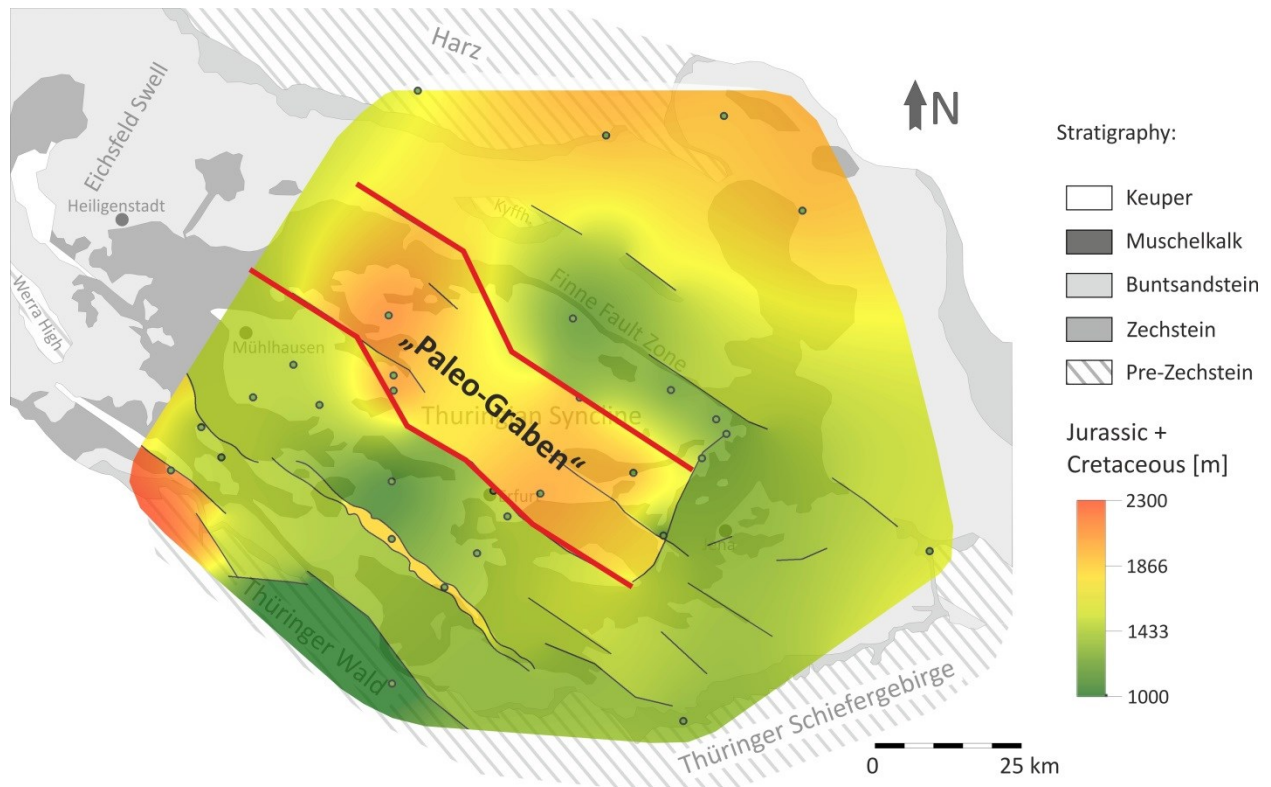
Fig. 22: The high reconstructed thicknesses of Jurassic and Cretaceous sediments in the centre of the Thuringian Syncline are interpreted here to reveal a Mesozoic "Paleo-Graben" (map in the background is modified after Puff 1994; black faults after Franke 2014).

4.4. Thermal evolution and compaction of the sediments

According to the best fit model the Zechstein sediments reached burial depths of 3900 m and maximum temperatures of 140°C in the centre of the Thuringian Syncline in Campanian (Late Cretaceous) time, where the overburden of Jurassic and Cretaceous sediments was maximum (see in Fig. 22 the paleo-graben with the highest thickness of Jurassic and Cretaceous sediment). In the area around this paleo-graben structure the

maximum depth was 3200 m and the maximum temperature was 120°C. Hence, the organic matter of the Zechstein Formation was in the range of the gas window. Gas extraction from the Buntsandstein sandstones in the western part of the Thuringian Syncline (Kästner 2003) corroborates these estimated depths and temperatures. The sandstones of the Calvörde Formation reached maximum burial depths of 3650 m and maximum temperatures of 140 °C in the area of deepest burial. Outside of the paleo-graben structure the maximum depth was 2950 m and maximum temperature was 120 °C. Therefore, it is suggested that the Middle Buntsandstein was in temperature conditions of > 100 °C during deepest burial (red and green line in Fig. 23).
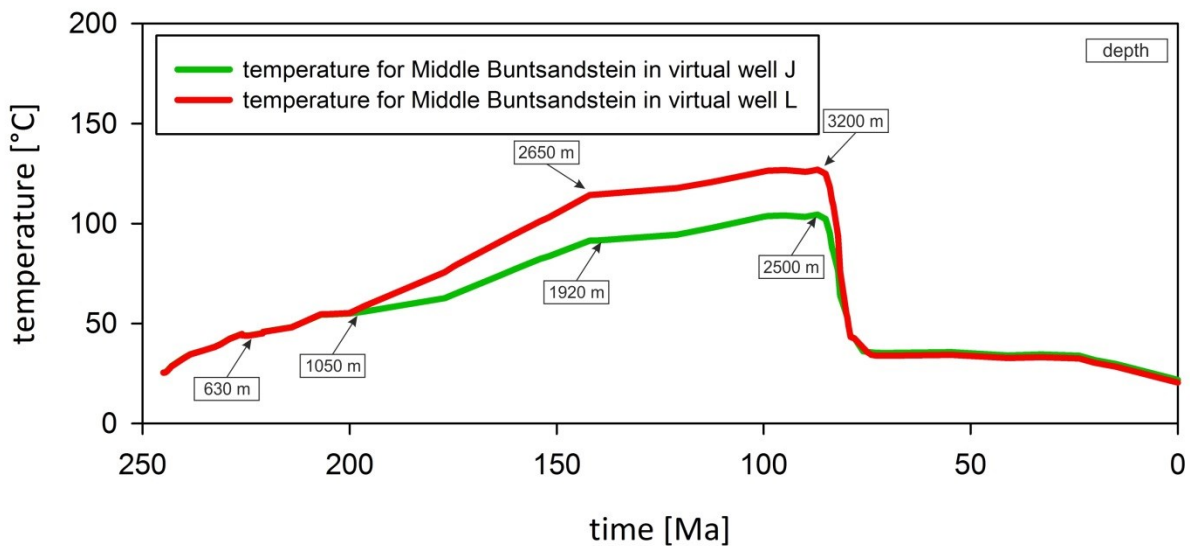
Fig. 23: Thermal evolution of the Middle Buntsandstein (Hardegsen Formation) through time. Well L is located in the centre of the syncline (red) and well J at the margin of the syncline (green).

Compaction of the Buntsandstein took place during burial and is increasing with depth. Many factors are influencing the degree of compaction; hence a prediction of the porosity only on the basis of the reached maximum depth provides a range of estimated porosity: based on the porosity-depth curve from Allen & Allen (2005) and Giles (1997), the porosity for the Middle Buntsandstein sandstone (Hardegsen Formation) at 3.2 km depth is between 7 % and 22 % (Fig. 24). The porosity reduction curve after Ehrenberg et al. (2009) shows for 592 samples from Triassic sandstones worldwide a median porosity of approximately 13 % at 3.2 km depth (Fig. 24). An exact prediction of the porosity is not possible, because many factors influence the pore space evolution in

sandstone. Nevertheless a total porosity loss up to 33 % can be assumed, because of the burial depth of the sandstones (initial porosity of 40 %, cf. Ehrenberg 1989 and Houseknecht 1989). The factors for porosity and permeability evolution in the Buntsandstein sandstones are described in detail in chapters 5.3 and 5.4.
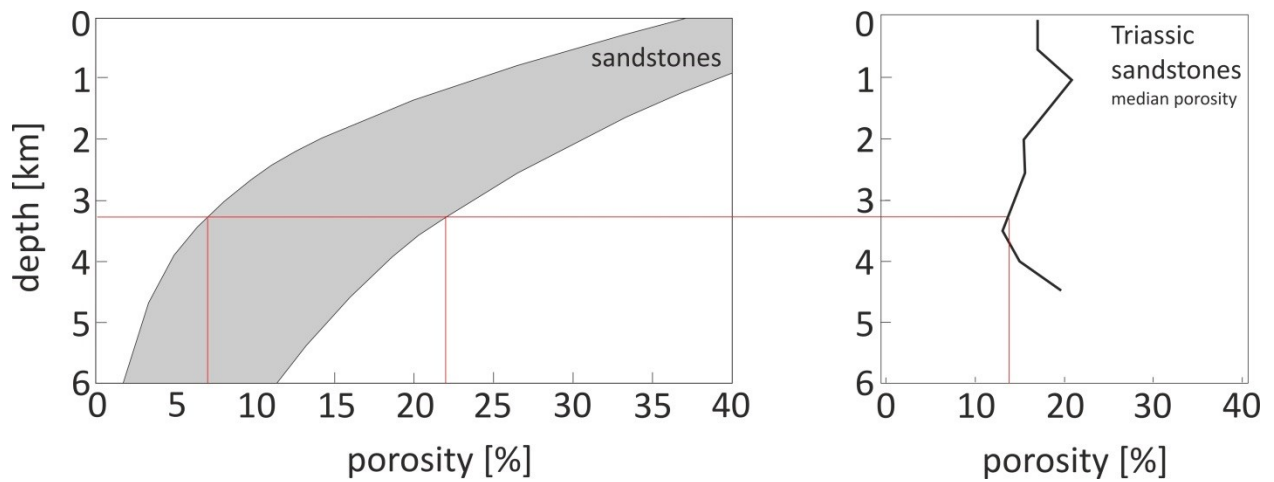
Fig. 24: Porosity reduction due to the burial. Left: sandstones from 3.2 km depth show porosities between 7 % and 22 % (diagram is modified after Giles 1997 and Allen & Allen 2005); right: diagram of median porosity of Triassic clastic reservoirs shows a porosity of 13 % at 3.2 km depth (diagram is modified after Ehrenberg et al. 2009).

5. Sedimentology, petrography, petrophysics and diagenesis of the Buntsandstein sandstones

Commonly the sedimentary facies is influencing the diagenesis (Füchtbauer 1979, Giles 1997); diagenetic processes are controlling reservoir properties, like porosity and permeability (Morad et al. 2010). So a correlation of depositional environment and reservoir properties can be assumed. Differences in facies and diagenetic evolution of Buntsandstein sandstones in the Thuringian Syncline result in remarkable differences in texture, mineral composition, cementation, compaction, porosity and permeability. Therefore facies analysis, petrological and mineralogical investigations, and petrophysical measurements were performed.

5.1. Depositional environment (facies types)
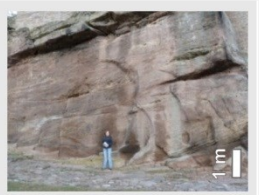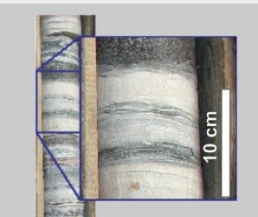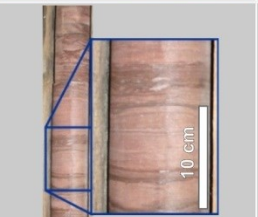
Fig. 25: Outcrop and core photos of the four distinguished depositional environments. Outcrop photos made by Kunkel (in prep.). Lacustrine outcrop: quarry Ferna; sandflat outcrop: Vollenborn; fluvial outcrop: Hanstein; eolian outcrop: Sondershausen; lacustrine, sandflat and eolian core: Rks2; fluvial core: Ballst-1.

Four general depositional environments (see Fig. 25 and Table 5) could be determined by a macroscopic study of outcrops and cores in the Thuringian Syncline: (i) lacustrine units, (ii) fluvial and mixed (iii) sandflat deposits and (iv) eolian sand sheet to dune facies. The facies classification and interpretation for the Buntsandstein samples were

made by Kunkel (in prep.). Differentiation of facies was achieved through a detailed analysis of primary depositional features including macroscopic texture, bedding, and sedimentary structures, as well as biogenic and chemical overprints such as bioturbation and pedogenic features (Kunkel et al. 2012, 2013; Kunkel in prep.).

Table 5: Influence of facies types on sandstone-characteristics for investigated Buntsandstein sandstones in the Thuringian Syncline (content of cement and clay by point counting; porosity and permeability by plug measurement; ratio of sandstone to mudstone estimated by Kunkel (in prep.)).

	lacustrine (24 samples)	sandflat (83 samples)	fluvial (16 samples)	eolian (23 samples)
deposits	heterolith	sand/mud sheet	channel	desert sand
main formation	suC, suB	smV, smD, smH	smS, smH	smV, smD, smH
ratio of sandstone to mudstone	high (1:1)	moderate (2:1)	low (10:1)	very low (50:1)
sandstone thickness	centimetres	decimetres	metres	centimetres to decimetres
mean grain size	0.15 mm	0.22 mm	0.23 mm	0.44 mm
mean carbonate cement content	6.1 %	2.1 %	4.8 %	2.7 %
mean sulphate cement content	0.9 %	2.7 %	5.0 %	6.7 %
mean blocky cement content	11.7 %	9.5 %	14.5 %	13.6 %
mean clay content (cutans and detrital matrix)	2.5 %	7.9 %	2.0 %	3.1 %
special features	fine grained	various characteristics	less clay	coarser grained
mean porosity	11.5 %	13.0 %	11.9 %	13.4 %
mean permeability	4.1 mD	27.2 mD	57.8 mD	108.7 mD

5.2. Composition and textural properties

Analysis of sandstone thin sections revealed differences in texture and composition between the facies types (Fig. 26). The composition of the sandstones is consisting of two parts: the detrital and the authigenic components. Detrital components are depending on the provenance and depositional environment, while authigenic minerals are controlled by diagenetic processes.
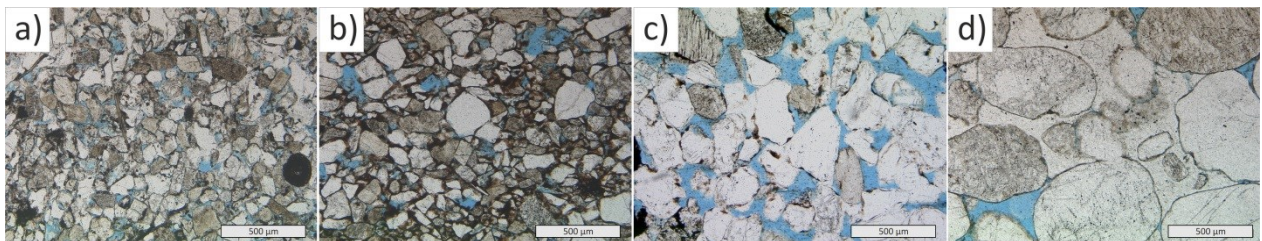
Fig. 26: Thin section images in normal light of: a) lacustrine sandstone (sample Rks2-18, Bernburg Formation), b) sandflat sandstone (sample Rks2-10, Volpriehausen Formation), c) fluvial sandstone (sample Rks2-32, Solling Formation) and d) eolian sandstone (Rks2-14, Volpriehausen Formation).

5.2.1. Texture

The grains of the lacustrine sandstone are the smallest of the four identified facies with a mean grain size of 0.15 mm. These lacustrine sandstones are well sorted and the grains are subangular to subrounded (Fig. 27). The sandflat and fluvial sandstones are mostly moderately well to well sorted. The grains are coarser than those of the lacustrine sandstones (0.22 mm and 0.23 mm mean grain size) and mainly subrounded (Fig. 27). The sandstones of the eolian facies have the coarsest grain size with a mean of 0.44 mm. The grains are rounded and they are moderately well sorted (Fig. 27). The frequent bimodal grain size distribution in the eolian sandstones affects the sorting negatively.

Hence, the lacustrine sandstones have the finest grain size and the eolian sandstones are the coarsest ones. The grain size correlates positively with the degree of rounding and negatively with the sorting.
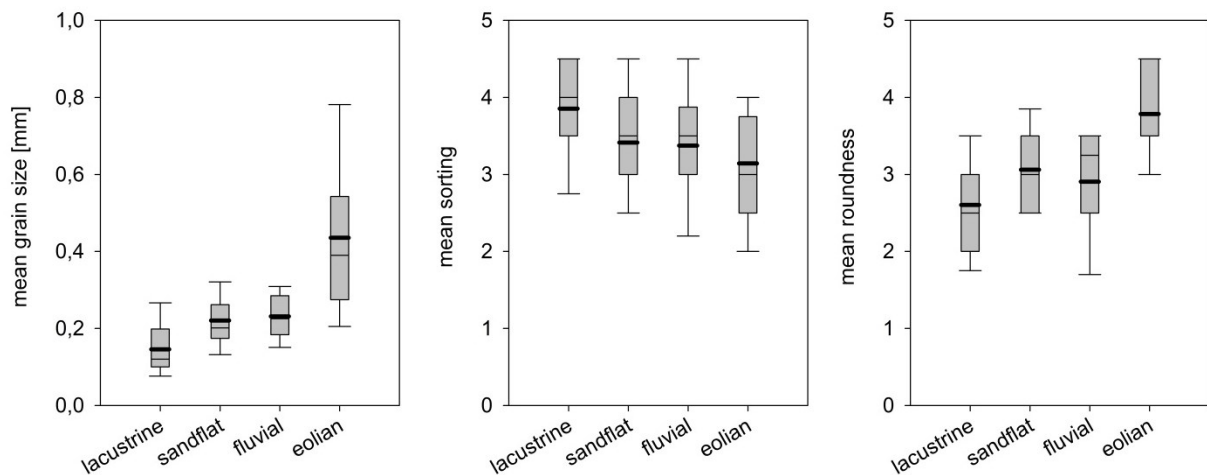
Fig. 27: Grain size, sorting (1 – poorly, 2 – moderately, 3 – moderately well, 4 – well, 5 – very well) and roundness (1 – angular, 2 – subangular, 3 – subrounded, 4 - rounded, 5 – well rounded) of particular Buntsandstein sandstones facies. The error bars indicate the 90th and 10th percentiles, thick black lines are the mean values.

5.2.2. Detrital components

Most of the sandstones can be classified as subarkose (in particular the fluvial facies) and arkose (in particular the lacustrine facies); lithic subarkose and quartzarenite also occur in the fluvial and in the eolian facies (classification according to McBride 1963) (Fig. 28). The most abundant detrital component is quartz grains (52 % on average in all sandstones), followed by feldspar grains, ooids (if they are present), clay, mica, lithic fragments and heavy minerals (see appendix 10.I.3. for thin section images). Below their abundance in the different facies is described (sorted by abundance).

1) The eolian sandstones have the highest mean quartz content with 61 %, whereas the lacustrine sandstones have the lowest with 46 %.

2) The highest amounts of feldspar, 24 %, occur in the fine-grained lacustrine sandstones and the lowest amounts of 11 %, in the coarse-grained eolian sandstones. Hence feldspar content correlates negatively with grain size. Commonly the feldspar grains are corroded, particularly in the lacustrine and fluvial facies, or they are partly albitized. Plagioclase occurs only with < 1 %.

3) Dolomitic ooids are present with up to 26 % in some lacustrine sandstones of the Lower Buntsandstein (Fig. 34a). Chemical composition of the ooids is similar to

their surrounding dolomite cements (Fig. 34b, Fig. 34c). The only differences are integrated small Al-rich fragments, probably caused by clay minerals, and a Si-rich quartz core in the centre of the ooid (Fig. 34c).

4) The mean detrital clay content in the sandflat sandstones is with 8 % the highest and 5 % - 6 % higher than in the other facies types. The fluvial sandstones have the lowest clay content with 2 %.

5) Mica is observable with 3 % in the lacustrine sandstones and 1 % in the sandflat and fluvial sandstones; it is absent in the eolian sandstones.

6) Rock fragments are rare (1 %). They are of felsic volcanic, felsic plutonic and sedimentary origin.

7) The heavy minerals zircon and monazite are present in traces only (< 1 %).
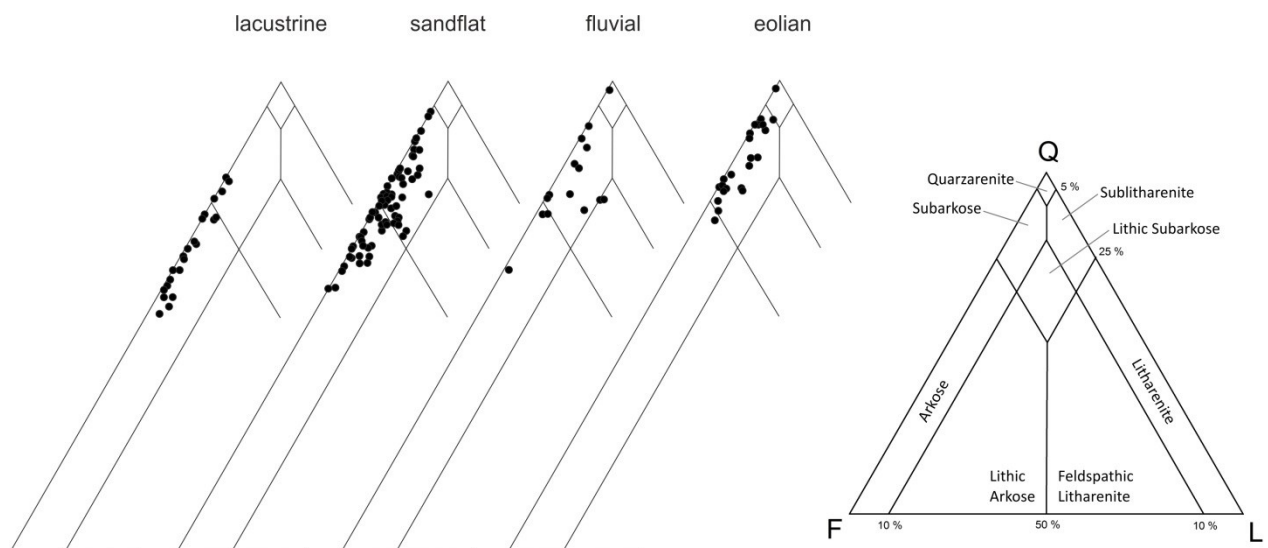
Fig. 28: Detrital composition of the Buntsandstein sandstones distinguished by their facies (diagram after McBride 1963; Q – Quartz, F – Feldspar, L – Lithic fragments).

5.2.3. Authigenic components

The most abundant authigenic minerals (Fig. 29) are carbonate cements, followed by sulphate cements, then cements of quartz, hematite, illite, kaolinite, feldspar, titanium oxide and salt (see appendix 10.I.3. for thin section images).

48
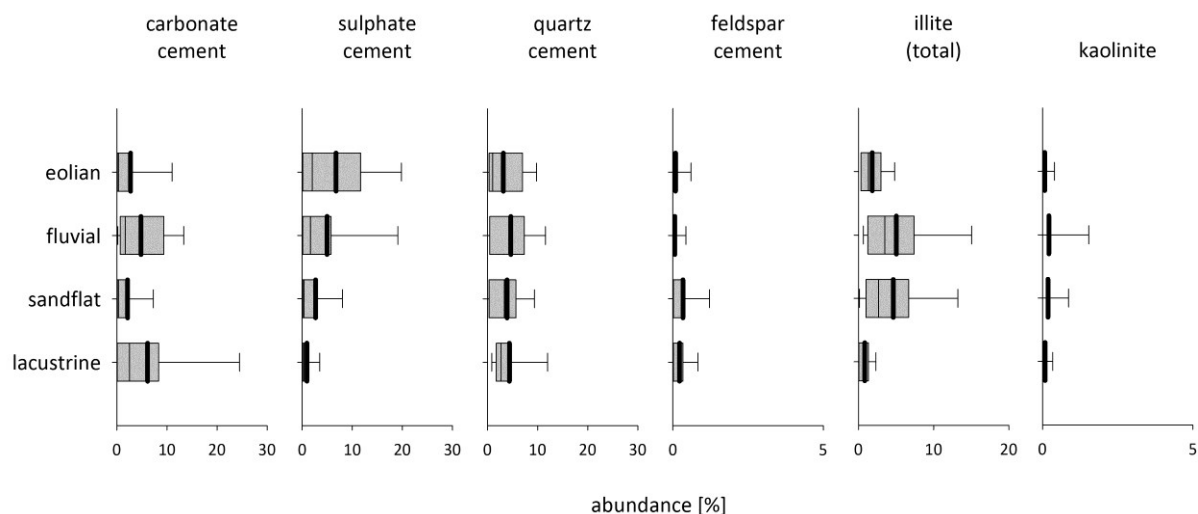
Fig. 29: Abundance of authigenic minerals in the sandstones of different facies type. The error bars indicate the 90th and 10th percentiles, thick black lines are the mean values.

The abundance in the different facies is described (sorted by abundance) as follows:

1) Hypidiomorphic heterogenic carbonate cement is the most common cement. Idiomorphic rhombohedral crystals are only sporadically present. The carbonate cement occurs as nodules that surrounds several detrital grains (nodule size: 1 – 2 mm) and as heterogenic patches. No clay cutans are present on grains surrounded by carbonate nodules. Carbonate cement occurs in all facies types (on average 6 % in the lacustrine sandstone; 2 % in the sandflat sandstone; 5 % in the fluvial sandstones and 3 % in the eolian sandstones). The MgO content of the carbonate is between 15 and 20 %, which is typical of dolomite. Also calcite and dolomite rich in iron (and rarely ankerite) were found. At least four generations of carbonate growth were distinguished (Fig. 30). The oldest generation occurs heterogenically as hypidiomorphic dolomite crystals between detrital grains. This generation contains 0.1 wt% FeO and is rich in MgO with 20 wt%. It is slightly corroded and exhibits micro porosity. The FeO content increases with time (second and third generation, Fig. 30), whereas the MgO content decreases. The youngest generation contains more FeO (7.1 wt%) and less MgO (15.7 wt%) than the older ones (Fig. 30). The corrosion of the three youngest generations is less intensive than for the first generation. Occasionally carbonate cements occur as replacements of detrital feldspar and quartz grains.
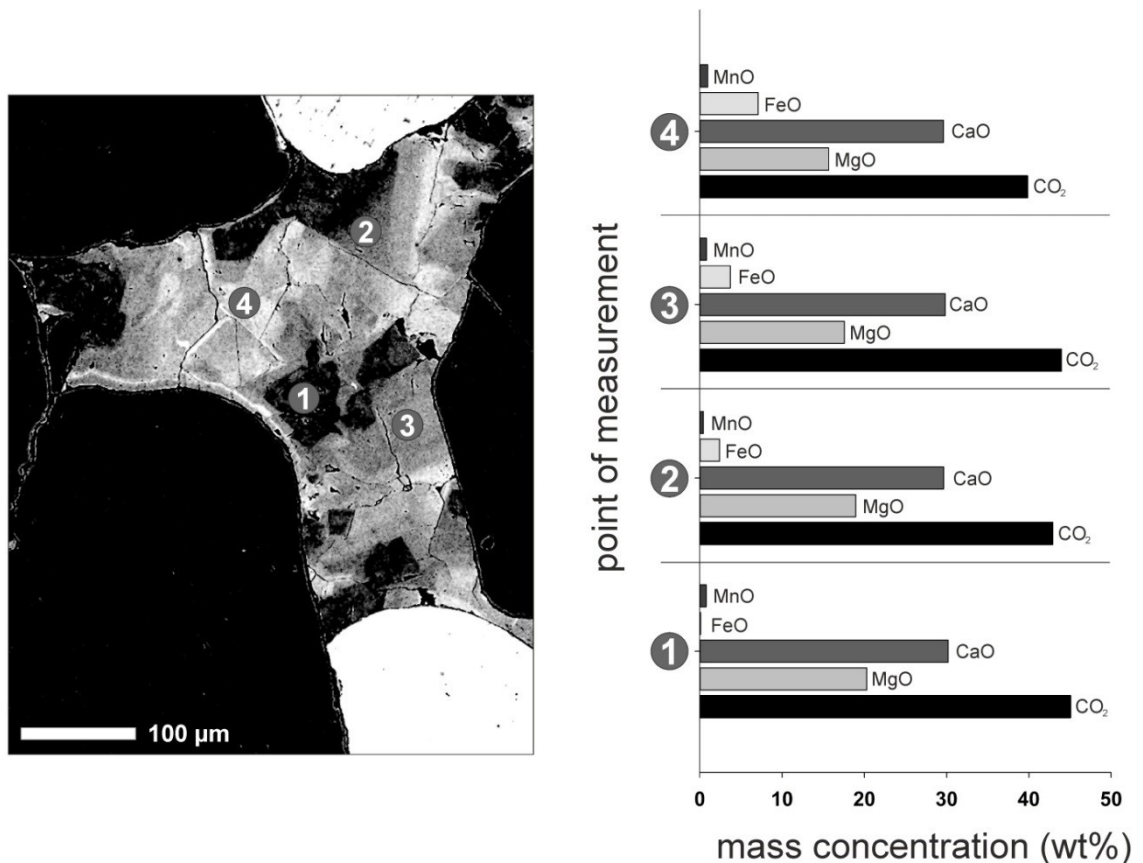
Fig. 30: Backscattered electron image and chemical composition (measured by wavelength-dispersive X-ray spectroscopy) of the four cement generations of carbonate cement (Sample Ag-14, Volpriehausen Formation, sandflat facies). 1: oldest generation; 4: youngest generation.

2) The second most frequent pore-filling cement is sulphate cement. The mean sulphate cement contents are 1 % in the lacustrine sandstones, 3 % in the sandflat sandstones, 5 % in the fluvial sandstones and 7 % in the eolian sandstones. The dominant part of the sulphate cement is gypsum and anhydrite. Barite was observed sparsely. The texture of gypsum is mainly poikilitic. Small anhydrite crystals (ca. 250 µm) completely surrounded by gypsum are present (Fig. 32e, Fig. 32f).

3) Homoaxial quartz cement overgrowths on quartz grain surfaces are very common (Fig. 32a, Fig. 32c, Fig. 32d). The mean quartz cement contents are 4 % in the lacustrine sandstones, 4 % in the sandflat sandstones, 5 % in the fluvial sandstones and 3 % in the eolian sandstones. In sandstones with large amounts of clay matrix and rims (> 10 %) the development of quartz cement is minor.

Sandstones with quartz cements exceeding 10 % were only observed in sandstones that did not contain significant amounts of detrital clay.

4) Iron oxide rims (e.g. hematite) and clay cutans occur as coatings around the grains. The coatings vary in thickness from 1 - 10 μm.

5) The mean total illite contents are 1 % in the lacustrine sandstones, 5 % in the sandflat and fluvial sandstones and 2 % in the eolian sandstones. Illite occurs dominantly as tangential cutans, but also as overgrowths (Fig. 32b) and meshworks (Fig. 33e). Their abundance is shown in Fig. 31. Sometimes both forms appear in close proximity to each other. Some of the overgrowths are only recognizable by electron microscopy, owing to their small size of 1 μm in thickness. Additionally, illite occurs as precipitates in secondary pores within feldspars, feldspar bearing lithoclasts and in relationship with micas.
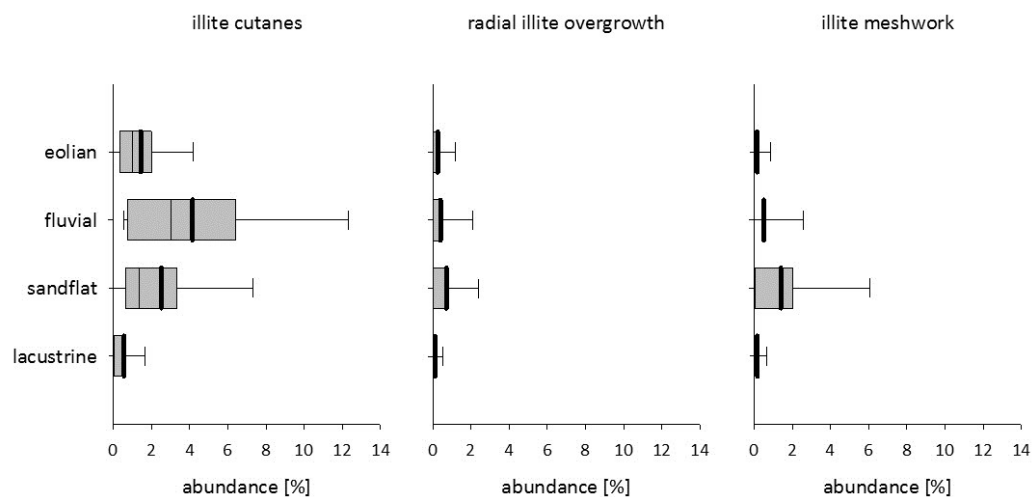
Fig. 31: Illite distribution in the sandstones of different facies type. The error bars indicate the 90th and 10th percentiles, thick black lines are the mean values.

6) Kaolinite is less common than authigenic illite. When present it occurs to < 3 %. The crystals have a vermicular shape (Fig. 33c, Fig. 33d). They occur in pore throats and in relics of completely corroded/dissolved feldspars. Furthermore, the precipitation of kaolinite takes place in between and close to altered micas (Fig. 33c).

7) Also authigenic titanium oxide is rare with < 1 % (Fig. 33d), occurring within corroded feldspar grains or lithoclasts.

8) Sporadic homoaxial feldspar overgrowths occur. In general, the feldspar grains and their surrounding cements are corroded and have etch-pits along cleavage planes (Fig. 32a). The feldspar grains are partly albitized.

9) Authigenic halite is seldom preserved in the analysed sandstones, but it can be assumed to have been present because this cement is thought to have prevented compaction in some eolian desert sands (Glennie 1970, Gaupp & Okkerman 2011).
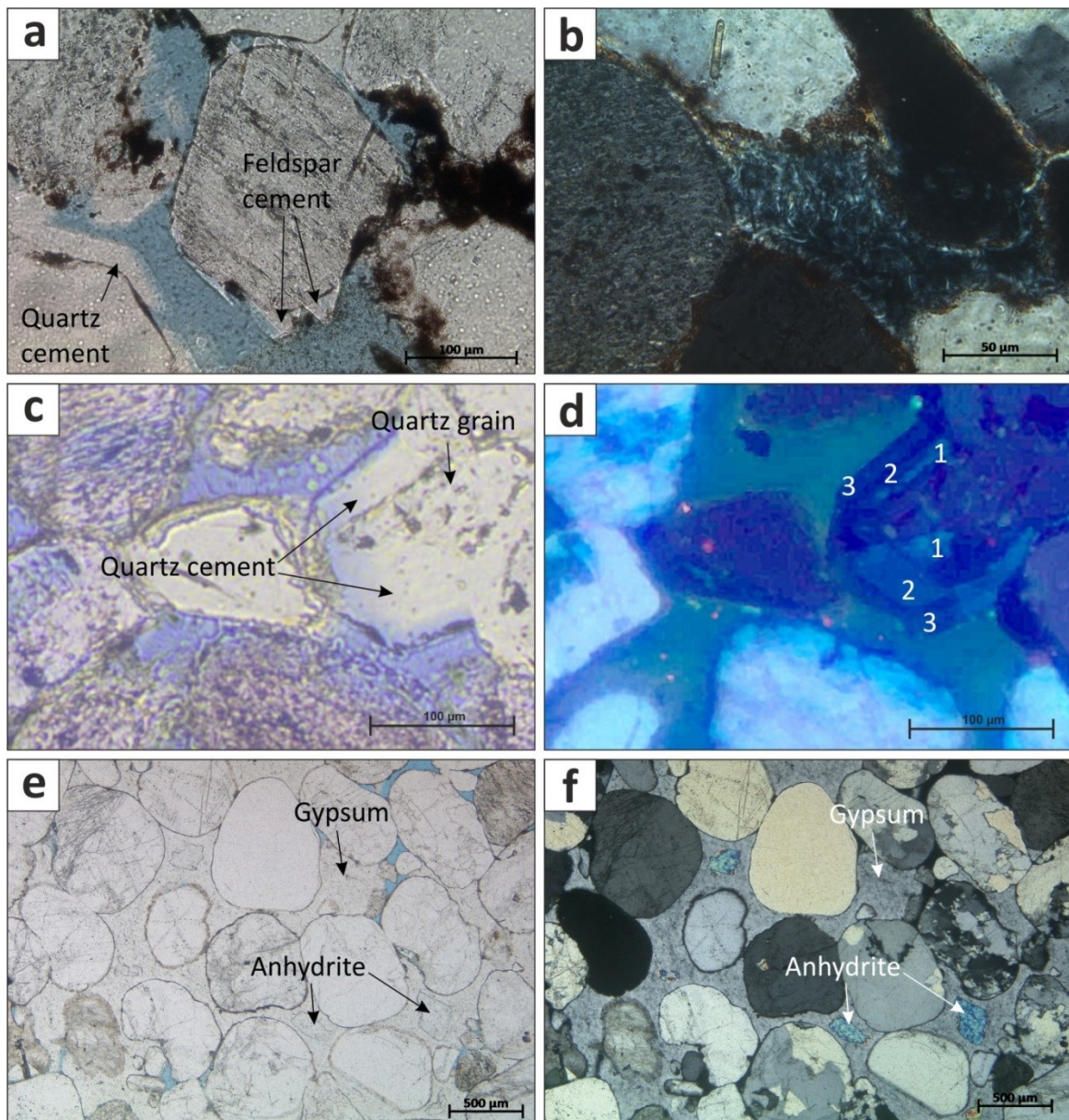
Fig. 32: Thin section images of Buntsandstein sandstones: a) feldspar and quartz overgrowth (sample Fh13-57, Detfurth Formation, eolian facies); b) illite cutans and overgrowths on the grains and rudimentary meshwork between the grains (sample Fh13-8, Hardegsen Formation, sandflat facies); c) and d) three quartz cement generations in normal light and in a cathodoluminescence-image (sample La35-15, Solling Formation, fluvial facies); e) and f) remnants of anhydrite surrounded by poikilitic gypsum in an eolian sandstone in normal light and in crossed nicols (sample Rks2-14, Volpriehausen Formation, eolian facies).
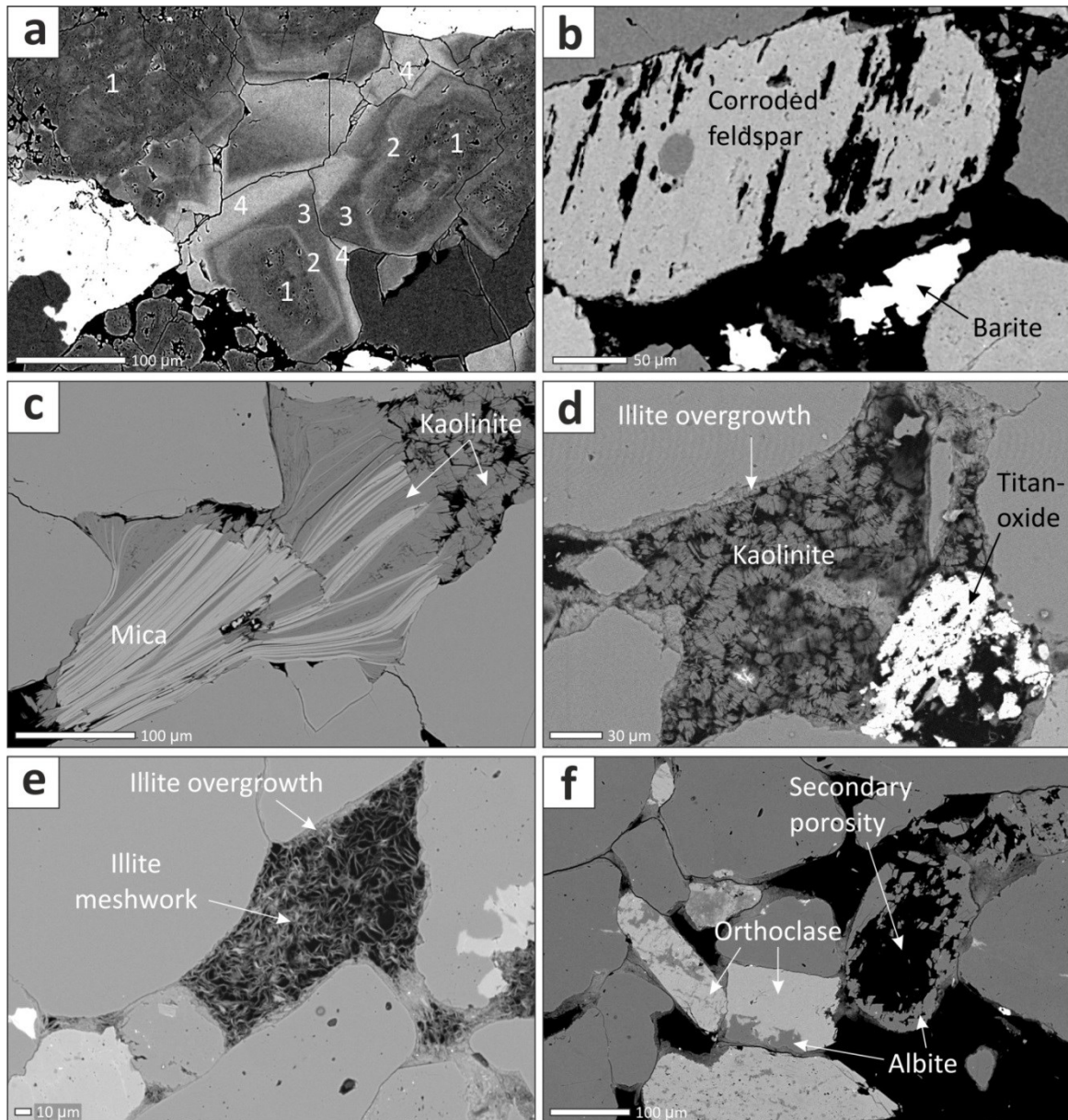
Fig. 33: Backscattered electron images of Buntsandstein sandstone: a) four generations of dolomite cement (sample Ballst-11, Bernburg Formation, lacustrine facies); b) barite and corroded K-feldspar (sample La35-15, Hardegsen Formation, sandflat facies); c) muscovite and its alteration product kaolinite in a sandstone sample taken from an outcrop (sample Br-2, Solling Formation, fluvial facies); d) illite, kaolinite and titanium oxide (sample Gü1-26, Hardegsen Formation, sandflat facies); e) illite overgrowth on grain surfaces and meshwork between grains (sample Ag-14, Volpriehausen Formation, sandflat facies); f) albitized K-feldspar (sample Ag-3, Volpriehausen Formation, sandflat facies).
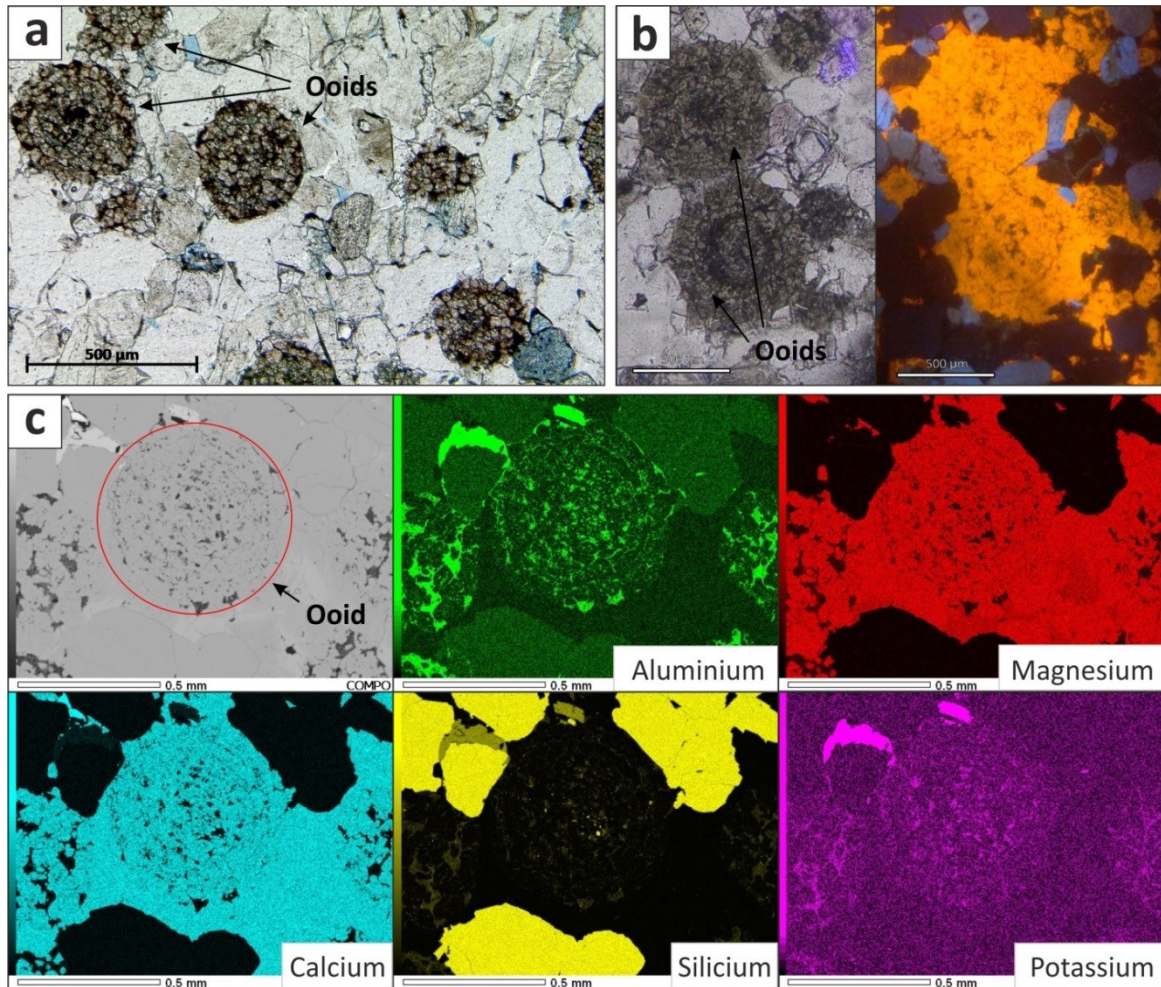
Fig. 34: Analysis of ooids (sample Ballst-11, Bernburg Formation, lacustrine facies): a) optical microscope image of ooids; b) ooids imaged by optical microscope (left) and cathodoluminescence (right), which reveals orange colours caused by trace elements like Mn^{2+} and Pb^{2+}; c) backscattered electron image of ooid and the corresponding element mapping. A complete dolomitisation is observeable on the distribution of magnesium. Moreover, a silica core in the centre of the ooid is detected in the distribution of silicium.

5.3. Factors for petrophysical properties

For better understanding the influence on petrophysical properties the most important sandstone factors on porosity and permeability are described below. The effect of sorting on porosity and permeability is only minor and not described here.

5.3.1. Grain size

The grain size affects the permeability stronger than the porosity (Fig. 35 I), especially in the lacustrine and sandflat facies. In these facies the coarse grained sandstones have higher permeability than in fine grained sandstones (Fig. 35 Ia and Fig. 35 Ib). In the eolian facies the fine grained sandstones have the highest porosities and permeabilities (Fig. 35 Id).

Because the amount of blocky cement is correlated with the porosity and permeability, it is important to mention here that with increasing grain size the amount of blocky cement is increasing: The fine-grained sandstones have medium amounts of blocky cement with an average of 7 %; Moderately- to coarsely-grained sandstones are well cemented with an average of 13 % cement.

5.3.2. Amount of cement

In all facies types the porosity and permeability decreases with increasing cement content (Fig. 35 II). In sandstones with relatively low porosity (< 8 %) the mean cement content is high (23 %). Lacustrine sandstones with ooids have large amounts of dolomitic cement (up to 30 %) and their mean permeability is 1.5 mD (Fig. 35 IIa). In the other facies types the high blocky cement content is a result of quartz, carbonate and sulphate cements. In the coarse grained eolian sandstones the amount of blocky cement is high due to sulphate cements, but these sandstones also have a high permeability. However, the most permeable of the eolian sandstones with > 100 mD have a cement content < 20 % (Fig. 35 d).

5.3.3. Amount of detrital clay

Relative high clay content (>10 %) only occurs in porous sandstones (porosity > 8 %; Fig. 35: III). The mean clay content is relatively low (2 %) in sandstones with a porosity < 8 %. In the lacustrine, fluvial and eolian facies types the effect of clay is minor. In the sandflat sandstones the clay content is enhanced in the moderately porous and permeable sandstones. In relatively highly permeable sandstones (> 110 mD) the abundance of clay is relatively low with a mean value of 1 %.
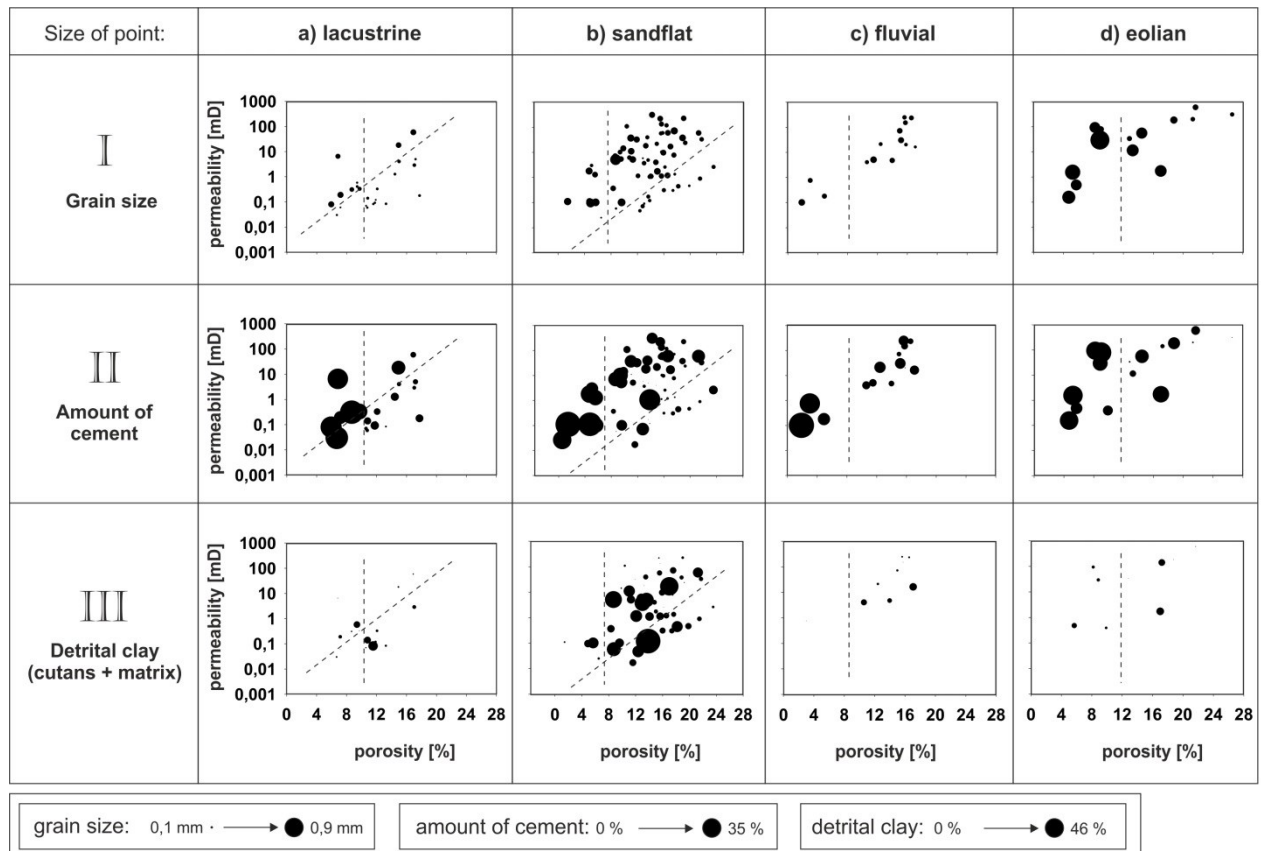
Fig. 35: Porosity and permeability of the analysed Buntsandstein sandstone samples distinguished by their facies type, relative grain size and amount of detrital clay and cement. The dashed lines separate sandstone groups with different grain size.

5.3.4. Porosity loss

It can be assumed, that the initial porosity of the sandstones was about 40 % after deposition (cf. Ehrenberg 1989 and Houseknecht 1989). A theoretical loss of porosity during burial is shown in Fig. 24. In Table 5 the mean porosity of the Buntsandstein sandstones in the present day is listed (measured on plugs). The porosity, cements and intergranular volume measured with point-counting are shown in Fig. 36. A relatively high mean cement content of ca. 14 % and a high mean intergranular volume of ca. 21 % were measured for the sandstones of the fluvial and eolian facies (Fig. 36, cement and intergranular volume). Using the formula of Lundegard (1992), the mean cementational porosity loss in the fluvial and eolian facies is 12 % and 11 %, which is higher than in the sandflat and lacustrine facies with 8 % and 9 %, respectively (porosity loss by cementation, Fig. 36); for all sandstones the mean porosity loss by compaction is much

higher with average 26 % (porosity loss by compaction, Fig. 36). The mean porosity loss by compaction is in the lacustrine sandstones 26 %, in the sandflat sandstones 27 % and in the fluvial and eolian sandstones 23 %. In 88 % of the samples the dominant porosity loss was caused by mechanical compaction. In the lacustrine and the sandflat facies the mean intergranular volume of 18 % and 16 % is ca. 3 % to 5 % lower than in the fluvial or eolian facies (Fig. 36). The porosity loss by compaction is also shown in the appendix chapter 10. I.6. (porosity loss according to Houseknecht 1987 and Ehrenberg 1989).
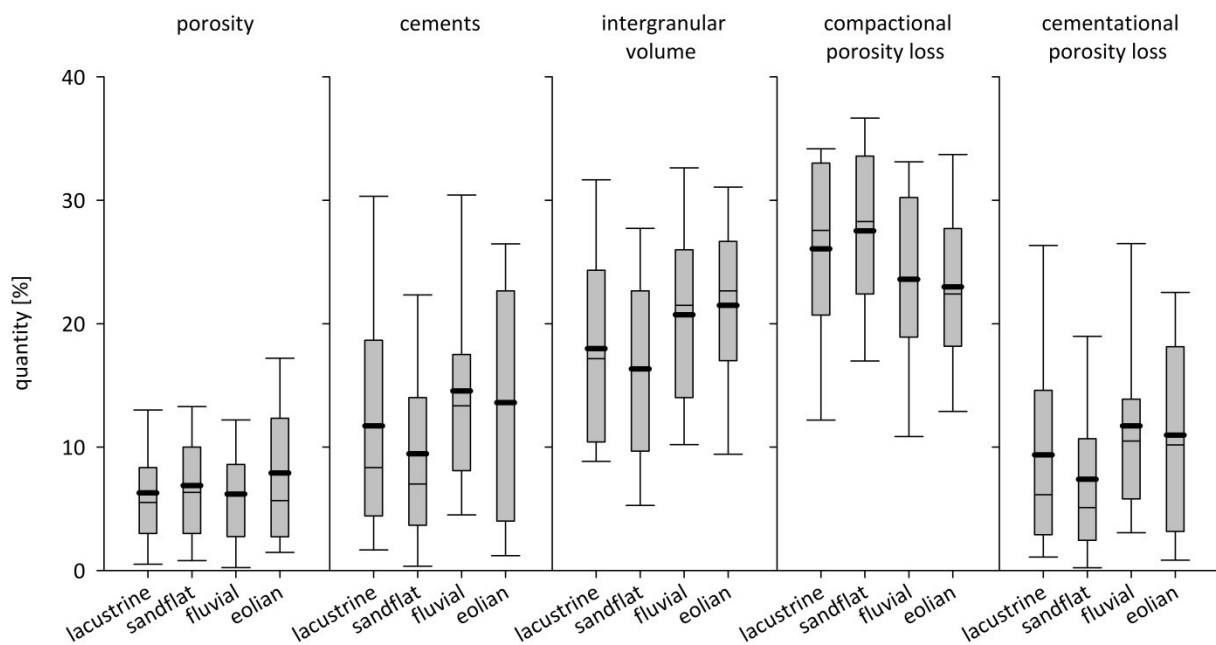
Fig. 36: Intergranular porosity, amount of blocky cement, intergranular volume (igv), compactional porosity loss (copl) and cementational porosity loss (cepl) for the different facies types. copl and cepl are according to Lundegard (1992). Porosity, cements and intergranular volume were measured with point-counting. The error bars indicate the 90th and 10th percentiles, thick black lines are the mean values.

5.3.5. Intragranular porosity

In addition to the intergranular porosity also an intragranular porosity is present. This secondary porosity occurs predominantly in corroded feldspar grains. The sandstones with the highest secondary porosity are of the lacustrine and sandflat facies type with

1.2 %. The mean intragranular porosity is well below 1 % in the eolian and fluvial sandstones. The intragranular porosity correlates with the abundance of detrital feldspar. (For a more detailed description of pore space classification see chapter 6.1.1.)

5.3.6. Red and grey coloured sandstones

Differences between reddish and greyish sandstones are shown in Fig. 37. The mean amount of clay cutans and matrix is lower in the greyish sandstones than in the reddish sandstones. Blocky cements are more abundant in the greyish sandstones. These cements caused a lower compactional porosity loss and a higher cementational porosity loss. Nevertheless the grey coloured sandstones show higher permeabilities (Fig. 37). Greyish sandstones are present in all facies types: 50 % of the lacustrine sandstones, 47 % of the sandflat sandstones, 88 % of the fluvial sandstones and 61 % of the eolian sandstones are grey sandstones.
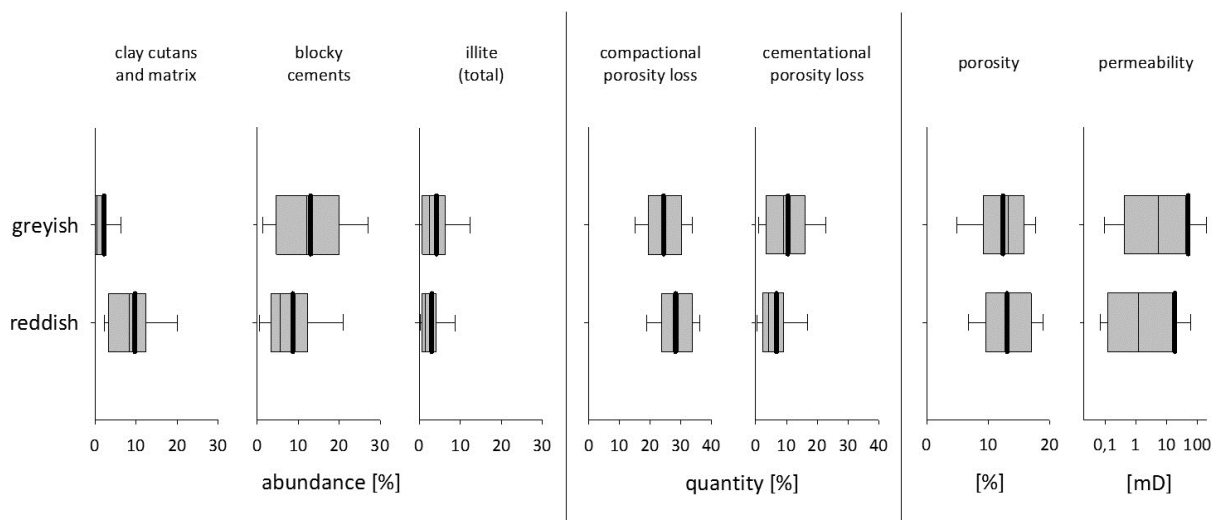
Fig. 37: Characteristics of red and grey coloured sandstones. The red colour of the sandstone is caused by iron oxide minerals. The mean permeability is slightly higher in the grey coloured sandstones. The error bars indicate the 90th and 10th percentiles, thick black lines are the mean values.

5.3.7. Present-day depth

Only sandstone samples from deep bore holes (> 400 m depth) located in the centre of the Thuringian Syncline have so far been described. The sandstone permeabilities from the deep boreholes are relatively low compared with the permeabilities of sandstones

taken from shallow boreholes (depth < 160 m) and outcrops (Fig. 39; see Fig. 2 for the locations). The purpose of this brief comparison is to demonstrate the importance of the sandstone present depth on petrophysical properties.
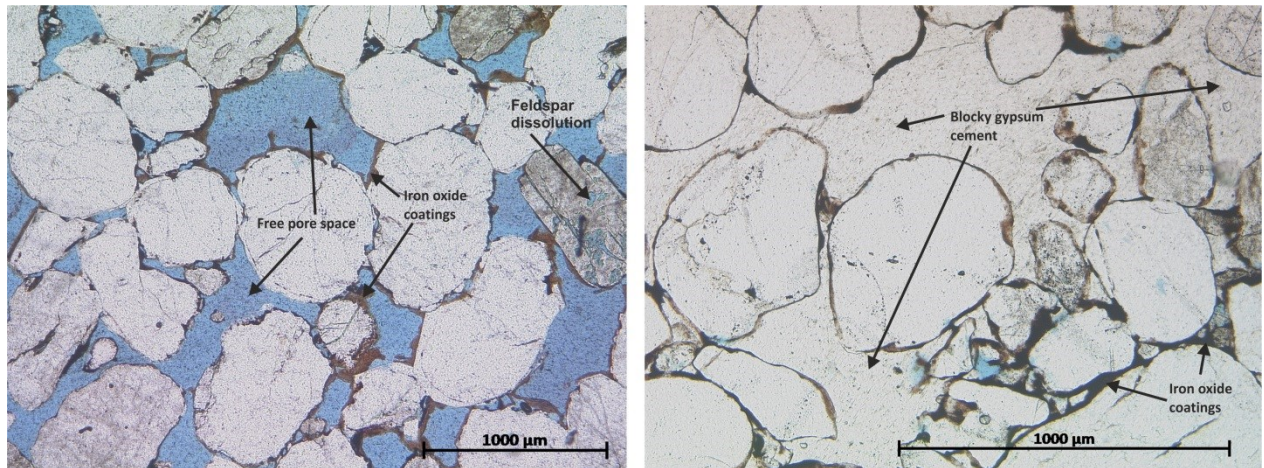
Fig. 38: Thin section images of sandstones from the Volpriehausen Formation. Left: outcrop ("Am Knorrenkopf") in the NW of the Thuringian Syncline. Right: Borehole in the centre of the Thuringian Syncline (sample Rks2-8, Volpriehausen Formation, eolian facies). Sulphate cement is not observable in the sandstones from outcrops or shallow boreholes.

Sandstones from outcrops and shallow boreholes at the margin of the Thuringian Syncline have a mean porosity of 18 %, which is about 5 % more than the porosity measured for samples from deep boreholes (see Table 5). Furthermore, high mean permeabilities of 628 mD in outcrops and 436 mD in shallow boreholes were measured (Fig. 39). The composition and texture of the Buntsandstein sandstones from deeper boreholes and from shallow boreholes and outcrops are not differing significantly. However, sulphate cement was not observed in sandstones from outcrops or shallow boreholes at the margin of the Thuringian Syncline (Fig. 38).
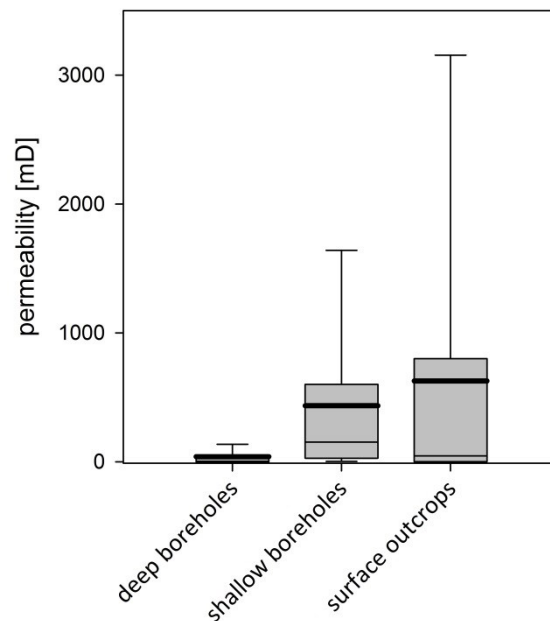
Fig. 39: Sandstone permeabilities in relation to their location/depth. The error bars indicate the 90th and 10th percentiles, thick black lines are the mean values.

5.4. Diagenetic evolution

The permeability of sandstones is both related to their depositional environment and to the diagenetic evolution (e.g. Shepherd 1989, Detmer 1995). The paragenetic sequence (see Fig. 40) is crucial to understand the effect of facies and other control factors on the diagenesis of Buntsandstein sandstones. The diagenetic stages eodiagenesis, mesodiagenesis and telodiagenesis that are used here are described by Worden & Burley (2003): Eodiagenesis is characterized by the interaction of meteoric water with the sediment at shallow burial; mesodiagenesis takes place during deeper burial and telodiagenesis during and after uplift in interaction with meteoric water.

5.4.1. Common diagenetic evolution in all facies types

Eodiagenesis

The first eodiagenetic process was the formation of carbonate nodules as indicated by the absence of clay cutans on grains surrounded by carbonate nodules (cf. Wilson & Pittman 1977). Calcretes are observable in all Buntsandstein formations and they are

caused by evaporation of ascending carbonate rich waters in a semi-arid climate (Paul 1999a). Thereafter tangential illite cutans and detrital clay matrix were formed in still open poresystems. Typically they form by infiltration of clay suspensions that are stained with Fe(III) oxides and clay minerals (Gaupp 1996, Worden & Morad 2003) like smectite and illite in the meteoric-vadose zone above groundwater table. It is assumed that the hematite grain coatings and clay cutans formed at a similar time under oxygen-rich porewater conditions during the shallow burial phase (cf. Muchez et al. 1992, Gaupp et al. 1993). Fig. 32 b shows how hematite coating and illite cutans are located intermingled on grain surfaces. Blocky gypsum and halite cement also formed at an early stage as a consequence of high evaporation rates, caused by a fluctuating ground water table and the semi-arid climate. Where this blocky cement occurred, it supported an existing grain fabric that inhibited further mechanical compaction (cf. Glennie 1970). The low amount of feldspar cement (< 1 %) on the feldspar grains had only a small effect on the absolute porosity loss. With increasing overburden the degree of mechanical compaction rose, as indicated by the low amount of eodiagenetic and mesodiagenetic cement and by high values of porosity loss by compaction. Thereafter, feldspar was (partially) dissolved. This can be seen by the small etch-pits along cleavage planes and inhomogeneous patchy corrosion (Fig. 32a, Fig. 33b). This secondary porosity contributes only a small part to the total porosity of the samples. Dissolution of feldspar took place predominantly under humid conditions (Worden & Morad 2003). Such fluctuating climate conditions (from arid to humid) may force chemical mineral instability (Pettijohn et al. 1987). Concurrently, quartz overgrowths started to grow as thin rims on quartz grain surfaces lacking clay coatings. The quartz growths are probably linked to the dissolution and transformation of feldspar to albite and kaolinite (Worden & Morad 2000). This requires acid conditions and low ion concentrations in the fluid (Emery et al. 1990). The vermicular shape of the kaolinite minerals is caused by fast growth, which is linked to fast transport of Al and Si ions in meteoric water (Hurst & Irwin 1982). Today soil is the main source for vermicular kaolinite (Fitzpatrick 1980). This is in accordance both with the proofed pedogenic phases for the Middle Buntsandstein (Rettig 1996) and with the identification of pedogenic carbonates nodules in the Middle Buntsandstein sandstones (Voigt 2000, Lippmann 2012). In such an environment a mineral precipitation within the pH range 4/5 – 8 that was controlled by Al and Si ions (Curtis 1983) is plausible. Primary dolomite cement precipitation under surface conditions is uncommon (Tucker & Wright 1990). Therefore dolomitisation of primary calcite can be assumed for the late eodiagenetic or the mesodiagenetic phase. A

reason for that could be the increase of the Mg:Ca ratio caused by the precipitation of sulphate cement (cf. Rahimpour-Bonab et al. 2010). Eodiagenetic replacement of halite cement by gypsum is also probable. The absence of organic material may be primary due to limited plant growth under arid climate conditions or due to complete decay of organics caused by oxygen saturation of pore waters.

Mesodiagenesis

The dissolution of quartz at grain to grain contacts is generally accompanied by mechanical compaction (Worden & Burley 2003). The precipitation of homoaxial quartz overgrowths continues due to grain to grain dissolution. This process is supported by the release of Si in the transformation of smectite to illite during burial (Worden & Morad 2003). Variations in the amount of quartz cement results in differences in the compaction rates of the Buntsandstein sandstones. For example, in sandstones with < 8 % quartz cement the mechanical compaction is strong with mean porosity loss by compaction of 27 %. In samples with > 8 % quartz cement the mean porosity loss by compaction is 20 %. Subsequent a phase of carbonate und sulphate cementation followed. The observed carbonate cements generally have an irregular and inhomogeneous shape. A reason for this could be just temperature increase or interruptions of the mineral growth process owing to changing fluid pathways during compaction and cementation. Additionally, such changes in fluid pathways may result in changes in the chemical composition of pore fluids. Indeed, at least four carbonate dissolution and precipitation phases could be traced in some sandstone (see Fig. 30). Ferrous carbonate minerals precipitated in burial-related deeper regions during mesodiagenesis and under reducing conditions (Morad 1998). In a reducing environment Fe^{2+} and Mn^{2+} ions are available for carbonate precipitation. Gypsum dehydrated to anhydrite with increasing pressure, salinity and temperature (Testa & Lugli 2000). It can be assumed that in the final phase of mesodiagenesis (prior to uplift in more than 2 km depth, see Fig. 23), all gypsum was transformed to anhydrite (cf. Worden & Burley 2003). The precipitated barite may be related to high salinity brines from deeper-seated barium-containing Paleozoic or basement rocks. Another source could be the dissolution of feldspar (barium in traces) in the Buntsandstein and Rotliegend formations. The smectite to illite transformation continues with increasing temperature and depth (McKinley et al. 2003). During late mesodiagenesis patchy albite precipitated mainly within K-feldspar. This is a typical reaction at temperatures

between 75°C and 100°C (Morad et al. 1990). The albitization consumed Na, which is available in most formation waters, and provides K+ to the fluid, which was consumed for the precipitation of illite (McKinley et al. 2003). Illite precipitated predominantly as two morphotypes: as radial overgrowth on detrital grains and as intra-pore illite meshwork (distinguished after Deutrich 1993). In chapter 4.4. is described, that the organic matter of the Zechstein Formation was in the range of the gas window. A migration of hydrocarbons from the Zechstein rocks to the Buntsandstein sandstones is possible in the late mesodiagenesis. An oxidation of hydrocarbons results in organic acids and CO_2, which lowered the pH value, Fe ions were mobilized (Fe reduction) and a bleaching of the Buntsandstein sandstone took place (cf. Shebl & Surdam 1996). Furthermore, small patches of rocks are bleached close to mudstone clasts. This observation can be linked to an anaerobic oxidation of organic carbon in the mudstones (Canfield et al. 1993).

Telodiagenesis

During and after uplift the temperature decreases and the fresh water content increases in the circulating fluids (Worden & Burley 2003). Pressure release may form new fluid path-ways through joints, faults and fractures as well as an increasing water flow through the sandstone.

Both sandstones from drill cores and from outcrops have nearly a similar diagenetic history. The major difference between them is the presence of blocky gypsum cement only in the sandstones samples from deep drill cores. Therefore we distinguish two phases of telodiagenesis: telo A, which is recorded both for drill core and outcrop sandstones, and telo B, which was only recognized in outcrop sandstones and shallow boreholes (depth < 160 m). Telo A proceeded with the uplift and telo B occurred in the basin margin area of the Thuringian Syncline. Telo B resulted in mineral dissolution and alteration phenomena. For the central Thuringian Syncline the uplift of the Buntsandstein sandstones was insufficient for an overprint by meteoric water at shallow depths.

In telo A the precipitation of illite meshworks decreased with progressive uplift. Anhydrite cement was transformed to gypsum due to hydration. In some cases this transformation is not yet complete as proven by relics of anhydrite within gypsum cement minerals (cf. Testa & Lugli 2000).

Telo B is restricted to lithologies exposed at the erosional basin margin, where the infiltration of surface (rain-) water is high. This oxygen rich waters (probably with bacterial influence) forced weathering and corrosion of the sandstones. The infiltration resulted in bleaching phenomena linked to fractures or sheet boundaries (Hilse in prep.). For the absence of sulphate cement in sandstones < 170 m depth (analysed on drill cores and outcrops) sulphate dissolution by under-saturated meteoric water is considered. Intensity of feldspar dissolution increased with the intensive influx of meteoric waters. Corrosion of feldspars is accompanied by precipitation of kaolinite. Petrographic observations reveal late stage kaolinite formation linked to the dissolution of feldspar and the alteration of mica, especially muscovite (Fig. 33c).

5.4.2. Facies control on specific diagenetic features

Diagenesis of lacustrine deposits

The lack of early hematite staining in the lacustrine sandstones is linked to common low oxygen contents in bottom waters of lakes (cf. Einsele 1992). This is typical of lacustrine sediments. Instead hematite coatings tend to be most common in subaerially deposited floodplain sediments under arid to semi-arid climate (Gaupp et al. 1993, Worden & Burley 2003). Therefore reddish lacustrine sandstones could have been caused by lake regressions. Because infiltrated clay cutans were rarely observed, the lake was dried out only occasionally (cutans could only form when the lake bottom was exposed to the air and meteoric waters). The common weak and discontinuous clay cutination on quartz grains of the lake sandstones instead favoured large volumes of quartz overgrowth. Furthermore, dissolution of the calcareous ooids probably contributed with carbonate ions for the observed intense carbonate cementation (cf. Langbein 1985). The high amount of carbonate cement and the small grain size in the lacustrine sandstones lead to lower permeabilities than in the sandstones of all other facies types. A consistently strong carbonate cementation results in very low mean permeability of 1 mD in lacustrine rocks with a carbonate content > 5 %. The intense corrosion of feldspar and resulting higher secondary porosity compared to the other facies types is due to the higher detrital feldspar content in the studied lacustrine Buntsandstein sandstones. Nevertheless, the total permeability seems to be slightly affected.

Diagenesis of sandflat deposits

Pedogenic phases and the related formation of dolcretes occur predominantly in clastic sandflat deposits of arid to semi-arid regions (Morad 1998). The common dolcretes inhibit mechanical compaction, whereas sandflat sandstones with surface-related dolomite underwent a great mechanical compaction due to the low amount of pore-stabilizing cement. Due to the depositional environment the infiltration of clay suspension is increased. A particularly high content in clay cutans, matrix, ductile mudclasts and mica then promotes mechanical compaction (Worden et al. 2000). For these reasons, the mean porosity loss by compaction (copl) is with 28 % the greatest in comparison to the other facies types. Eodiagenetic kaolinite was observed in the sandflat sandstone. Since kaolinite occurs as inclusions within blocky gypsum and carbonate cement, an early formation prior to these cement types is assumed. Petrophysical data suggest that kaolin minerals have a minor influence on rock permeabilities. This can be explained by smooth mineral surfaces and the sporadic occurrence in clusters.

Diagenesis of fluvial channel deposits

Fluvial sandstones underwent a weak compaction during mesodiagenesis due to the quartz cementation, low abundance of clay and a larger grain size and better sorting. This results in good permeability characteristics and aquifer properties. Gypsum is more abundant than carbonate cement, since potential ion sources for carbonate cement like ooids are absent. A late stage transformation of mica to kaolinite and dissolution of gypsum is observed in this facies type. These processes are most likely related to high connectivity and permeability of fluvial sandstone during meteoric water infiltration.

Diagenesis of eolian units

An early lithification by early halite cement is a common feature of eolian facies (Glennie 1970), but relicts of halite were scarcely observed in the core material and neither in outcrops of the Thuringian Buntsandstein. It is assumed that halite was replaced by gypsum and that primary halite cements were leached during drilling or at the surface. The high amounts of quartz grains lead the rock to a mechanically and chemically stable framework (cf. Bloch 1994). Hence mechanical compaction is lower than in the other facies. The precipitation of gypsum cement is related to coarser-grained sandstone as supersaturated fluids prefer large pores for precipitation (Putnis & Mauthe 2001, Pape et al. 2005). This is the most important factor for porosity loss in

primarily highly porous eolian sediments. Although the residual (intergranular) porosities are low, permeabilities are commonly high owing to a weak mechanical compaction and the coarse grain size. During telodiagenesis the dissolution of sulphate or halite cement results in a significant increase in rock permeability (up to > 600 mD, measured on outcrop samples of sandstone).

Time	Triassic			Recent
Stage	**Eodiagenesis**	**Mesodiagenesis**		**Telodiagenesis**
Burial	Shallow	Intermediate	Deep	Intermediate

Diagenetic Process				
Infiltration of clay				
Halite				
Carbonate (pedogenic)				
Fe-oxide (hematite)				
Tangential illite				
Feldspar cement				
Quartz cement				
Dissolution of feldspar				
Kaolinite				
Ti-oxide				
Mechanical compaction				
Carbonate cement				
Calcite				
Dolomite				
Ankerite/Siderite				
Sulfate cement				
Gypsum + Anhydrite				
Barite				
Dissolution of cement				
Illite overgrowth				
Illite meshwork				
Replacement of feldspar				
Hydrocarbon migration				
Hydration of anhydrite				
Late kaolinite				
Fracturing				
Bleaching				
Late meteoric cement dissolution				

Fig. 40: Schematic diagenetic sequence for Buntsandstein sandstones from the Thuringian Syncline. Not all processes took place in all analysed sandstones. The bar indicates the duration of the process.

6. Characterisation of pore space and mineral surface area in the Buntsandstein sandstones

Porosity is the most important factor for permeability, but a high porosity in sandstone is not always a guarantee for a high permeability. Pores, which are not connected with other pores, are not increasing the permeability of the sandstone. The origin of these unconnected pores is diverse. For a better understanding of facies related differences in rock permeability a more detailed investigation with digital image analysis of the pore space was carried out (cf. Kayser 2006, Abram 2007 and Kohlhepp 2012).

If a fluid is flowing through permeable sandstone, the inner surface area of the rock is interacting with the fluid, depending on chemical equilibria. It is not possible to describe this process only with the petrographic composition of the sandstone, because not every detrital mineral or grain is in contact with the pore space. With a specific analysis of the surface area in sandstone it was possible to estimate fluid-rock interactions.

For the estimation of mineral surface areas it was necessary, that the examined sandstone was with porosity (> 5 %). In sandstone without porosity, no surface areas (in contact with open pore space) are measurable. In this chapter a specification of pore space and mineral surface area of the Buntsandstein sandstones in regard to their facies type is given.

6.1. Qualitative evaluation of pore space

6.1.1. Classification of the pores

These pore classifications are common for clastic sediments:

1) **Origin**: pores, which are develop during deposition between grains are primary; and pores, which are develop during diagenesis by dissolution of grains or cements are secondary (cf. Schmidt & MacDonald 1979). If a complete grain was dissolved, an oversized pore could remain (Moncure et al. 1984). The size of an oversized pore is often larger than the average pore size in the sample and nearly the size of a grain (Fig. 41).

2) **Size**: pores can be distinguished between micropores (diameter < 5 μm) and macropores (diameter > 5 μm) (Marfil et al. 1996, Fischer & Gaupp 2004).

3) **Position**: porosity inside a grain is intragranular porosity; porosity between grains is intergranular porosity. Intergranular porosity is predominantly caused by corrosion of grains.
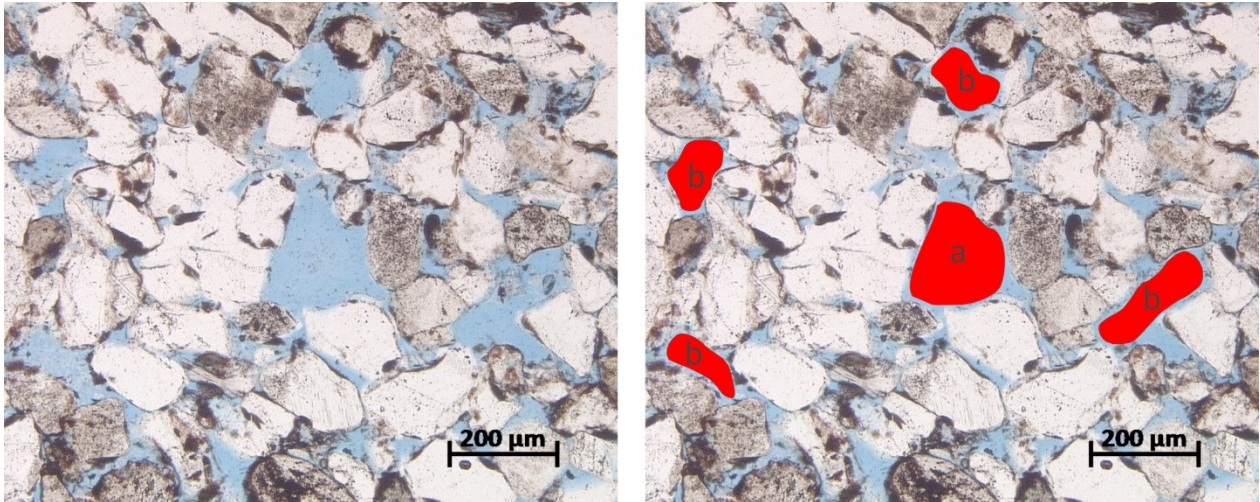
Fig. 41: In the sandstone samples some oversized pores exist, but it is not possible to identify their exact origin. Pore (a) is surely a dissolved grain, the other large pores (b) may be caused by dissolution of cement or grain, or they could be also primary (sample Rks2-1, Hardegsen Formation, sandflat facies).

Primary and secondary pores are hard to differentiate; only the intragranular pores (inside feldspars, see chapter 5.3.) are surely secondary in their origin. Some oversized pores are observable in the samples. As visible in Fig. 41 these oversized pores were probably caused by dissolution of grains (a) or cements (b). It seems that in the lacustrine sandstones the secondary porosity is predominantly caused by dissolved grains (Table 6). It is also assumable that in the sandflat sandstones dissolved cements and grains form the secondary pore space (Table 6). In the fluvial and in the eolian sandstones the secondary pore space seems predominantly caused by dissolved cement (Table 6) due to the fact that dissolved large grains (for mean grain size see Table 5) would lead to large oversized pores, which are not observable in these samples.

Table 6: Estimated secondary pore space in the different facies types (mean porosity by plug measurement with helium).

	lacustrine	sandflat	fluvial	eolian
measured mean porosity	12 %	13 %	12 %	13 %
estimated secondary porosity by dissolved cement	< 1 %	1 % - 3 %	1 % - 3 %	2 % - 5 %
estimated secondary porosity by dissolved grains	1 % - 4 %	1 % - 3 %	< 1 %	< 1 %

6.1.2. Connectivity of the pores

Connected pores are fundamental for permeable sandstones (Tiab & Donaldson 2004). Hence, poor-connected pores in sandstone lead to a poor permeability, in contrast permeable sandstones feature a well-connected pore system. The factors, which are influencing the pore space and the permeability, are described in chapter 5. Here, a qualitative estimation of pore connectivity in the Buntsandstein sandstones is visualized (Fig. 42):

(1) Poorly connected pores in low porosity sandstones cause very low permeability in all facies types. The porosity in the lacustrine and sandflat sandstones is higher than in the fluvial and eolian sandstones.

(2) Pores are better connected, but they are only present in clusters. The pore size is proportional with the sandstones grain size: small pores in the lacustrine sandstones, larger pores in the eolian sandstones.

(3) Pores are distributed more homogenously/randomly. The pore area (pore space) is not much higher than in class 2. The pore size is proportional with the sandstones grain size.

(4) Well-connected larger pores are distributed homogenously in the sandstone. Pores of the lacustrine sandstones are smaller than the pores in the other facies types, even if they are well connected the permeabilities are only medium (e.g. sample Ballst-7: 58.6 mD). In the other facies types are permeabilities possible up to 300 mD.

(A quantitative determination of pore connectivity in the sandstones is described in chapter 6.3.)
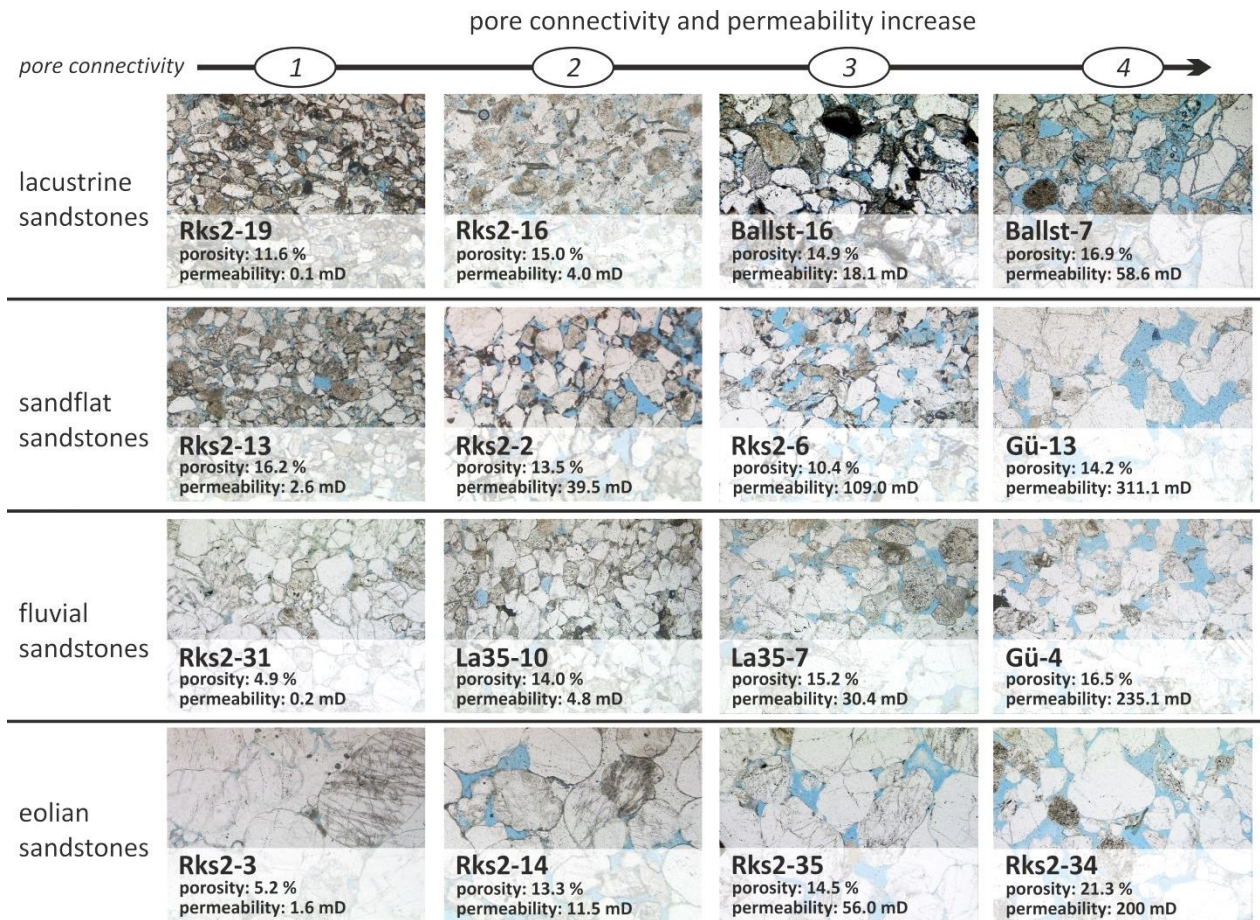
Fig. 42: Four observed pore connectivity classes for the sandstones of different facies type. A good connection between the pores yields a higher permeability and vice versa. Microphotos have same magnification and scale.

6.2. Pore size distribution evaluated with digital image analysis

6.2.1. Porosity measurement

Macroporosity measured with image analysis does not distinguish between intra- and intergranular porosity or primary and secondary pores, because all pores were identified by blue stained resin which is identical for all pore types. Also micropores (< 1 µm²) are not measureable due to this method.
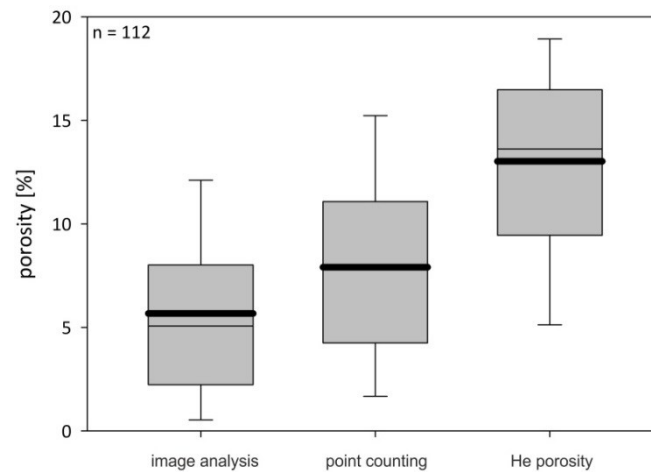
Fig. 43: The porosity of the sandstone samples measured with digital image analysis, point counting and Helium porosimetry. The error bars indicate the 90th and 10th percentiles, thick black lines are the mean values.

Porosity values which result from image analysis are in average smaller than porosity values from point counting or He- porosities (Fig. 43). One explanation is the precision (in connection to the scale) of the method. Small pores and micropores which are not covered with blue resin are underestimated and not measureable by microscopic image analysis. The porosity measured by Helium porosimetry is a quite exact method (c.f. Kazimierz et al. 2004), which is also measuring the microporosity in the sandstones. It is assumable, that the difference between the porosity measured with image analysis and the porosity measured with Helium is the microporosity of the sandstone (Fig. 44). The mean of thus determined microporosity is between 6 % and 8 % in the different facies types (lowest in the fluvial sandstones, highest in the lacustrine sandstones). Furthermore, microporosity higher than 8 % is only determined in sandstones with a mean grain size smaller 0.4 mm.
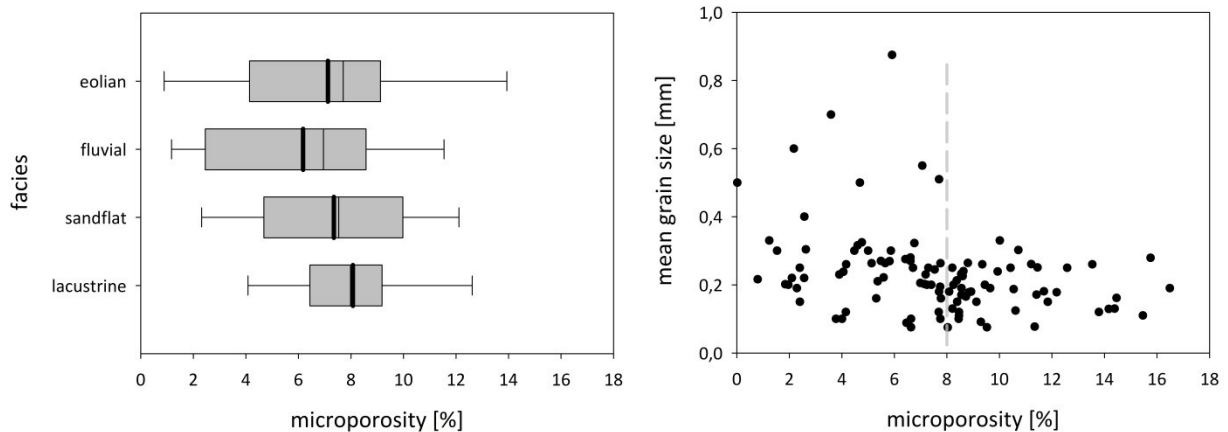
Fig. 44: Estimated microporosity is linked slightly with the facies type and the mean grain size of the sandstone. A microporosity higher 8 % is only present in sandstones with a mean grain size smaller 0.4 mm. The error bars indicate the 90th and 10th percentiles, thick black lines are the mean values.

Correlation between the porosity measured with Helium porosimetry and the measured permeability in the sandstones is quite hard to find. Many factors influence the relationship (see chapter 5.3.). Nevertheless the calculated regression (second order) between the porosity measured with digital image analysis and permeability (r^2 = 0.43) is stronger than between the He porosity and permeability (r^2 = 0.30) (plots with regression lines in Fig. 45). Also is the porosity measured with digital image analysis or point counting performed only on "images", which means it is only a 2D method. Sandstones in 3D are inhomogeneous and a 2D image is not representing the rock completely.
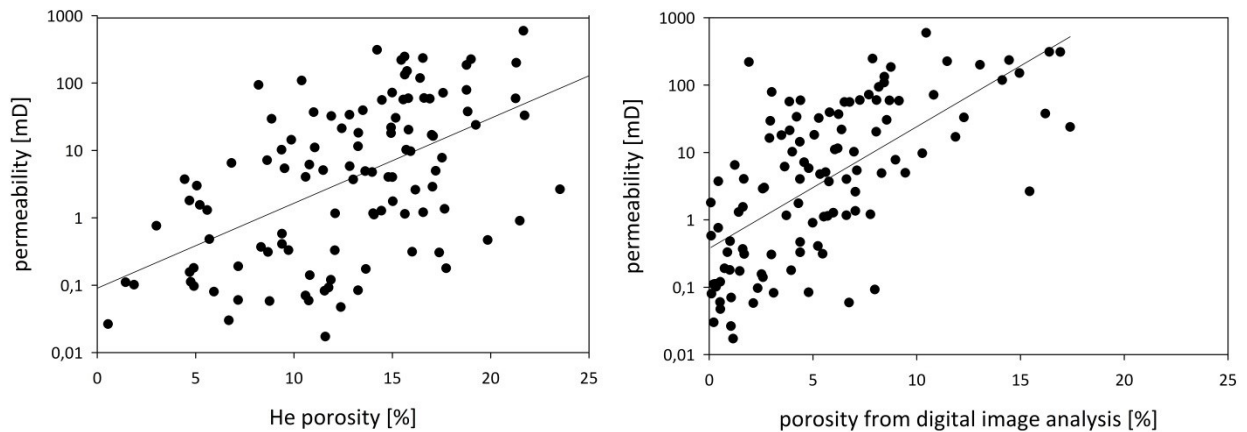
Fig. 45: Helium porosity correlates poorly with the permeability (left). The porosity measured with image analysis correlates stronger (right). The black line is the linear regression for the data.

6.2.2. Pore classes

As a result of digital image analysis, small pores (1-1000 µm²) are very frequent in the lacustrine sandstones (Fig. 46). Medium pores (1000-10000 µm²) are equally frequent in all sandstones. Large (10000-50000 µm²) and very large pores (> 50000 µm²) are most frequent in the eolian sandstones and low frequent in the lacustrine sandstones (Fig. 46).
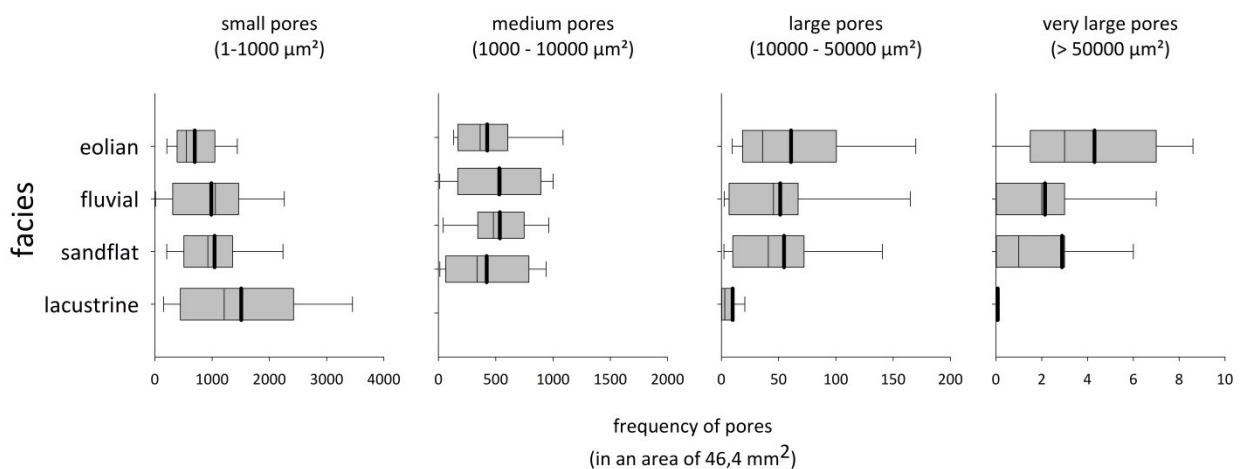
Fig. 46: The frequency of pores in a pore class in the four facies types in an area of 46.4 mm². The error bars indicate the 90th and 10th percentiles, thick black lines are the mean values.

The lacustrine facies shows a high percentage of small pores of the total porosity (about 50 %) and the percentage of large and very large pores is low (0 % – 5 %). One common feature of all facies types is a very frequent occurrence of medium-sized pores (40 % – 45 %; Fig. 47).
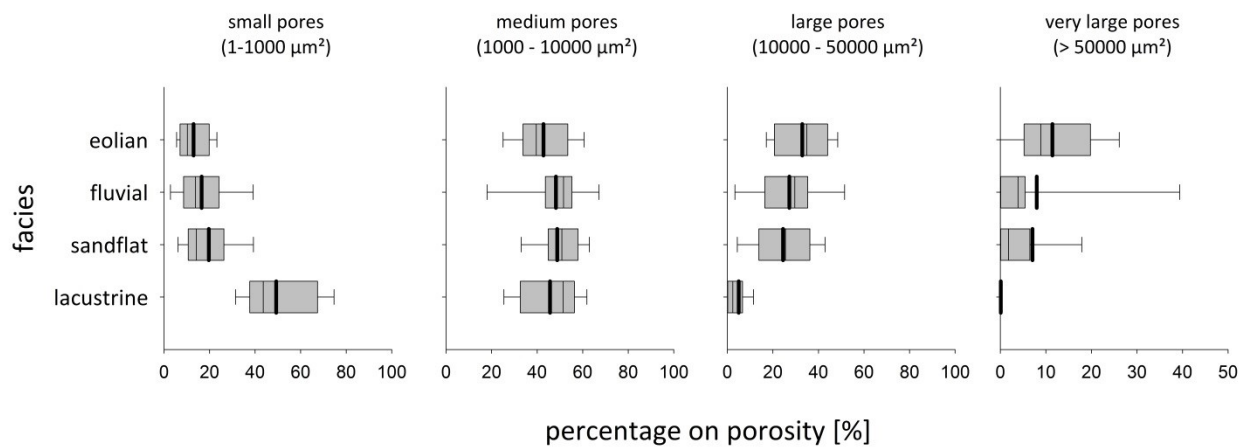
Fig. 47: Ratio of pore classes normalized to the porosity in the sandstones of the four facies types. The error bars indicate the 90th and 10th percentiles, thick black lines are the mean values.

6.2.3. Pore density

The measured pore density includes information about the spatial frequency of pores in a defined area. The average amount of pores is in between 20 and 40 pores in an area of 1 mm². The lowest mean pore density is in the eolian facies, the highest is in the lacustrine facies (Fig. 48). There is no correlation between pore density and the sandstone permeability (Fig. 48). A high pore density is associated with a high frequency of small pores and vice versa.
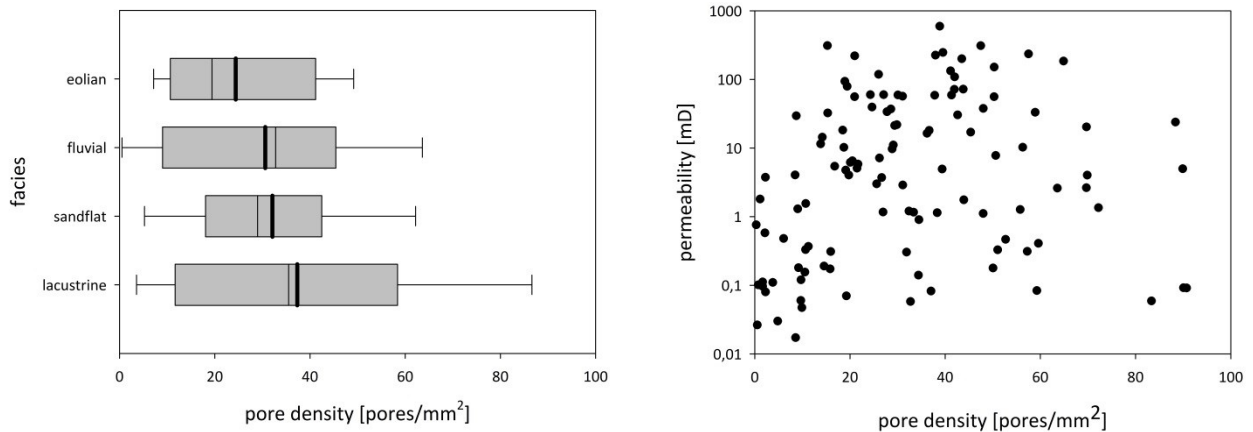
Fig. 48: The pore density in the sandstones is associated with their facies type, not with the sandstones permeability. The error bars indicate the 90th and 10th percentiles, thick black lines are the mean values.

6.2.4. Pore perimeter

The sum of the pore-mineral interface per area is very similar in all facies types (Fig. 49). The total perimeter per area correlates slightly with the permeability (Fig. 49). Although lacustrine sandstones contain a high amount in small pores, their perimeter/area is similar to facies types with predominantly large pores such as eolian facies type. For this reason, the pore perimeter is no significant parameter for the discrimination of fluid flow properties.
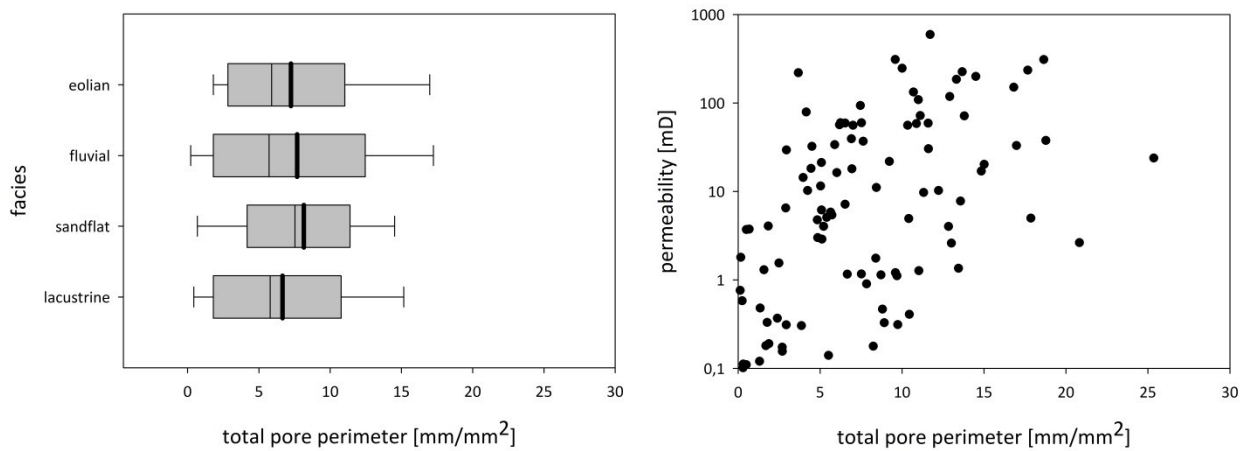
Fig. 49: The total pore perimeter in the four facies types and the relation between the permeability and the total pore perimeter. The error bars indicate the 90th and 10th percentiles, thick black lines are the mean values.

In the lacustrine sandstones the pore-mineral interfaces (the perimeters of the pores) are formed up to 60 % by small pores and to nearly 40 % by medium pores (Fig. 50). In contrast, in the other three facies types the pore-mineral interfaces are fabricated 30 % by small pores, 50 % by medium pores, between 15 % and 20 % by large pores and around 5 % by very large pores (Fig. 50). Only 15 % to 25 % of the pore-mineral interfaces are fabricated by large and very large pores (in the sandflat, fluvial and eolian sandstones, Fig. 50).
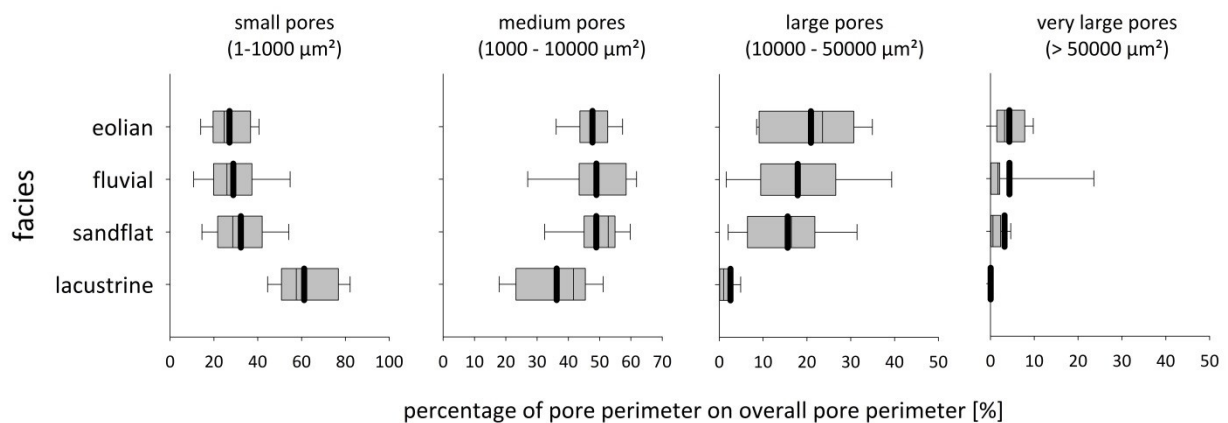
Fig. 50: The percentage of pore perimeter of pore class on sandstones overall pore perimeter. The error bars indicate the 90th and 10th percentiles, thick black lines are the mean values.

6.3. Relationship between rock fabric and pore structure

6.3.1. Influence of large pores on fluid flow

As described in chapter 5, the sandstones with higher mean permeabilities are the sandflat, fluvial and the eolian sandstones. The main difference to the lacustrine sandstones is the abundance of large and very large pores in these sandstones. This means, that a high abundance of large pores (pore area of class III and IV > 500000 μm^2 in an area of 52544556 μm^2) results in an increased mean porosity and mean permeability. Furthermore low abundances of this large pores results in a decreased mean porosity and mean permeability (Fig. 51). For this reason the most important pore classes for fluid flow and therefore aquifer properties are the classes III and IV (large

and very large pores). As these large pores act as the major fluid conduits, even one percent of the well-connected sandstone porosity (measured with digital image analysis) within the pore class III and IV results in relatively good petrophysical properties (Fig. 51).
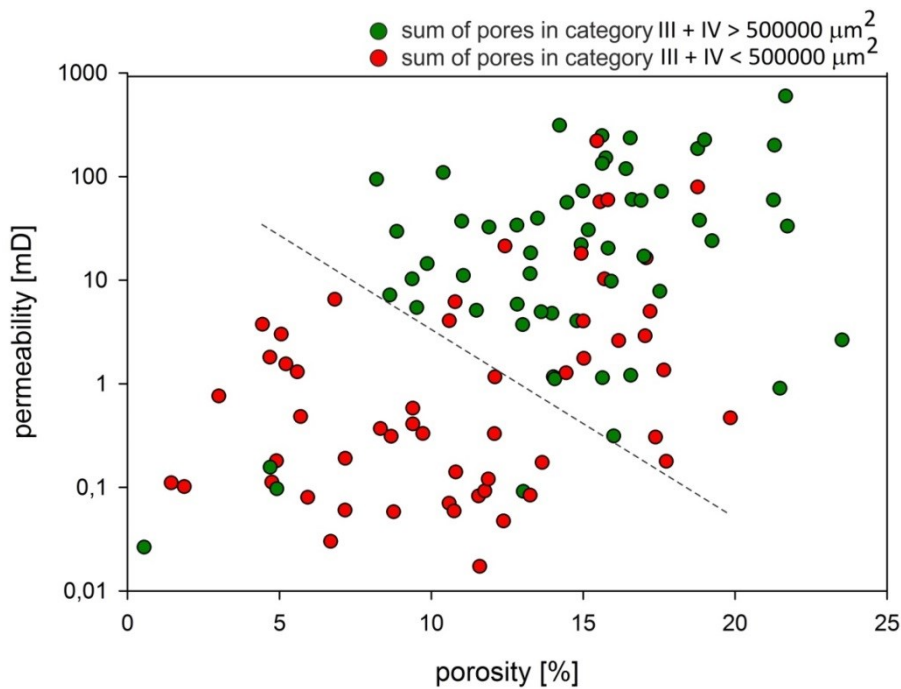
Fig. 51: Most samples in which the area of all pores from class III and IV exceeds 500000 µm² in an area of 52544556 µm² (green symbols) have relatively high permeability and porosity. The sum of large pores is high in some samples with poor petrophysical properties, because grains were broken out in these samples during preparation. These broken out grains are forming large pores (green symbols in the lower left).

If there is a fluid in these sandstones, it will interact with the minerals at the measured pore-mineral interface (perimeter of the pores). As described the large and very large pores are important for fluid flow, but also their pore-mineral interface is very low (Fig. 50). Hence is the fluid flowing predominantly in large and very large pores, the interacting of the fluid with the minerals will be low because of the low pore-mineral interface.

6.3.2. Pore connectivity

Sandstones with the highest pore density are lacustrine sandstones, as they are smaller grained in average and have smaller pore size. Sandstones with large grain size like the eolian sandstones have more large pores than fine grained sandstones. Hence grain size correlates positively with the frequency of large pores. Exceptions from this relationship are coarser grained sandstones with high percentage of blocky cements. Sulphate or carbonate cements occlude large pores in this type of sandstones (see chapter 5.4.). The percentage of large pores (pore class III) on the porosity of a sample is correlated with the mean grain size of the samples, an exception are those samples with more than 15 % of blocky cements (Fig. 52). Reason for that is a preferred cementation of large pores in coarse grained sandstones during the diagenesis (see chapter 5.4.)
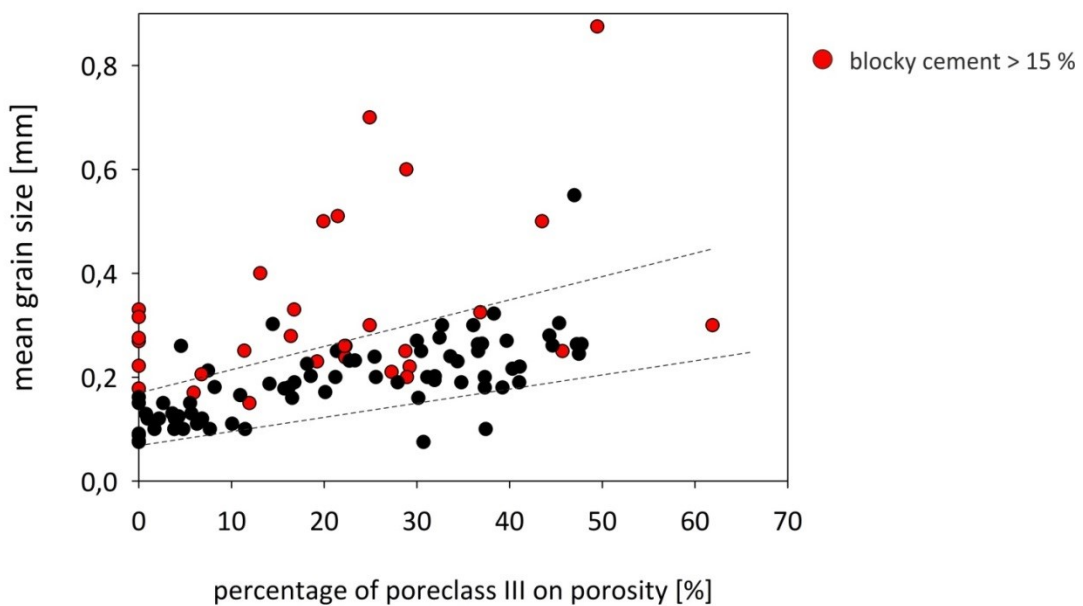
Fig. 52: The percentage of large pores (pore class III) on sandstones porosity is increasing with increasing grain size. Exceptions are coarse grained strongly cemented sandstones (red dots).

Both parameters pore density and porosity (measured with image analysis) include information about the pore connectivity. A high porosity (> 7 %) in combination with a low pore density (< 65 pores/mm²) is a result of a well-connected pore system and a good permeability (> 50 mD) (Fig. 53). Porous sandstone with high porosity and high pore density are only slightly moderately permeable (< 50 mD), while the most of the non-porous sandstones (< 7 % porosity) are also slight permeable, accordingly (Fig. 53).

Sandstone samples with the features of well-connected pores (porosity: > 7 %; pore density < 65 pores/mm^2) are rare in the lacustrine sandstones: 4 % of the lacustrine sandstones have these properties. In the other facies types such sandstones are more frequent: 31 % of the sandflat sandstones, 36 % of the fluvial sandstones and 31 % of the eolian sandstones have these features. 62 % of the samples with these properties have a permeability > 50 mD.
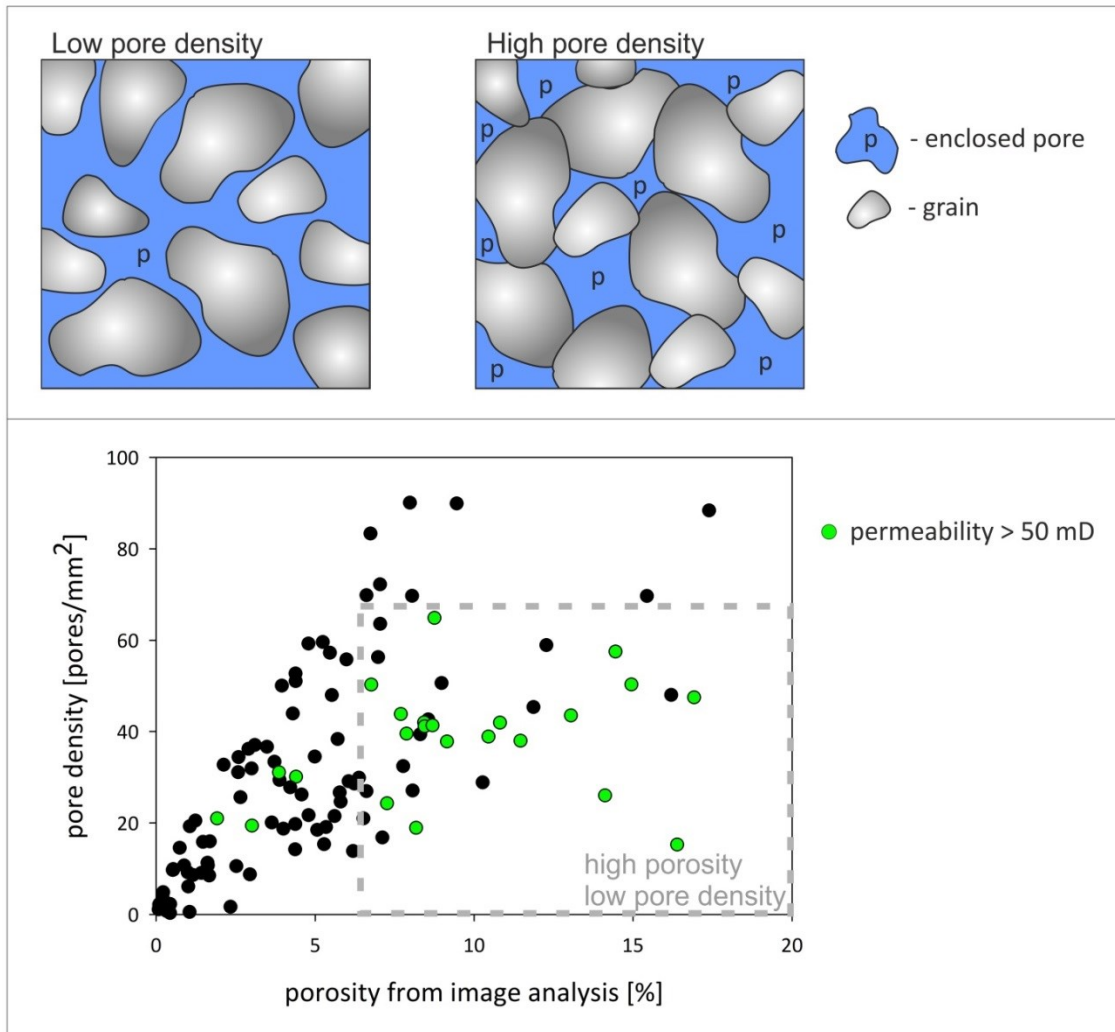
Fig. 53: In highly porous sandstone the connectivity between the pores is linked with the overall pore density in the analysed area. In the sandstone sketch on the left the pores are well connected, which results from a high porosity and low pore density. In contrast the sandstone sketch on the right has poor connection between the pores. The plot shows that samples with high permeability (green) have high porosity and low pore density.

6.4. Mineral surface areas evaluated with digital image analysis

6.4.1. Sandstones with and without iron oxide coatings

For the measurement of the mineral surface areas it was necessary to divide the sandstones into two groups: sandstones with and without iron oxide coatings around grains. If coatings are present in sandstone, all other measured surface areas are minor compared to measured surface area of the iron oxide coatings (Fig. 54).
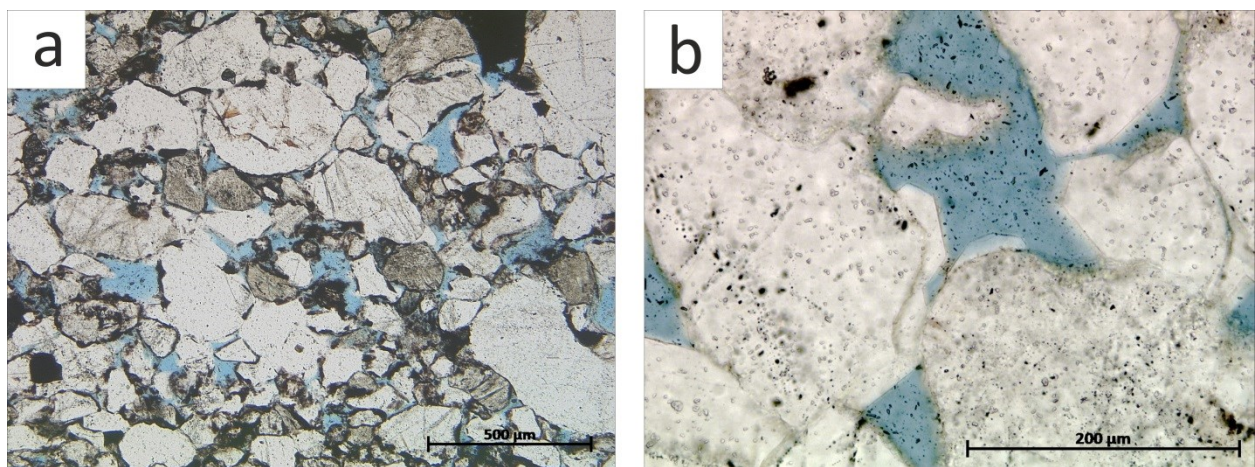
Fig. 54: In image a) the most surface areas, which are exposed to the pore space, consist of iron oxide coatings (sample Te-18, Hardegsen Formation, sandflat facies). In image b) the surface areas consist of grains and authigenic minerals (sample Gü1-15, Hardegsen Formation, sandflat facies).

The measured surface areas consist mainly of quartz, feldspar, quartz cement and iron oxide coatings (Fig. 55). In sandstones with coatings, the most abundant surface areas in average are iron oxide coatings (38.8 %), followed by quartz (24.5 %), feldspar (17.2) and quartz cement (13.4 %). In sandstones almost without iron oxide coatings (mean abundance is 1.9 %), the hierarchy of the abundant minerals is the same, but the frequency is much higher (mean surface area of quartz: 42.2 %; feldspar: 28.9 %; quartz cement: 14.3 %).
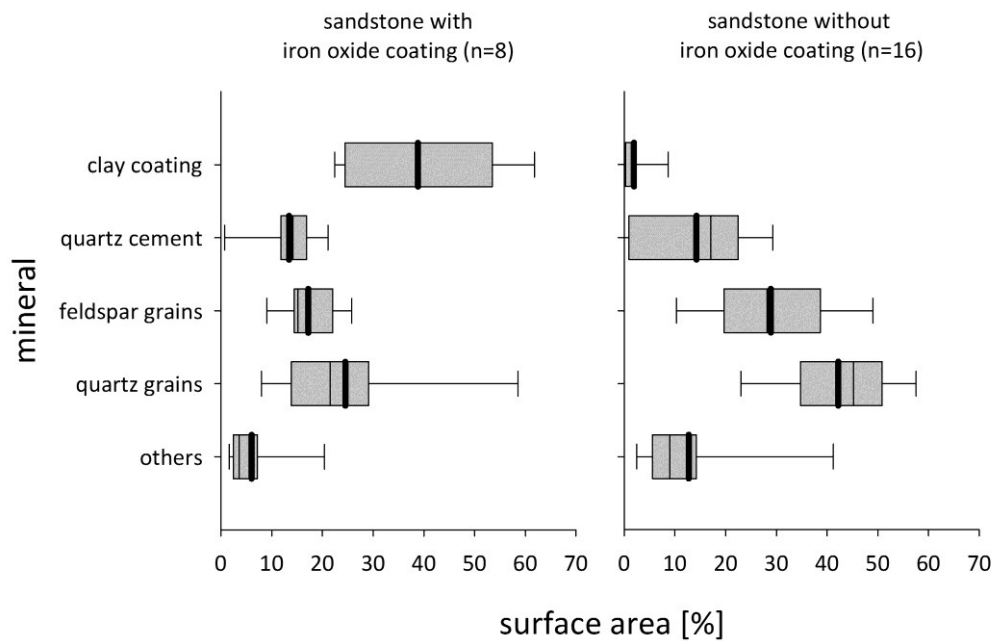
Fig. 55: The surface areas in sandstones with and without iron oxide coatings. The error bars indicate the 90th and 10th percentiles, thick black lines are the mean values.

6.4.2. Influence of the facies type for sandstones without iron oxide coatings

To identify the influence of the facies type on the mineral surface areas only the sandstones without iron oxide coatings were analysed. Fig. 56 shows the influence of the facies type on the sandstone surface area. Quartz grains are the most important sandstone grain surfaces in all facies types (40 % in average). The second most important surface area are feldspar grains, which are frequent in the lacustrine sandstones (approx. 40 %), less abundant in the sandflat and fluvial sandstones (25 % – 30 % in average) and lowest in the eolian sandstones (approx. 12 %). Also very important for surface area measurements are quartz cements, because they were precipitated on quartz grains and they are in contact with the open pore space. The surface area of quartz cement in lacustrine sandstones is low (5 % in average), in sandflat sandstone moderate (13 % in average) and higher in fluvial and eolian sandstones (17 % – 22 %). If ooids are present in the lacustrine sandstones, the surface area is highly influenced by ooids and carbonate cements (up to 35 % of the surface area). Also sulphate cements, like anhydrite and gypsum, have effect on the surface area (e.g. in the eolian sandstones up to 21 %). Other mineral surface areas (lithic fragments, feldspar cement, micas, heavy minerals, iron oxide coating, opaque

minerals, illite and kaolinite) are present predominantly in sandflat and eolian sandstones (Fig. 56).
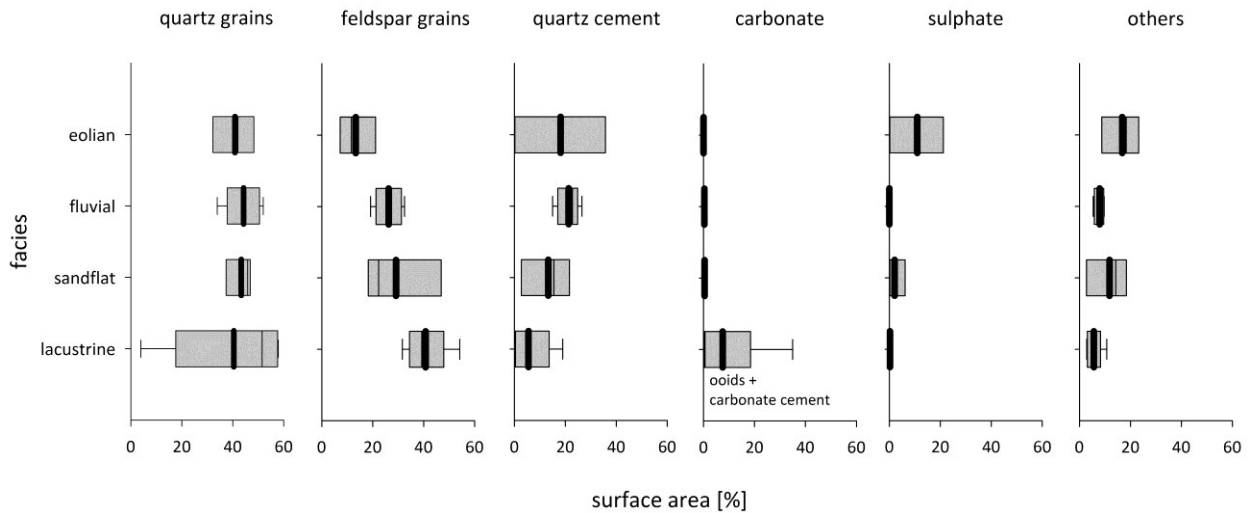
Fig. 56: Measured surface areas in sandstones (without clay coatings) of different facies type. Number of samples is 16 (4 for each facies type). The error bars indicate the 90th and 10th percentiles, thick black lines are the mean values.

6.4.3. Measured surface areas compared with mineral composition

The most important influence on the measured mineral surface area is the mineral composition of sandstone. The detrital composition of sandstone is mirrored in his surface area, but with other proportions. For example there are more feldspars present in the lacustrine sandstones than in the other sandstones, hence also their surface area of feldspar is higher.

The mean contents of quartz grain surface areas are lower than the mean quartz contents in the sandstones; while feldspars have higher surface area than mineral content (Table 7). Especially cements, which were precipitated on grains, are relevant for developing surface areas, which are exposed to the open pore space. Therefore quartz cements, which are present in the sandstones with 3 % to 8 % in the measured samples, are creating surface areas up to 21 % (Table 7). The surface areas of carbonate cements are in average low (between 0 % and 1 %). Only if ooids are present in the sandstones, carbonate mineral surfaces are up to 24 % (mean content in the lacustrine

sandstones is 5.3 %, but the maximum value is 24 %). The surface area of sulphate cement is in average lower than the mineral content.

If illite overgrowth would be more present in the sandstone, their effect would even be more intensive. Because of the minor presence of these clay minerals and the small size, their surface area is not measured with digital image analysis in a mentionable way (main surfaces measured in the sandstones are shown in Fig. 56).

*Table 7: Mean values of mineral contents in sandstones of different facies type, compared with the mean values of mineral surface areas in these sandstones. Mineral content is determined with point-counting. Mineral surface area is measured with digital image analysis. Only sandstones measured for mineral surface areas are compared here (n = 24). Mineral content * x = mineral surface area.*

		quartz grain			feldspar grain			quartz cement			carbonate			sulphate		
		mean content [%]	mean surface area [%]	x	mean content [%]	mean surface area [%]	x	mean content [%]	mean surface area [%]	x	mean content [%]	mean surface area [%]	x	mean content [%]	mean surface area [%]	x
with iron oxide coating	eolian	58.9	31.3	0.53	12.1	18.7	1.55	2.7	10.4	3.85	4.3	0.5	0.12	3.3	1.0	0.30
	fluvial	37.7	13.3	0.35	24.3	14.6	0.60	7.7	21.1	2.74	1.3	0.0	0.00	2.3	0.0	0.00
	sandflat	50.9	24.5	0.48	23.8	14.9	0.63	3.7	13.0	3.51	0.1	0.8	8.00	3.9	0.1	0.03
	lacustrine	62.7	16.2	0.26	16.0	22.3	1.39	4.0	16.0	4.00	0.7	0.0	0.00	0.0	15.9	/
without iron oxide coating	eolian	62.0	40.8	0.66	6.9	13.3	1.93	6.6	18.1	2.74	0.2	0.0	0.00	14.4	11.0	0.76
	fluvial	54.7	44.2	0.81	15.3	26.3	1.72	5.7	21.3	3.74	3.5	0.3	0.09	1.1	0.0	0.00
	sandsflat	53.3	43.3	0.81	24.2	29.1	1.20	3.7	13.3	3.59	1.8	0.4	0.22	0.2	2.1	10.50
	lacustrine	45.5	40.4	0.89	26.3	40.8	1.55	5.9	5.5	0.93	4.9	5.3	1.08	0.9	0.2	0.22

6.5. Sandstone internal surface area evaluated with BET analysis

BET analyses give information about the total mineral surface area within studied sandstone. After Lowell et al. (2004) is the size and the shape of a particle related to his surface area: small sized or irregularly formed particles have higher surface area than large sized or regularly formed particles (in a certain volume). A high BET surface area also indicates a high roughness of grains and minerals inside the sandstone (cf. Anbeek 1992). Especially between "large" grains/authigenic cements (e.g. quartz overgrowth) and "small" clay minerals the difference of surface area is high due to their mineral shape. After Scheffer and Schachtschabel (2009) the specific surface area of synthetic illite is 50 - 200 m^2/g and of hematite is 50 – 150 m^2/g. After White et al. (1996) is the BET surface area of clay: 3 – 20 m^2/g; iron oxyhydroxide: 2 – 3 m^2/g; quartz: 0.1 – 0.2 m^2/g; and of feldspar: 0.4 – 1.5 m^2/g (surface area in clay and feldspar is increasing with weathering state; measured on soil minerals). In the Buntsandstein sandstones the measured surface area with image analysis as well as the measured BET surface area indicates that the most of the surface areas are exposed by iron oxide coatings or quartz and feldspar mineral surfaces, otherwise the BET surface area would be much higher (Fig. 57). Macroscopic features like etch pits or defects in the minerals discovered by optical microscope do not contribute significantly to BET surface area (Anbeek 1992, Brantley et al. 1999). The highest mineral surface area is documented for some sandflat sandstones, probably caused by grain coatings consisting of clay minerals and iron oxide. The sandstones of the eolian and fluvial facies have a low BET surface area due to their mineral composition. The finer grained lacustrine and sandflat sandstones have higher BET surface area (2 m^2/g to 4 m^2/g) than the fluvial and eolian sandstones (approx. 1 m^2/g). Fluvial and eolian sandstones have higher quartz cement content, which may change the shape of the quartz grains from irregular to regular and decrease BET surface area in these sandstones sparsely.
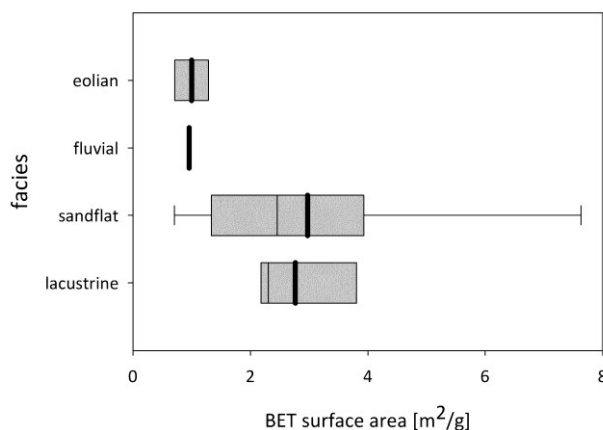
Fig. 57: Surface area measured by BET within Buntsandstein sandstones of different facies types. Number of samples is 26. The error bars indicate the 90th and 10th percentiles, thick black lines are the mean values.

6.6. Reactivity of the rocks

A storage of different gases, like hydrocarbons, carbon dioxide and hydrogen, is possible in sandstones of the Buntsandstein. It is important to know, how these fluids interact with the sandstone reservoir in order to prevent a change in the reservoir quality. For an estimation of sandstone reactivity, the surface areas are the most important factor: fluids react first only with the surface areas inside the rock, not with the whole sandstone.

The reactivity of a rock (or the rock-fluid-interaction) is predominantly influenced by the following factors:

- Permeability and connectivity of pores are important for some dissolution processes, because flowing fluids are necessary for ion transport (Bjorlykke et al. 1989).
- The mineral roughness, which is influenced by the size of the surface area (BET surface area) measured on a sandstones sample (cf. Fischer & Gaupp 2004). The reaction rate between mineral and fluid is affected by this roughness. A rock composed of highly rough minerals exhibit a high BET surface area and therefore a high area of potential reaction.

- The petrography, because the dissolution rate of a component depends on the kind of mineral (cf. Holdren & Speyer 1985). It is relevant which mineral surface is in contact with the fluid.

- The kind of fluid interacting with the rock. For example: the fluids hydrocarbons or CO_2 may cause acidic conditions by forming organic acid (Surdam et al. 1993) or carbonic acid (Rochelle et al. 2004); the gas hydrogen in aqueous solution may react with sulphur to hydrogen sulphide (Foh et al. 1979); the fluid water may oxidise iron minerals, if it is oxygen rich, and under-saturated waters may dissolve sulphate and salt minerals (e.g. meteoric waters).

6.6.1. Reactivity of mineral surfaces

Iron oxide coating

Many grains in the sandstones are covered with coatings or cutans. Hence the reacting surface area is first the coating, than the grain below it. On approximately half of the Buntsandstein sandstones clay coatings around grains are present. In these reddish stained sandstones about 40 % of mineral surfaces are iron oxide coatings mixed with clay mineral cutans (Fig. 55).

A reaction between iron oxide and liquid hydrocarbon in sandstones were discussed by many authors, the consequences for sandstone are redox reactions, bleaching and enhancement of porosity (e.g. Surdam et al. 1993, Parry et al. 2004, Ajdukiewicz et al. 2010).

Quartz and feldspar

Quartz is a very resistant mineral and the dissolution rate in shallow depths is low (Dove & Elston 1992). The dissolution rate of plagioclase and K-feldspar is higher than of quartz in acidic fluids (Holdren & Speyer 1985). Plagioclase grains are more instable than K-feldspar grains in acidic fluids (cf. Nesbitt et al. 1997), but the abundance of

plagioclase in the sandstones is only < 1 % and their mineral surface areas are insignificant for reactions.

Carbonate and sulphate

The most abundant cements in the Buntsandstein sandstones are the carbonate and sulphate cements. Carbonate cements will be dissolved in contact with acidic fluids. Sulphate cements and salt can be dissolved by under saturated waters (e.g. meteoric water). Also a thermochemical sulphate reduction of sulphate minerals caused by hydrocarbons is possible (Cross et al. 2004).

6.6.2. Assumed reactivity of the facies types

After all factors were taken into account, the reactivity for the Buntsandstein sandstones is expectable. The estimated reactivity for the four facies types of the sandstones is summarized in Table 8.

Table 8: Estimated reactivity for the Buntsandstein sandstones. Important factors are surface area and mineralogical composition as well as permeability of the sandstone.

depositional environment	fluid flow	BET surface area/ pore density	mineral surface areas/ (petrography)	expected reaction
lacustrine	low permeability (about 4 mD)	high BET surface area (about 3 mm²/g); high pore density	feldspars and carbonate	carbonate and feldspar dissolution
sandflat	medium permeability (about 27 mD)	high BET surface area (about 3 mm²/g); medium pore density	grain coatings are common	bleaching and alteration of grain coatings
fluvial	medium permeability (about 58 mD)	low BET surface area (about 1 mm²/g); medium pore density	quartz, quartz cement and feldspar (carbonate and sulphate)	carbonate, sulphate, feldspar dissolution
eolian	high permeability (about 109 mD)	low BET surface area (about 1 mm²/g); low pore density	low content of feldspars, high content of gypsum	dissolution of gypsum

Lacustrine sandstones

Relatively high BET surface area, high frequency of small pores and pore diameter indicate a large area of mineral-fluid-interaction. Instable minerals like feldspars and carbonate ooids and cements form up to 60 % of the total mineral surfaces in many lacustrine sandstones. A mineral reaction or corrosion on these mineral surfaces is probable, if the fluid is acidic and the permeability is high enough for fluid flow.

Sandflat sandstones

The high BET surface area and the internal roughness of the rocks is supporting a reaction between mineral and fluid. This roughness is predominantly caused by iron oxide coatings mixed with clay minerals. A reaction with acidic fluids will increase porosity (cf. Surdam et al. 1993). This is important for potential hydrocarbon storage in the Buntsandstein sandstones, because acidic fluids caused by hydrocarbons may change the pore space.

Fluvial sandstones

BET mineral surface area is relatively low, due to smooth mineral surfaces of detrital quartz and quartz cements (Fig. 56) and the low abundance of clay cutans and matrix. Carbonate and sulphate minerals are present in the fluvial sandstones, but the measured mineral surface area of them is very low (Fig. 56). Assumed reactivity of fluvial sandstones is only minor due to the absence of instable cements and/or detrital grains in the measured mineral surface areas. A corrosion of feldspars and carbonate cements in an acidic environment is possible.

Eolian sandstones

High permeability supports reactivity in these rocks, but the internal roughness is low due to a low BET surface area. Many surface areas consist of sulphate cements, which are susceptible to under-saturated waters. Dissolution in contact with meteoric water is expected (see also chapter 5.3.).

7. Discussion: burial history, mineral surfaces and regional comparison

7.1. Influence of the burial history on the evolution of reservoir quality

Due to the burial depth and the predominant P/T and chemical conditions, the diagenesis processes have been different in the Buntsandstein sandstones during eo-, mesodiagenesis and telodiagenesis (Fig. 40 and Fig. 58). The burial history of the Buntsandstein sandstones in the Thuringian Syncline depend on by their location, i.e. centre or margin of the syncline. The maximum depth and temperature during burial are influenced by the subsidence phase and the present depth of the sandstones is influenced by the uplift phase. Some processes of the telodiagenesis (telo B, see chapter 5.4.1.) are only been present in sandstones uplifted to a depth less than 160 m, at the margin of the syncline. All Buntsandstein sandstones from the Thuringian Syncline centre have been buried deeper than 2000 m and were heated to temperatures higher than 100°C during mesodiagenesis (see chapter 4.4. for thermal evolution).
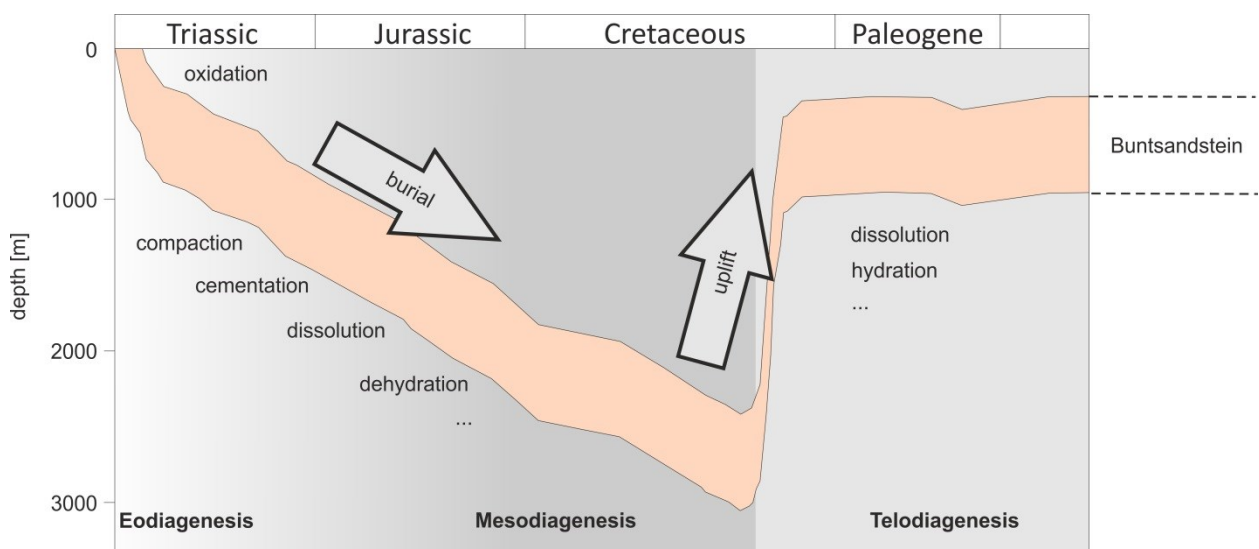
Fig. 58: Sketch of the connection between burial history and diagenesis. See also Fig. 40 for the paragenetic sequence. Burial history of the Buntsandstein is from virtual well C (centre of the Thuringian Syncline).

The higher calculated thicknesses of Jurassic and Cretaceous sediments in the central part of the Thuringian Syncline indicate that this part of the syncline was buried deeper than the rest of the syncline during Jurassic and Cretaceous times. This part can be interpreted as a paleo-graben in the centre of the Thuringian Syncline, which has been active during Jurassic and Cretaceous times. The paleo-graben described in chapter 4 suggests that the sandstones from borehole 3, 4, 6 and 8 (boreholes located in the area of the paleo-graben, Fig. 59) differ with respect to their thermal history, diagenesis and compaction rate than the other sandstones from outside of the paleo-graben due to their deeper burial. Sediments of the graben area were 700 m deeper and temperature was 20°C higher than outside of the graben during maximum burial.
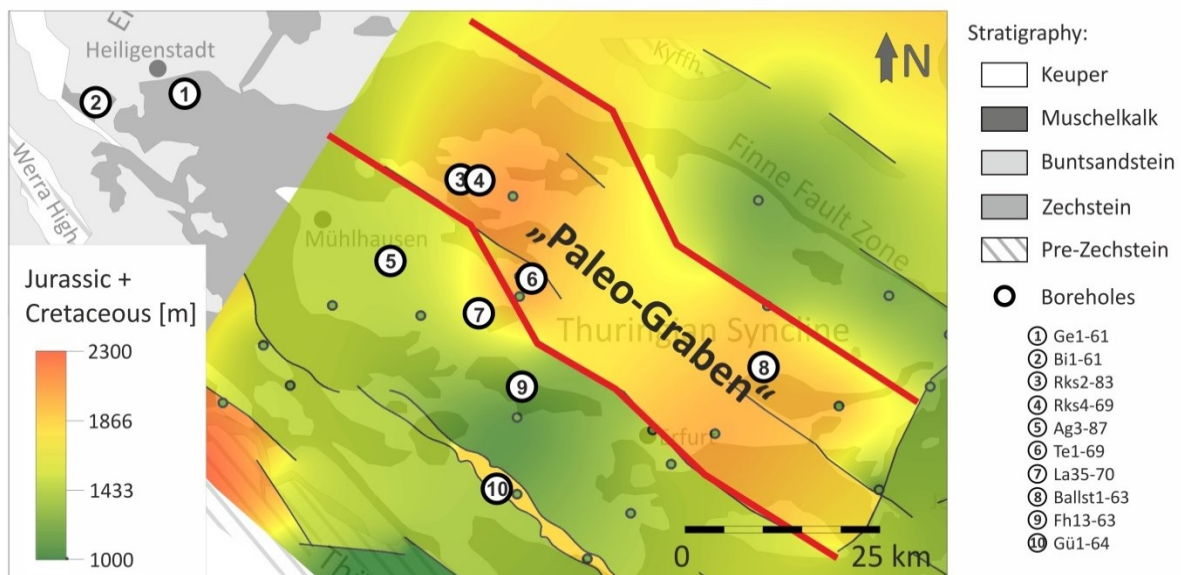
Fig. 59: Boreholes inside and outside of the interpreted paleo-graben structure. Inside the paleo-graben the Buntsandstein sediments were about 700 m deeper than outside at the end of Cretaceous time. Map in the background is modified after Puff 1994; black faults after Franke 2014.

The abundance of authigenic minerals, porosity loss by cementation/compaction and petrophysical properties for the sandstones from inside and outside the paleo-graben are shown in Fig. 60. It was possible to compare sandflat, fluvial and eolian sandstones from outside the graben with sandstones from inside the paleo-graben. Carbonate cements are slightly more abundant in the sandstones from outside the paleo-graben, whereas sulphate cements are more abundant inside the graben (especially in the fluvial sandstones, Fig. 60). Cementation or dissolution of these cements might have been influenced by the contact with different pore water in the deeper subsurface. The

relatively early precipitation of quartz was not affected by the subsidence situation in the basin (Fig. 60). Illite meshwork is more abundant in the sandflat sandstones from outside the graben in comparison with inside the graben (Fig. 60). This is in accordance with the amount of mean secondary porosity by feldspar dissolution, which is slightly higher outside of the paleo-graben (1.3 %) than inside (0.6 %): feldspar dissolution is the major ion source for potassium, aluminium and silicium, and therefore feldspar dissolution controls the growth of authigenic illite. However, increased illite growths or chlorite minerals inside the graben due to higher temperatures were not observed. This is unusual, because according to the common knowledge (e.g. Platt 1993) illite precipitation could start above a kinetic temperature threshold of 70°C and differences in temperature could influence the growth of illite (or chlorite) minerals. Due to higher sulphate cement content in the fluvial sandstones from the paleo-graben, the porosity loss by cementation is higher (and the porosity loss by compaction is lower) than in the sandstones from the surround area (Fig. 60). Eolian sandstones contain more carbonate cement outside the paleo-graben than inside the paleo-graben (mean sulphate and quartz cement content is equal), and hence the porosity loss by cementation is also higher for the eolian sandstones from outside the paleo-graben. In consequence the mean porosity and permeability (and therefore reservoir quality) in the eolian sandstones is slightly lower outside and higher inside the paleo-graben (Fig. 60). Hence, the maximum burial depth had slightly influenced the diagenesis in the Buntsandstein sandstones. It is likely that a change of fluid pathways by a deeper burial in the paleo-graben sediments caused a less pronounced growth of authigenic illite, enhanced precipitation of sulphate cement in the fluvial sandstones and dissolution of carbonate cement in the eolian sandstones.
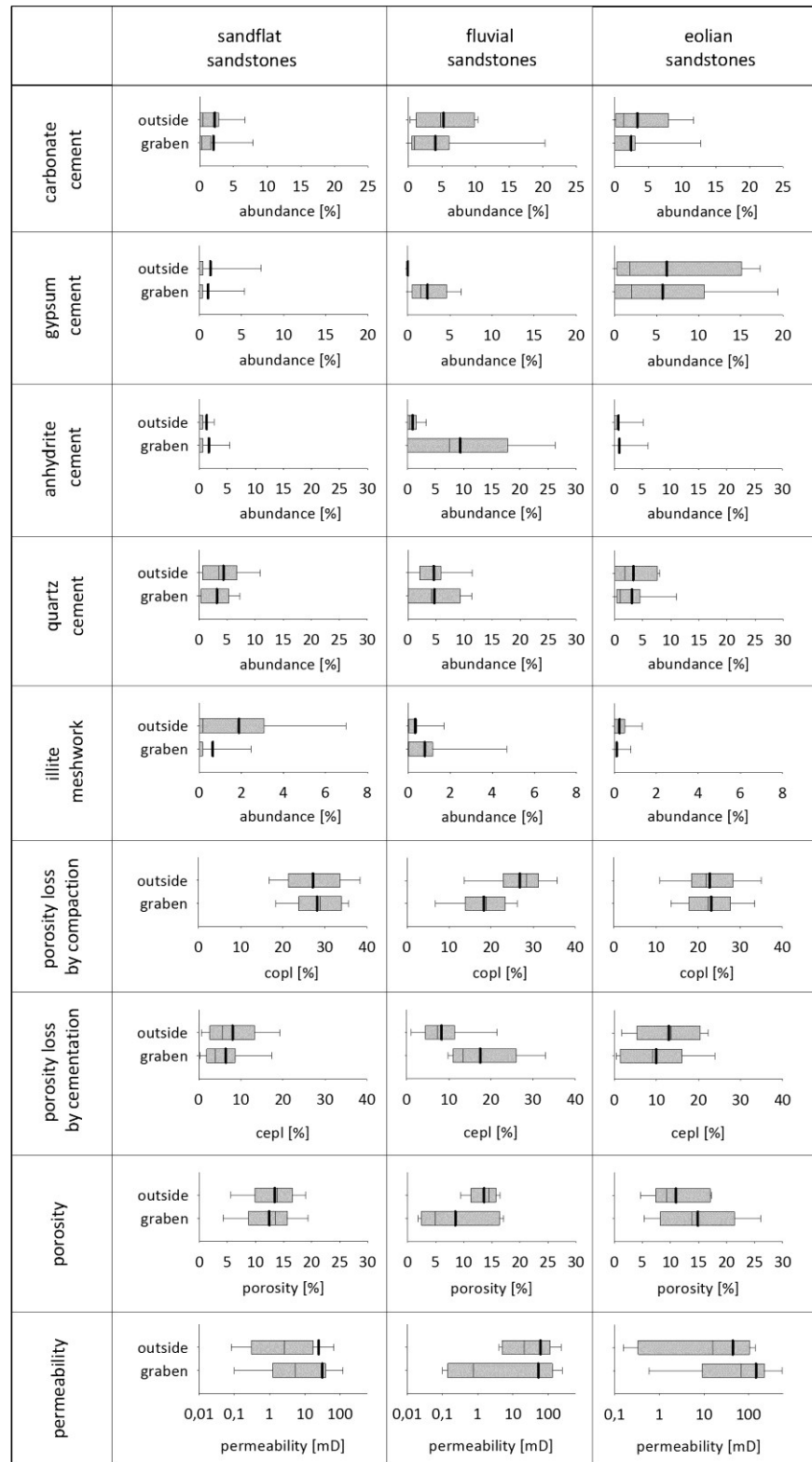
Fig. 60: Sandstones from inside the paleo-graben (location: graben) compared with sandstones from the same facies type, but outside of the paleo-graben (location: outside). All analyzed lacustrine sandstones are from the interior graben. For this reason lacustrine sandstones are not compared with other facies types. The error bars indicate the 90th and 10th percentiles, and the thick black lines represent the mean values.

The modelled burial history indicates that Zechstein source rocks have been buried into depths of the oil and gas window. For this reason it is likely that hydrocarbons were theoretically able to ascend from the Zechstein source rocks to potential reservoir rocks. Hydrocarbons were observed in the Zechstein rocks and in the sandstones of the Middle Buntsandstein in the west of the Thuringian Syncline (Kästner 2003). Hydrocarbon migration and the required temperatures are reached, as it has been proven in the burial history simulation of this study (see chapter 4.1.)

As there are no iron oxides in the investigated bleached sandstones, it is very likely that a reaction between the sandstones and the hydrocarbons took place due to the migration of hydrocarbons into the Buntsandstein sandstones during diagenesis. The relationship between hydrocarbon-migration and bleaching has been described by Surdam et al. (1993). He describes, that combined with the bleaching also dissolution of carbonates by acidic acids takes place. Natural gas in the Buntsandstein has been found only in a few boreholes in the west of the Thuringian Syncline (Fig. 5), but iron oxide coatings are absent in many Buntsandstein sandstones from the entire Thuringian Syncline. As the most Buntsandstein sandstones do not contain natural gas today, the absence of the hematite could be either primary (that means, hematite have never been formed) or secondary (hematite has been dissolved during chemical bleaching). With the bleaching process also a precipitation of pyrite and chlorite is accompanied (Shebl & Surdam 1996), but these minerals are not present in the Buntsandstein sandstones. Therefore the absence of iron oxide cutans in some sandstone is probably primary or caused by pre oil acidic fluids.

The calculated porosity of the Buntsandstein sandstones, based on porosity/depth curves with an expected maximum depth of 3.2 km, should theoretically be between 7 % and 22 % (according to the diagram of Giles 1997), or around 13 % (according to the diagram of Ehrenberg et al. 2009). The measured helium-porosities of the analysed Buntsandstein sandstone samples are approximately between 11% and 14 %, depending on the facies type. The measured mean helium porosities are in the same range of the calculated mean porosity from the porosity/depth curves; hence the calculated maximum burial depth for these sandstones is realistic. Furthermore it means that the sandstones are predominantly affected by compaction than cementation, which is approved in chapter 5.3. (in this chapter the factors on porosity and permeability evolution are described).

7.2. The connection between depositional environment, diagenesis, porosity/permeability and sandstone reactivity

Due to their depositional environment, the sandstones of the Buntsandstein differ in sandstone architecture, sand to clay ratio, sandstone texture, petrography, diagenesis, porosity/permeability, pore space distribution and mineral surface areas. The connections between these parameters for the sandstones of different depositional environment are described in the following text.

Lacustrine sandstones

The particular features for the lacustrine sandstones are high feldspar content and occurrence of ooids. The high content of carbonate cement in the lacustrine sandstones is very likely related to the partially dissolution of ooids and a primary oversaturated pore water with respect to carbonate. The small grain size and a related relative high mechanical compaction as well as a high content in carbonate cement are reasons for a low frequency of large pores (pore category III and IV). This is an indication of poor porosity and permeability characteristics. The frequency of small pores is high in the lacustrine sandstones. A high frequency of small pores also results in a high pore density. The high pore density and the low porosity lead to poor pore connectivity in the lacustrine sandstones. Well-connected pores are rare in the lacustrine sandstones. The secondary porosity in the sandstones is probably caused by dissolved feldspar grains. Due to both, feldspar dissolution and a small grain size, the lacustrine sandstones also have the highest determined microporosity. The microporosity cannot be measured with digital image analysis due to the small size of the pores. It can be assumed, that these small pores are also not available for fluid flow, because the porosity measured with image analysis shows a stronger correlation with the permeability than with the porosity measured with Helium. With regard to the pore-mineral interfaces which are exposed to the open pore space, the reactive minerals are predominantly feldspars, ooids and carbonate cements in the lacustrine sandstones. These minerals are all reactive in contact with acidic fluids in the future (cf. Morad 1998, Zhu et al. 2006). They are available for dissolution by acid treatment / or acid natural groundwater and an enhancement of porosity.

Sandflat sandstones

A relatively high amount of clay cutans and matrix is generally abundant in the sandflat sandstones. Detrital feldspars are frequent, but not as often as in the lacustrine sandstones. The presence of inherited iron oxide cutans and clay coatings in the sandflat sandstones inhibited the precipitation of quartz cement and other blocky cements (cf. McBride 1989, Lander & Walderhaug 1999). In sandstones that contain clay matrix between the clasts, the precipitation of fabric supporting quartz cement, carbonate and sulphate cements did not take place. This and the mechanical softness of matrix as well as the chemical dissolution at the clay (matrix)-quartz boundary lead to a higher compaction state in sandstones with primary matrix. Hence the mean compactional porosity loss is higher than in the other facies types. Large pores are rare due to the intensive compaction and the sporadic cements, but they are more abundant than in the lacustrine sandstones. Therefore the mean permeability is higher than in the lacustrine sandstones, but not as good as in the fluvial or eolian sandstones. The internal mineral surface area (BET) is also higher due to the frequent presence of iron oxide coatings in combination with clay minerals. Thus a large reactive surface area is available for fluid-mineral reaction (cf. Fischer & Gaupp 2004), but as the permeability is low, fluid flow and reaction rates are potentially low. However, the sandflat sandstones are highly diverse and the clay content is not high in all sandstones. Between 15 % and 20 % of the pore-mineral interfaces occur in large and very large pores in the sandflat sandstones. In these pores a reaction between the minerals and the fluid can likely take place. Based on the proximity to the pores and on the pores in which the minerals appear, the minerals will react in the following sequence with a pore fluid: first the iron oxide cutans and the cements will react with the fluid, then the detrital grains. A bleaching of the sandstones is possible due to a reduction of the iron oxide minerals.

Fluvial sandstones

The feldspar content is lower in the fluvial sandstones than in the lacustrine and sandflat sandstones, but the carbonate, sulphate and quartz cement contents are higher. In the fluvial sandstones the mechanical compaction is lower than in the other facies types, due to the fabric supporting early quartz cement and the low clay content (cf. Lander & Walderhaug 1999). Low mechanical compaction results in a relatively high

abundance of large pores. The frequency of large pores and the pore connectivity is also better than in the lacustrine or sandflat sandstones, but not as high as in the eolian sandstones. The abundance of large pores, the relative large grain size and the good sorting lead to relatively good porosity and permeability. High permeabilities ensure a fluid flow and therefore a contact between mineral and fluid. The mineral surfaces areas predominantly consist of quartz (detrital grains and cement) and minor feldspar. Carbonate and sulphate cement are enclosed between grains and hence they are not available for mineral-fluid reaction. The assumed reactivity of the fluvial sandstones is relatively low, due to a minor abundance of instable minerals in contact with a potential fluid.

Eolian sandstones

The eolian medium- to coarse-grained sandstones have relatively low feldspar content. This facies type typically contains a higher amount of fabric supporting and pore-occluding sulphate cement than in the other facies types. Therefore is the cementational porosity loss relatively high and the compactional porosity loss is low. The frequency of large pores is also higher than in the other sandstones, because the amount of large pores normally correlates positively with the mean grain size. Nevertheless the eolian sandstones lost a part of their primary large pores by cementation, because a supersaturated fluid prefers larger pores instead of small pores for precipitation (cf. Putnis & Mauthe 2001, Pape et al. 2005). In sandstones with a great amount of pore-filling blocky cement the frequency of large pores is lower. This leads to the evidence that large pores can evolve from the dissolution of originally cemented large pores (formed early in diagenesis). But generally the overall porosity and permeability situation in the investigated rocks is relatively good due to the frequent occurrence of large pores and the low frequency of clay. 20 % to 25 % of the pore-mineral interfaces are located in larges pores. Important mineral surfaces exposed to open pore space in the eolian sandstones are detrital quartz, authigenic quartz and sulphate cement. The frequency of feldspar surface areas is lower than in the other facies types. Moreover quartz is a stable mineral in respect to dissolution, the sulphate cement has a higher solubility in water and therefore dissolution by infiltrating undersaturated water can be assumed. Due to the presence of sulphate cement in formerly large pores, dissolution would open these pores and the porosity/permeability would intensively increase. This

process took place in eolian sandstones near the margin of the Thuringian Syncline at shallow depths (see chapter 5.4.2.).

7.3. Comparison of the Thuringian Buntsandstein with other Middle European locations
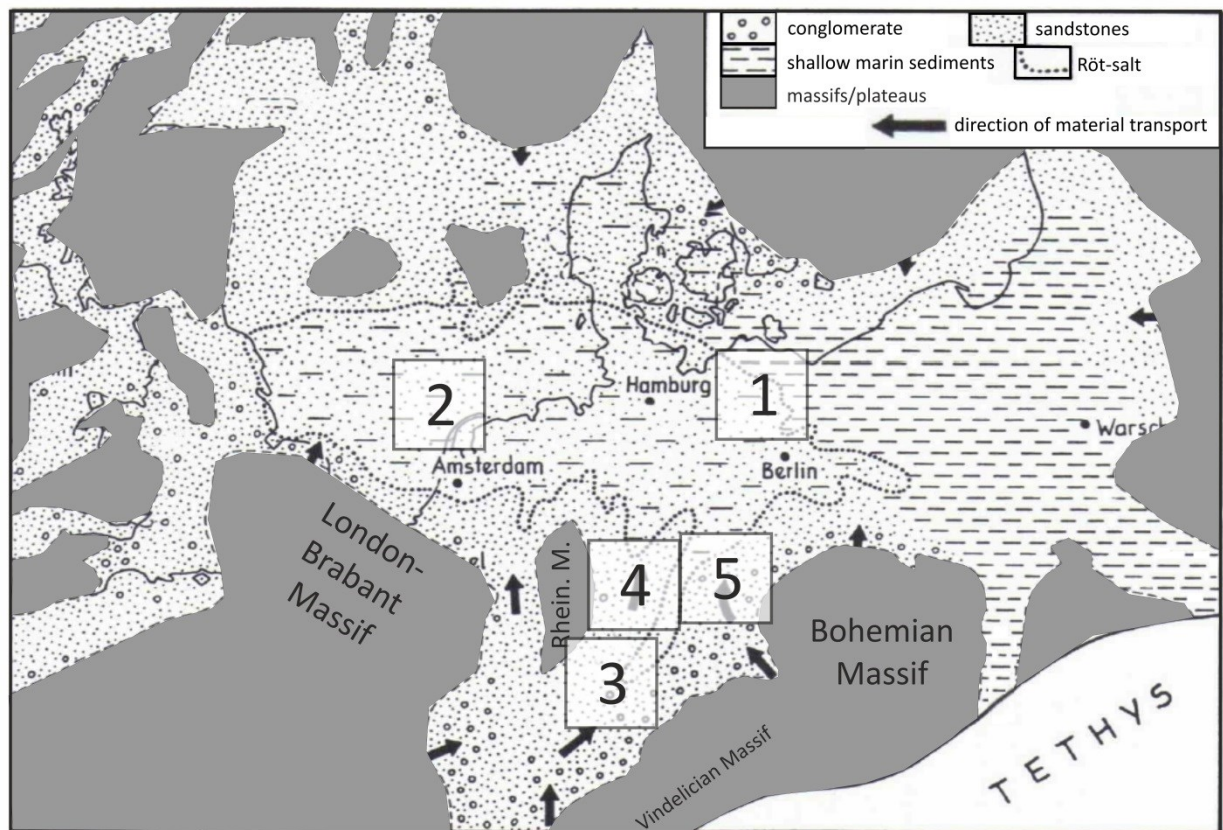
Fig. 61: Locations of the Buntsandstein sandstones, which were compared with the Buntsandstein from the Thuringian Syncline (paleogeographic map of the Buntsandstein modified after Faupl 2000). 1 – North German Basin, 2 – Netherlands, 3 – SW Germany, 4 – Hesse, 5 – Thuringia.

Buntsandstein sandstones were compared from different locations out of the Central European Basin (Fig. 61): the North German Basin [1] in the northeast, The Netherlands [2] in the central west, Southwest Germany [3], Hesse [4] and other locations of Thuringia [5] in the south. Their features are compared in Table 9. The locations near the centre of the Central European Basin ([1] and [2]) are characterized by sediments of a distal sedimentary basin and a shallow marine influence, whereas the locations in the south ([3],[4] and [5]) have been deposited in a more proximal area of the basin with

conglomerate input (Fig. 61). Nevertheless, for these locations the authors describe predominantly the fluvial and eolian sediments, because they are the most suitable reservoirs. The present depth of the Buntsandstein sediments vary due to their different burial and uplift history (Fig. 62): e.g. the Central North German Basin or the Central Graben has not been uplifted. In contrast, the sediment of the Thuringian Syncline were 1.5 - 3 km uplifted (Fig. 16).
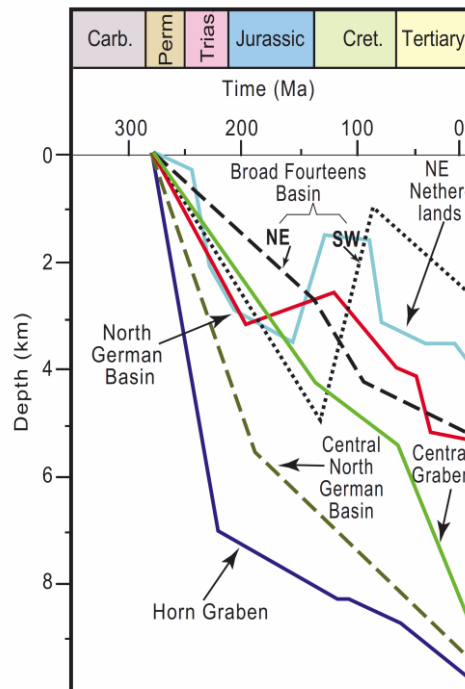
Fig. 62: Burial history curves from different locations. North German Basin shows only small amounts of uplift, whereas parts of the Netherlands were uplifted by some kilometers. The lines reflect the basin depocentres; graphic from Gaupp & Okkermann (2011), modified after Ziegler (2006) and Cornford (1998).

The sandstones are mostly described as fine to medium grained with a various sorting and usually they are classified as arkose or subarkose (lithic fragment content is increasing with decreasing material transport way). These characteristics are consistent with the sandstones from the Thuringian Syncline. Ooids are more abundant in the northern part near the centre of the basin ([1] and [2]). In Thuringia ooid-bearing sandstones are present, but they do not occur in the area south of Thuringia. In general (red coloured) clay cutans and primary matrix are abundant at all locations ([1]-[5]); in many studies a bleaching of reddish to greyish sediments is described. The cements carbonate, sulphate, quartz and feldspar are abundant in the sandstones of all locations.

The clay minerals illite and kaolinite are described in most studies. Chlorite is abundant in sandstones, which experienced a deep burial with relative high temperatures, like sandstones from the North German Basin, Rhine Graben or the Netherlands (see Table 9). Porosity and permeability values show a high variance. Sandstones from the North German Basin have relatively high porosity (25 % – 30 %) and permeability (> 500 mD) values (Wolfgramm et al. 2008), probably caused by early stabilizing cements and a dissolution of them later in the mesodiagenesis. The detrital composition of the sandstones from the North German Basin is like the composition of fluvial or eolian sandstone from the Thuringian Buntsandstein. A high percentage of eolian sandstones could be a reason for high permeability values in the North German Basin (cf. Wolfgramm 2002). The porosity (5 % – 20 %) and permeability (0.01 mD – 150 mD) of the Buntsandstein sandstones from the Netherlands (Purvis & Okkerman 1996) are relatively similar to the Thuringian Syncline, even if the sandstone composition is different (ooids, halite and chlorite are present)(Table 9). The Buntsandstein sandstones from SW Germany have higher lithic fragments content and the porosity and permeability is comparable with the Buntsandstein sandstones from the Thuringian Syncline (Table 9). The main factors influencing porosity and permeability are facies, texture, compaction, cements and clay minerals. Also bleaching processes by hydrocarbons (The Netherlands, Geluk 2007), CO_2 (Hesse, Wendler et al. 2012) or hydrothermal fluids (Rhine Graben, Baaske 1999) influenced the porosity and permeability.

Table 9: Listed features of the Buntsandstein sandstones from different locations compared with the Buntsandstein from the Thuringian Syncline. Locations are shown in Fig. 61. Indirectly description is in () and not described is - (su – Lower Buntsandstein; sm – Middle Buntsandstein).

author	this work	Paul (1982)	Wolfgramm (2002)	Wolfgramm et al. (2008)	Purvis & Okkerman (1996)	Geluk (2007)	Leggewie et al. (1977)	Baaske (1999)	Junghans (2003)	Klapperer (2009)
location	**Thuringian Syncline**	**North German Basin [1]**			**Netherlands [2]**		**SW Germany [3]**			
stratigraphy	su + sm	su	su + sm	sm	sm	su + sm	sm	su + sm	sm	su + sm
depth	0 – 1040 m	-	1100 – 2800 m	1300 – 2100 m	3600 - 4300 m	0 – 7000 m	-	0 m	300 – 470 m	0 – 2900 m
main facies type	lacustrine, sandflat, fluvial, eolian	playa lake	fluvial, eolian	-	fluvial, eolian	fluvial, eolian	fluvial, eolian	fluvial	fluvial	fluvial, eolian
mean grain size	fine-medium	fine	-	fine - medium	fine - medium	-	various	fine - medium	medium - coarse	fine - coarse
mean sorting	moderately well - well	-	poor - well	moderately well - well	moderately - well	-	-	fine - coarse	poor - well	moderately - well
detritus	arkose - subarkose	-	subarkose	subarkose	arkose - sublitharenite	(sub-)arkose	subarkose	lithic subarkose	-	subarkose - litharenite
ooids	rare	oolithic	-	traces	rare	oolite beds	-	-	-	-
clay cutans / matrix	0 – 40 %	yes	0 – 20 %	10 – 16 %	yes	yes	yes	0 – 4 %	yes	yes
bleaching	yes	yes	-	-	(yes)	-	-	yes	-	yes
fluids/hydrocarbons	natural gas?	-	(gas)	-	gas	gas	-	hydrothermal fluids	-	bitumen
blocky cements	carbonate, sulphate, quartz, feldspar	carbonate, sulphate, quartz	carbonate, sulphate, quartz	carbonate, sulphate, rarely pyrite and galenite	carbonate, sulphate, halite, quartz	carbonate, quartz, halite	quartz, carbonate, sulphate, feldspar	quartz, feldspar, jarosit	?	quartz, carbonate, feldspar
clay minerals	illite, kaolinite	-	illite, kaolinite, chlorite	illite, kaolinite, glauconite	illite, chlorite	-	illite	illite, kaolinite, chlorite	(illite)	illite
max. burial depth	3200 m	-	(3000 m)	-	-	-	-	3200 m	-	-
max. burial temp.	140 °C	-	-	-	-	-	-	-	-	-
uplifted	yes	-	slightly	-	-	-	-	yes	-	-
mean porosities	11 – 14 %	-	-	25 – 30 %	5 – 20 %	-	-	9 – 20 %	8 – 11 %	5 – 23 %
mean permeabilities	4 – 110 mD	-	-	>500 mD	0.01 – 150 mD	-	-	0 – 1900 mD	0.09 – 1 mD	0.01 – 700 mD

Table 9 continuation

author	this work	Wendler et al. (2012)	Langbein (1985)	Lang (2001)	Maaß (2010)	Fensterer (2009)	Fritsch (2010)	Hilse et al. (2010)
location	**Thuringian Syncline**	**Hesse [4]**	**Thuringia [5]**	**West + East Thuringia [5]**	**SE Thuringia [5]**	**East Thuringia [5]**		**SW Thuringia [5]**
stratigraphy	su + sm	su	s	sm	su	su	su + sm	su + sm
depth	0 – 1040 m	30 – 80 m	-	0 – 455 m	0 m	0 m	0 – 240 m	-
main reservoir facies	lacustrine, sandflat, fluvial, eolian	-	fluvial, lacustrine, eolian	lacustrine, fluvial	lacustrine, fluvial, eolian	lacustrine, fluvial, eolian	fluvial, eolian	fluvial
mean grain size	fine-medium	fine-medium	fine-medium	fine - medium	fine-medium	fine-medium	fine-coarse	fine-medium
mean sorting	moderately well - well	-	poorly- well	moderately well - well	poorly- well	well	moderately - well	-
detritus	arkose - subarkose	arkose - subarkose	feldspathic litharenite - arkose	subarkose	feldspathic litharenite	subarkose – lithic subarkose	subarkose	subarkose
ooids	rare	-	yes	-	-	yes	yes	-
clay cutans and matrix	0 – 40 %	yes	yes	yes	yes	yes	yes	yes
bleaching	yes	yes	yes	yes	yes	(yes)	(yes)	yes
fluids/hydrocarbons	natural gas?	CO_2	-	-	-	-	-	CO_2
blocky cements	carbonate, sulphate, quartz, feldspar	carbonate, quartz, feldspar	carbonate, sulphate, quartz, feldspar, pyrite	carbonate, quartz (+karneol), feldspar, sulphate,	quartz, sulphate	carbonate, quartz, feldspar	quartz, carbonate, feldspar	carbonate, quartz, feldspar
clay minerals	illite, kaolinite	illite, chlorite	illite, kaolinite	illite	illite, kaolinite	illite, chlorite	illite, kaolinite	illite, chlorite
max. burial depth	3200 m	-	1500 m	-	-	-	-	-
max. burial temp.	140 °C	-	-	-	-	-	-	-
uplifted	yes	yes	yes	-	-	-	-	-
mean porosities	11 – 14 %	4 – 18 %	-	-	-	-	5 – 11 %	-
mean permeabilities	4 – 110 mD	0.1 – 10 mD	-	-	-	-	-	-

The primary characteristics of the sediments were influenced by the topography and the associated depositional facies. The paleo-topographic map in Fig. 63 shows where the different depositional environments were formed. The arid to semi-arid climate and the low angle dipping formed a fluvial plain with a branched braided river system. Closely to the erosion area channel deposits were predominant and the lithic fragment content was increased (Buntsandstein from South Germany). Northwards the depositional environment was characterized by migratory rivers, sheet floods, floodplains, lakes and dune sands (results are alternating sandstones and mudstones with eolian input, what matches with the sediments of the Thuringian Buntsandstein). The sediments of the North German Basin or The Netherlands show shallow marine influence and a sabkha-like depositional environment (Ziegler 1990). The higher subsidence of the basin centre also resulted in a greater layer thicknesses (cf. Mazur et al. 2005). The abundance of oversaturated water with respect to carbonate caused the formation of ooliths and stromatolites (Paul 1999b).
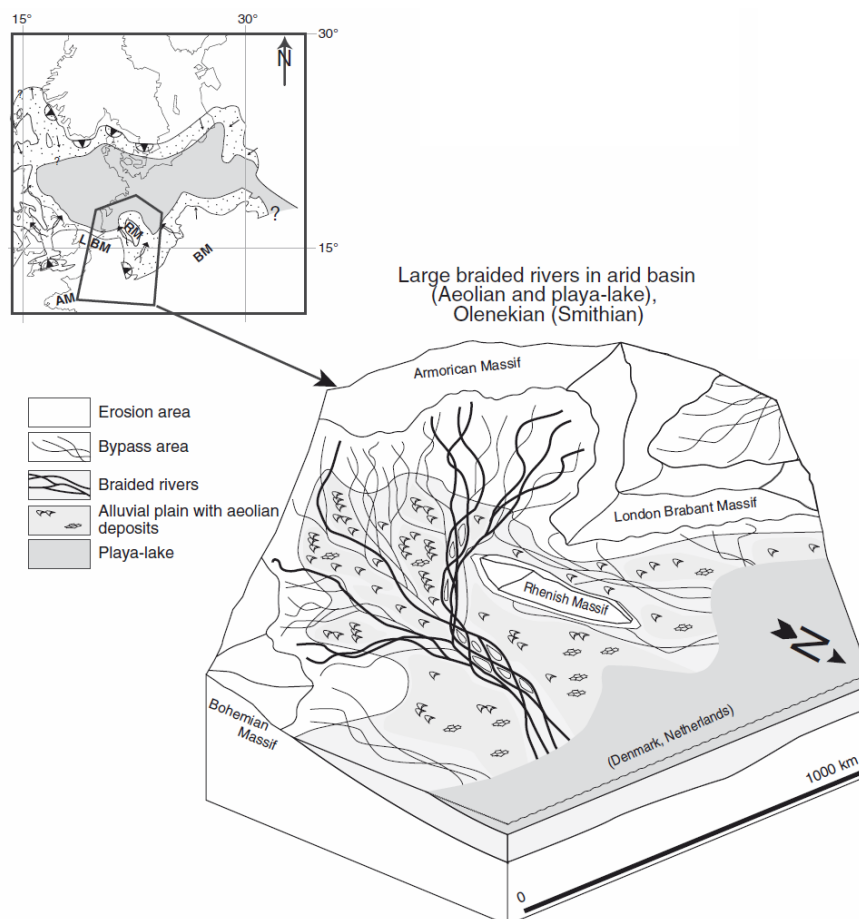
Fig. 63: The Lower Triassic paleo-topographic map with depositional environments (Bourquin et al., 2009) from the Hinterland to the centre of the Central European Basin. The sedimentation is affected by braided rivers, a large alluvial (fluvial) plain with eolian dune sands and a playa-lake at the centre of the basin.

8. Conclusions

The depositional environment influenced the diagenesis as well as the porosity and permeability evolution of the Buntsandstein sandstones during burial history. The following conclusions are relevant for the future use of Buntsandstein aquifers, e.g. for geothermal energy or underground storage wells.

Burial history

a) The Thuringian Syncline was influenced by an extensional phase in the middle Mesozoic and a contractional phase in the end of the Mesozoic. Fault-related subsidence caused the evolution of a graben structure downthrown by 500 m to 650 m in the axis of the Thuringian Syncline in post-Triassic time.

b) During the Late Cretaceous shortening event normal faults in the centre of the Thuringian Syncline were reactivated as reverse faults and set to nearly zero displacement. This shows that the inversion, which is well documented for sub-basins of the North German Basin system (e.g. Lower Saxony Basin, Central Graben, Polish Trough and the Central Netherland Basin) was also active on the southern basin margin.

c) The Buntsandstein sandstones reached temperatures up to 120°C in the centre of the syncline during burial. Some Buntsandstein rocks acted as reservoirs for ascending gas from Zechstein source rocks, which reached the temperature of the gas window. It is likely that hydrocarbons affected the diagenesis of Buntsandstein rocks in the vicinity of faults, where the gases were ascending.

Sedimentology, petrography, petrophysics and diagenesis

a) Eolian sandstones are the best aquifers and reservoirs, followed by the fluvial, sandflat and lacustrine facies types.

b) The Buntsandstein sandstones lost a great amount of porosity by mechanical compaction during burial. The maximum burial depth of the Buntsandstein sandstones was with 3200 m (centre of the Thuringian Syncline) much higher than their depth today. Buntsandstein sandstones from the North German Basin or the Rhine Graben were buried to comparable depths, but exhibit higher porosity and permeability values.

c) The dissolution of cements, e.g. gypsum, may increase the permeability at least by an order of magnitude. This situation has occurred in areas, where the Buntsandstein sandstone where uplifted to depths < 160 m. This enables meteoric water to infiltrate the sandstones during telodiagenesis (during Paleogene and Neogene times).

d) In the Lower Buntsandstein the mean permeability of sandstone in the central syncline is low. Reasons are small grain sizes and high cement content according to the predominant lake environment. In the Middle Buntsandstein sandflat, fluvial and eolian sandstones are common. These sandstones have moderate to good permeabilities because of their larger grain size and lower cement content.

Pore space and mineral surface areas

a) The facies type also influences the structure of pores in the Buntsandstein sandstones. In lacustrine sandstones the amount of small pores is very high, in contrast the eolian sandstones have a high amount of large pores.

b) In sandstones with clay coatings on grains, other mineral surfaces exposed to open pore space are present only in small amounts. In sandstones without clay coatings the petrography influences the mineral surface area significantly. In lacustrine sandstones the mineral surfaces of feldspar are higher than in the other sandstones, while eolian sandstones show less feldspar but more quartz and sulphate cement surface areas.

c) The BET surface area is high in the sandflat and lacustrine sandstones, because they have a high clay (mineral) content or a large amount of small pores and less quartz cement overgrowths.

d) Potential reactions between rock and fluid depend on the fluid type, permeability, petrography of the rock and the mineral surface area inside the rock. These reactions are more likely than others for the sandstones: carbonate dissolution (lacustrine sandstones), iron reduction (sandflat sandstones) and sulphate dissolution (eolian sandstones).

The Buntsandstein sandstone is a good example that texture, composition, diagenesis, pore space and petrophysical aquifer properties are still predominantly controlled by the original depositional environments. Therefore facies models, burial history and information about diagenesis and pore space are an important precondition for petrophysical reservoir/aquifer models.

9. References

Abram, P. (2007): Relations between seismic signals and reservoir properties of deep gas reservoirs in Northwest-Germany - Wustrow member, Rotliegend. – Diss., Univ. Jena.

Ajdukiewicz, P., Nicholson, H., Esch, W. L. (2010): Prediction of deep-reservoir quality using early diagenetic process models in the Jurassic Norphlet Formation, Gulf of Mexico. – AAPG Bulletin, 94: 1189–1227.

Allen, P. A. & Allen, J. R. (2005): Basin Analysis: Principles and Applications. – Blackwell Scientific Publications, Cambridge: 451 S.

Anbeek, C. (1992): Surface roughness of minerals and implications for dissolution studies. – Geochim. Cosmochim. Acta, 56: 1461–1469.

Anjos, S. M. C., de Ros, L. F., Silva, C. M. A. (2003): Chlorite authigenesis and porosity preservation in the Upper Cretaceous marine sandstones of the Santos Basin, offshore eastern Brazil. – Int. Assoc. Sedimentol. Spec. Publ., 34: 291–316.

Baaske, U. P. (1999): Untersuchungen zur Diagenese des Buntsandsteins am Westrand des Rheingrabens (Region Bad Dürkheim / Neustadt a. d. Weinstraße). – Diplomarbeit, Institut für Geowissenschaften Johannes Gutenberg-Universität, 90 S.

Bachmann, G. H., Hauschke, N., Kozur, H. W. (2009): Buntsandstein cyclicity and conchostracan biostratigraphy of the Halle (Saale) area, Central Germany. – 6th International Field Workshop on the Triassic of Germany, Martin-Luther-Univ. Halle-Wittenberg, Institut für Geowissenschaften, Halle (Saale), 1-30.

Bai Bin, Zhu Rukai, Wu Songtao, et al. (2013): Multi-scale method of Nano(Micro)-CT study on microscopic pore structure of tight sandstone of Yanchang Formation, Ordos Basin. – Petroleum Exploration and Development, 40(3): 329–333.

Bayer, U., Brink, H.-J., Gajewski, D., Littke, R. (2008): Characteristics of complex intracontinental sedimentary basins. – In: Littke, R., Bayer, U., Gajewski, D., Nelskamp, S. (ed.): Dynamics of Complex Intracontinental Basins - The Central European Basin System, Springer-Verlag, Berlin-Heidelberg, 1–12.

Bär, K. (2012): Untersuchung der tiefengeothermischen Potenziale von Hessen. – Diss., Fachbereich Material- und Geowissenschaften, Technische Universität Darmstadt, 265 S.

Betz, D., Führer, F., Greiner, G., Plein, E. (1987): Evolution of the Lower Saxony Basin. – Tectonophysics, 137: 127–170.

Beutler, G. & Szulc, J. (1999): Die paläogeographische Entwicklung des Germanischen Beckens in der Trias und die Verbindung zur Tethys. – In: Hauschke, N. & Wilde, V. (ed.): Trias - Eine ganz andere Welt. – München (Pfeil Verlag), 71–80.

Bliefnick, D. M., and J. G. Kaldi (1996): Pore geometry: control on reservoir properties, Walker Creek field, Columbia and Lafayette Counties, Arkansas. – American Association of Petroleum Geologists Bulletin, 80: 1027–1044.

Bloch, S. (1994): Effect of detrital mineral composition on reservoir quality. – In: Wilson, M. D. (ed.): Reservoir quality assessment and prediction in clastic rocks. – SEPM Short Course, 30: 161–82.

Bourquin, S., Guillocheau, F., Peron, S. (2009): Braided rivers within an arid alluvial plain (example from the Lower Triassic, western German Basin): recognition criteria and expression of stratigraphic cycles. – Sedimentology, 56: 2235–2264.

Brantley, S. L., White, A. F., Hodson, M. E. (1999): Surface area of primary silicate minerals. – In: Jamtveit, B. and Meakin, P. (eds.): Growth, Dissolution and Pattern Formation in Geosystems. – Kluwer Academic Publishers, 291–326, Dordrecht.

Bricker, O. P., Paces, T., Johnson, C. E., Sverdrup, H. (1994): Weathering and erosion aspects of small catchment research. – In: Moldan, B., Cerny, J. (eds.): Biogeochemistry of small catchments: a tool for environmental research. – Wiley and Sons Ltd, Chichester, England, 85–105.

Brosin, P. (2013): Die Erdölgewinnung in Thüringen – Von Anfang des 20. Jahrhunderts bis in die 1970er Jahre. – Thür. Geol. Verein e. V., Sonderband: 154 S., Weimar.

Brunauer, S., Emmet, P. H., Teller, E. (1938): Adsorption of gases in multimolecular layers. – J. Am. Chem. Soc. (60): 309–319.

Canfield, D. E., Jorgensen, B. B., Fossing, H., Glud, R., Gundersen, J., Ramsing, N. B., Thamdrup, B., Hansen, J. W., Nielsen, L. P., Hall, P. O. J. (1993): Pathways of organic carbon oxidation in three continental margin sediments. – Mar. Geol., 113: 27–40.

Cerepi, A., Durand, C., Brosse, E. (2002): Pore microgeometry analysis in low-resistivity sandstone reservoirs. – Journal of Petroleum Science and Engineering, 35: 205–232.

Cornford, C. (1998): Source rocks and hydrocarbons of the North Sea. – In: Glennie, K. W. (ed.): Introduction to the Petroleum Geology of the North Sea. – Fourth edition: Oxford, U. K., Blackwell Science Ltd.: 376–462.

Cross, M. M., Manning, D. A. C., Bottrell, S. H., Worden, R. H. (2004): Thermochemical sulphate reduction (TSR): experimental determination of reaction kinetics and implications of the observed reaction rates for petroleum reservoirs. –Org. Geochem., 35: 393–404.

Curtis, C. D. (1983): Link between aluminium mobility and the destruction of secondary porosity. – Bull. Am. Assoc. Petrol. Geol., 67: 380–393.

Dadlez, R. (2003): Mesozoic thickness pattern in the Mid-Polish Trough. – Geological Quarterly, 47 (3): 223–240.

Dolezalek, B. (1955): Die Finnestörung bei Bad Sulza, Eckartsberga und Rastenberg. – Abh. der dt. Akademie der Wiss. Kl. Math. und Naturwiss., 5: 139–173.

De Jager, J. (2007): Geological development. – In: Wong, Th. E., Batjes, D. A. J. & de Jager, J. (eds): Geology of the Netherlands. – Royal Netherlands Academy of Arts and Sciences, Amsterdam, 5–26.

Detmer, D. M. (1995): Permeability, porosity and grain-size distribution of selected Pliocene and Quaternary sediments in the Albuquerque Basin. – New Mexico Geology, 17: 79–87.

Deutrich, T. (1993): Tonmineral-Diagenese in Rotliegend-Sandsteinen des Norddeutschen Beckens. – Diss., Univ. Mainz, 179 S.

Dove, P. M., and Elston, S. F. (1992): Dissolution kinetics of quartz in sodium chloride solutions: Analysis of existing data and a rate model for 25°C. – Geochim. Cosmochim. Acta, 56: 4147–4156.

Drozdzewski, G. (2003): Geologische Entwicklung und tektonischer Bau. – In: Geologischer Dienst NRW (ed.): Geologie im Weser- und Osnabrücker Bergland. Krefeld: 16–30.

Ehrenberg, S. N. (1989): Assessing the Relative Importance of Compaction Processes and Cementation to Reduction of Porosity in Sandstones: Discussion; Compaction and Porosity Evolution of Pliocene Sandstones, Ventura Basin, California: Discussion. – AAPG Bulletin, 73(10): 1274–1276.

Ehrenberg, S. N., Nadeau, P. H., Steen, Ø. (2009): Petroleum reservoir porosity versus depth: Influence of geological age. – AAPG Bulletin, 93(10): 1281–1296.

Einsele, G. (1992): Sedimentary Basins, Evolution, Facies and Sediment Budget: 632 S., Berlin (Springer).

Emery, D., Myers, K. J., and Young, R. (1990): Ancient subaerial exposure and freshwater leaching in sandstones. – Geology, 18: 1178–1181.

Ernst, W. (2003): 4.5.2 Jura. – In: Seidel, G. (ed.): Geologie von Thüringen: 392–399, Stuttgart (Schweizerbart).

Faupl, P. (2000): Historische Geologie. Eine Einführung: 270 S., UTB für Wissenschaft: Uni-Taschenbücher.

Fensterer, M. (2009): Stratigraphie und Fazies der Bernburg Formation in Ost-Thüringen. – Forschungspraktikum, Institut für Geowissenschaften, Universität Jena, 103 S.

Fischer, C. & Gaupp, R. (2004): Multi-scale rock surface area quantification—a systematic method to evaluate the reactive surface area of rocks. – Chemie der Erde, 64: 241–256.

Fitzpatrick, E. A. (1980): Soils. Their Formation Classification and Distribution (2nd edition): 453 S., London (Longman).

Flügel, E. (2004): Microfacies of Carbonate Rocks – Analysis, Interpretation and Application: 976 S., Berlin Heidelberg (Springer).

Foh, S., Novil, M., Rockar, E., Randolph, P. (1979): Underground Hydrogen Storage Final Report. – Brookhaven National Laboratory, Upton-New York., p. 145.

Folk, R. L. (1968): Bimodal supermature sandstones. Product of the desert floor. – XXIII Internat. Geol. Cong. Proc., 8: 9–32.

Fritsch, S. (2010): Fazies und Architektur der Bernburg- und Volpriehausen-Formation in Ostthüringen. – Diplomarbeit, Institut für Geowissenschaften, Universität Jena, 71 S.

Franke, D. (2014): Regionale Geologie von Ostdeutschland – Ein Wörterbuch. – Website www.regionalgeologie-ost.de.

Fryberger, S. G. and Schenk, C. J. (1988): Pin stripe lamination: A distinctive feature of modern and ancient eolian sediments. – In: Hesp, P. & Fryberger, S. G. (ed.): Eolian Sediments – Sediment. Geol., 55: 1–15.

Füchtbauer, H. (1979): Die Sandsteindiagenese im Spiegel der neueren Literatur. – Geologische Rundschau, 68: 1125–1151.

Gaupp, R. (1996): Diagenesis types and their application in diagenesis mapping. – Zentralblatt für Geologie und Paläontologie Teil I, 11/12: 1183–1199.

Gaupp, R., Matter, A., Platt, J., Ramseyer, K. & Walzebuck, J. (1993): Diagenesis and Fluid Evolution of Deeply Buried Permian (Rotliegende) Gas Reservoirs, Northwest Germany. – American Association of Petroleum Geologists Bulletin, 77 (7): 1111–1128.

Gaupp, R., Voigt, T., Lützner, H. (1998): Stratigraphy and sedimentological evolution of Lower and Middle Triassic deposits in the SE part of the Germanic Triassic Basin. International Symposium on the Epicontinental Triassic, Hallesches Jahrbuch für Geowissenschaften, Beiheft, 6, 99-120.

Gaupp, R. & Okkerman, J. A. (2011): Diagenesis and reservoir quality of Rotliegend sandstones in the northern Netherlands - a review. – In: Grötsch, J. & Gaupp, R. (eds.): The Permian Rotliegend of the Netherlands – SEPM Special Publication, 9: 193–226.

Geluk, M. C. (2007): Triassic. – In: Wong, T. E., Batjes, D. A. J. & De Jager, J. (ed.): Geology of the Netherlands – Royal Netherlands Academy of Arts and Sciences, Amsterdam: 85–106.

Gibling, M. R. (2006): Width and thickness of fluvial channel bodies and valley fills in the geological record: a literature compilation and classification. – Journal of Sedimentary Research, 76: 731–770.

Giles, M. R. (1997): Diagenesis: a Quantitative Perspective: 526 S., Dordrecht (Kluwer Academic Publishers).

Giles, M. R., Stevenson, S., Martin, S. V., Cannon, S. J. C., Hamilton, P. J., Marshall, J. D., Samways, G. M. (1992): The reservoir properties and diagenesis of the Brent Group: a regional perspective. – In: Morton, A. C., Haszeldine, R. S., Giles, M. R., Brown, S. (ed.): Geology of the Brent Group. – Geological Society London Special Publications, 61: 289–328.

Glennie, K. W. (1970): Developments in Sedimentology 14 - Desert sedimentary environments: 222 S., Amsterdam (Elsevier).

Götze, M. (2011): Numerische Modellierung der Versenkungsgeschichte der Thüringer Mulde mit Inkohlungsdaten des Unteren Keuper. – Diplomarbeit, Institut für Geowissenschaften, Universität Jena, 98 S.

Gregg, S. J., Sing, K. S. W. (1982): Adsorption, surface area and porosity, second ed. Academic Press, London.

Grobleben, J. (2007): Paläothermische Rekonstruktion und Kohlenwasserstoff-Generierung der permokarbonen Senken im Untergrund der Thüringer Mulde. – Diplomarbeit, Institut für Geowissenschaften, Universität Jena, 119 S.

Hampton, B. A. & Horton, B. K. (2007): Sheetflow fluvial processes in a rapidly subsiding basin, Altiplano plateau, Bolivia. – Sedimentology, 54: 1121–1147.

Hantschel, T., and Kauerauf, A.I. (2009): Fundamentals of Basin and Petroleum Systems Modeling. – Springer Verlag, Berlin: 476 S. Germany.

Haq, B. U., Hardenbol, J. and Vail, P. R. (1987): Chronology of Fluctuating Sea Levels Since the Triassic.– Science, 235: 1156-1167.

Houseknecht, D. W. (1987): Assessing the relative importance of compaction processes and cementation to reduction of porosity in sandstones. – AAPG Bulletin, 71: 633–642.

Harzer, E. (2003): Grundwasserneubildungsdynamik im Buntsandstein des Spessarts - Ermittlung über die Durchströmung der ungesättigten Zone. – Diss., Uni. Würzburg, 185 S.

Hilse, U., Pudlo, D., Gaupp, R. (2010): Mineralogische und geochemische Unterschiede von "red bed" Sedimenten (Buntsandstein, Rotliegend) in der Bohrung Metzels 1/64 (Thüringische Vorderrhön). – Exkursionsführer/Tagungsband „150. Geburtstag von Johannes Walther - Fazies der Trias in Ostthüringen" zur 20. Jahreshauptversammlung (Vortrags- und Exkursionsveranstaltung) vom 04. bis 06. Juni 2010 in Jena, Jena.

Hilse, U., Aehnelt, M., Köster, J., Pudlo, D., Heide, K., Gaupp, R. (in prep.): Bleaching diversity of Lower Triassic Buntsandstein sandstones in Thuringia and NE-Hesse.

Holdren, G. R., Jr. and Speyer, P. M. (1985): Reaction rate-surface area relationships during the early stages of weathering - I. Initial observations. – Geochim. Cosmochim. Acta, 49: 675–681.

Hoppe, W. (1957): Gliederung des Mittleren Buntsandsteins im Gebiet von Sondershausen in Thüringen. – Ber. Geol. Ges. DDR, 2: 183-198; Berlin.

Hoppe, W. (1968): Zyklen und Rhythmen, Zeit- und Faziesgrenzen im Buntsandstein, Geologie, 17, 1130–1137.

Hoppe, W. (1976a): Zur Bildungsgeschichte des Buntsandsteins im Germanischen Buntsandsteinbecken. – Z. geol. Wiss., 4(11): 1457–1471.

Hoppe, W. (1976b): Die paläogeographisch-fazielle Entwicklung im Südteil des Germanischen Buntsandstein Beckens. – Schriftenr. Geol. Wiss., 6: 5–62.

Houseknecht, D. W. (1989): Assessing the Relative Importance of Compaction Processes and Cementation to Reduction of Porosity in Sandstones: Reply[1]. – The American Association of Petroleum Geologists Bulletin, 73: 1277–1279.

Huckriede, H. & Zander, I. (2010): Geologische Charakterisierung der Speicher- und Barrieregesteine im tieferen Untergrund des Freistaats Thüringen (Deutschland). Geological characterisation of reservoir and barrier rocks in the deeper subsurface of the

Free State of Thuringia (Germany). – In: ...... (Hrsg.). Speicher-Kataster Deutschland. – In: Schriftenreihe der Deutschen Gesellschaft für Geowissenschaften, 74, ..-..; Hannover.

Hurst, A. & Irwin, H. (1982): Geological modelling of clay diagenesis in sandstones. – Clay Miner., 17: 5–22.

IUPAC (1985): Reporting Physisorption Data for Gas/Solid Systems. – Pure Appl. Chem., (57): 603–619.

Junghans, W.-D. (2003): Fazies, Zyklizität, Petrophysik und Palaomagnetik im Buntsandstein der Bohrung Kraichgau 1002 (SW-Deutschland). – Diss., Geowissenschaftlichen Fakultät der Eberhard Karls Universität Tübingen.

Karnin, W.-D., Idiz, E., Merkel, E., Ruprecht, E. (1996): The Zechstein Stassfurt Carbonate hydrocarbon system of the Thuringian Basin, Germany. – Petroleum Geoscience, 2: 53–58.

Kayser, A. (2006): Herkunft, Auftreten und Visualisierung von Permeabilitätsbarrieren in einer Gaslagerstätte in Sandsteinen des Rotliegenden (Südliches Permbecken, Deutschland): Bedeutung für Diagenese, Fluidfluß und Produktion. – Diss, Universität Marburg, 206 S.

Kazimierz, T., Jacek, T., Stanisław, R. (2004): Evaluation of Rock Porosity Measurement Accuracy with a Helium Porosimeter. – Acta Montanistica Slovaca Ročník, 9(3): 316–318.

Kästner, H. (2003): Erdöl/Erdgas/Kohlendioxid. – In: Seidel, G. (ed.): Geologie von Thüringen: 483–486, Stuttgart (Schweizerbart).

Kästner, H., Seidel, G., Wiefel, H. (2003): Regionalgeologische Stellung und Gliederung. – In: Seidel, G. (ed.): Geologie von Thüringen: 14–23, Stuttgart (Schweizerbart).

Klapperer, S. (2009): Sedimentologisch-fazielle Untersuchungen des Odenwälder Buntsandsteins und Korrelation mit Kernen der Bohrung Römerberg 1. – Diplomarbeit, Institut für Geowissenschaften, Universität Jena, 81 S.

Klaua, D. (2003): 4.5.3 Kreide. – In: Seidel, G. (ed.): Geologie von Thüringen: 399–403, Stuttgart (Schweizerbart).

Kley, J. & Voigt, T. (2008): Late Cretaceous intraplate thrusting in central Europe: Effect of Africa-Iberia-Europe convergence, not Alpine collision. – Geology, 36(11): 839–842.

Knox, R. W. O., Burgess, W. G., Wilson, K. S. and Bath, A. H. (1984): Diagenetic influences on reservoir properties of the Sherwood Sandstone (Triassic) in the Marchwood geothermal borehole. – Clay Minerals, 19: 441–456.

Kockel, F., Wehner, H. and Gerling, P. (1994): Petroleum Systems of the Lower Saxony Basin, Germany. – In: Magoon, L. B., and Dow, W. C. (eds.): The petroleum system-from source to trap. – AAPG Memoir 60: 573–586.

Kockel, F. (2002): Rifting processes in NW-Germany and the German North Sea Sector. – Geologie En Mijnbouw-Netherlands Journal of Geosciences, 81: 149-158.

Kohlhepp, B. (2012): Untersuchungen zu Fazies, Diagenese und Poren-/Mineralgrenzflächen an Rotliegend-Sandsteinen im Rahmen einer Analogstudie zur Wirkung von CO2 auf Gasspeichersysteme. – Diss., Institut für Geowissenschaften, Universität Jena, 243 S.

Kunkel, C., Voigt, T, Beyer, D., Hilse, U., Aehnelt, M., Pudlo, D. & Gaupp, R. (2012): Towards a better understanding of facies and spatial variations of Lower and Middle Buntsandstein sediments in the Thuringian Basin: From outcrop to model. – Schriftenreihe der Deutschen Geologischen Gesellschaft, 80: 523.

Kunkel, C., Beyer, D., Hilse, U., Aehnelt, M., Voigt, T., Gaupp, R. (2013): 3D-small-scale modelling of facies development and variations of the Lower and Middle Buntsandstein formations in the Thuringian Syncline. – Abstract Sedimentary Basins 2013, Jena.

Kunkel, C. (in prep.): Architectural design, facies, 3D modeling and aquifer characterization of the German Triassic Buntsandstein in the North Hessian Trough and the Thuringian Syncline. – Diss., Univ. Jena.

Lander, R. H. & Walderhaug, O. (1999): Predicting Porosity through Simulating Sandstone Compaction and Quartz Cementation. – AAPG Bulletin, 83 (3): 433–449.

Landis, C. R. & Castaño, J. R. (1995): Maturation and bulk chemical properties of a suite of solid hydrocarbons. – Org. Geochem. 22(1): 137–149.

Lang, S. (2001): Zur Sedimentologie der Solling-Formation (Trias, Buntsandstein) im Thüringer Becken. – Diplomarbeit, Institut für Geowissenschaften, Universität Jena, 201 S.

Langbein, R. (1970): Zur Petrologie des Thüringer Buntsandsteins. – Beiheft zur Zeitschrift Geologie, 68, 131 S., Berlin.

Langbein, R. (1985): Fluvial-Marine Transitional Depositional Environment Influencing the Diagenesis in the Buntsandstein of Thuringia (German Democratic Republic). – In: Mader, D. (ed.): Aspects of fluvial sedimentation in the Lower Triassic Buntsandstein of Europe. – Lecture Notes in Earth Sci., 4: 561–590.

Leggewie, R., Füchtbauer, H. & El-Najjar, R. (1977): Zur Bilanz des Buntsandsteinbeckens (Korngrößenverteilung und Gesteinsbruchstücke). – Geologische Rundschau, 66: 551-577.

Lepper, J. & Röhling, H. G. (1998): Buntsandstein. – Hallesches Jb. Geowiss., Reihe B, 6: 27–34.

Lippmann, R. (2012): Diagenesis in Rotliegend, Triassic and Jurassic clastic hydrocarbon reservoirs of the Central Graben, North Sea. – Diss., Institut für Geowissenschaften, Universität Jena, 226 S.

Lowell, S., Shields, J. E., Thomas, M. A., Thommes, M. (2004): Characterization of Porous Solids and Powders: Surface Area, Pore Size and Density. – Springer, Dordrecht, the Netherlands.

Lundegard, P. D. (1992): Sandstone porosity loss - A "Big Picture" view of the importance of compaction. – J. of Sediment. Petrol., 62: 250–260.

Maaß, K. (2010): Die Ablagerungsbedingungen des Unteren Buntsandsteins im Ostteil der Thüringer Mulde. – Diplomarbeit, Institut für Geowissenschaften, Universität Jena, 144 S.

Malz, A. & Kley, J. (2012): The Finne fault zone (Central Germany): structural analysis of a partially inverted extensional fault zone by balanced cross-sections. – International Journal of Earth Sciences, 101: 2167-2182.

Marchand, A. M. E., Craig Smalley, P., Stuart Haszeldine, R., Fallick, A. E. (2002): Note on the importance of hydrocarbon fill for reservoir quality prediction in sandstones. – AAPG Bulletin, 86 (9): 1561–1571.

Marfil, R., Scherer, M., Turrero, M. J. (1996): Diagenetic processes influencing porosity in sandstones from the Triassic Buntsandstein of the Iberian Range, Spain. – Sedimentary Geology, 105: 203–219.

Martini, H. J. (1940): Saxonische Zerrungs- und Pressungsformen im Thüringer Becken. – Geotekt. Forsch., 5: 125–133.

Mazur, S., Scheck-Wenderoth, M., Krzywiec, P. (2005): Different modes of the Late Cretaceous–Early Tertiary inversion in the North German and Polish basins. – Int. J. Earth. Sci. (Geol Rundsch), 94: 782–798.

März, K. (1977): Hydrogeologische und hydrochemische Untersuchungen im Buntsandstein und Muschelkalk Nordbayerns. – Hydrochem. hydrogeol. Mitt., 2: 1–170.

McBride, E. F. (1963): A classification of common sandstones. – J. Sediment. Petrol., 33: 664–669.

McBride, E. F. (1989): Quartz cement in sandstones: a review. – Earth-Science Reviews, 26: 69-112.

McKinley, J. M., Worden, R. H., Ruffell, A. H., Morad, S. (2003): Smectite in sandstones: a review of the controls on occurrence and behaviour during diagenesis. – In: Worden, R. H. & Morad, S. (ed.): Clay minerals in sandstones. – Special Publication of the International Association of Sedimentologists, 34: 109–128.

Ménard, G. & Molnar, P., (1988): Collapse of a Hercynian Tibetan Plateau into a late Paleozoic European Basin and Range province. – Nature, 334: 235-237.

Miall, A. D. (1996): The Geology of Fluvial Deposits: 582 S., Berlin (Springer).

Moncure, G. K., Lahann, R. W., Siebert, R. M. (1984): Origin of Secondary Porosity and Cement Distribution in a Sandstone/Shale Sequence from the Frio Formation (Oligocene): Part 2. Aspects of Porosity Modification. – In: MacDonald, D. A. & Surdam, R. C. (eds.): Clastic diagenesis. – Am. Assoc. Petrol. Geol. Mem., 37: 151-61.

Morad, S. (1998): Carbonate cementation in sandstones: distribution patterns and geochemical evolution. – Spec. Publs. int. Ass. Sediment., 26: 1–26.

Morad, S., Bergan, M., Knarud, R., Nystuen, J. P. (1990): Albitization of detrital plagioclase in Triassic reservoir sandstones from the Snorre Field, Norwegian North Sea. – Journal of Sedimentary Petrology, 60(3): 411–425.

Morad, S., Al-Ramadan, K., Ketzer, J. M., De Ros, L. F. (2010): The impact of diagenesis on the heterogeneity of sandstone reservoirs: A review of the role of depositional facies and sequence stratigraphy. – AAPG Bulletin, 94(8): 1267–1309.

Muchez, Ph., Viaene, W., Dusar, M. (1992): Diagenetic control on secondary porosity in flood plain deposits: an example of the Lower Triassic of northeastern Belgium. – Sediment. Geol., 78: 285–298.

Nagtegaal, P. J. C. (1978): Sandstone-framework instability as a function of burial diagenesis. – J. Geol. Soc. Lond., 135: 101–105.

Naumann, D. (2013): Fazieller Einfluss auf die Diagenese- und Porenraumentwicklung in Sedimenten des Buntsandsteins, Bohrung Ballstedt 1/63. – Diploma thesis, Univ. Jena, 64 S.

Nesbitt H. W., Fedo, C. M., Young, G. M. (1997): Quartz and Feldspar Stability, Steady and Non-steady-State Weathering, and Petrogenesis of Siliciclastic Sands and Muds[1]. – The Journal of Geology, 105: 173–191.

Niedersächsisches Landesamt für Bodenforschung (1991): Erdöl und Erdgas in der Bundesrepublik, Deutschland 1990. - Hannover.

Nover, G. (2005): Electrical Properties of Crustal and Mantle Rocks – A Review of Laboratory Measurements and their Explaination. – Surveys in Geophysics, 26 (5): 593–651.

Pape, H., Clauser, C., Iffland, J., Krug, R., Wagner, R. (2005): Anhydrite Cementation and Compaction in Geothermal Reservoirs: Interaction of Pore-Space Structure with Flow, Transport, P-T-conditions, and Chemical Reactions. – Int. J. Rock Mechanics and Mining Sciences, 42: 1056–1069.

Parnell, J. (1994): Hydrocarbons and other fluids: paragenesis, interactions and exploration potential inferred from petrographic studies. – In: Parnell, J. (ed.): Geofluids: Origin, Migration and Evolution of Fluids in Sedimentary Basins. – Geological Society Special Publication, 78: 275–291.

Parry, W. T., Chan, M. A., Beitler, B. (2004): Chemical bleaching indicates episodes of fluid flow in deformation bands in sandstone. – AAPG Bulletin, 88(2): 175–191.

Paul, J. (1982): Der Untere Buntsandstein des Germanischen Beckens. – Geologische Rundschau, 71: 795–811.

Paul, J. (1999a): Fazies und Sedimentstrukturen des Buntsandsteins. – In: Hauschke, N. & Wilde, V. (eds.): Trias - Eine ganz andere Welt: 105–114, München (Pfeil Verlag).

Paul, J. (1999b): Oolithe und Stromatolithen im Unteren Buntsandstein. – In: Hauschke, N. & Wilde, V. (ed.): Trias - Eine ganz andere Welt: 263-270, München (Pfeil Verlag).

Peisker, J. (2011): Rekonstruktion der Versenkungsgeschichte des Thüringer Beckens mit Inkohlungswerten aus dem Kupferschiefer. – Forschungsarbeit, Institut für Geowissenschaften, Universität Jena, 51 S.

Pettijohn, F. J., Potter, P. E., Siever R. (1987): Sand and Sandstone: 553 S., New York (Springer).

Platt, J. D. (1993): Controls on clay mineral distribution and chemistry in the Early Permian Rotliegend of Germany. – Clay Minerals, 28: 393–416.

Pudlo, D., Gaupp, R., Adelmann, D., Elsner, M., Hilse, U., Goepel, A. (2010): DFG-Project AD 315/1-1: Long-term impact of CO_2 on the stability of mineral assemblages in porous reservoir sandstones – Analogue study in natural CO_2 reservoirs from Central Europe. – DFG Final report.

Puff, P. (1969): Über den Unteren Buntsandstein am Südrand des Thüringer Beckens. – Abhandlungen des Zentralen Geologischen Instituts, 13, Berlin.

Puff, P. (1976): Gliederung der Solling-Folfe (Trias, Buntsandstein) im südlichen Thüringen mittels Violetter Horizonte. – Schriftenr. geol. Wiss., 6: 81–96.

Puff, P. (1994): Thüringen – Geologische Übersicht 1 : 400 000, Gotha (Perthes).

Puff, P. & Seidel, G. (2009): Schichtausfälle und Faziesänderungen im Unteren Buntsandstein des Thüringer Beckens. – Geow. Mitt. Thüringen, 13: 169–180.

Puff, P. & Langbein, R. (2003): 4.5.1.1 Buntsandstein. – In: Seidel, G. (ed.): Geologie von Thüringen: 326–341, Stuttgart (Schweizerbart).

Purvis, K. & Okkerman, J. A. (1996): Inversion of reservoir quality by early diagenesis: an example from the Triassic Buntsandstein, offshore the Netherlands. – In: Rondeel et al. (eds): Geology of gas and oil under the Netherlands. – Kluwer Academic Publishers, Netherlands, 179–189.

Putnis, A. & Mauthe, G. (2001): The effect of pore size on cementation in porous rocks. – Geofluids, 1: 37–41.

Radzinski, K.-H. (1995): Zum Unteren und Mittleren Buntsandstein im Unstruttal bei Nebra (Sudwestrand der Querfurter Mulde). – Mitt. Geol. Sachsen-Anhalt, 1: 85–103.

Rahimpour-Bonab, H., Esrafili-Dizaji, B., Tavakoli, V. (2010): Dolomitization and anhydrite precipitation in Permo-Triassic carbonates at the South Pars gas Field, Offshore Iran: controls on reservoir quality. – J. Pet. Geol, 33: 43–66.

Rauche, H. & Franzke, H. J. (1990): Stress field evolution at the northern part of the South German Block on the territory the G.D.R. – Gerlands Beitr. Geophysik, Leipzig, 99: 441-461.

Rettig, B. (1996): Die Solling-Folge (Mittlerer Buntsandstein) im Grenzgebiet Niedersachsen – Thüringen – Hessen. – Mitt. geol. Inst. Univ. Hannover, 35.

Rochelle, C. A., Czernichowski-Lauriol, I., Milodowski, A. E. (2004): The impact of chemical reactions on CO2 storage in geological formations: a brief review. – Geological Society of London, Special Publications, 233: 87–106.

Roman, A. (2004): Sequenzstratigraphie und Fazies des Unteren und Mittleren Buntsandsteins im östlichen Teil des Germanischen Beckens (Deutschland, Polen): 1247 S., Dissertation, Martin Luther Univ. Halle Wittenberg, Halle (Saale).

Rödiger, T. (2005): Charakterisierung und Modellierung des Buntsandsteinfließsystems im Osten des Thüringer Beckens: 180 S., Diss. Univ. Jena.

Scheffer, F. & Schachtschabel, P. (1998): Lehrbuch der Bodenkunde. – Enke-Verlag: 570 S., Stuttgart.

Schmidt, V. & MacDonald, D. A. (1979): The role of secondary porosity in the course of sandstone diagenesis. – In: Scholle, P. A. and Schluger, P. R. (eds.): Aspects of diagenesis. – SEPM Spec. Pub., Tulsa (26): 175-207.

Schöner, R. (2006): Comparison of Rotliegend sandstone diagenesis from the northern and southern margin of the North German Basin. – Diss., Univ. Jena., 160 S.

Seidel, G. (1972): Zur Petrographie der Gerölle im mittleren Teil des Buntsandsteins des Thüringer Beckens. – Geologie, 21 (7): 770–685.

Seidel, G. (1992): Thüringer Becken. – Sammlung Geologischer Führer, Bd. 85., Bornträger (Berlin, Stuttgart).

Seidel, G. (1995): Zur Ausbildung des Oberen Buntsandsteins bei Hildburghausen. – Geowiss. Mitt. von Thüringen, 3: 123–134.

Seidel, G. (2003): Saxonische Tektonik. – In: Seidel, G. (ed.): Geologie von Thüringen: 403–408, Stuttgart (Schweizerbart).

Senglaub, Y., Brix, M. R., Adriasola, A. C. and Littke, R. (2005): New information on the thermal history of the southwestern Lower Saxony Basin, northern Germany, based on fission track analysis. – International Journal of Earth Sciences (Geologische Rundschau), 94: 876–896.

Senglaub, Y., Littke, R., and Brix, M. (2006): Numerical modelling of burial and temperature history as an approach for an alternative interpretation of the Bramsche anomaly, Lower Saxony Basin. –International Journal of Earth Sciences, 95: 204–224.Shepherd, R. (1989): Correlations of Permeability and Grain Size. – Ground Water, 27(5): 633–638.

Shebl, M. A. & Surdam, R. C. (1996): Redox reactions in hydrocarbon clastic reservoirs: experimental validation of this mechanism for porosity enhancement. – Chemical Geology 132: 103–117.

Shepherd, R. (1989): Correlations of Permeability and Grain Size. – Ground Water, 27(5): 633–638.

Steinmüller, A. (2003): 4.6.1 Tertiär. – In: Seidel, G. (ed.): Geologie von Thüringen: 409–423, Stuttgart (Schweizerbart).

Stow, D. A. V. (2003): Sedimentary Rocks in the Field – A Colour Guide: 320 S., London (Manson Publishing Ltd).

Surdam, R. C., Boese, S. & Crossey, L. J. (1984): Chemistry of secondary porosity. – AAPC Memoir, 37: 127–149.

Surdam, R. C., Jiao, Z. S., MacGowan, D. B. (1993): Redox Reactions Involving Hydrocarbons and Mineral Oxidants: A Mechanism for Significant Porosity Enhancement in Sandstones[1]. – The American Association of Petroleum Geologists Bulletin, 77(9): 1509–1518.

Sweeney, J. J. & Burnham, A. K. (1990): Evaluation of a simple model of vitrinite reflectance based on chemical kinetics. AAPG Bulletin, 74: 1559–1570.

Szurlies, M. (2001): Zyklische Stratigraphie und Magnetostratigraphie des Unteren Buntsandsteins in Mitteldeutschland. – Diss., Univ. Halle-Wittenberg, 150 S.

Testa, G. & Lugli, S. (2000): Gypsum-anhydrite transformations in Messinian evaporites of central Tuscany (Italy). – Sediment. Geol., 130: 249–268.

Tiab, D. & Donaldsen, E. C. (2004): Petrophysics (second edition). – Elsevier: 889 S., Amsterdam.

Thomson, S. & Zeh, A. (2000): Fission-track thermochronology of the Ruhla Crystalline Complex: new constrains on the post-variscan thermal evolution of the NW-Saxo-Bohemian Massif. – Tectonophysics, 324: 17–35.

Tucker, M. E. & Wright, V. P. (1990): Carbonate Sedimentology: 496 S., Oxford (Blackwell Scientific Publications).

Udluft, P. (1971): Hydrogeologie des Oberen Sinntales. – Geologica Bavarica, 64: 365–384.

Voigt, T. (2000): Exkursionsführer Trias und Bausteine in und um Jena, 2.4. Exkursion, Exkursionspunkt 1, Rabenschüssel - Eichberg bei Maua (Mittlerer Buntsandstein). – In: Katzschmann, L. (ed.): Trias in Thüringen. – Exkursionsführer und Kurzreferate zur 10. Jahreshauptversammlung (Vortrags- und Exkursionstagung) vom 16.-18.06.2000 in Jena/Thüringen, 30–31.

Voigt, T. (2011): Fazielle und petrographische Eigenschaften der Sandsteine im Buntsandstein Ostthüringens und ihr Einfluss auf die Werkstein-Eignung. IFS-Bericht 40/2011, 7-16.

Voigt, T. & Gaupp, R. (2000): Die fazielle Entwicklung an der Grenze zwischen Unterem und Mittlerem Buntsandstein im Zentrum der Thüringer Senke. – Beiträge Geologie Thüringen, 7: 55–71.

Voigt, T., Gaupp, R., Röhling, H.-G. (2011): Lake deposits of the Early Triassic Buntsandstein in Central Germany: Type localities of oolites and stromatolites. – 5th Int. Limnogeological Congress (Konstanz 2011) Abstract-Volume and Fieldguide: 191–211.

Waldmann, S. (2011): Geological and mineralogical investigation of Rotliegend gas reservoirs in the Netherlands and their potential for CO2 storage. – Diss., Institut für Geowissenschaften, Universität Jena, 171 S.

Walker, R. G. (2006): Facies models revisited: Introduction. – In: Posamentier, H. W. & Walker, R. G. (eds.): Facies models revisited. – SEPM Special Puplication, 84: 1–18.

Walter, R. (1992): Geologie von Mitteleuropa. – Schweizerbart'sche Verlagsbuchhandlung, Stuttgart: 561 S.

Wardlaw, N. C, and Taylor, R. P., (1976): Mercury capillary pressure (sic) curves and the interpretation of pore structure and capillary behavior in reservoir rocks. – Can. Pet. Geol. Bull., 24: 225 – 262.

van Wees, J. D., Beekman, F. (2000): Lithosphere rheology during intraplate basin extension and inversion; inferences from automated modeling of four basins in Western Europe. – Tectonophysics, 320 (3–4): 219–242.

Wendler, J., Köster, J., Götze, J., Kasch, N., Zisser, N., Kley, J., Pudlo, D., Nover, G., Gaupp, R. (2012): Carbonate diagenesis and feldspar alteration in fracture-related bleaching zones (Buntsandstein, central Germany): possible link to CO2-influenced fluid–mineral reactions. – Int. J. Earth Sci. (Geol. Rundsch.), 101: 159–176.

White, A. F., Blum, A. E., Schulz, M. S., Bullen, T. D., Harden, J. W., and Peterson, M. L. (1996): Chemical weathering rates of a soil chronosequence on granitic alluvium: I. Quantification of mineralogical and surface area changes and calculation of primary silicate reaction rates. – Geochim. Cosmochim. Acta, 60, 2533–2550.

Williams, G. (1964): Some aspects of aeolian saltation load. – Sedimentology, 3: 257–287.

Wilson, M. D. & Pittman, E. D. (1977): Authigenic clays in sandstones: recognition and influence on reservoir properties and paleoenvironmental analysis. – J. of Sed. Pet., 47(1): 3–31.

Wilson, M. D. & Stanton, P. T. (1994): Diagenetic mechanism of porosity and permeability reduction and enhancement. – In: Wilson, M.D. (ed.): Reservoir Quality

Assessment and Prediction in Clastic Rocks. – Society of Economic Paleontologists and Mineralogists, Short Course, 30: 59–118.

Wolfgramm, M. (2002): Fluidentwicklung und Diagenese im Nordostdeutschen Becken - Petrographie, Mikrothermometrie und Geochemie stabiler Isotope. – Dissertation, Mathematisch-Naturwissenschaftlich-Technische Fakultät, Martin-Luther-Universität,170 pp., Halle-Wittenberg.

Wolfgramm, M., Rauppach, K., Seibt, P. (2008): Reservoir-geological characterization of Mesozoic sandstones in the North German Basin by petrophysical and petrographical data. – Zeitschrift für geologische Wissenschaften, 36: 249–265.

Worden, R. H. & Morad, S. (2000): Quartz Cementation in Oil Field Sandstones: A Review of the Key Controversies. – In: Worden, R. H. & Morad, S. (ed.): Quartz Cementation in Sandstones. – Special Publication of the International Association of Sedimentologists, 29: 1–20.

Worden, R.H. & Morad, S. (2003): Clay minerals in sandstones: controls on formation, distribution and evolution. – In: Worden, R. H. & Morad, S. (ed.): Clay minerals in sandstones. – Special Publication of the International Association of Sedimentologists, 34: 3–41.

Worden, R. H. & Burley, S. D. (2003): Sandstone Diagenesis: The Evolution of Sand to Stone. – In: Burley, S. D. & Worden, R. H. (eds.): Sandstone Diagenesis: Recent and Ancient, 3–43.

Worden, R. H., Mayall, M. J., Evans, I. J. (2000): The effect of ductile-lithic sand grains and quartz cement on porosity and permeability in Oligocene and Lower Miocene elastics, South China Sea: prediction of reservoir quality. – American Association of Petroleum Geologists Bulletin, 84: 345 – 359.

Yalcin M. N., Littke, R., Sachsenhofer, R. F. (1997): Thermal history of sedimentary basins. – In: Welte, D. H. et al. (eds.): Petroleum and Basin Evolution, Berlin (Springer-Verlag): 73-167.

Zhu, C., Veblen, D. R., Blum, A. E., Chipera, S. J. (2006): Naturally weathered feldspar surfaces in the Navajo Sandstone aquifer, Black Mesa, Arizona: electron microscopic characterization. – Geochimica et Cosmochimica Acta 70: 4600–4616.

Ziegler, P. A. (1978): North-Western Europe: tectonics and basin development. – Geologie en Mijinbouw, 57: 589–626.

Ziegler, P. A. (1990): Geological Atlas of Western and Central Europe: 239 S., Amsterdam (Elsevier).

Ziegler, K. (2006): Clay minerals of the Permian Rotliegend Group in the North Sea and adjacent areas. – Clay Minerals, 41: 355–393.

Zisser, N., Nover, G., Dürrast, H., Siegesmund, S. (2007): Relationship between electrical and hydraulic properties of sedimentary rocks. – Z. dt. Ges. Geowiss., 158(4): 883–894.

10. Appendix

10. I. Plates

10. I.1. Virtual wells
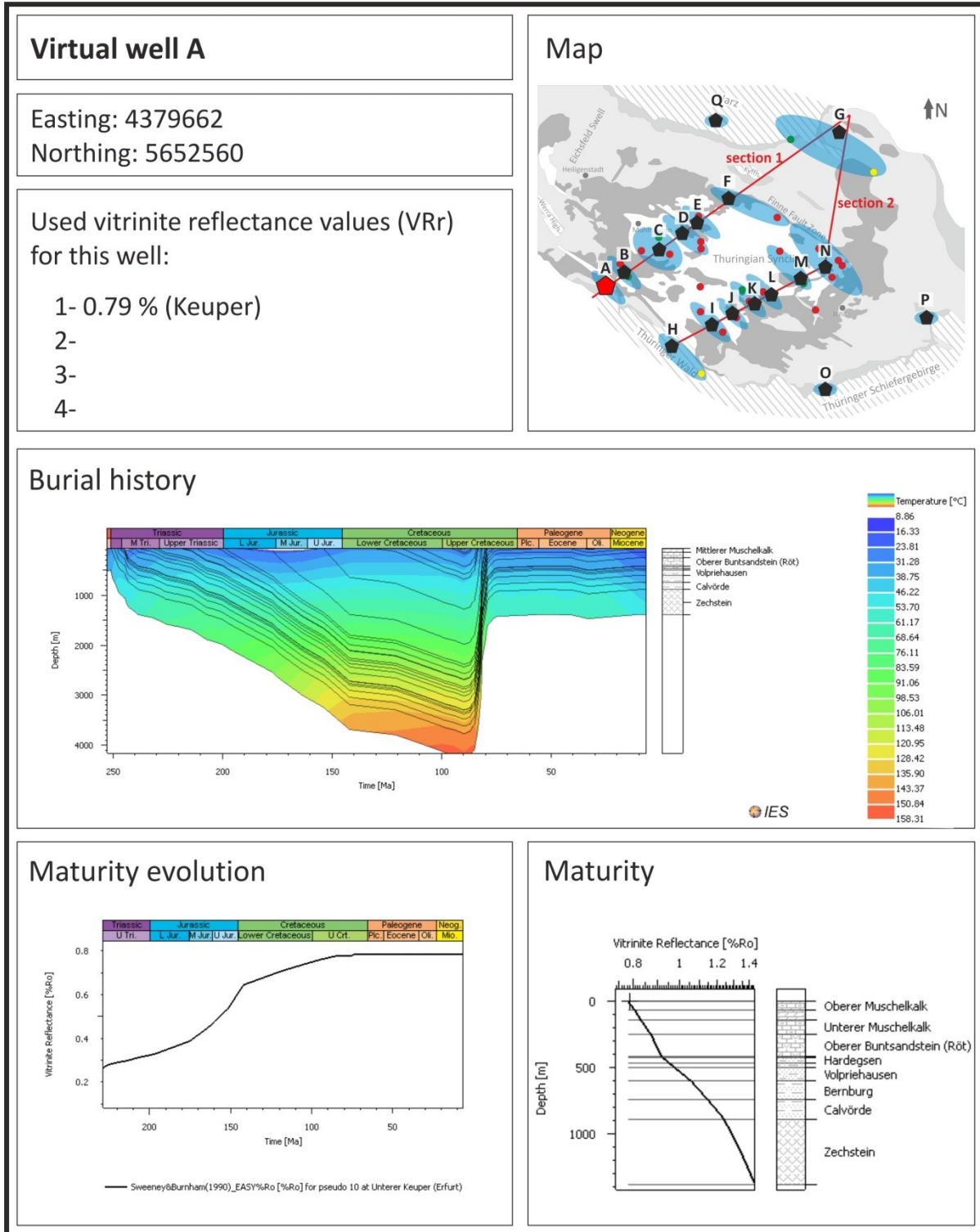
Fig. A 1: Characteristics of virtual well A.
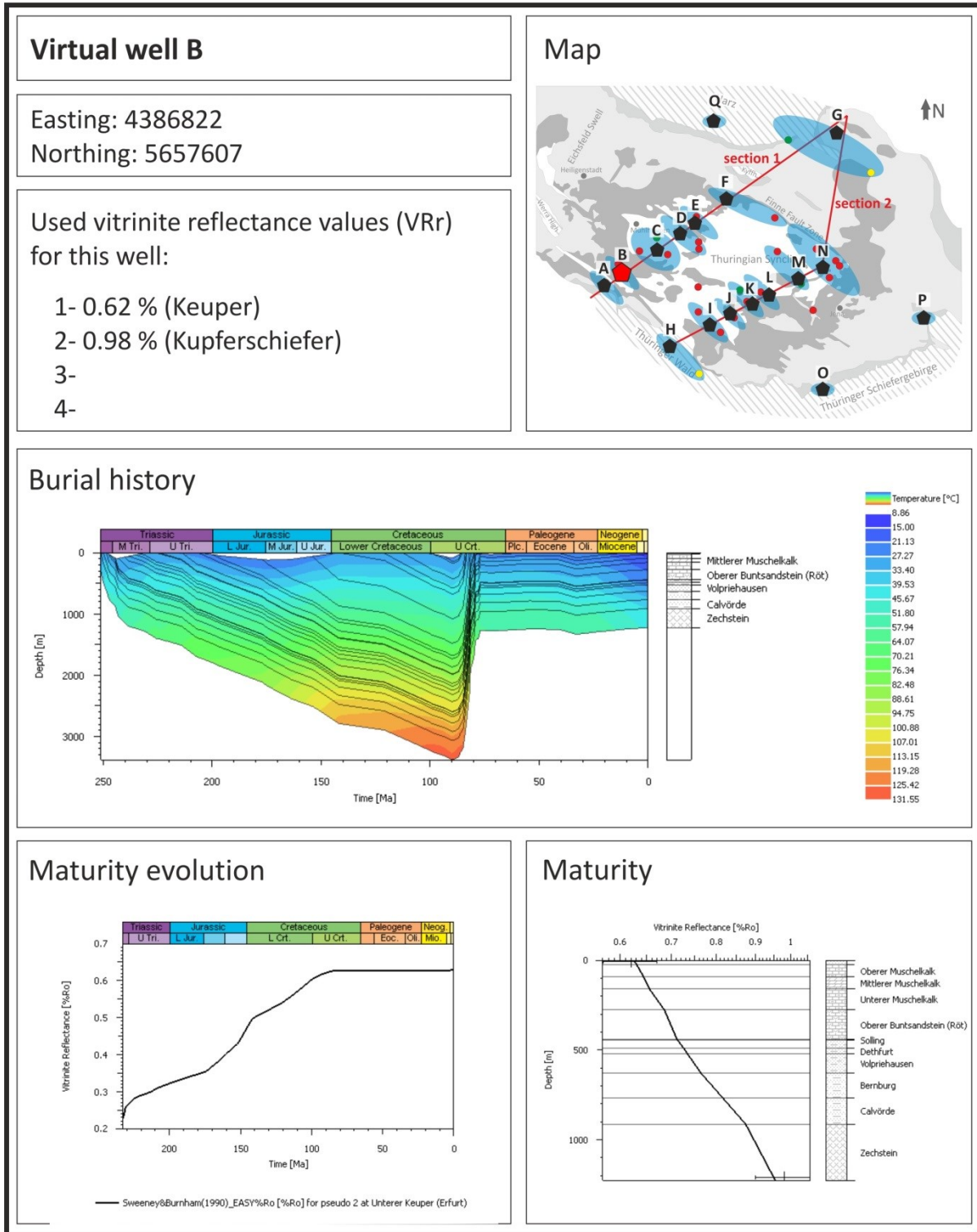
Fig. A 2: Characteristics of virtual well B.

Fig. A 3: Characteristics of virtual well C.

Virtual well D

Easting: 4408402
Northing: 5672825

Used vitrinite reflectance values (VRr)
for this well:

1- 0.79 % (Keuper)
2- 0.55 % (Keuper)
3-
4-

Map

Burial history

Maturity evolution

Maturity
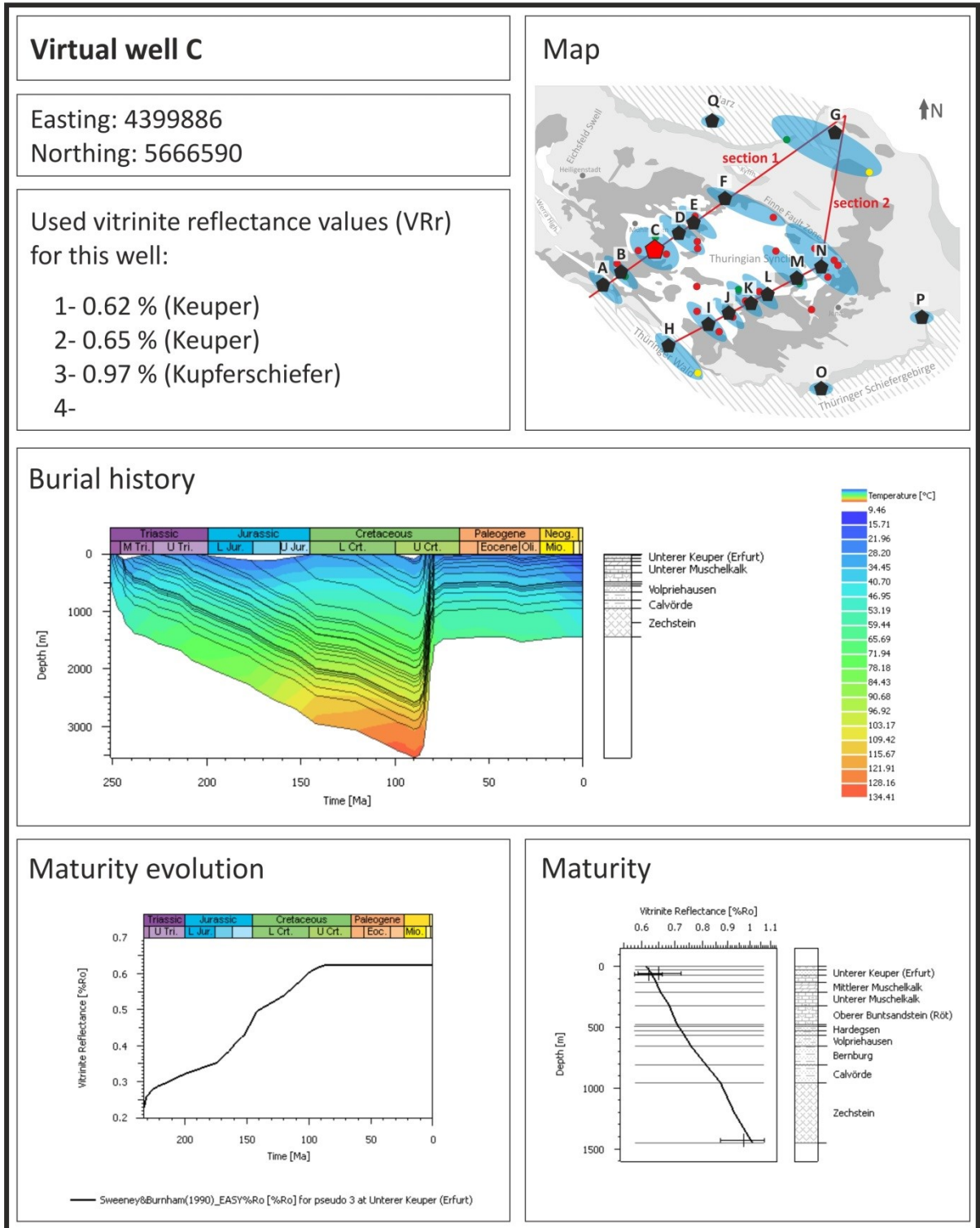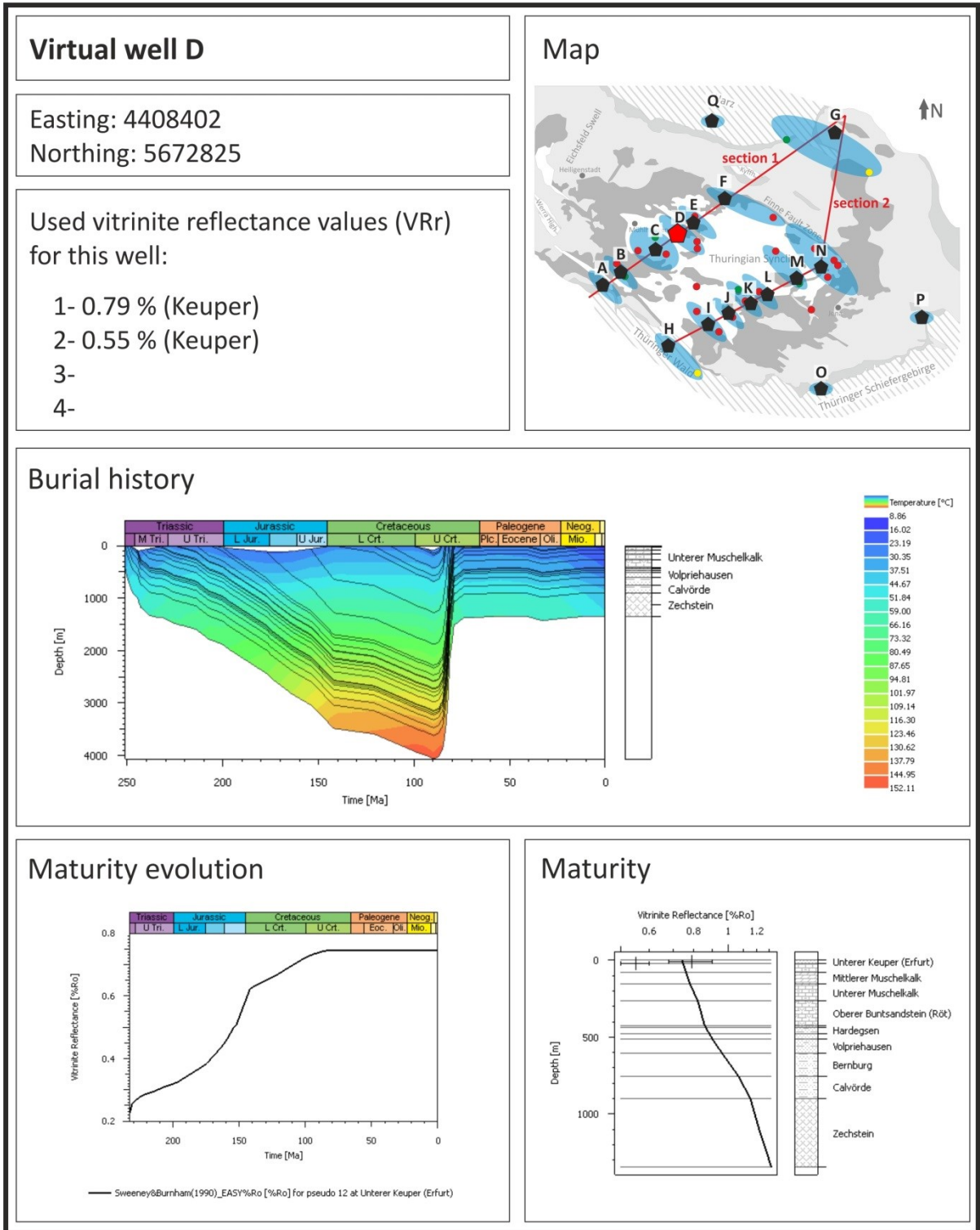
Fig. A 4: Characteristics of virtual well D.

Fig. A 5: Characteristics of virtual well E.

Fig. A 6: Characteristics of virtual well F.

Virtual well G

Easting: 4470043
Northing: 5712978

Used vitrinite reflectance values (VRr)
for this well:

1- 1.14 % (Kupferschiefer)
2- 1.32 % (Kupferschiefer)
3- 2.4 % (Wettin F.)
4- 2.8 % (Mansfeld F.)

Map

Burial history

Maturity evolution

Maturity

Fig. A 7: Characteristics of virtual well G.

Virtual well H

Easting: 4403941
Northing: 5628582

Used vitrinite reflectance values (VRr)
for this well:

1- 1.8 % (Manebach F.)
2-
3-
4-

Map

Burial history

Maturity evolution

Sweeney&Burnham(1990)_EASY%Ro [%Ro] for pseudo 11 at Manebach

Maturity

Fig. A 8: Characteristics of virtual well H.

Virtual well I

Map

Easting: 4420245
Northing: 5637123

Used vitrinite reflectance values (VRr)
for this well:

1- 0.75 % (Keuper)
2- 0.64 % (Keuper)
3-
4-

Burial history

Maturity evolution

Maturity

Fig. A 9: Characteristics of virtual well I.
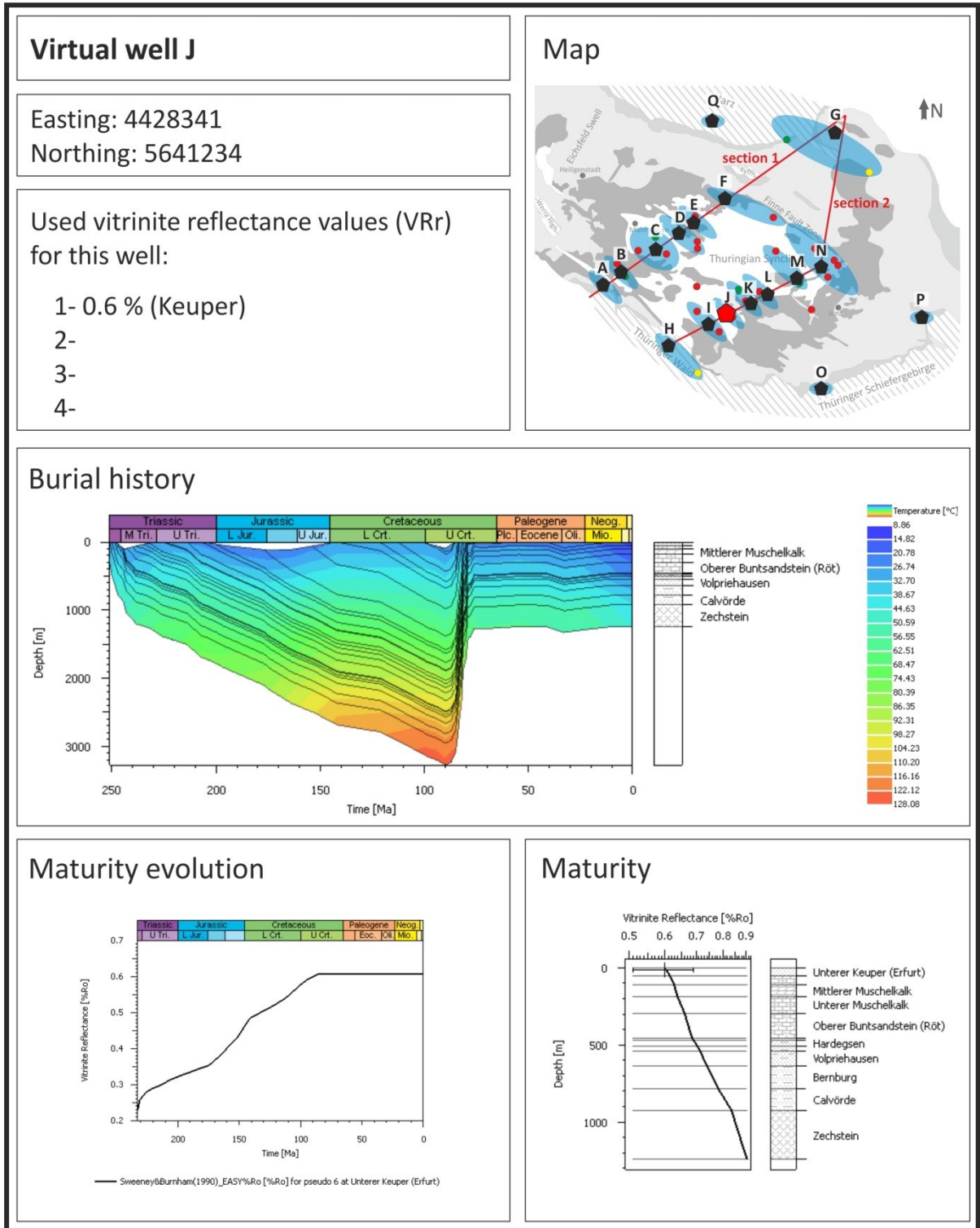
Fig. A 10: Characteristics of virtual well J.

Virtual well K

Easting: 4436412
Northing: 5645420

Used vitrinite reflectance values (VRr)
for this well:

1- 0.68 % (Keuper)
2- 0.89 % (Kupferschiefer)
3-
4-

Map

Burial history

Maturity evolution

— Sweeney&Burnham(1990)_EASY%Ro [%Ro] for pseudo 18 at Unterer Keuper (Erfurt)

Maturity
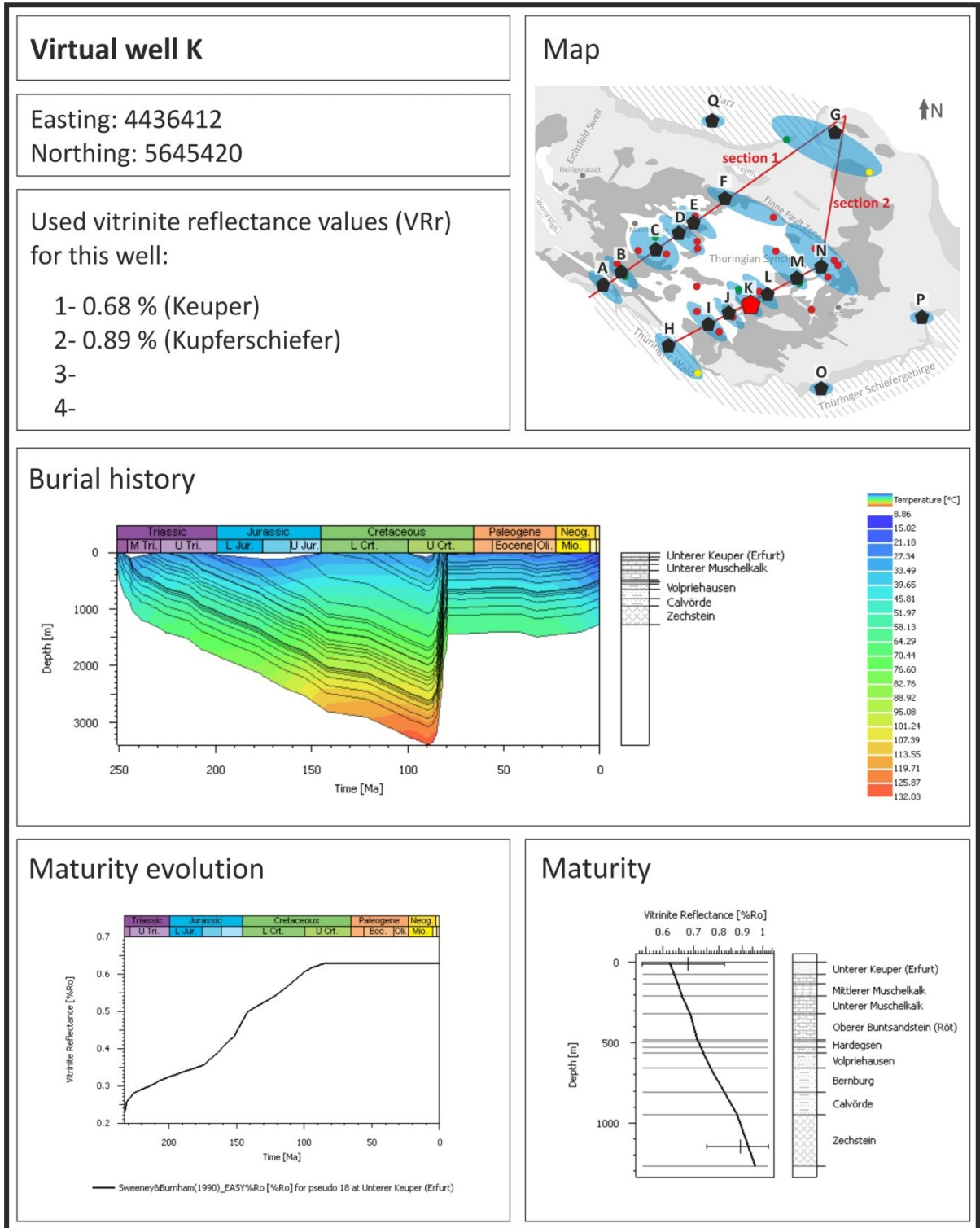
Fig. A 11: Characteristics of virtual well K.
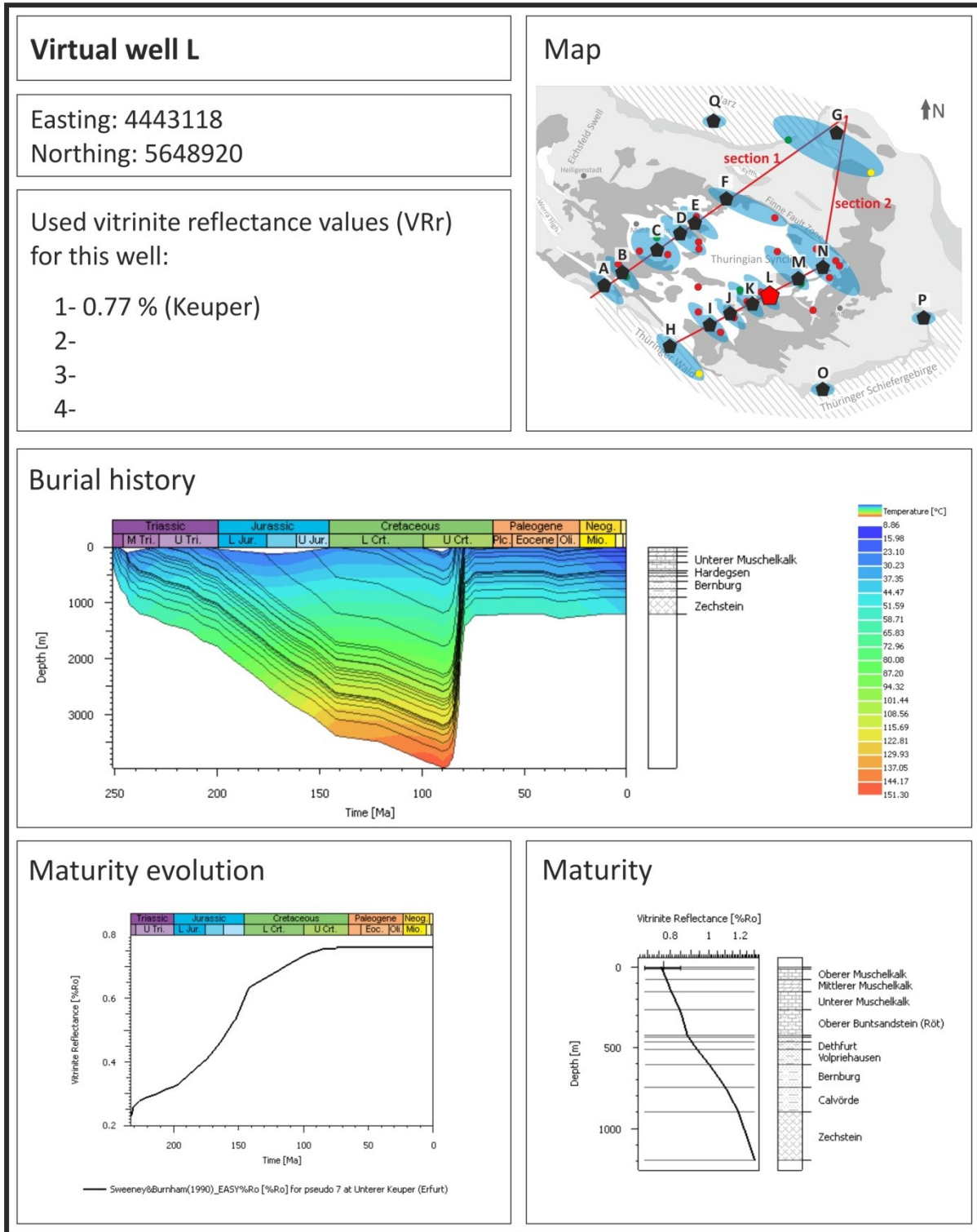
Fig. A 12: Characteristics of virtual well L.

Virtual well M

Easting: 4454350
Northing: 5654674

Used vitrinite reflectance values (VRr)
for this well:

1- 0.86 % (Keuper)
2- 1.16 % (Kupferschiefer)
3-
4-

Map

Burial history

Maturity evolution

Maturity
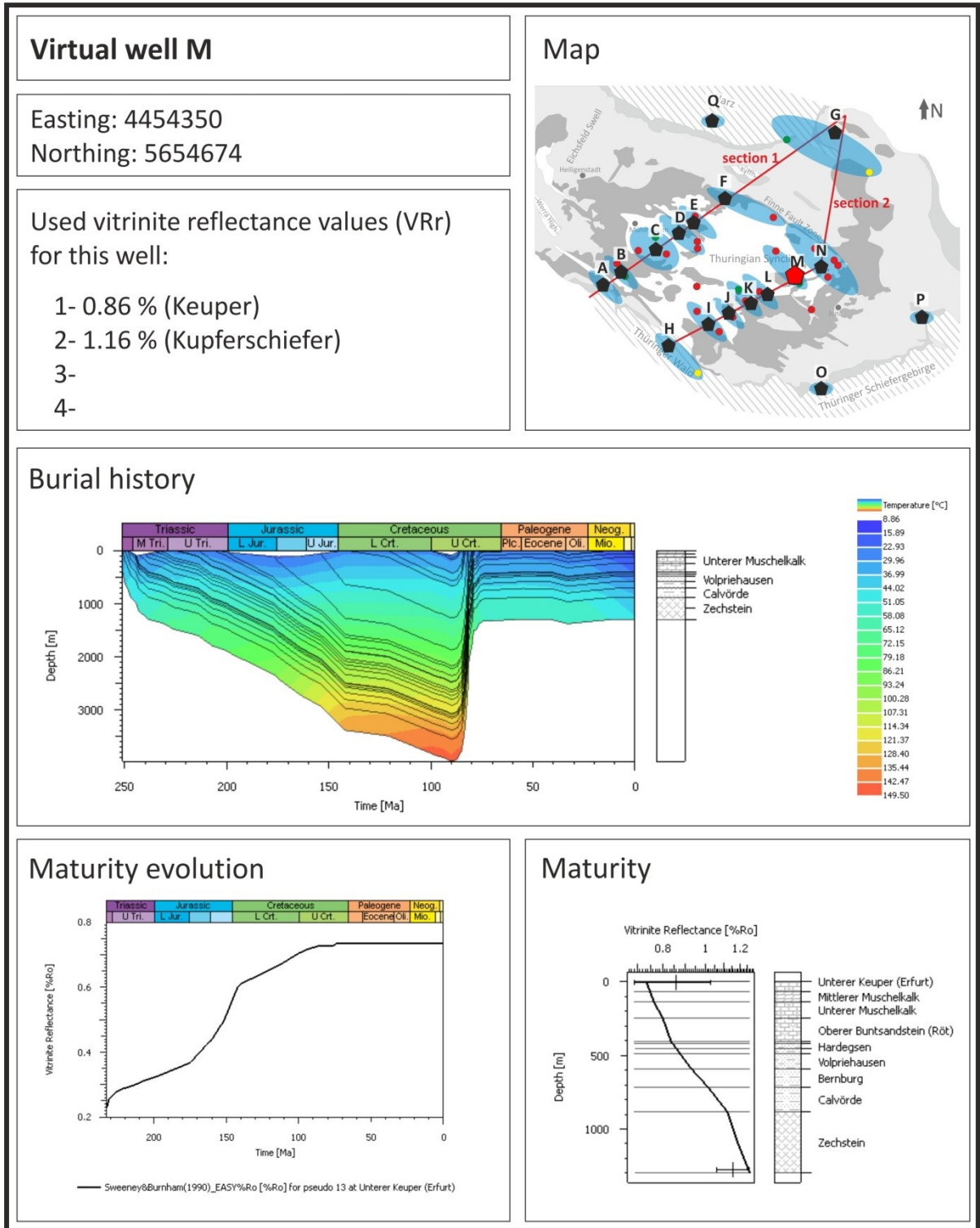
Fig. A 13: Characteristics of virtual well M.

Virtual well N

Easting: 4463810
Northing: 5658970

Used vitrinite reflectance values (VRr)
for this well:

1- 0.56 % (Keuper)
2- 0.57 % (Keuper)
3- 0.54 % (Keuper)
4- 0.57 % (Keuper)

Map

Burial history

Maturity evolution

Maturity
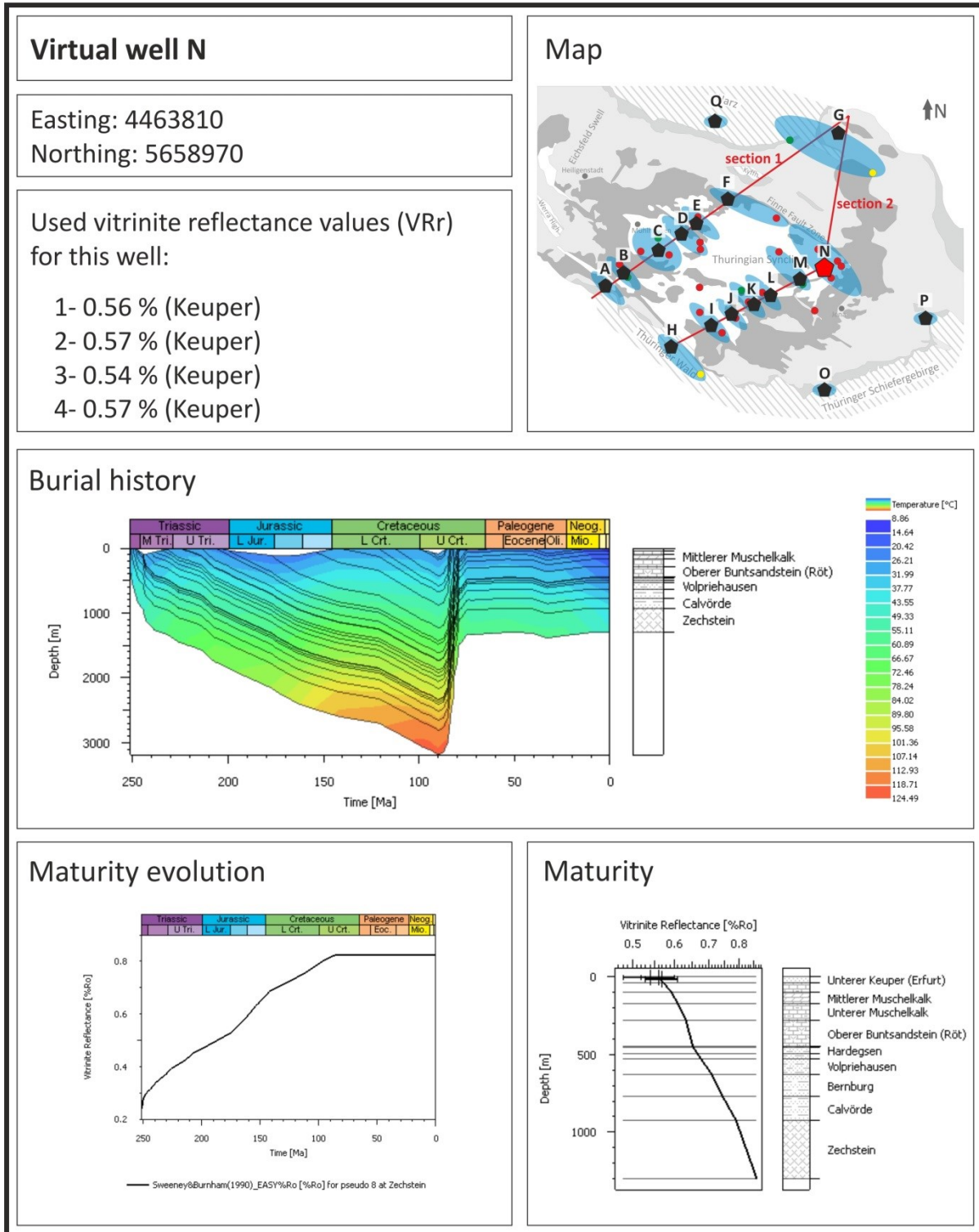
Fig. A 14: Characteristics of virtual well N.

Virtual well O

Map

Easting: 4463413
Northing: 5612070

Used vitrinite reflectance values (VRr) for this well:

1- 0.83 % (Kupferschiefer)
2-
3-
4-

Burial history

Maturity evolution

Sweeney&Burnham(1990)_EASY%Ro [%Ro] for pseudo 15 at Zechstein

Maturity
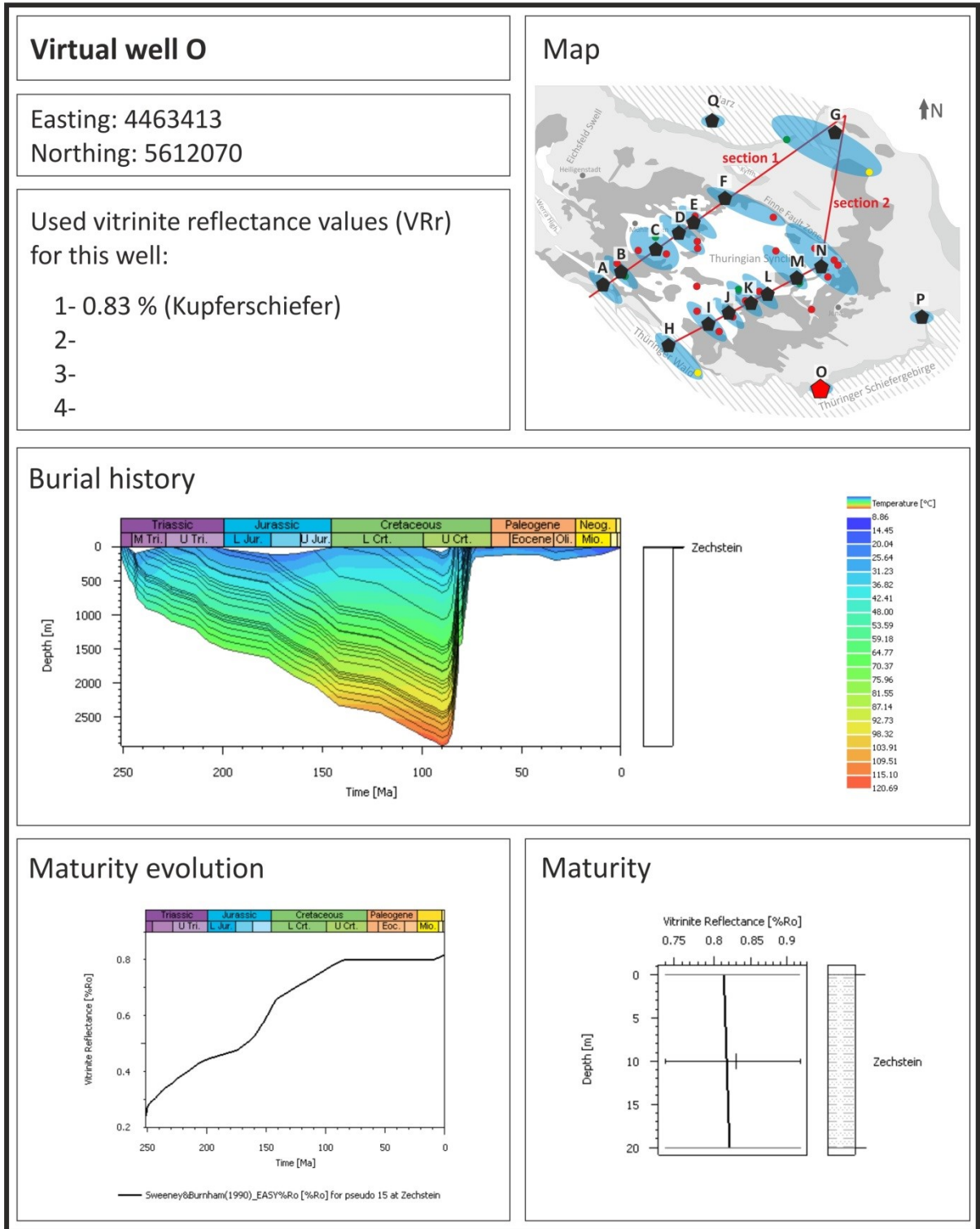
Fig. A 15: Characteristics of virtual well O.
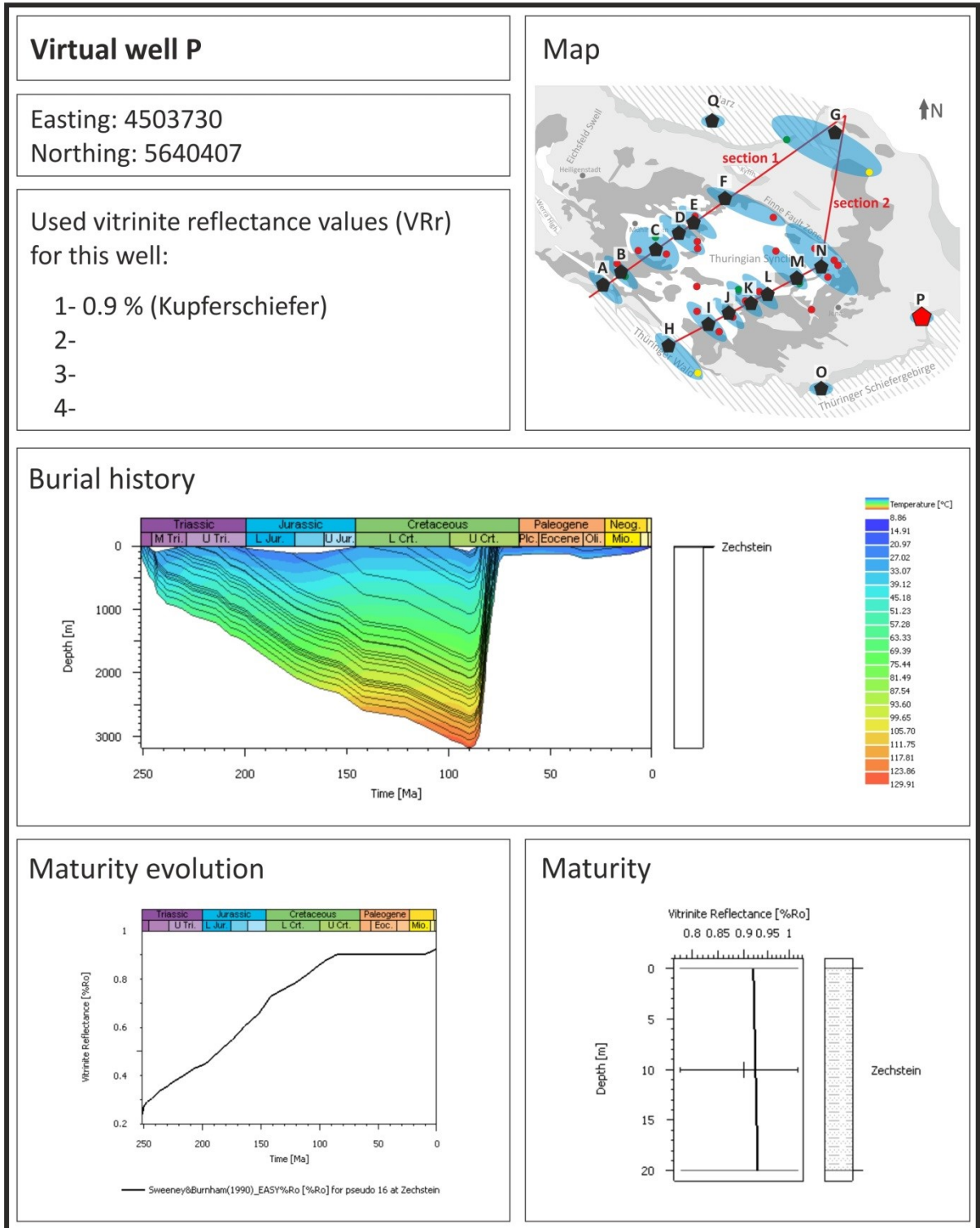
Fig. A 16: Characteristics of virtual well P.

Virtual well Q

Easting: 4419905
Northing: 5717220

Used vitrinite reflectance values (VRr)
for this well:

1- 1.45 % (Netzkater F.)
2-
3-
4-

Map

Burial history

Maturity evolution

Sweeney&Burnham(1990)_EASY%Ro [%Ro] for pseudo 19 at Rotliegend

Maturity
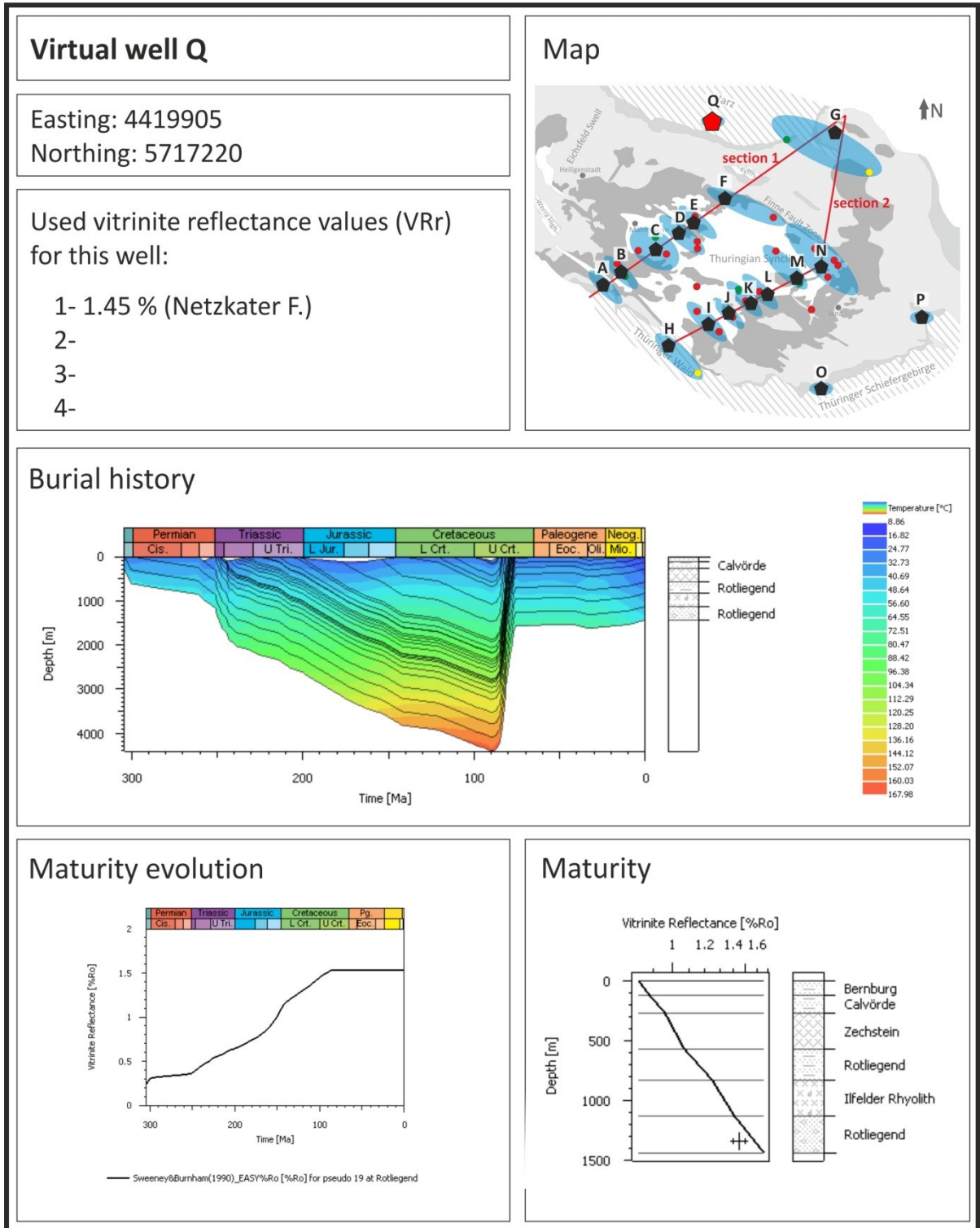
Fig. A 17: Characteristics of virtual well Q.

10. I.2. Core photos
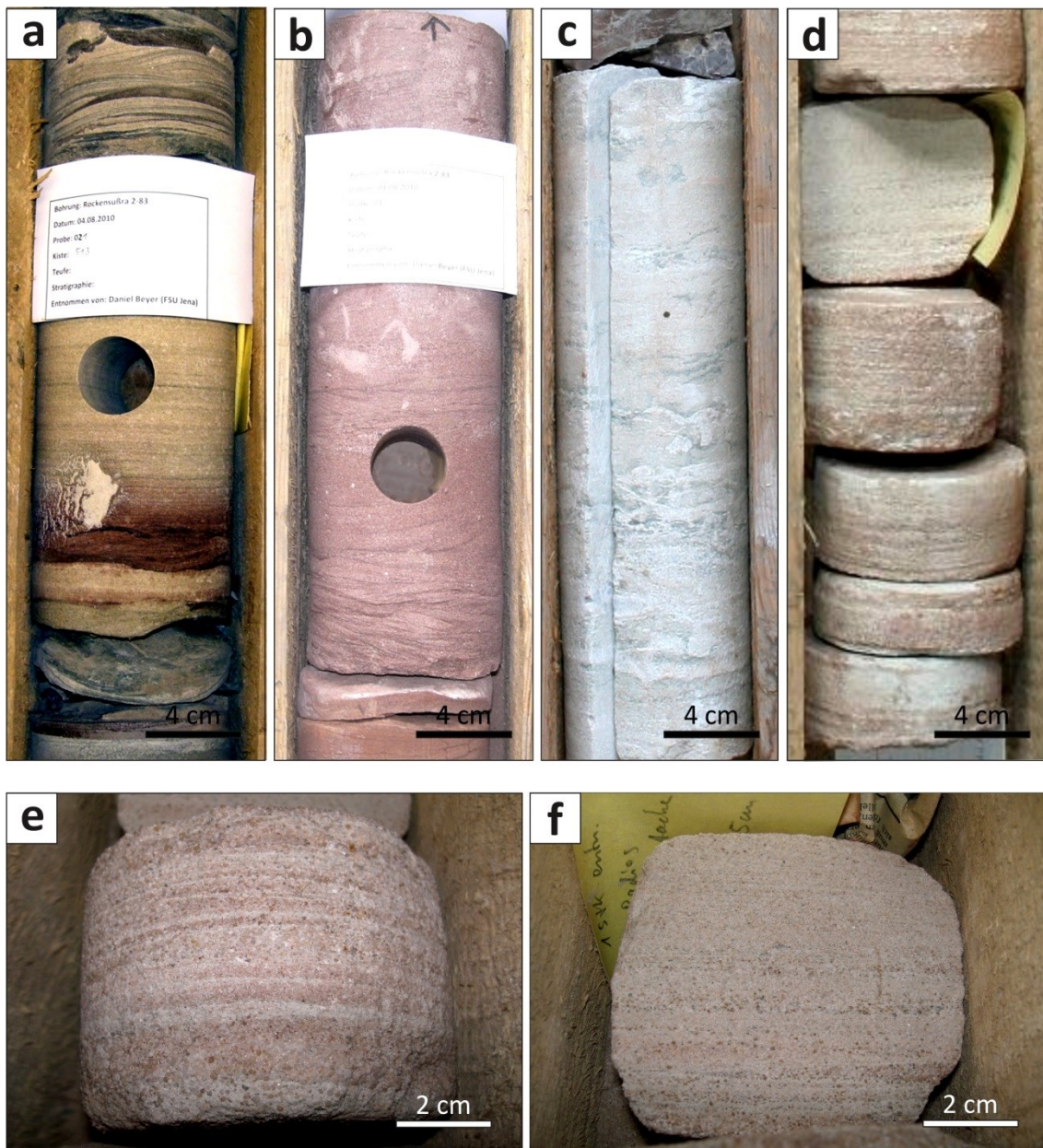
Fig. A 18: Drilling core Rks2, photos: a) lacustrine sandstone (sample Rks2-21, Bernburg Formation); b) sandflat sandstone (sample Rks2-1, Hardegsen Formation); c) fluvial sandstone (sample Rks2-31, Solling Formation); d) + e) + f) eolian sandstone (sample Rks2-34, Detfurth Formation).

Fig. A 19: Drilling core Fh13, photos: a) sandflat sandstone (sample Fh13-46, Fh13-47, Fh13-50, Detfurth Formation); b) eolian sandstone (sample Fh13-88, Detfurth Formation); c) sandflat sandstone (sample Fh13-12, Hardegsen Formation); d) sandflat sandstone (sample Fh13-85, Volpriehausen Formation).

Fig. A 20: Drilling core Ballst, photos: a) lacustrine sandstone (sample Ballst-8, Bernburg Formation); b) lacustrine sandstone (sample Ballst-9, Bernburg Formation); c) sandflat sandstone (sample Ballst-5, Volpriehausen Formation); d) sandflat sandstone (sample Ballst-1, Volpriehausen Formation).

Fig. A 21: Drilling core Gü1, photos: a) fluvial sandstone (sample Gü1-2, Solling Formation); b) fluvial sandstone (sample Gü1-6, Solling Formation); c) sandflat sandstone (sample Gü1-9, Hardegsen Formation); d) sandflat sandstone (sample Gü1-25, Hardegsen Formation).

Fig. A 22: Drilling core La35, photos: a) fluvial sandstone (samples La35-7, La35-8, La35-9, La35-10, La35-11, La35-12, Solling Formation); b) sandflat sandstone (samples La35-29, La35-30, La35-31, La35-32, Hardegsen Formation).

10. I.3. Thin sections
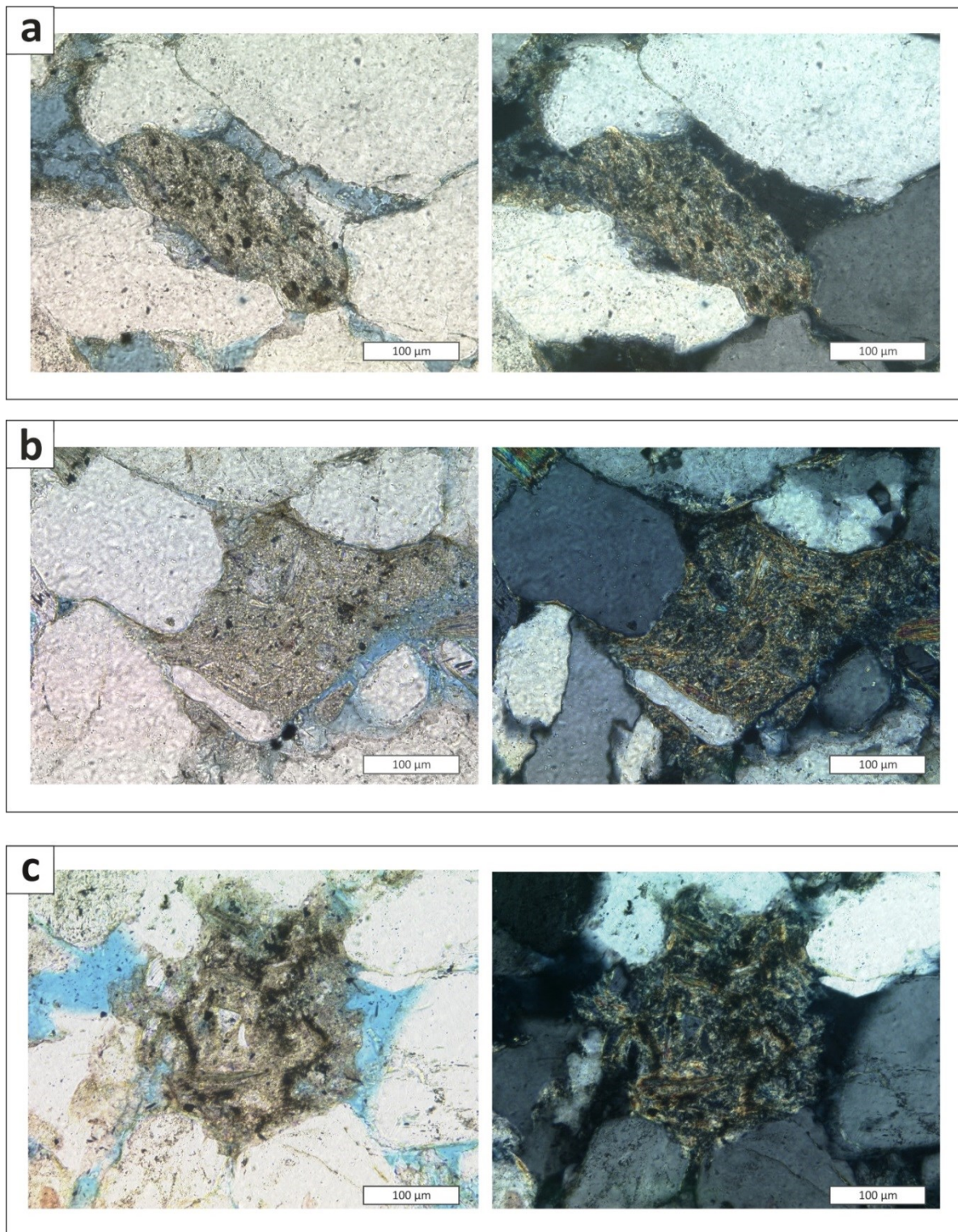
Fig. A 23: Thin section images (left: normal light, right: crossed nicols) of sedimentary lithic fragments: a) sample Gü1-4 (fluvial facies, Solling Formation); b) sample Gü1-26 (sandflat facies, Hardegsen Formation); c) sample Gü1-28 (sandflat formation, Hardegsen Formation).
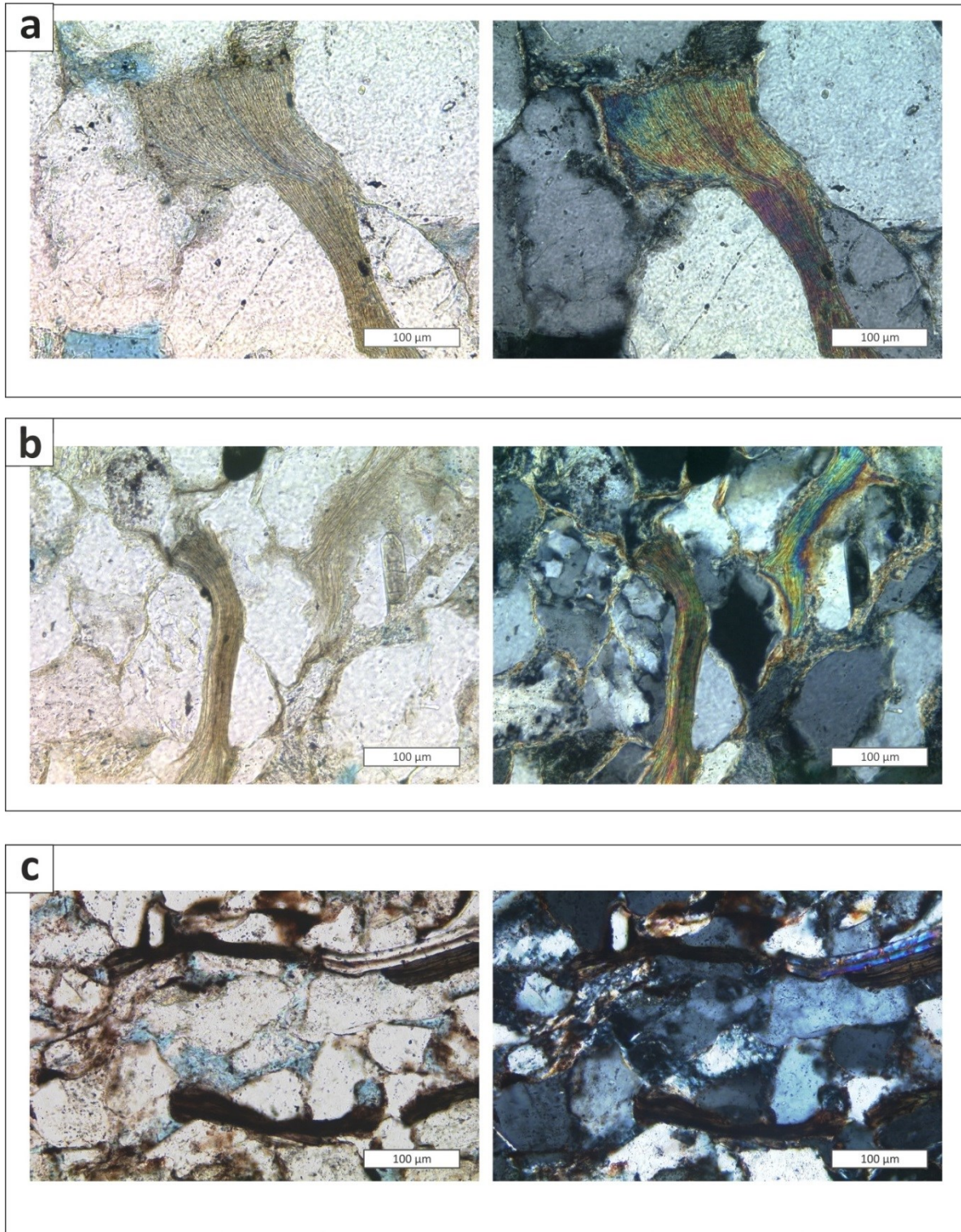
Fig. A 24: Thin section images (left: normal light, right: crossed nicols) of detrital micas: a) sample Gü1-26 (sandflat facies, Hardegsen Formation); b) sample Gü1-24 (sandflat facies, Hardegsen Formation); c) corroded/oxidized mica in sample Fh13-40 (sandflat facies, Detfurth Formation).
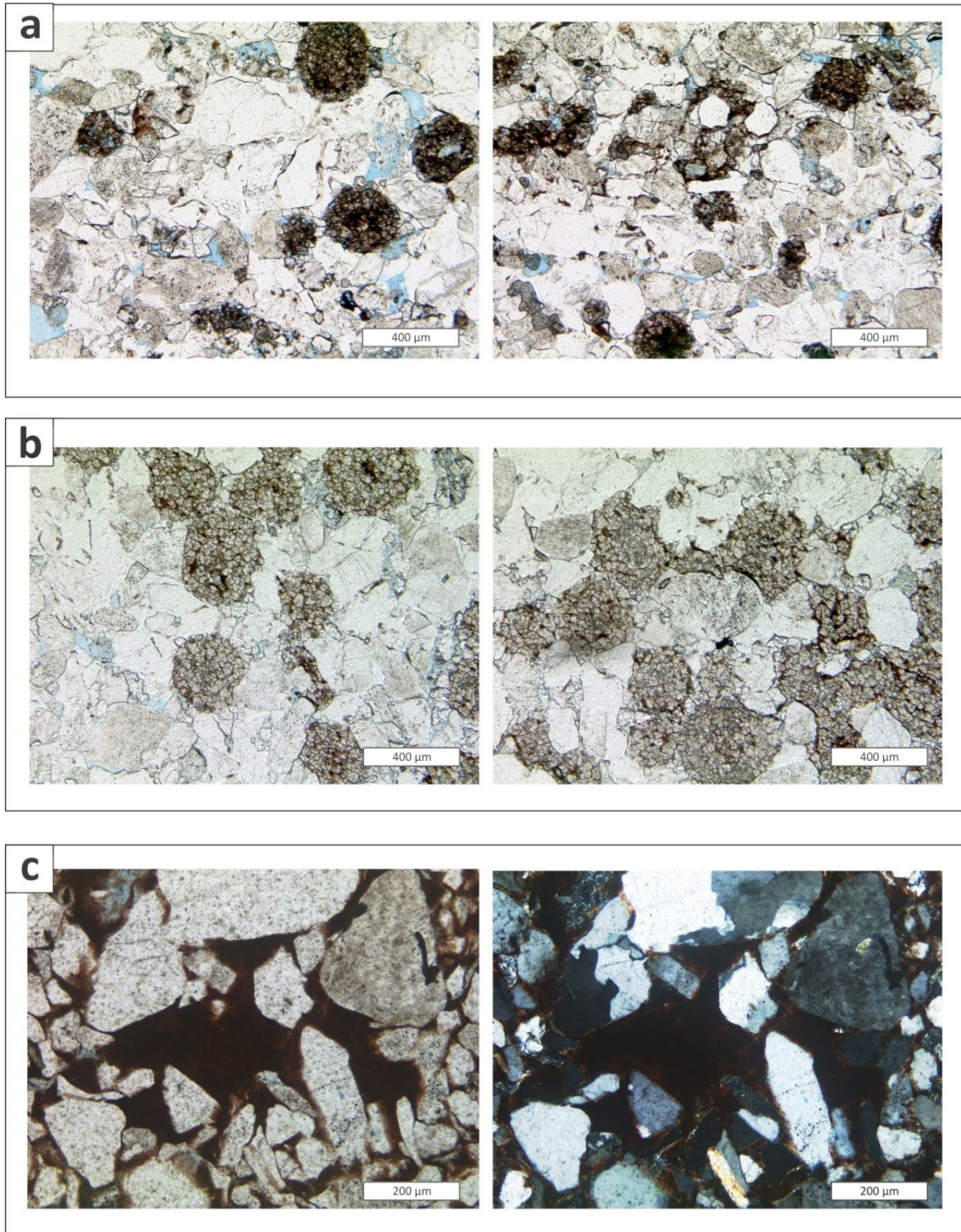
Fig. A 25: Thin section images (normal light) of ooids in a) sample Ballst-9 (lacustrine facies, Bernburg Formation); b) Ballst-8 (lacustrine facies, Bernburg Formation). Thin section image (left: normal light, right: crossed nicols) of c) ferrous clay matrix in sample Fh13-1 (sandflat facies, Hardegsen Formation).
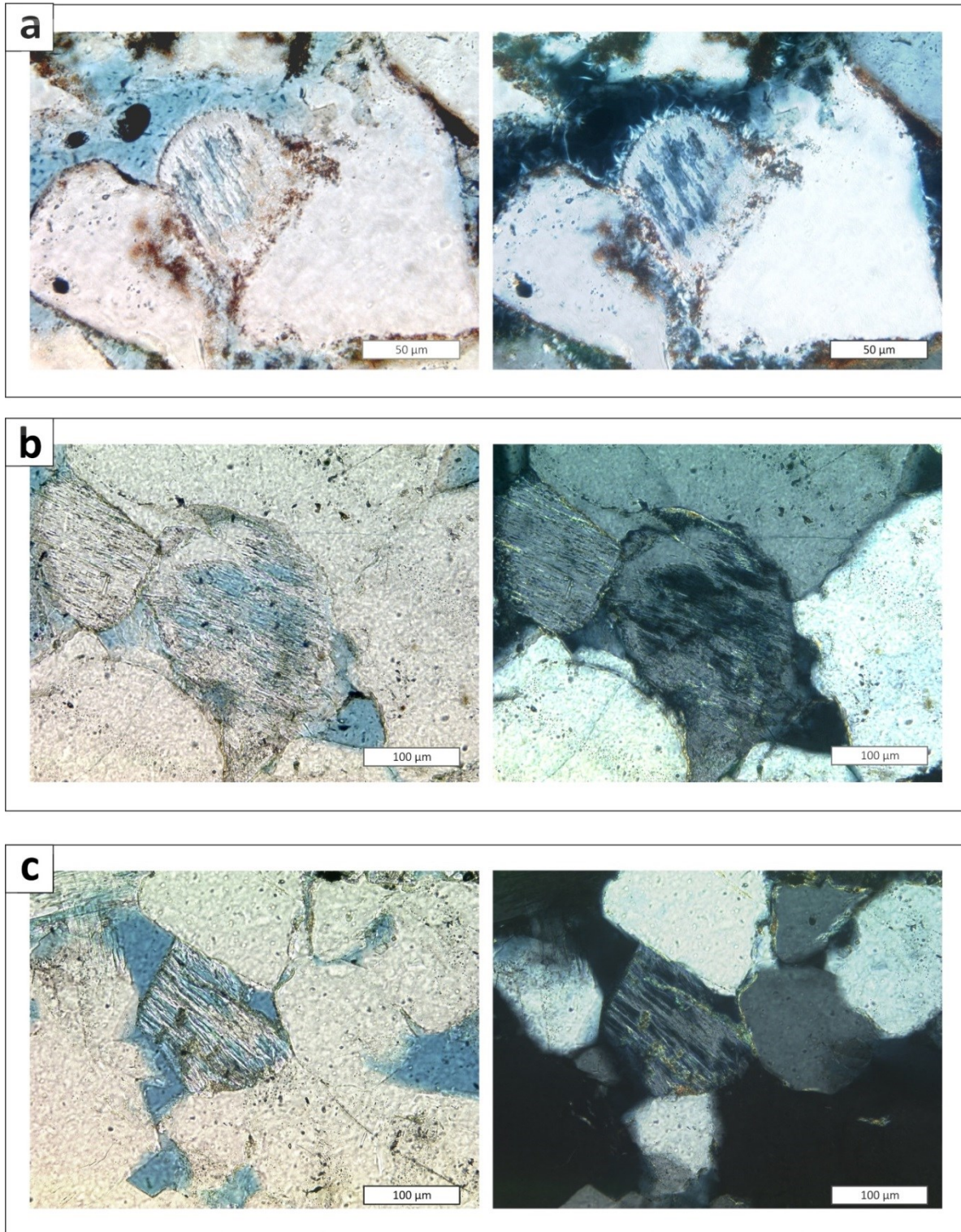
Fig. A 26: Thin section images (left: normal light, right: crossed nicols) of corroded feldspars: a) corroded feldspar with radial illite growth (sample Te1-7, sandflat facies, Hardegsen Formation); b) corroded feldspars (sample Gü1-26, sandflat facies, Hardegsen Formation); c) corroded feldspar with illite (sample Gü1-4, fluvial facies, Solling Formation).
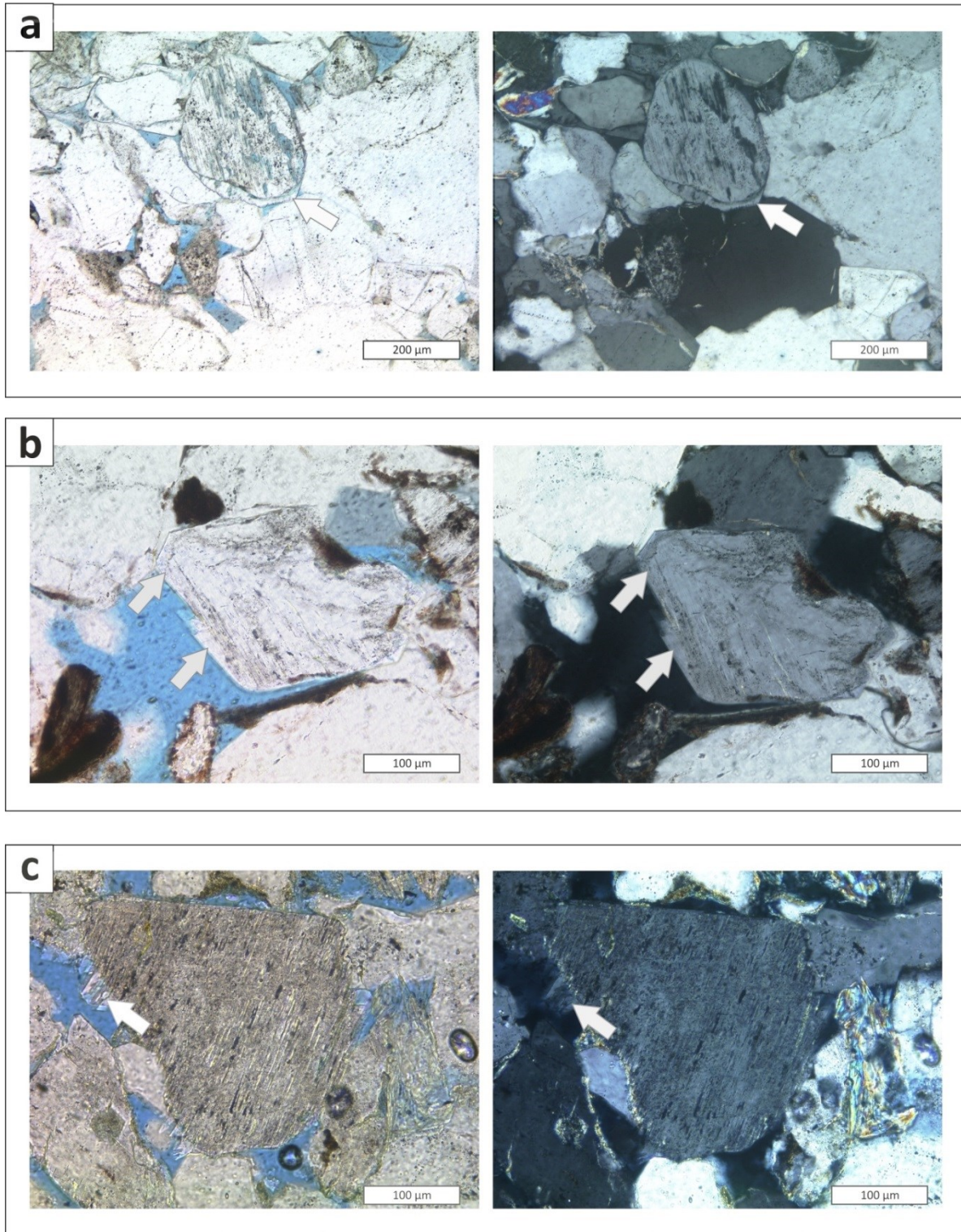
Fig. A 27: Thin section images (left: normal light, right: crossed nicols) of authigenic feldspar cement: a) sample La35-4 (fluvial facies, Solling Formation); sample Te1-16 (sandflat facies, Hardegsen Formation); c) sample Gü1-2 (fluvial facies, Solling Formation).
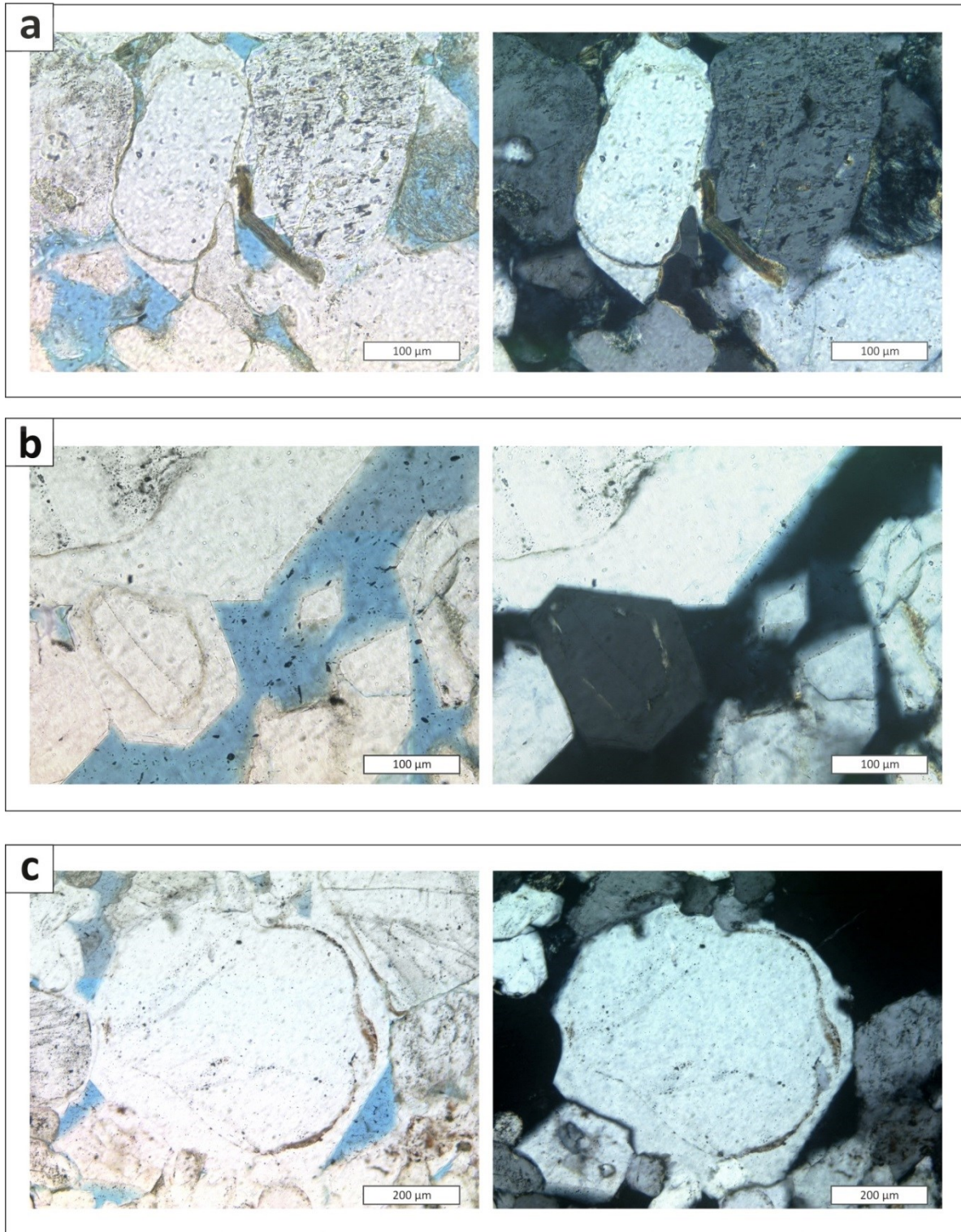
Fig. A 28: Thin section images (left: normal light, right: crossed nicols) of authigenic quartz cement: a) sample Gü1-23 (sandflat facies, Hardegsen Formation); b) sample La35-7 (fluvial facies, Solling Formation); c) sample La35-4 (fluvial facies, Solling Formation).
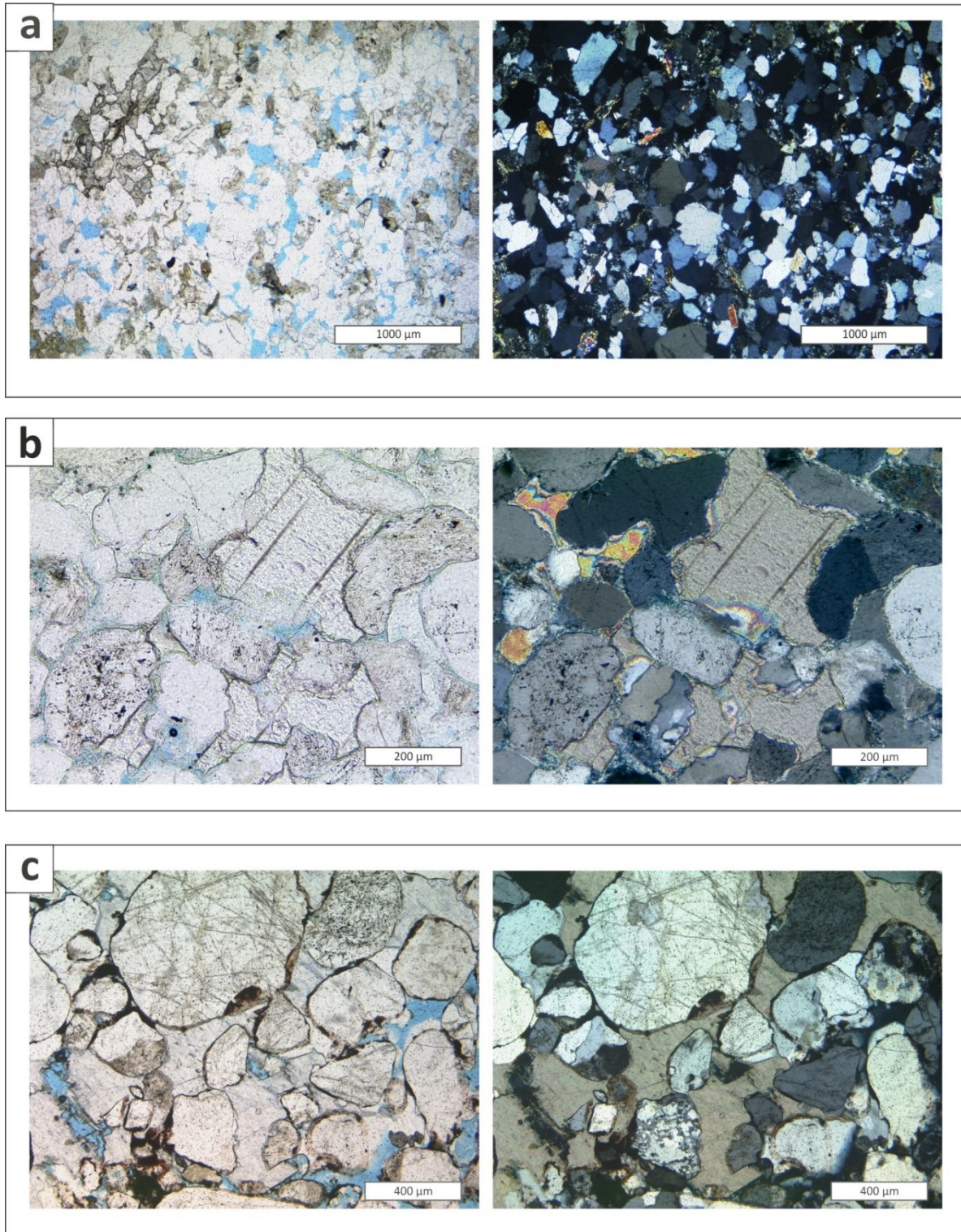
Fig. A 29: Thin section images (left: normal light, right: crossed nicols) of authigenic carbonate cement: a) carbonate patches in sample Gü1-6 (fluvial facies, Solling Formation); b) sample Rks2-31 (fluvial facies, Solling Formation); c) sample Fh13-57 (eolian facies, Detfurth Formation).
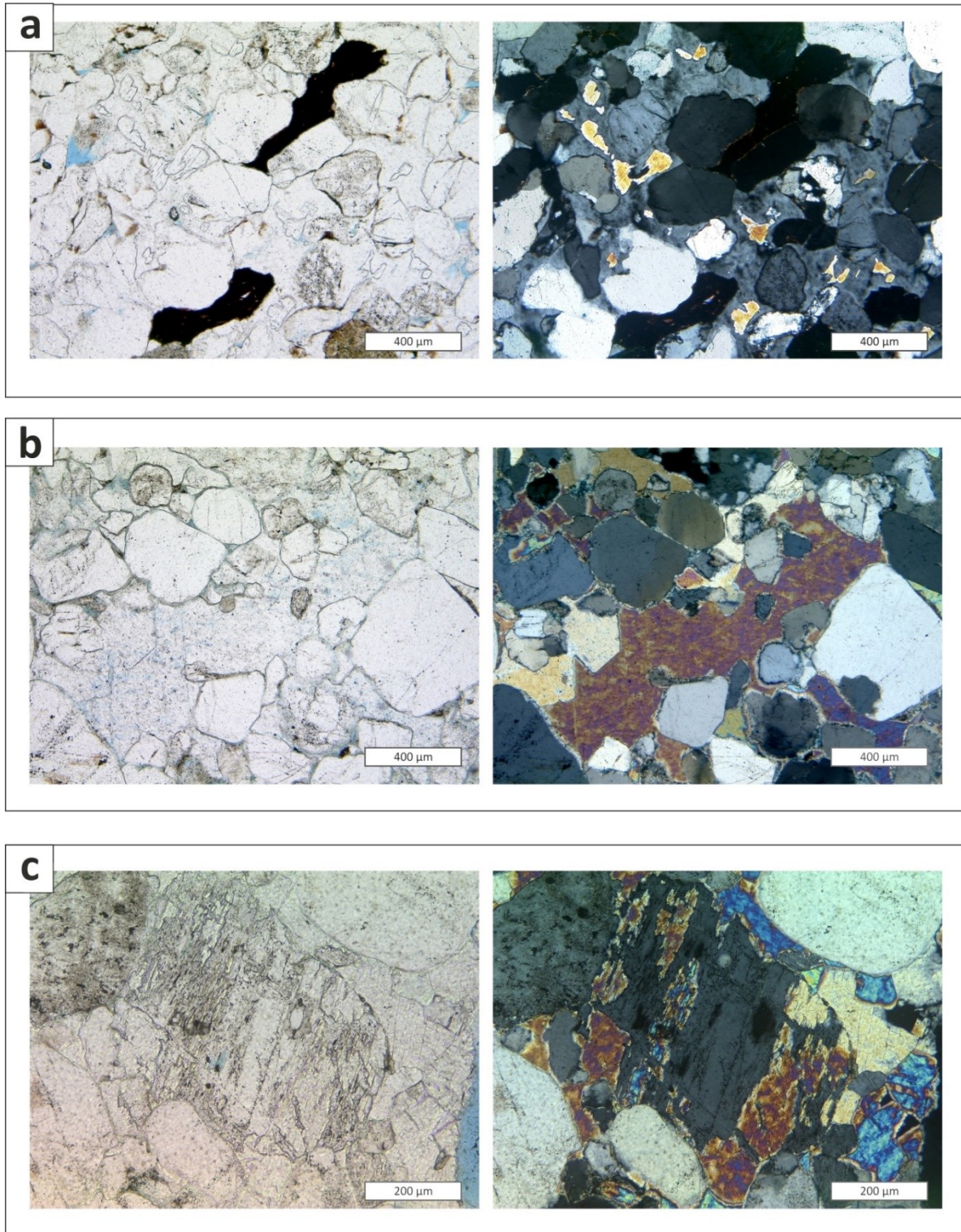
Fig. A 30: Thin section images (left: normal light, right: crossed nicols) of authigenic gypsum and anhydrite cement: a) sample Rks2-32 (fluvial facies, Solling Formation); b) sample Rks2-31 (fluvial facies, Solling Formation); c) sample Gü1-18 (sandflat facies, Hardegsen Formation).
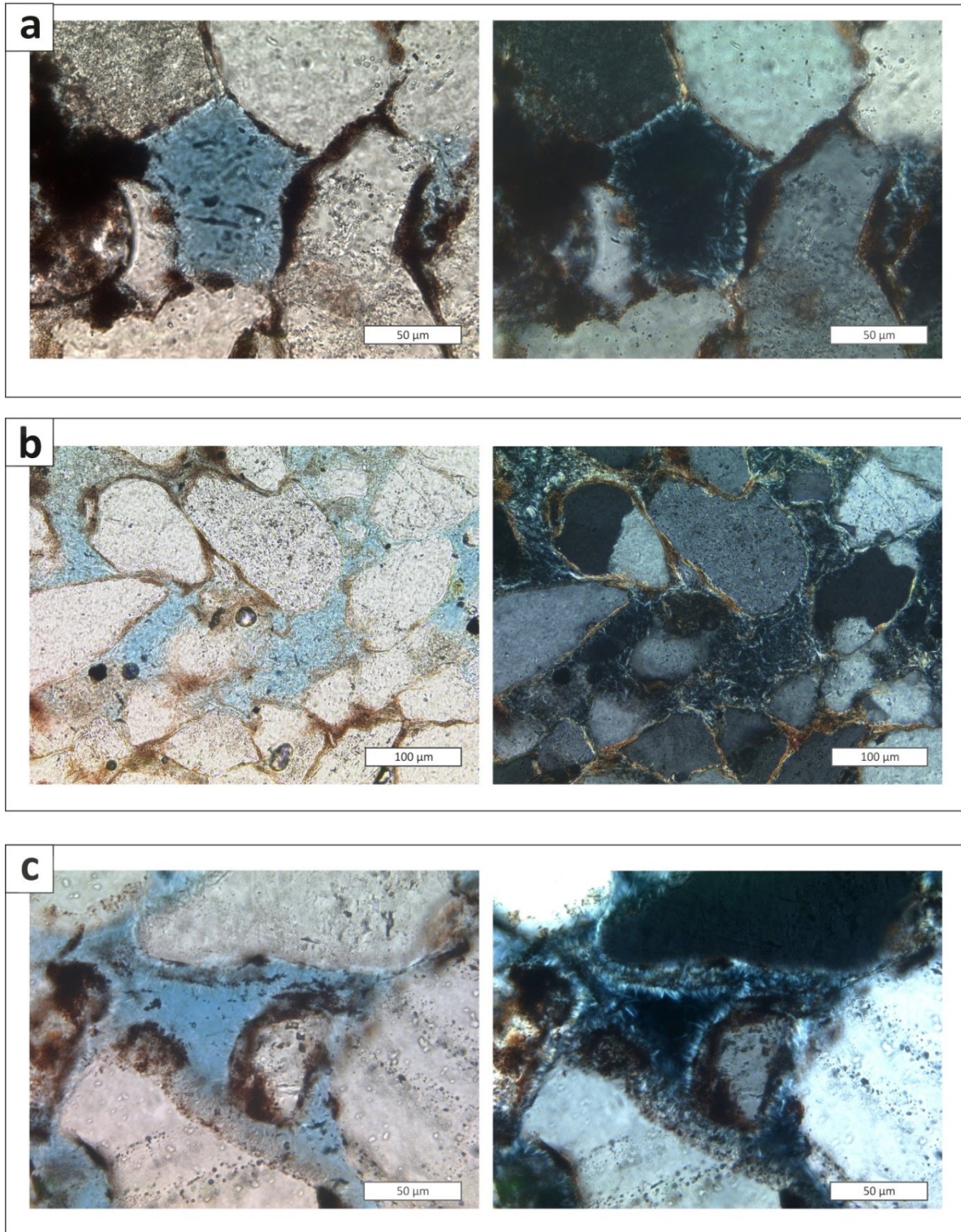
Fig. A 31: Thin section images (left: normal light, right: crossed nicols) of authigenic illite: a) sample Fh13-8 (sandflat facies, Hardegsen Formation); b) sample Fh13-4 (sandflat facies, Hardegsen Formation); c) sample Te1-18 (sandflat facies, Hardegsen Formation).
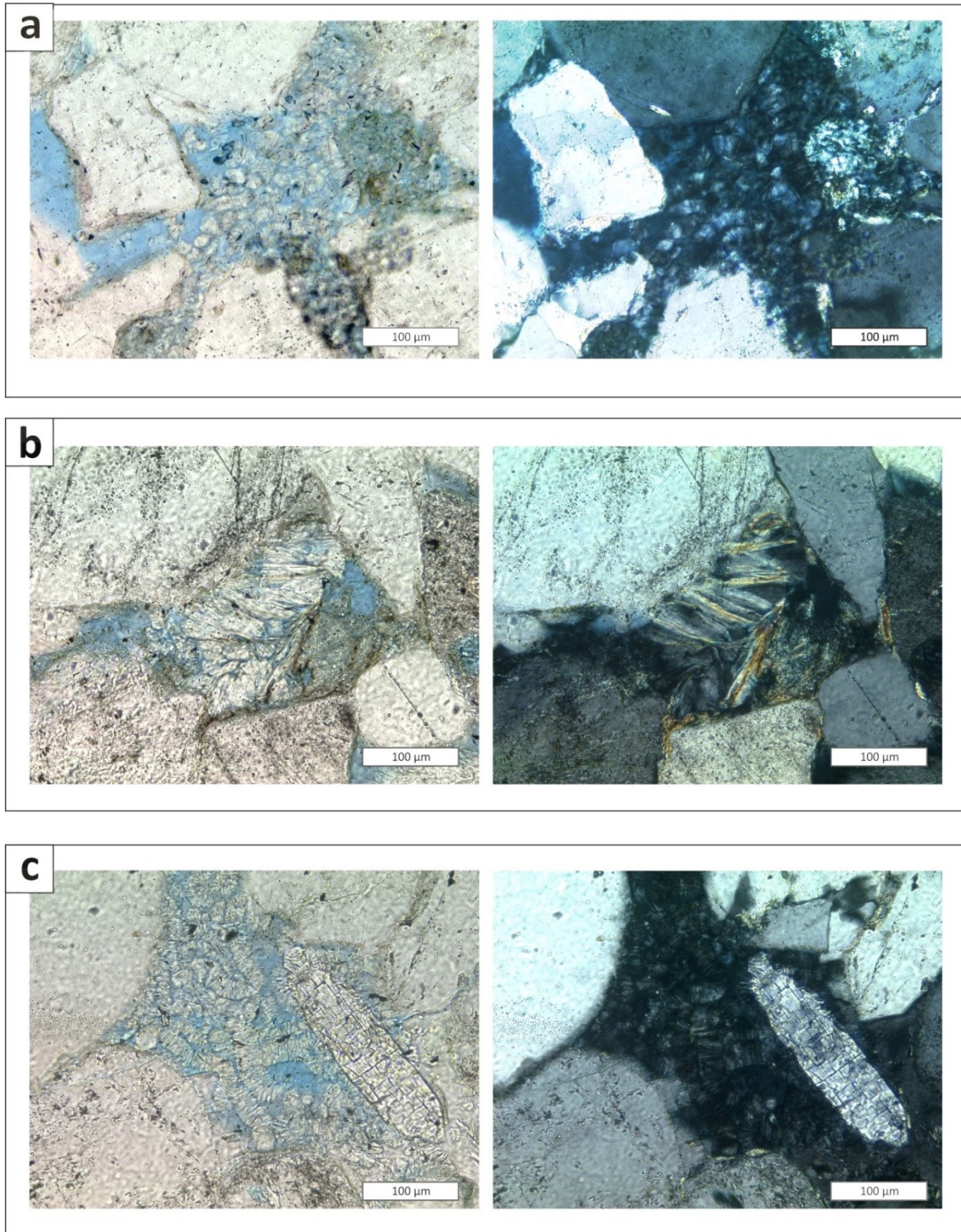
Fig. A 32: Thin section images (left: normal light, right: crossed nicols) of authigenic kaolinite: a) sample Gü1-28 (sandflat facies, Hardegsen Formation); b) sample Gü1-26 (sandflat facies, Hardegsen Formation); c) sample Gü1-26 (sandflat facies, Hardegsen Formation).

10. I.4. Microprobe
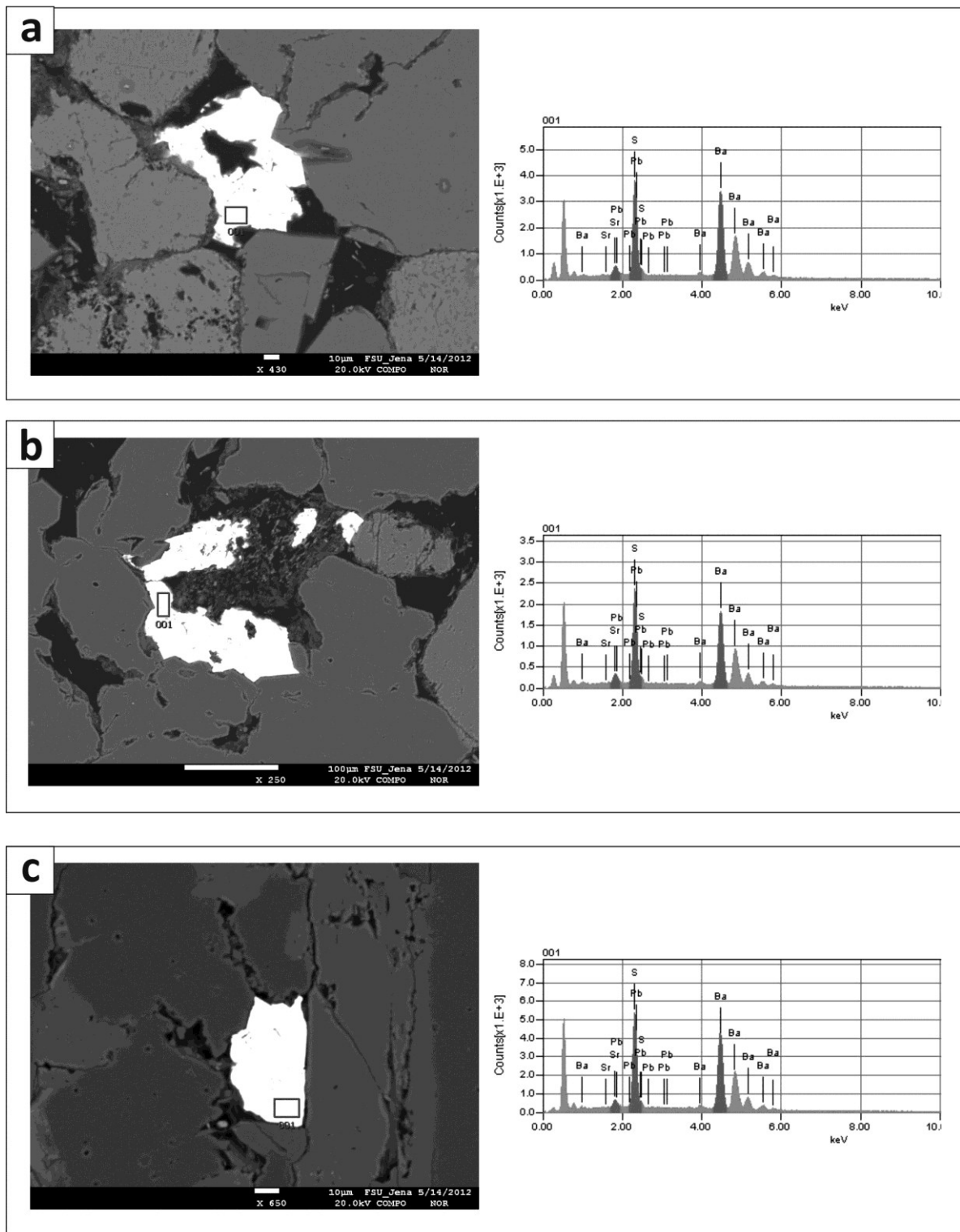
Fig. A 33: Backscattered electron images with the measured Energy-dispersive X-ray spectroscopy of barite: a) + b) sample La35-15 (sandflat facies, Hardegsen Formation); c) sample Ballst11 (lacustrine facies, Bernburg Formation).
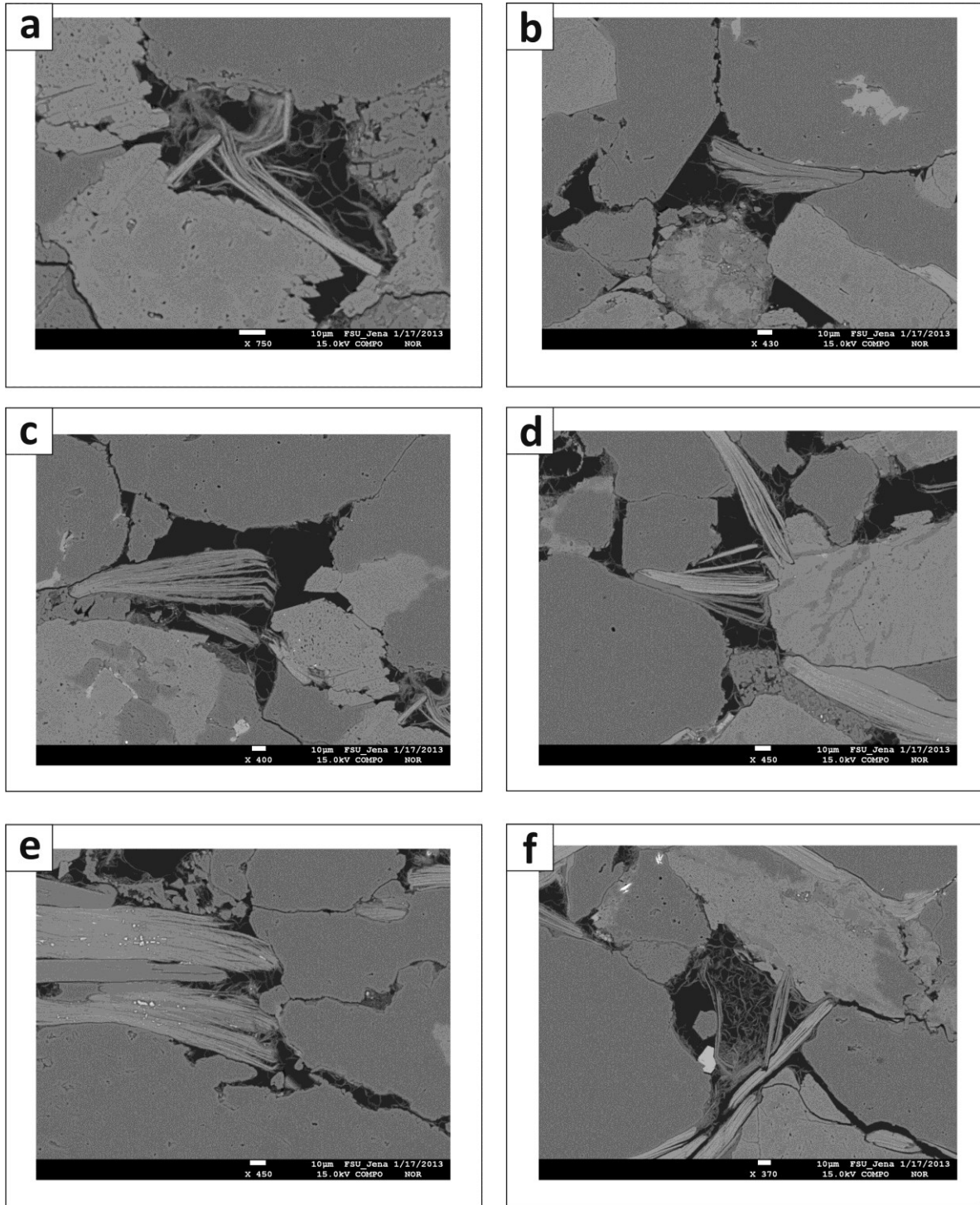
Fig. A 34: Backscattered electron images of illite associated with micas: a) – f) sample fh13-135 (sandflat facies, Volpriehausen Formation).
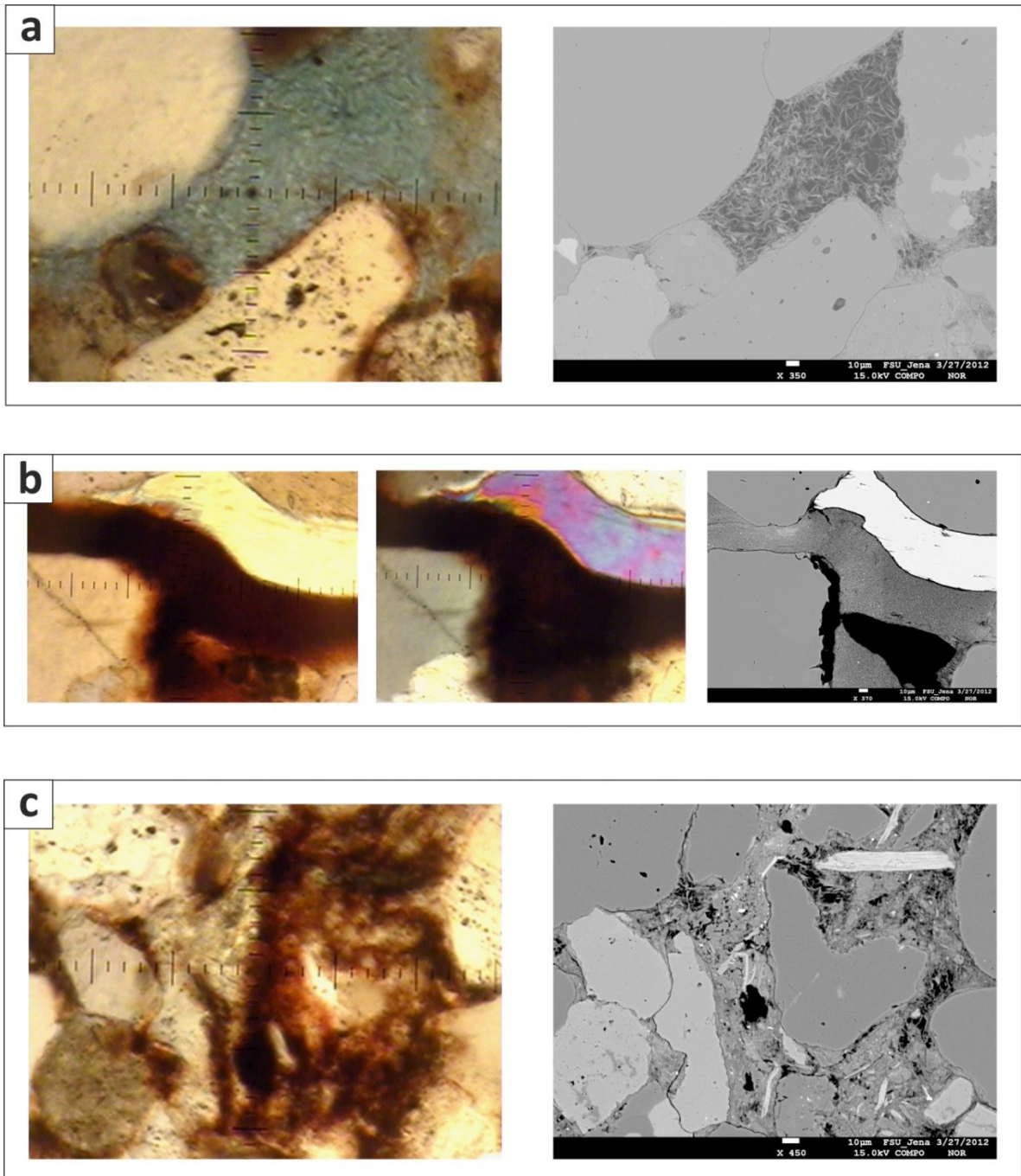
Fig. A 35: Comparison between images from microscope and microprobe: a) illite meshwork in normal light and as backscattered electron image (sample Ag-14, sandflat facies, Volpriehausen Formation); b) red coloured clay next to anhydrite cement in normal light, with crossed nicols and as backscattered electron image (sample Ag-3, sandflat facies, Volpriehausen Formation); c) red coloured clay in normal light and as backscattered electron image (sample Ag-14, sandflat facies, Volpriehausen Formation).
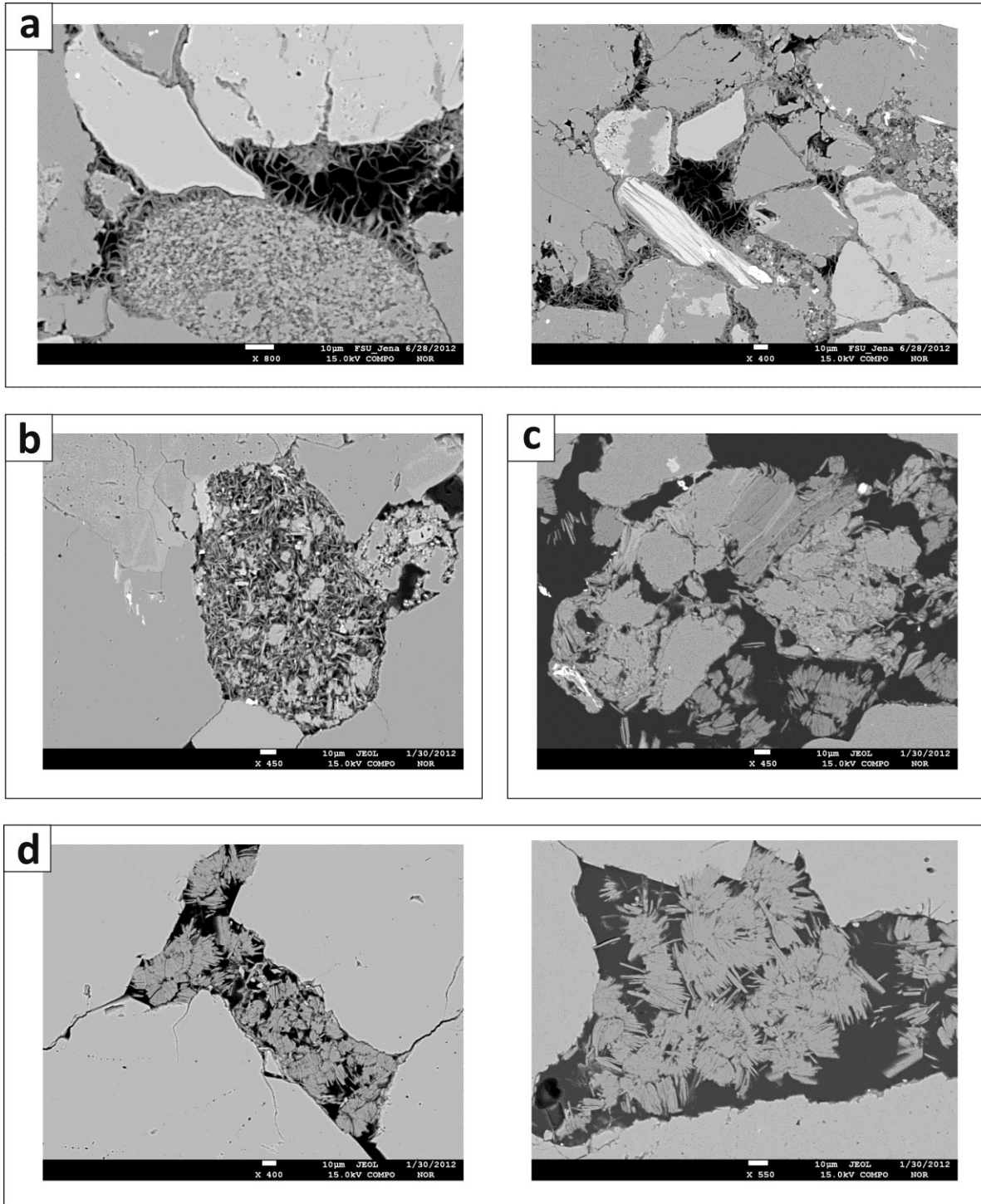
Fig. A 36: Backscattered electron images of illite and kaolinite: a) radial illite overgrowth (sample Ballst-17, lacustrine facies, Calvörde Formation); b) feldspar alteration to illite (sample Ballst-11, lacustrine facies, Bernburg Formation); c) + d) authigenic kaolinite (sample Br2, fluvial facies, Solling Formation).

10. I.5. Scanning electron microscope
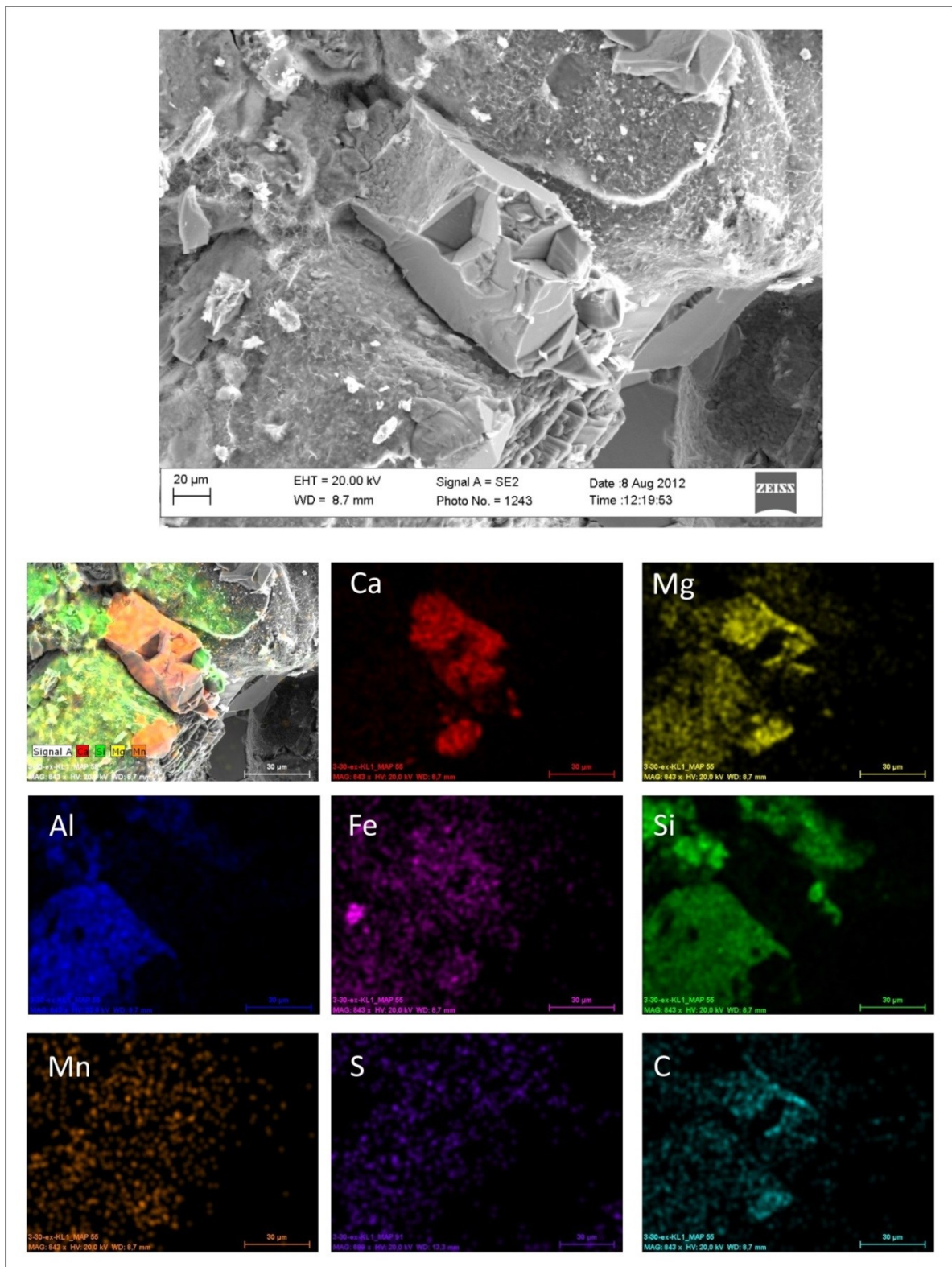
Fig. A 37: Secondary electron image of an authigenic carbonate mineral, with element mapping (sample Ag-3, sandflat facies, Volpriehausen Formation).
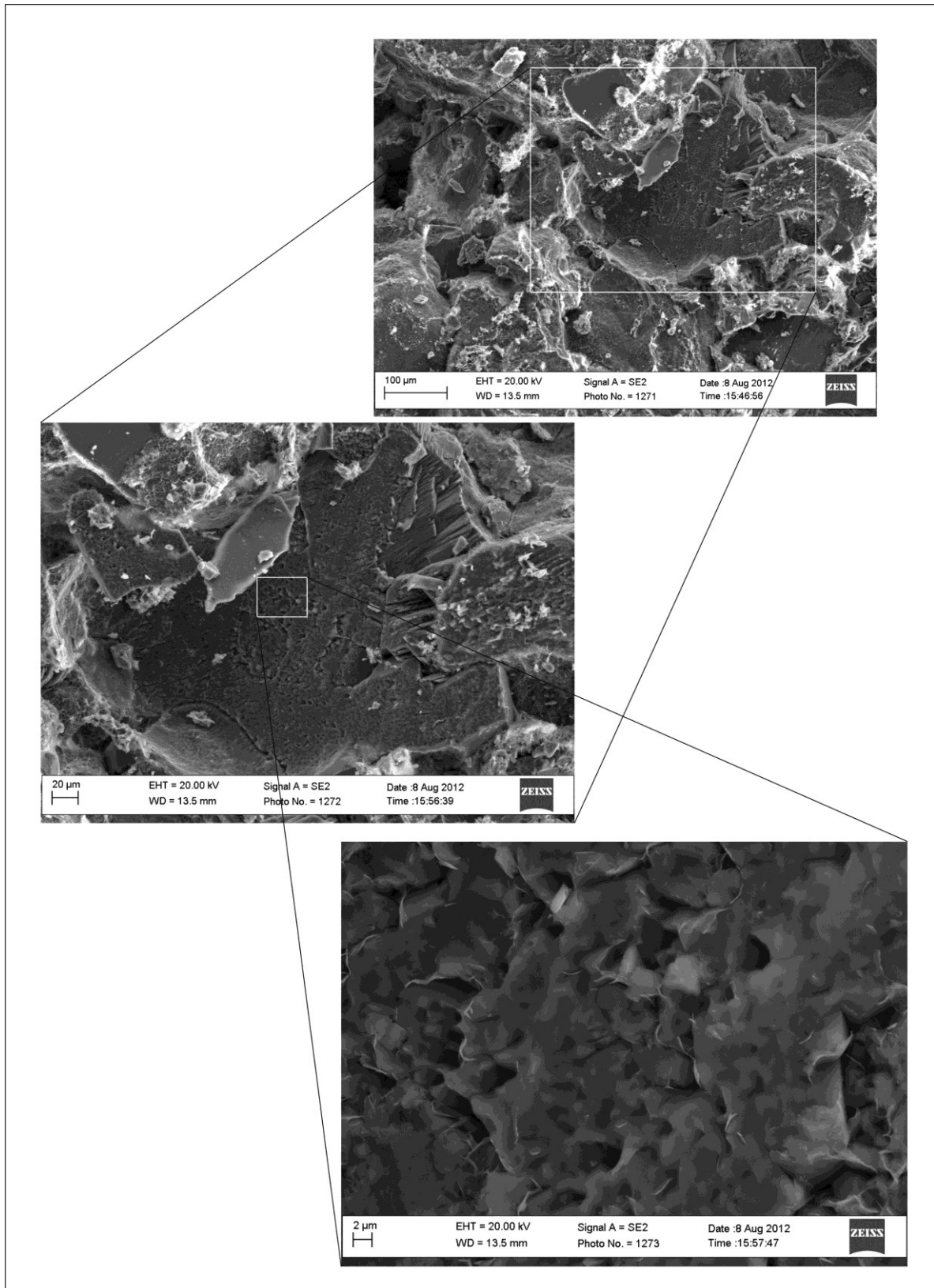
Fig. A 38: Secondary electron image of a notch of a broken out grain (sample Ag-3, sandflat facies, Volpriehausen Formation).
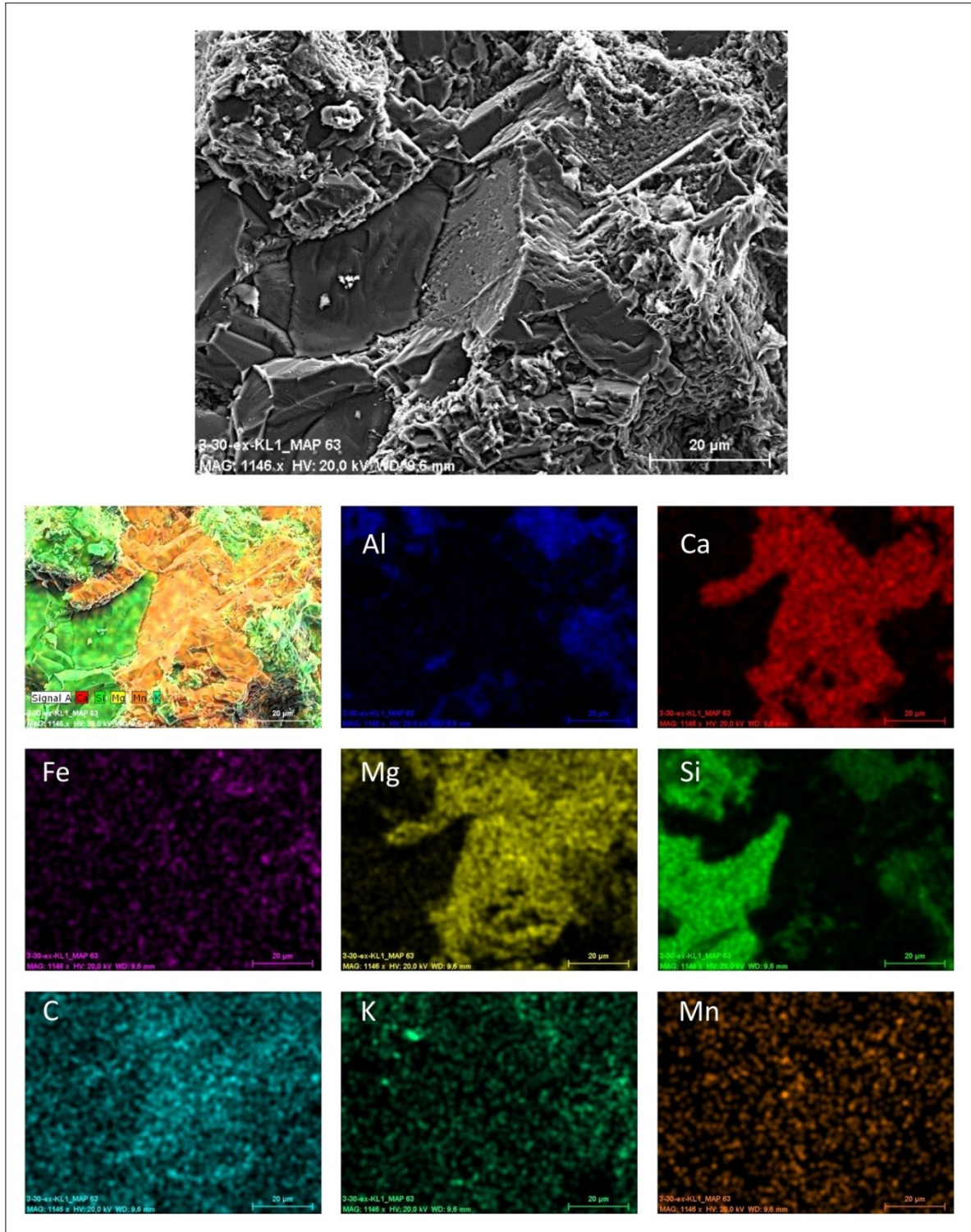
Fig. A 39: Secondary electron image of an authigenic carbonate mineral, with element mapping (sample Ag-3, sandflat facies, Volpriehausen Formation).
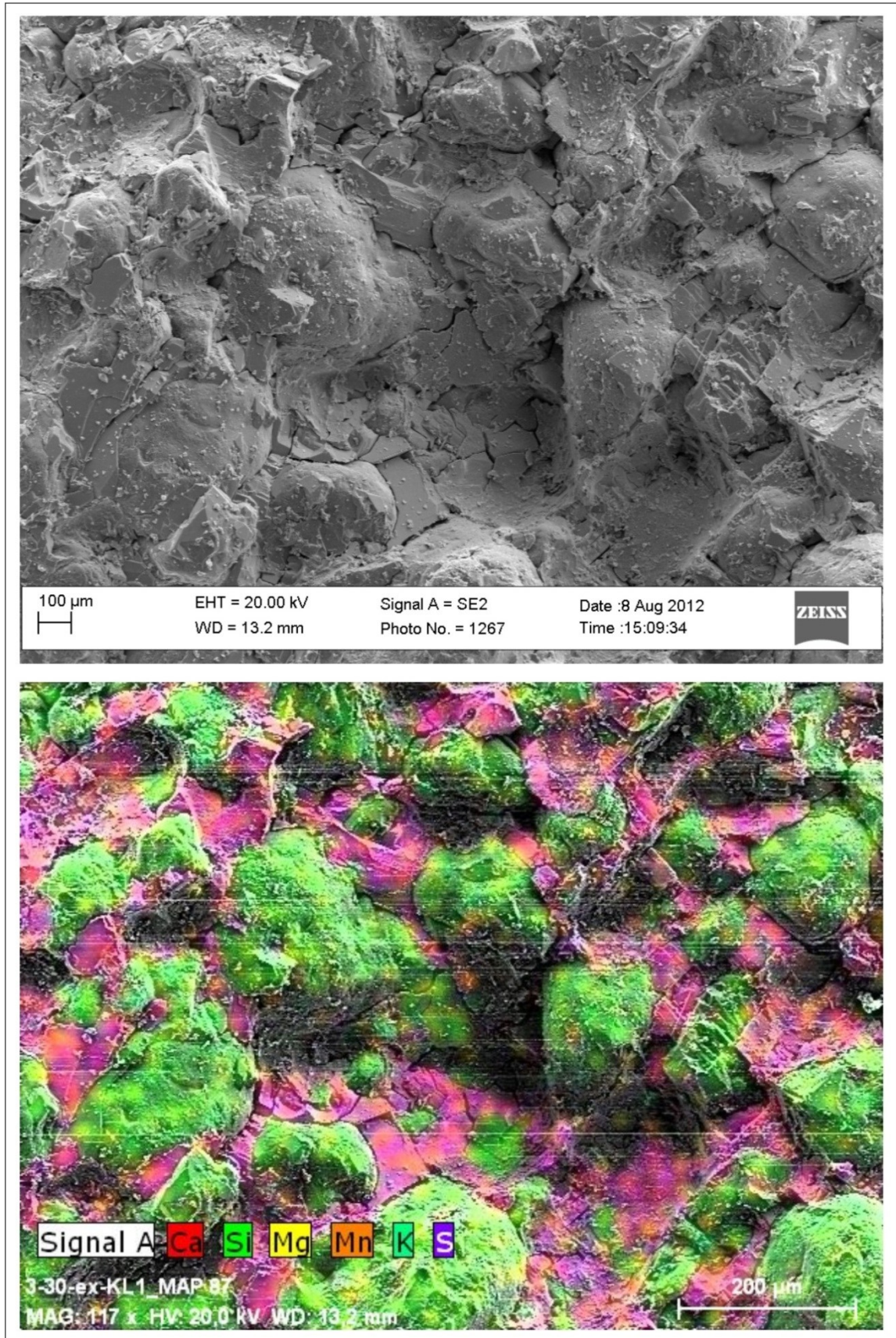
Fig. A 40: Secondary electron image of authigenic sulphate cement in between grains, with element mapping (sample Ballst-29, eolian facies, Detfurth Formation).
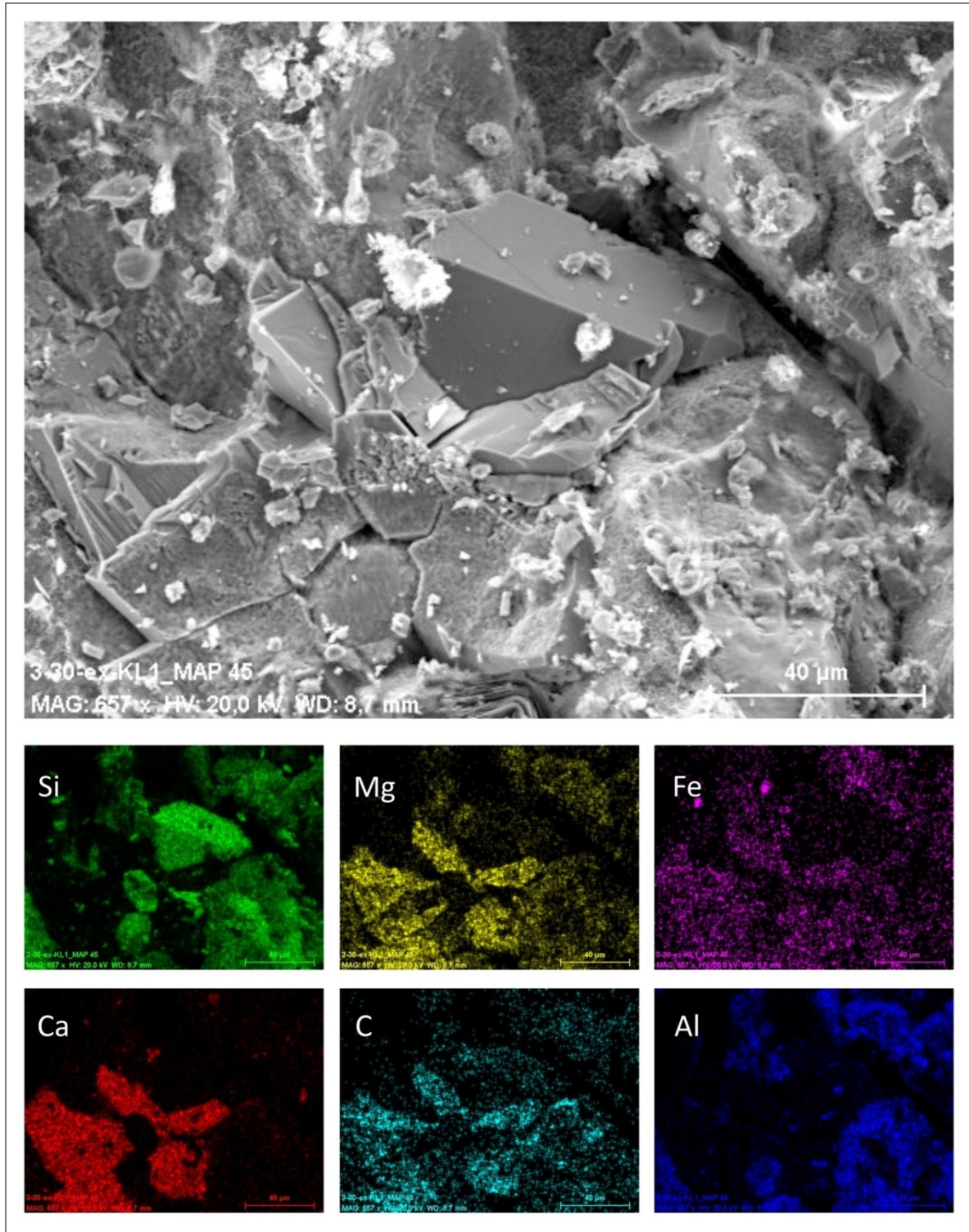
Fig. A 41: Secondary electron image of authigenic quartz cement, with element mapping (sample Ag-3, sandflat facies, Volpriehausen Formation).

10. I.6. Porosity loss by compaction accordingly Houseknecht (1987) and Ehrenberg (1989)
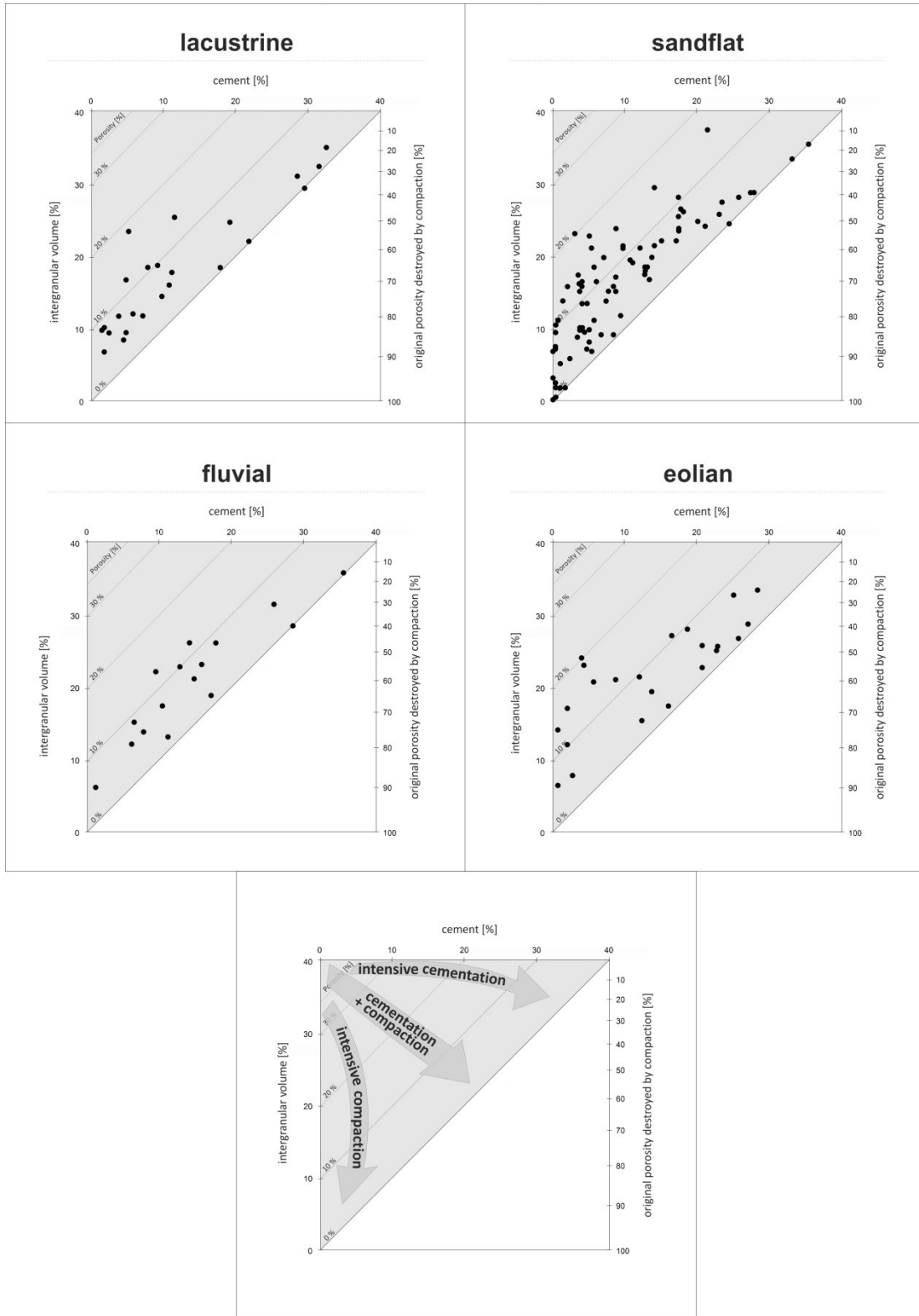
Fig. A 42: The intergranular volume and cement content gives information about the porosity loss by compaction for the Buntsandstein sandstones (according to Houseknecht 1987 and Ehrenberg 1989).

10. I.7. Pore space distribution
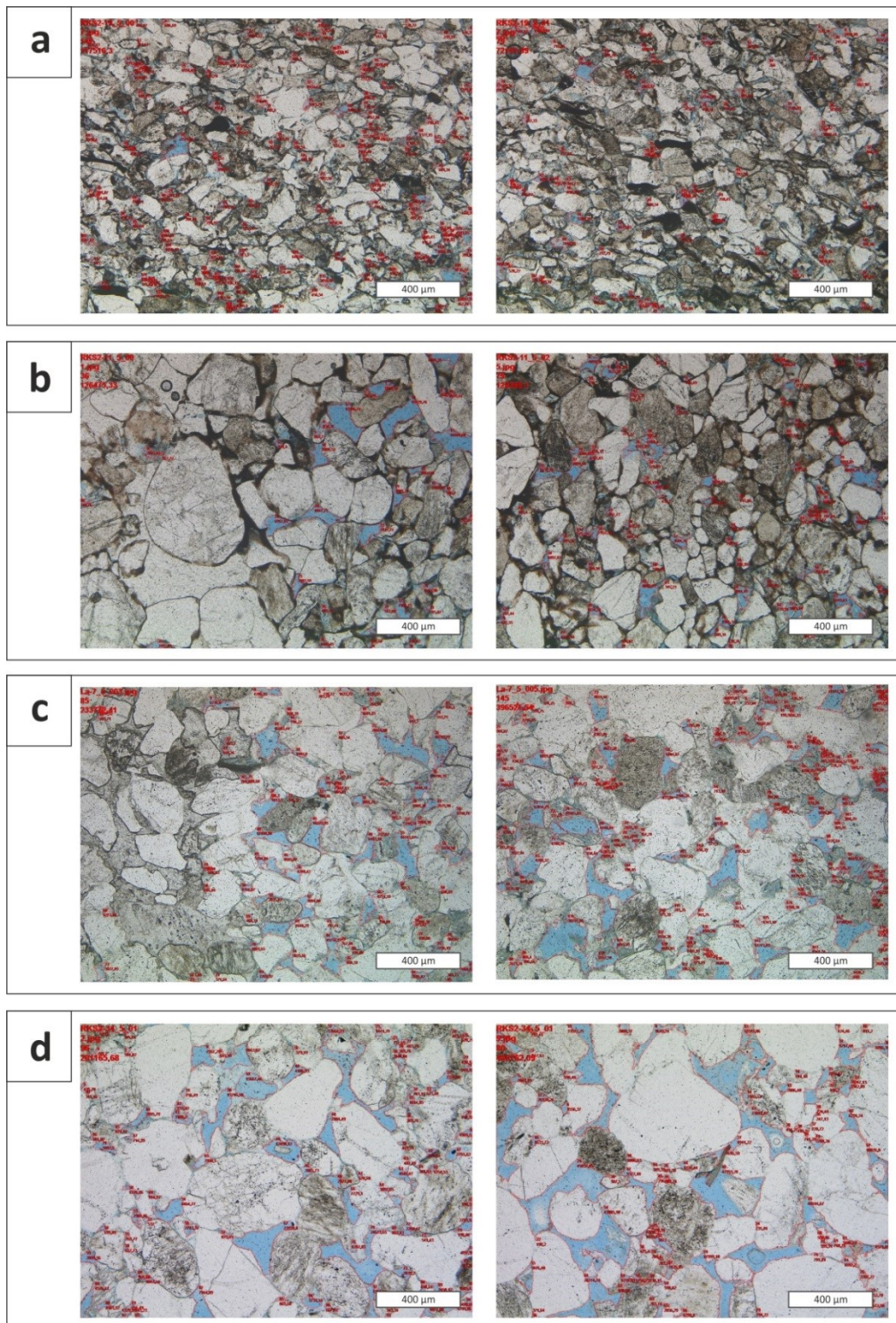
Fig. A 43: Pore space distribution with the program Axiovision© from Zeiss: a) sample Rks2-19 (lacustrine facies, Bernburg Formation); b) sample Rks2-11 (sandflat facies, Volpriehausen Formation); c) sample La35-7 (fluvial facies, Solling Formation); d) sample Rks2-34 (eolian facies, Detfurth Formation).

10. I.8. Mineral surface
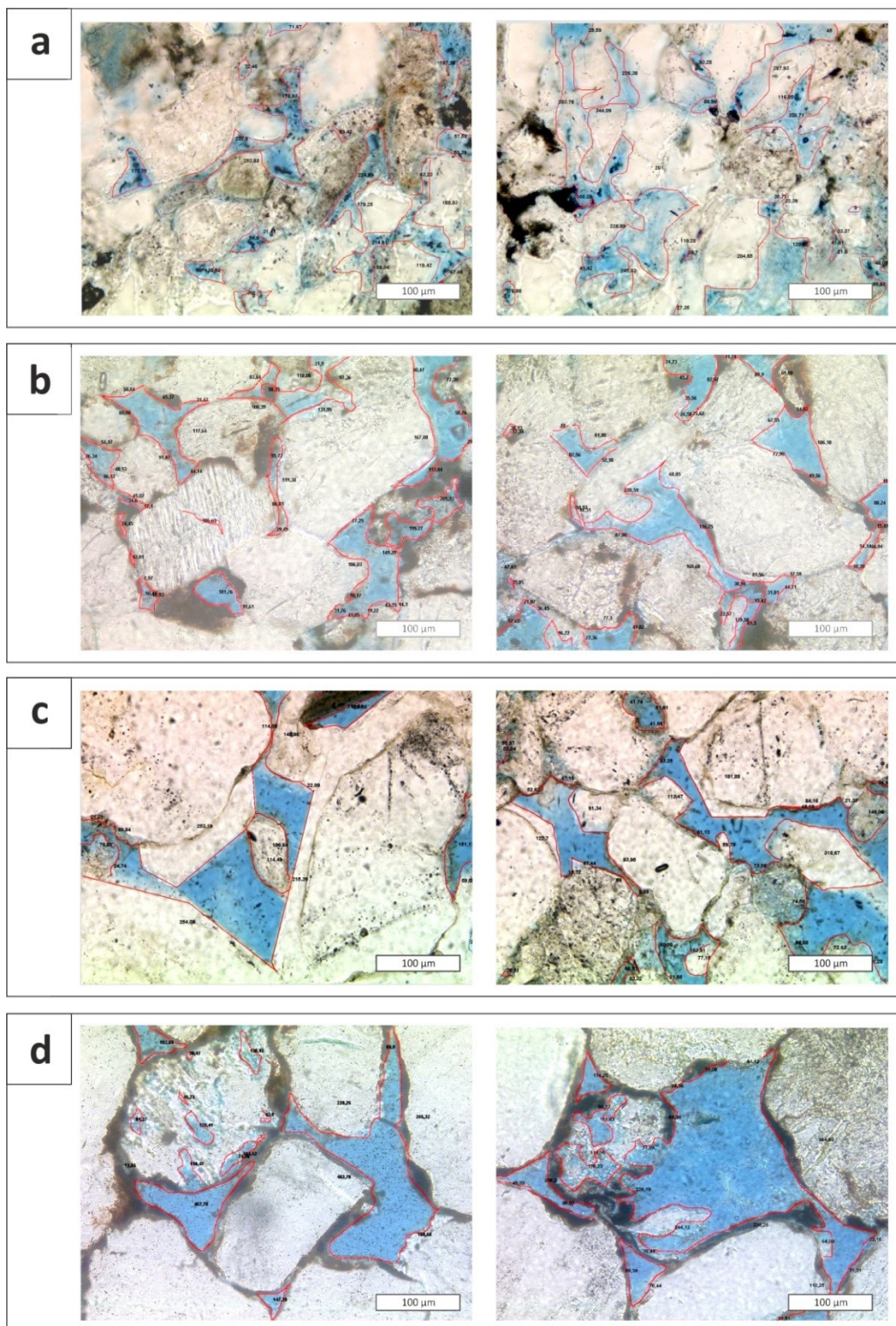
Fig. A 44: Mineral surface area measurement on thin section images with the program JMicroVision©: a) sample Rks2-27 (lacustrine facies, Calförde Formation); b) sample Rks2-6 (sandflat facies, Detfurth Formation); c) sample La35-7 (fluvial facies, Solling Formation); d) sample Rks2-36 (eolian facies, Volpriehausen Formation).

10. II. Tables

10. II.1. Samples and methods

Table A 1: Overview of the investigated Buntsandstein sandstone samples and the methods used.

thin section	facies type	formation	petrophysics	texture	composition (point counted)	pore space distribution	mineral surface area	BET	cathodoluminescence	microprobe	scanning electron microscope
Fh13 - 4	x	x		x	x	x		x			
Fh13 - 5	x	x	x	x	x	x					
Fh13 - 7	x	x	x	x	x	x					
Fh13 - 8	x	x	x	x	x			x			
Fh13 - 11	x	x	x	x	x	x					
Fh13 - 12	x	x	x	x	x	x					
Fh13 - 13	x	x	x	x	x	x	x				
Fh13 - 15	x	x	x	x	x	x					
Fh13 - 21	x	x	x	x	x	x		x			
Fh13 - 24	x	x	x	x	x	x		x			
Fh13 - 27	x	x	x	x	x	x		x			
Fh13 - 28	x	x		x	x	x	x				
FH13 - 30	x	x	x	x	x	x		x			
FH13 - 38								x			
Fh13 - 41	x	x	x	x	x	x		x			
Fh13 - 42	x	x	x	x	x	x					
FH13 - 46	x	x	x	x	x	x					
Fh13 - 47	x	x	x	x	x	x					
Fh13 - 50	x	x	x	x	x	x					
Fh13 - 51	x	x	x	x	x	x					
Fh13 - 52	x	x	x	x	x	x					
Fh13 - 88	x	x		x	x						
Fh13 - 57	x	x	x	x	x	x					
Fh13 - 59	x	x	x	x	x	x					
Fh13 - 60	x	x	x	x	x	x					
Fh13 - 64	x	x	x	x	x	x		x			
Fh13 - 70	x	x	x	x	x						
Fh13 - 78	x	x	x	x	x						
Fh13 - 79	x	x	x	x	x			x			
Fh13 - 82	x	x	x	x	x			x			
Fh13 - 84	x	x	x	x	x						
Fh13 - 85	x	x	x	x	x						
Fh13 - 93	x	x	x	x	x						
Fh13 - 96	x	x		x	x						
Fh13 - 97	x	x		x	x						
Fh13 - 110	x	x	x	x	x			x			
Fh13 - 130										x	
Fh13 - 134	x	x		x	x			x			
Fh13 - 135										x	
Fh13 - 140	x	x		x	x						
Fh13 - 141								x			
Fh13 - 148								x			

thin section	facies type	formation	petrophysics	texture	composition (point counted)	pore space distribution	mineral surface area	BET	cathodoluminescence	microprobe	scanning electron microscope
Fh13 - 158	x	x		x	x						
Fh13 - 160								x			
Fh13 - 170	x	x	x		x						
Fh13 - 171	x	x	x		x						
Fh13 - 35	x	x		x	x						
Gü1 - 2	x	x	x	x	x	x					
Gü1 - 4	x	x	x	x	x	x	x	x			
Gü1 - 6	x	x	x	x	x	x	x				
Gü1 - 9						x					
Gü1 - 11	x	x	x	x	x	x					
Gü1 - 13	x	x	x	x	x	x					
Gü1 - 15	x	x	x	x	x	x	x	x			
Gü1 - 16	x	x	x	x	x	x		x			
Gü1 - 18	x	x	x		x	x					
Gü1 - 20	x	x	x	x	x	x					
Gü1 - 22	x	x	x	x	x	x					
Gü1 - 25	x	x	x	x	x	x					
Gü1 - 26	x	x								x	
Gü1 - 28	x	x	x	x	x	x					
La35 - 2	x	x	x	x	x	x					
La35 - 3	x	x	x	x	x	x					
La35 - 4	x	x	(x)	x	x	x					
La35 - 7	x	x	x	x	x	x	x				
La35 - 10	x	x	x	x	x	x	x				
La35 - 11	x	x	x	x	x	x					
La35 - 12	x	x	x	x	x	x					
La35 - 13	x	x	x	x	x	x					
La35 - 14						x					
La35 - 15	x	x	x	x	x	x			x	x	
La35 - 16	x	x	x	x	x	x					
La35 - 18						x					
La35 - 19	x	x	x	x	x	x					
La35 - 23	x	x	x	x	x	x					
La35 - 24						x					
La35 - 28						x					
La35 - 29	x	x	x	x	x	x					
La35 - 31	x	x	x	x	x	x					
La35 - 32						x					
La35 - 33						x					
La35 - 34	x	x	x	x	x	x					
RKS4 - 5	x	x	x	x	x	x					
RKS4 - 7	x	x	x	x	x	x					
RKS4 - 17						x					
RKS4 - 19	x	x		x	x	x					
RKS4 - 23	x	x	x	x	x	x					
RKS4 - 27	x	x	x	x	x	x					
Te - 2	x	x	(x)	x	x	x					
Te - 3	x	x		x	x	x					
Te - 7	x	x	(x)	x	x	x					
Te - 11	x	x		x	x	x					
Te - 16	x	x		x	x	x					

thin section	facies type	formation	petrophysics	texture	composition (point counted)	pore space distribution	mineral surface area	BET	cathodoluminescence	microprobe	scanning electron microscope
Te - 18	x	x		x	x	x					
Te - 22	x	x		x	x	x					
Te - 26	x	x		x	x	x					
Te - 27						x					
Te - 29	x	x	(x)	x	x	x					
RKS2 - 1	x	x	x	x	x	x					
RKS2 - 2	x	x	x	x	x	x	x				
RKS2 - 3	x	x	x	x	x	x	x				
RKS2 - 4	x	x	x	x	x	x	x				
RKS2 - 5	x	x	x	x	x	x					
RKS2 - 6	x	x	x	x	x	x	x	x			
RKS2 - 7	x	x	x	x	x	x					
RKS2 - 8	x	x	x	x	x	x					
RKS2 - 9	x	x	x	x	x	x					
RKS2 - 10	x	x	x	x	x	x					
RKS2 - 11	x	x	x	x	x	x					
RKS2 - 12	x	x	x	x	x	x					
RKS2 - 13	x	x	x	x	x	x	x	x			
RKS2 - 14	x	x	x	x	x	x		x			
RKS2 - 15	x	x	x	x	x	x					
RKS2 - 16	x	x	x	x	x	x					
RKS2 - 17	x	x	x	x	x	x					
RKS2 - 18	x	x	x	x	x	x					
RKS2 - 19	x	x	x	x	x	x					
RKS2 - 20	x	x	x	x	x	x					
RKS2 - 21	x	x	x	x	x	x	x	x			
RKS2 - 22	x	x	x	x	x	x					
RKS2 - 23	x	x	x	x	x	x					
RKS2 - 24	x	x	x	x	x	x		x			
RKS2 - 25	x	x	x	x	x	x					
RKS2 - 26	x	x	x	x	x	x	x	x			
RKS2 - 27	x	x	x	x	x	x	x				
RKS2 - 31	x	x	x	x	x	x					
RKS2 - 32	x	x		x	x	x					
RKS2 - 33	x	x		x	x	x					
RKS2 - 34	x	x	x	x	x	x					
RKS2 - 35	x	x	x	x	x	x					
RKS2 - 36	x	x		x	x	x	x	x			
RKS2 - 37	x	x		x	x	x					
Ballst - 22	x	x	x	x	x	x	x				
Ballst - 23	x	x	x	x	x	x	x				
Ballst - 24	x	x	x	x	x	x	x				
Ballst - 25	x	x	x	x	x	x					
Ballst - 26	x	x	x	x	x	x					
Ballst - 27	x	x		x	x	x					
Ballst - 28	x	x	x	x	x	x	x				
Ballst - 29	x	x	x	x	x	x					x
Ballst - 30	x	x	x	x	x	x	x				
Ballst - 31	x	x	x	x	x	x					
Ballst - 32	x	x	x	x	x	x					
Ballst - 1	x	x	x	x	x	x					

thin section	facies type	formation	petrophysics	texture	composition (point counted)	pore space distribution	mineral surface area	BET	cathodoluminescence	microprobe	scanning electron microscope
Ballst - 2	x	x	x	x	x	x					
Ballst - 3	x	x	x	x	x	x	x				
Ballst - 4	x	x	x	x	x	x					
Ballst - 5	x	x	x	x	x	x				x	x
Ballst - 6	x	x	x	x	x	x					
Ballst - 7	x	x	x	x	x	x					
Ballst - 8	x	x	x	x	x	x				x	
Ballst - 9	x	x	x	x	x	x	x				
Ballst - 10	x	x	x	x	x	x					
Ballst - 11	x	x	x	x	x	x				x	x
Ballst - 12	x	x	x	x	x	x					
Ballst - 13	x	x	x	x	x	x					
Ballst - 14	x	x	x	x	x	x					
Ballst - 15	x	x	x	x	x	x					
Ballst - 16	x	x	x	x	x	x					
Ballst - 17	x	x	x	x	x	x				x	x	x
Ballst - 18	x	x	x	x	x	x	x				
Ballst - 19	x	x	x	x	x	x					
Ag - 1 (p1)	x	x	(x)								
Ag - 2 (p2)	x	x	(x)								
Ag - 3 (p3)	x	x	x							x	x
Ag - 4 (p4)	x	x	x								
Ag - 5 (p5)	x	x	x								
Ag - 6 (p6)	x	x	x								
Ag - 7 (p7)	x	x	x								
Ag - 8 (p8)	x	x	x								
Ag - 9 (p9)	x	x	x								
Ag - 10 (p10)	x	x	x								
Ag - 11 (p11)	x	x	x								
Ag - 12 (p12)	x	x	x								
Ag - 13 (p13)	x	x	x								
Ag - 14 (p14)	x	x	x							x	
Ge - 1	x	x	x								
Ge - 2	x	x	x								
Ge - 3	x	x	x								
Ge - 4	x	x	x								
Ge - 5	x	x	x								
Bi - 1	x	x	x								
Bi - 2	x	x	x								
Bi - 3	x	x	x								
Bi - 4	x	x	x								
Bi - 5	x	x	x								
Bi - 6	x	x	x								
Bi - 7	x	x	x								
Bi - 8	x	x	x								
Bi - 9	x	x	x								
Bi - 10	x	x	x								
Bi - 11	x	x	x								
Bi - 12	x	x	(x)								
Bi - 13	x	x	(x)								
Bi - 14	x	x									

thin section	facies type	formation	petrophysics	texture	composition (point counted)	pore space distribution	mineral surface area	BET	cathodoluminescence	microprobe	scanning electron microscope
Hartschwinden 1	x	x	x								
Hartschwinden 2	x	x	x								
Werraufer 1	x	x	x								
Werraufer 2	x	x	x								
Vacha 1	x	x	x								
Vacha 2	x	x	x								
Ludwigstein 1	x	x	x								
Ludwigstein 2	x	x	x								
Hanstein 1	x	x	x								
Hanstein 2	x	x	x								
Brehme 1 (Br-1)	x	x	x								
Brehme 2 (Br-2)	x	x	x							x	
Brehme 3 (Br-3)	x	x	x								
Heiligenstadt 2	x	x	x								

10. II.2. Virtual wells

Table A 2: Location of the virtual wells and which vitrinite reflectance values were taken into account in each virtual well. Keuper samples from Götze (2011), Kupferschiefer samples from Peisker (2011) and Siles and Rotliegend samples from Grobleben (2007).

model/ virtual well	Gauss- Krüger coordinates		Keuper samples VRr (%)				Kupferschiefer samples VRr (%)		Siles and Rotliegend samples VRr (%)	
	Easting	Northing	1	2	3	4	1	2	1	2
A	4379662	5652560	0.79	-	-	-	-	-	-	-
B	4386822	5657607	0.62	-	-	-	0.98	-	-	-
C	4399886	5666590	0.62	0.65	-	-	0.97	-	-	-
D	4408402	5672825	0.79	0.55	-	-	-	-	-	-
E	4416217	5678327	0.81	-	-	-	-	-	-	-
F	4426645	5685676	0.53	-	-	-	-	-	-	-
G	4470043	5712978	-	-	-	-	1.14	1.32	2.4	2.8
H	4403941	5628582	-	-	-	-	-	-	1.8	-
I	4420245	5637123	0.75	0.64	-	-	-	-	-	-
J	4428341	5641234	0.60	-	-	-	-	-	-	-
K	4436412	5645420	0.68	-	-	-	0.89	-	-	-
L	4443118	5648920	0.77	-	-	-	-	-	-	-
M	4454350	5654674	0.86	-	-	-	1.16	-	-	-
N	4463810	5658970	0.56	0.57	0.54	0.57	-	-	-	-
O	4463413	5612070	-	-	-	-	0.83	-	-	-
P	4503730	5640407	-	-	-	-	0.90	-	-	-
Q	4419905	5717220	-	-	-	-	-	-	1.45	-

Table A 3: Vitrinite reflectance data of the Keuper, Rotliegend and Siles/Rotliegend samples and their appearance in the virtual wells. Keuper samples from Götze (2011), Kupferschiefer samples from Peisker (2011) and Siles and Rotliegend samples from Grobleben (2007).

	Location	Depth [m]	VRr (%)	virtual well/model	depth in the model [m]
Keuper samples	Reisdorf	surface	0.54	N	5
	Eberstedt	surface	0.56	N	7
	Finnetunnel	surface	0.57	N	15
	Lauterbach	surface	0.62	B	5
	Freienbessingen	surface	0.81	E	10
	Hochstedt	surface	0.77	L	10
	Eischleben	surface	0.60	J	15
	Bad Langensalza	surface	0.65	C	60
	Magdala	surface	0.55	-	-
	Kb Schillingstedt	506	0.53	F	10
	Kleinvargula	surface	0.55	D	20
	Melchendorf	surface	0.68	K	8
	Tennstedt	surface	0.79	D	10
	Vogelsberg	surface	0.86	M	5
	Tröchtelborn	surface	0.53	-	-
	Kb Seebergen 1/64	402	0.64	I	5
	Hy Arnstadt 10/92	14	0.75	I	20
	Kb Apolda 1/65	250 m	0.57	N	10
	S4/Tb4-1 Kammerforst	20.5 m	0.62	C	65
	Eisenach	surface	0.79	A	1
	Netragraben	surface	0.99	-	-
	Buchberg 106	surface	1.24	-	-
Kupferschiefer samples	Altengottern 1/58	1652	0.97	C	1430
	Ettersburg 7/63	1279	1.16	M	1280
	Erfurt 1/64	1085	0.89	K	1145
	Hainich Berka 101/63	1215	0.98	B	1210
	Gera Märzenberg	Surface	0.90	P	10
	GTB Kamsdorf	Surface	0.83	O	10
	Mansfeld Fortschritt SF	542	1.32	G	540
	Wettelrode Röhrigschacht	162	1.14	G	535
Siles and Rotliegend samples	Querfurt 1/64	2500	2.40	G	1675
	Querfurt 1/64	3000	2.80	G	2175
	Ilfeld	1200	1.45	Q	1340
	Thuringian Forest	0	1.80	H	1570

Table A 4: Stratigraphic input data for all virtual wells.

Layer	virtual well A									virtual well B								
	top [m]	base [m]	thickness [m]	eroded [m]	depo. from [Ma]	depo. to [Ma]	eroded from [Ma]	eroded to [Ma]	lithology	top [m]	base [m]	thickness [m]	eroded [m]	depo. from [Ma]	depo. to [Ma]	eroded from [Ma]	eroded to [Ma]	lithology
Tertiär	0	0	0	80	41.0	33.0	33.0	10.0	Sandcongl	0	0	0	80	41.0	33.0	33.0	10.0	Sandcongl
Oberes Campan	0	0	0	0	73.0	41.0	-	-	none	0	0	0	0	73.0	41.0	-	-	none
höhere Oberkreide	0	0	0	0	89.0	73.0	-	-	none	0	0	0	0	89.0	73.0	-	-	none
tiefere Oberkreide (Turon)	0	0	0	65	93.5	89.0	87.0	86.0	LIMESTONE	0	0	0	65	93.5	89.0	87.0	86.0	LIMESTONE
tiefere Oberkreide (Cenoman)	0	0	0	35	99.0	93.5	86.0	85.0	LIMEmarly	0	0	0	35	99.0	93.5	86.0	85.0	LIMEmarly
höhere Unterkreide (Alb)	0	0	0	250	112.2	99.0	85.0	84.0	SANDSTONE	0	0	0	250	112.2	99.0	85.0	84.0	SANDSTONE
höhere Unterkreide (Apt)	0	0	0	150	121.0	112.2	84.0	83.5	SANDSTONE	0	0	0	150	121.0	112.2	84.0	83.5	SANDSTONE
tiefere Unterkreide	0	0	0	100	142.0	121.0	83.5	83.2	SANDSTONE	0	0	0	100	142.0	121.0	83.5	83.2	SANDSTONE
Oberer Jura (Malm)	0	0	0	600	154.0	142.0	83.2	82.0	LIMEmarly	0	0	0	400	154.0	142.0	83.2	82.0	LIMEmarly
Mittlerer Jura (Dogger)	0	0	0	700	177.0	154.0	82.0	81.5	SHALE&LIME	0	0	0	400	177.0	154.0	82.0	81.5	SHALE&LIME
Unterer Jura (Lias)	0	0	0	400	200.0	177.0	81.5	80.0	MARL	0	0	0	200	200.0	177.0	81.5	80.0	MARL
Oberer Keuper (Exter)	0	0	0	53	207.0	200.0	80.0	79.8	SANDSTONE	0	0	0	53	207.0	200.0	80.0	79.8	SANDSTONE
Mittlerer Keuper (Arnstadt)	0	0	0	134	214.0	207.0	79.8	79.5	MARL	0	0	0	134	214.0	207.0	79.8	79.5	MARL
Mittlerer Keuper (Weser)	0	0	0	112	224.5	214.0	79.5	79.0	GYPSUM	0	0	0	112	224.5	214.0	79.5	79.0	GYPSUM
Mittlerer Keuper (Stuttgart)	0	0	0	10	226.0	224.5	79.0	78.8	SANDSTONE	0	0	0	10	226.0	224.5	79.0	78.8	SANDSTONE
Mittlerer Keuper (Grabfeld)	0	0	0	145	232.5	226.0	78.8	76.0	GYPSUM	0	0	0	145	232.5	226.0	78.8	76.0	GYPSUM
Unterer Keuper (Erfurt)	0	2	2	40	235.0	232.5	76.0	74.0	SANDSTONE	0	26	26	22	235.0	232.5	76.0	74.0	SANDSTONE
Oberer Muschelkalk	2	67	65	0	238.5	235.0	-	-	LIMEmarly	26	91	65	0	238.5	235.0	-	-	LIMEmarly
Mittlerer Muschelkalk	67	137	70	0	240.0	238.5	-	-	DOLOMITE	91	161	70	0	240.0	238.5	-	-	DOLOMITE
Unterer Muschelkalk	137	253	116	0	243.0	240.0	-	-	LIMEmarly	161	277	116	0	243.0	240.0	-	-	LIMEmarly
Oberer Buntsandstein (Röt)	253	417	164	0	244.5	243.0	-	-	LIME&EVAP	277	441	164	0	244.5	243.0	-	-	LIME&EVAP
Solling	417	422	5	0	245.0	244.5	-	-	SANDshaly	441	446	5	0	245.0	244.5	-	-	SANDshaly
Hardegsen	422	465	43	0	247.0	245.0	-	-	SANDshaly	446	489	43	0	247.0	245.0	-	-	SANDshaly
Dethfurt	465	498	33	0	247.5	247.0	-	-	SANDshaly	489	522	33	0	247.5	247.0	-	-	SANDshaly
Volpriehausen	498	603	105	0	248.5	247.5	-	-	SANDshaly	522	627	105	0	248.5	247.5	-	-	SANDshaly
Bernburg	603	742	139	0	250.0	248.5	-	-	SAND&SHALE	627	766	139	0	250.0	248.5	-	-	SAND&SHALE
Calvörde	742	888	146	0	251.0	250.0	-	-	SAND&SHALE	766	912	146	0	251.0	250.0	-	-	SAND&SHALE
Zechstein	888	1388	500	0	258.0	251.0	-	-	EVAPORITE	912	1225	312	0	258.0	251.0	-	-	EVAPORITE
-	-	-	-	-	-	258.0	-	-	-	-	-	-	-	-	258.0	-	-	-

Layer	virtual well C									virtual well D								
	top [m]	base [m]	thickness [m]	eroded [m]	depo. from [Ma]	depo. to [Ma]	eroded from [Ma]	eroded to [Ma]	lithology	top [m]	base [m]	thickness [m]	eroded [m]	depo. from [Ma]	depo. to [Ma]	eroded from [Ma]	eroded to [Ma]	lithology
Tertiär	0	0	0	80	41.0	33.0	33.0	10.0	Sandcongl	0	0	0	80	41.0	33.0	33.0	10.0	Sandcongl
Oberes Campan	0	0	0	0	73.0	41.0	-	-	none	0	0	0	0	73.0	41.0	-	-	none
höhere Oberkreide	0	0	0	0	89.0	73.0	-	-	none	0	0	0	0	89.0	73.0	-	-	none
tiefere Oberkreide (Turon)	0	0	0	65	93.5	89.0	87.0	86.0	LIMESTONE	0	0	0	65	93.5	89.0	87.0	86.0	LIMESTONE
tiefere Oberkreide (Cenoman)	0	0	0	35	99.0	93.5	86.0	85.0	LIMEmarly	0	0	0	35	99.0	93.5	86.0	85.0	LIMEmarly
höhere Unterkreide (Alb)	0	0	0	250	112.2	99.0	85.0	84.0	SANDSTONE	0	0	0	250	112.2	99.0	85.0	84.0	SANDSTONE
höhere Unterkreide (Apt)	0	0	0	150	121.0	112.2	84.0	83.5	SANDSTONE	0	0	0	150	121.0	112.2	84.0	83.5	SANDSTONE
tiefere Unterkreide	0	0	0	100	142.0	121.0	83.5	83.2	SANDSTONE	0	0	0	100	142.0	121.0	83.5	83.2	SANDSTONE
Oberer Jura (Malm)	0	0	0	400	154.0	142.0	83.2	82.0	LIMEmarly	0	0	0	600	154.0	142.0	83.2	82.0	LIMEmarly
Mittlerer Jura (Dogger)	0	0	0	400	177.0	154.0	82.0	81.5	SHALE&LIME	0	0	0	600	177.0	154.0	82.0	81.5	SHALE&LIME
Unterer Jura (Lias)	0	0	0	200	200.0	177.0	81.5	80.0	MARL	0	0	0	400	200.0	177.0	81.5	80.0	MARL
Oberer Keuper (Exter)	0	0	0	53	207.0	200.0	80.0	79.8	SANDSTONE	0	0	0	53	207.0	200.0	80.0	79.8	SANDSTONE
Mittlerer Keuper (Arnstadt)	0	0	0	134	214.0	207.0	79.8	79.5	MARL	0	0	0	134	214.0	207.0	79.8	79.5	MARL
Mittlerer Keuper (Weser)	0	0	0	112	224.5	214.0	79.5	79.0	GYPSUM	0	0	0	112	224.5	214.0	79.5	79.0	GYPSUM
Mittlerer Keuper (Stuttgart)	0	0	0	10	226.0	224.5	79.0	78.0	SANDSTONE	0	0	0	10	226.0	224.5	79.0	78.0	SANDSTONE
Mittlerer Keuper (Grabfeld)	0	27	27	111	232.5	226.0	78.0	74.0	GYPSUM	0	0	0	130	232.5	226.0	78.0	74.0	GYPSUM
Unterer Keuper (Erfurt)	27	75	48	0	235.0	232.5	-	-	SANDSTONE	0	20	20	30	235.0	232.5	-	-	SANDSTONE
Oberer Muschelkalk	75	133	58	0	238.5	235.0	-	-	LIMEmarly	20	78	58	0	238.5	235.0	-	-	LIMEmarly
Mittlerer Muschelkalk	133	210	77	0	240.0	238.5	-	-	DOLOMITE	78	155	77	0	240.0	238.5	-	-	DOLOMITE
Unterer Muschelkalk	210	320	110	0	243.0	240.0	-	-	LIMEmarly	155	265	110	0	243.0	240.0	-	-	LIMEmarly
Oberer Buntsandstein (Röt)	320	480	160	0	244.5	243.0	-	-	LIME&EVAP	265	425	160	0	244.5	243.0	-	-	LIME&EVAP
Solling	480	493	13	0	245.0	244.5	-	-	SANDshaly	425	438	13	0	245.0	244.5	-	-	SANDshaly
Hardegsen	493	530	37	0	247.0	245.0	-	-	SANDshaly	438	475	37	0	247.0	245.0	-	-	SANDshaly
Dethfurt	530	565	35	0	247.5	247.0	-	-	SANDshaly	475	510	35	0	247.5	247.0	-	-	SANDshaly
Volpriehausen	565	658	93	0	248.5	247.5	-	-	SANDshaly	510	603	93	0	248.5	247.5	-	-	SANDshaly
Bernburg	658	807	149	0	250.0	248.5	-	-	SAND&SHALE	603	752	149	0	250.0	248.5	-	-	SAND&SHALE
Calvörde	807	955	148	0	251.0	250.0	-	-	SAND&SHALE	752	900	148	0	251.0	250.0	-	-	SAND&SHALE
Zechstein	955	1450	495	0	258.0	251.0	-	-	EVAPORITE	900	1345	445	0	258.0	251.0	-	-	EVAPORITE
-	-	-	-	-	-	258.0	-	-	-	-	-	-	-	-	258.0	-	-	-

Layer	virtual well E									virtual well F								
	top [m]	base [m]	thickness [m]	eroded [m]	depo. from [Ma]	depo. to [Ma]	eroded from [Ma]	eroded to [Ma]	lithology	top [m]	base [m]	thickness [m]	eroded [m]	depo. from [Ma]	depo. to [Ma]	eroded from [Ma]	eroded to [Ma]	lithology
Tertiär	0	0	0	80	41.0	33.0	33.0	10.0	Sandcongl	0	0	0	80	41.0	33.0	33.0	10.0	Sandcongl
Oberes Campan	0	0	0	0	73.0	41.0	-	-	none	0	0	0	0	73.0	41.0	-	-	none
höhere Oberkreide	0	0	0	0	89.0	73.0	-	-	none	0	0	0	0	89.0	73.0	-	-	none
tiefere Oberkreide (Turon)	0	0	0	65	93.5	89.0	87.0	86.0	LIMESTONE	0	0	0	65	93.5	89.0	87.0	86.0	LIMESTONE
tiefere Oberkreide (Cenoman)	0	0	0	35	99.0	93.5	86.0	85.0	LIMEmarly	0	0	0	35	99.0	93.5	86.0	85.0	LIMEmarly
höhere Unterkreide (Alb)	0	0	0	250	112.2	99.0	85.0	84.0	SANDSTONE	0	0	0	250	112.2	99.0	85.0	84.0	SANDSTONE
höhere Unterkreide (Apt)	0	0	0	150	121.0	112.2	84.0	83.5	SANDSTONE	0	0	0	150	121.0	112.2	84.0	83.5	SANDSTONE
tiefere Unterkreide	0	0	0	100	142.0	121.0	83.5	83.2	SANDSTONE	0	0	0	100	142.0	121.0	83.5	83.2	SANDSTONE
Oberer Jura (Malm)	0	0	0	600	154.0	142.0	83.2	82.0	LIMEmarly	0	0	0	200	154.0	142.0	83.2	82.0	LIMEmarly
Mittlerer Jura (Dogger)	0	0	0	700	177.0	154.0	82.0	81.5	SHALE&LIME	0	0	0	300	177.0	154.0	82.0	81.5	SHALE&LIME
Unterer Jura (Lias)	0	0	0	400	200.0	177.0	81.5	80.0	MARL	0	0	0	200	200.0	177.0	81.5	80.0	MARL
Oberer Keuper (Exter)	0	0	0	53	207.0	200.0	80.0	79.8	SANDSTONE	0	0	0	53	207.0	200.0	80.0	79.8	SANDSTONE
Mittlerer Keuper (Arnstadt)	0	0	0	134	214.0	207.0	79.8	79.5	MARL	0	0	0	134	214.0	207.0	79.8	79.5	MARL
Mittlerer Keuper (Weser)	0	0	0	112	224.5	214.0	79.5	79.0	GYPSUM	0	0	0	112	224.5	214.0	79.5	79.0	GYPSUM
Mittlerer Keuper (Stuttgart)	0	0	0	8	226.0	224.5	79.0	78.0	SANDSTONE	0	0	0	8	226.0	224.5	79.0	78.0	SANDSTONE
Mittlerer Keuper (Grabfeld)	0	0	0	141	232.5	226.0	78.0	76.0	GYPSUM	0	0	0	141	232.5	226.0	78.0	76.0	GYPSUM
Unterer Keuper (Erfurt)	0	20	20	47	235.0	232.5	76.0	74.0	SANDSTONE	0	1	1	47	235.0	232.5	76.0	74.0	SANDSTONE
Oberer Muschelkalk	20	84	64	0	238.5	235.0	-	-	LIMEmarly	1	65	64	0	238.5	235.0	-	-	LIMEmarly
Mittlerer Muschelkalk	84	157	73	0	240.0	238.5	-	-	DOLOMITE	65	138	73	0	240.0	238.5	-	-	DOLOMITE
Unterer Muschelkalk	157	266	109	0	243.0	240.0	-	-	LIMEmarly	138	247	109	0	243.0	240.0	-	-	LIMEmarly
Oberer Buntsandstein (Röt)	266	425	159	0	244.5	243.0	-	-	LIME&EVAP	247	406	159	0	244.5	243.0	-	-	LIME&EVAP
Solling	425	436	11	0	245.0	244.5	-	-	SANDshaly	406	417	11	0	245.0	244.5	-	-	SANDshaly
Hardegsen	436	476	40	0	247.0	245.0	-	-	SANDshaly	417	457	40	0	247.0	245.0	-	-	SANDshaly
Dethfurt	476	509	33	0	247.5	247.0	-	-	SANDshaly	457	490	33	0	247.5	247.0	-	-	SANDshaly
Volpriehausen	509	611	102	0	248.5	247.5	-	-	SANDshaly	490	592	102	0	248.5	247.5	-	-	SANDshaly
Bernburg	611	737	126	0	250.0	248.5	-	-	SAND&SHALE	592	718	126	0	250.0	248.5	-	-	SAND&SHALE
Calvörde	737	902	165	0	251.0	250.0	-	-	SAND&SHALE	718	883	165	0	251.0	250.0	-	-	SAND&SHALE
Zechstein	902	1219	317	0	258.0	251.0	-	-	EVAPORITE	883	1300	417	0	258.0	251.0	-	-	EVAPORITE
-	-	-	-	-	-	258.0	-	-	-	-	-	-	-	-	258.0	-	-	-

Layer	top [m]	base [m]	thickness [m]	eroded [m]	depo. from [Ma]	depo. to [Ma]	eroded from [Ma]	eroded to [Ma]	lithology
									virtual well G
Tertiär	0	0	0	80	41.0	33.0	33.0	10.0	Sandcongl
Oberes Campan	0	0	0	0	73.0	41.0	-	-	none
höhere Oberkreide	0	0	0	0	89.0	73.0	-	-	none
tiefere Oberkreide (Turon)	0	0	0	65	93.5	89.0	87.0	86.0	LIMESTONE
tiefere Oberkreide (Cenoman)	0	0	0	35	99.0	93.5	86.0	85.0	LIMEmarly
höhere Unterkreide (Alb)	0	0	0	250	112.2	99.0	85.0	84.0	SANDSTONE
höhere Unterkreide (Apt)	0	0	0	150	121.0	112.2	84.0	83.5	SANDSTONE
tiefere Unterkreide	0	0	0	100	142.0	121.0	83.5	83.2	SANDSTONE
Oberer Jura (Malm)	0	0	0	600	154.0	142.0	83.2	82.0	LIMEmarly
Mittlerer Jura (Dogger)	0	0	0	500	177.0	154.0	82.0	81.5	SHALE&LIME
Unterer Jura (Lias)	0	0	0	400	200.0	177.0	81.5	80.0	MARL
Oberer Keuper (Exter)	0	0	0	53	207.0	200.0	80.0	79.8	SANDSTONE
Mittlerer Keuper (Arnstadt)	0	0	0	134	214.0	207.0	79.8	79.5	MARL
Mittlerer Keuper (Weser)	0	0	0	112	224.5	214.0	79.5	79.0	GYPSUM
Mittlerer Keuper (Stuttgart)	0	0	0	8	226.0	224.5	79.0	78.8	SANDSTONE
Mittlerer Keuper (Grabfeld)	0	0	0	141	232.5	226.0	78.8	78.5	GYPSUM
Unterer Keuper (Erfurt)	0	0	0	48	235.0	232.5	78.5	78.0	SANDSTONE
Oberer Muschelkalk	0	0	0	64	238.5	235.0	78.0	77.7	LIMEmarly
Mittlerer Muschelkalk	0	0	0	73	240.0	238.5	77.7	77.5	DOLOMITE
Unterer Muschelkalk	0	0	0	109	243.0	240.0	77.5	77.2	LIMEmarly
Oberer Buntsandstein (Röt)	0	0	0	159	244.5	243.0	77.2	76.5	LIME&EVAP
Solling	0	0	0	11	245.0	244.5	76.5	76.3	SANDshaly
Hardegsen	0	0	0	40	247.0	245.0	76.3	76.0	SANDshaly
Dethfurt	0	0	0	33	247.5	247.0	76.0	75.9	SANDshaly
Volpriehausen	0	0	0	102	248.5	247.5	75.9	75.7	SANDshaly
Bernburg	0	0	0	126	250.0	248.5	75.7	75.0	SAND&SHALE
Calvörde	0	0	0	165	251.0	250.0	75.0	74.5	SAND&SHALE
Zechstein	0	550	550	100	258.0	251.0	10	0	EVAPORITE
Rotliegend	550	1360	810	0	300.0	258.0	-	-	SAND&SHALE
Wettin	1360	1690	330	0	301.0	300.0	-	-	SAND&SHALE
Mansfeld	1690	2170	480	0	304.0	301.0	-	-	SAND&SHALE
-	-	-	-	-	-	304.0	-	-	-

Layer	top [m]	base [m]	thickness [m]	eroded [m]	depo. from [Ma]	depo. to [Ma]	eroded from [Ma]	eroded to [Ma]	lithology
					virtual well H				
Tertiär	0	0	0	80	41.0	33.0	33.0	10.0	Sandcongl
Oberes Campan	0	0	0	0	73.0	41.0	-	-	none
höhere Oberkreide	0	0	0	0	89.0	73.0	-	-	none
tiefere Oberkreide (Turon)	0	0	0	65	93.5	89.0	87.0	86.0	LIMESTONE
tiefere Oberkreide (Cenoman)	0	0	0	35	99.0	93.5	86.0	85.0	LIMEmarly
höhere Unterkreide (Alb)	0	0	0	250	112.2	99.0	85.0	84.0	SANDSTONE
höhere Unterkreide (Apt)	0	0	0	150	121.0	112.2	84.0	83.5	SANDSTONE
tiefere Unterkreide	0	0	0	100	142.0	121.0	83.5	83.2	SANDSTONE
Oberer Jura (Malm)	0	0	0	100	154.0	142.0	83.2	82.0	LIMEmarly
Mittlerer Jura (Dogger)	0	0	0	100	177.0	154.0	82.0	81.5	SHALE&LIME
Unterer Jura (Lias)	0	0	0	200	200.0	177.0	81.5	80.0	MARL
Oberer Keuper (Exter)	0	0	0	53	207.0	200.0	80.0	79.8	SANDSTONE
Mittlerer Keuper (Arnstadt)	0	0	0	134	214.0	207.0	79.8	79.5	MARL
Mittlerer Keuper (Weser)	0	0	0	112	224.5	214.0	79.5	79.0	GYPSUM
Mittlerer Keuper (Stuttgart)	0	0	0	10	226.0	224.5	79.0	78.8	SANDSTONE
Mittlerer Keuper (Grabfeld)	0	0	0	140	232.5	226.0	78.8	78.5	GYPSUM
Unterer Keuper (Erfurt)	0	0	0	50	235.0	232.5	78.5	78.0	SANDSTONE
Oberer Muschelkalk	0	0	0	60	238.5	235.0	78.0	77.7	LIMEmarly
Mittlerer Muschelkalk	0	0	0	75	240.0	238.5	77.7	77.5	DOLOMITE
Unterer Muschelkalk	0	0	0	110	243.0	240.0	77.5	77.2	LIMEmarly
Oberer Buntsandstein (Röt)	0	0	0	160	244.5	243.0	77.2	76.5	LIME&EVAP
Solling	0	0	0	30	245.0	244.5	76.5	76.3	SANDshaly
Hardegsen	0	0	0	40	247.0	245.0	76.3	76.0	SANDshaly
Dethfurt	0	0	0	30	247.5	247.0	76.0	75.9	SANDshaly
Volpriehausen	0	0	0	80	248.5	247.5	75.9	75.7	SANDshaly
Bernburg	0	0	0	100	250.0	248.5	75.7	75.0	SAND&SHALE
Calvörde	0	0	0	100	251.0	250.0	75.0	74.5	SAND&SHALE
Zechstein	0	0	0	210	258.0	251.0	10	0	EVAPORITE
Elgersburg	0	0	0	425	284.0	258.0	-	-	Sandstone (typical)
Oberhof	0	975	975	175	292.0	284.0	-	-	SAND&SILT
Goldlauter	975	1400	425	0	295.0	292.0	-	-	SANDcongl
Manebach	1400	1575	175	0	297.0	295.0	-	-	SANDcongl
-	-	-	-	-	-	297.0	-	-	-

Layer	virtual well I									virtual well J								
	top [m]	base [m]	thickness [m]	eroded [m]	depo. from [Ma]	depo. to [Ma]	eroded from [Ma]	eroded to [Ma]	lithology	top [m]	base [m]	thickness [m]	eroded [m]	depo. from [Ma]	depo. to [Ma]	eroded from [Ma]	eroded to [Ma]	lithology
Tertiär	0	0	0	80	41.0	33.0	33.0	10.0	Sandcongl	0	0	0	80	41.0	33.0	33.0	10.0	Sandcongl
Oberes Campan	0	0	0	0	73.0	41.0	-	-	none	0	0	0	0	73.0	41.0	-	-	none
höhere Oberkreide	0	0	0	0	89.0	73.0	-	-	none	0	0	0	0	89.0	73.0	-	-	none
tiefere Oberkreide (Turon)	0	0	0	65	93.5	89.0	87.0	86.0	LIMESTONE	0	0	0	65	93.5	89.0	87.0	86.0	LIMESTONE
tiefere Oberkreide (Cenoman)	0	0	0	35	99.0	93.5	86.0	85.0	LIMEmarly	0	0	0	35	99.0	93.5	86.0	85.0	LIMEmarly
höhere Unterkreide (Alb)	0	0	0	250	112.2	99.0	85.0	84.0	SANDSTONE	0	0	0	250	112.2	99.0	85.0	84.0	SANDSTONE
höhere Unterkreide (Apt)	0	0	0	150	121.0	112.2	84.0	83.5	SANDSTONE	0	0	0	150	121.0	112.2	84.0	83.5	SANDSTONE
tiefere Unterkreide	0	0	0	100	142.0	121.0	83.5	83.2	SANDSTONE	0	0	0	100	142.0	121.0	83.5	83.2	SANDSTONE
Oberer Jura (Malm)	0	0	0	500	154.0	142.0	83.2	82.0	LIMEmarly	0	0	0	300	154.0	142.0	83.2	82.0	LIMEmarly
Mittlerer Jura (Dogger)	0	0	0	500	177.0	154.0	82.0	81.5	SHALE&LIME	0	0	0	400	177.0	154.0	82.0	81.5	SHALE&LIME
Unterer Jura (Lias)	0	0	0	400	200.0	177.0	81.5	80.0	MARL	0	0	0	200	200.0	177.0	81.5	80.0	MARL
Oberer Keuper (Exter)	0	0	0	53	207.0	200.0	80.0	79.8	SANDSTONE	0	0	0	53	207.0	200.0	80.0	79.8	SANDSTONE
Mittlerer Keuper (Arnstadt)	0	0	0	134	214.0	207.0	79.8	79.5	MARL	0	0	0	134	214.0	207.0	79.8	79.5	MARL
Mittlerer Keuper (Weser)	0	0	0	112	224.5	214.0	79.5	79.0	GYPSUM	0	0	0	112	224.5	214.0	79.5	79.0	GYPSUM
Mittlerer Keuper (Stuttgart)	0	0	0	10	226.0	224.5	79.0	74.0	SANDSTONE	0	0	0	10	226.0	224.5	79.0	78.0	SANDSTONE
Mittlerer Keuper (Grabfeld)	0	0	0	140	232.5	226.0	10.0	0.0	GYPSUM	0	0	0	140	232.5	226.0	78.0	76.0	GYPSUM
Unterer Keuper (Erfurt)	0	25	25	45	235.0	232.5	-	-	SANDSTONE	0	50	50	0	235.0	232.5	76.0	74.0	SANDSTONE
Oberer Muschelkalk	25	83	58	0	238.5	235.0	-	-	LIMEmarly	50	108	58	0	238.5	235.0	-	-	LIMEmarly
Mittlerer Muschelkalk	83	160	77	0	240.0	238.5	-	-	DOLOMITE	108	185	77	0	240.0	238.5	-	-	DOLOMITE
Unterer Muschelkalk	160	270	110	0	243.0	240.0	-	-	LIMEmarly	185	295	110	0	243.0	240.0	-	-	LIMEmarly
Oberer Buntsandstein (Röt)	270	430	160	0	244.5	243.0	-	-	LIME&EVAP	295	455	160	0	244.5	243.0	-	-	LIME&EVAP
Solling	430	443	13	0	245.0	244.5	-	-	SANDshaly	455	468	13	0	245.0	244.5	-	-	SANDshaly
Hardegsen	443	480	37	0	247.0	245.0	-	-	SANDshaly	468	505	37	0	247.0	245.0	-	-	SANDshaly
Dethfurt	480	515	35	0	247.5	247.0	-	-	SANDshaly	505	540	35	0	247.5	247.0	-	-	SANDshaly
Volpriehausen	515	608	93	0	248.5	247.5	-	-	SANDshaly	540	633	93	0	248.5	247.5	-	-	SANDshaly
Bernburg	608	757	149	0	250.0	248.5	-	-	SAND&SHALE	633	782	149	0	250.0	248.5	-	-	SAND&SHALE
Calvörde	757	897	140	0	251.0	250.0	-	-	SAND&SHALE	782	922	140	0	251.0	250.0	-	-	SAND&SHALE
Zechstein	897	1217	320	0	258.0	251.0	-	-	EVAPORITE	922	1242	320	0	258.0	251.0	-	-	EVAPORITE
-	-	-	-	-	-	258.0	-	-	-	-	-	-	-	-	258.0	-	-	-

Layer	virtual well K									virtual well L								
	top [m]	base [m]	thickness [m]	eroded [m]	depo. from [Ma]	depo. to [Ma]	eroded from [Ma]	eroded to [Ma]	lithology	top [m]	base [m]	thickness [m]	eroded [m]	depo. from [Ma]	depo. to [Ma]	eroded from [Ma]	eroded to [Ma]	lithology
Tertiär	0	0	0	80	41.0	33.0	33.0	10.0	Sandcongl	0	0	0	80	41.0	33.0	33.0	10.0	Sandcongl
Oberes Campan	0	0	0	0	73.0	41.0	-	-	none	0	0	0	0	73.0	41.0	-	-	none
höhere Oberkreide	0	0	0	0	89.0	73.0	-	-	none	0	0	0	0	89.0	73.0	-	-	none
tiefere Oberkreide (Turon)	0	0	0	65	93.5	89.0	87.0	86.0	LIMESTONE	0	0	0	65	93.5	89.0	87.0	86.0	LIMESTONE
tiefere Oberkreide (Cenoman)	0	0	0	35	99.0	93.5	86.0	85.0	LIMEmarly	0	0	0	35	99.0	93.5	86.0	85.0	LIMEmarly
höhere Unterkreide (Alb)	0	0	0	250	112.2	99.0	85.0	84.0	SANDSTONE	0	0	0	250	112.2	99.0	85.0	84.0	SANDSTONE
höhere Unterkreide (Apt)	0	0	0	150	121.0	112.2	84.0	83.5	SANDSTONE	0	0	0	150	121.0	112.2	84.0	83.5	SANDSTONE
tiefere Unterkreide	0	0	0	100	142.0	121.0	83.5	83.2	SANDSTONE	0	0	0	100	142.0	121.0	83.5	83.2	SANDSTONE
Oberer Jura (Malm)	0	0	0	400	154.0	142.0	83.2	82.0	LIMEmarly	0	0	0	500	154.0	142.0	83.2	82.0	LIMEmarly
Mittlerer Jura (Dogger)	0	0	0	400	177.0	154.0	82.0	81.5	SHALE&LIME	0	0	0	600	177.0	154.0	82.0	81.5	SHALE&LIME
Unterer Jura (Lias)	0	0	0	200	200.0	177.0	81.5	80.0	MARL	0	0	0	500	200.0	177.0	81.5	80.0	MARL
Oberer Keuper (Exter)	0	0	0	53	207.0	200.0	80.0	79.8	SANDSTONE	0	0	0	53	207.0	200.0	80.0	79.8	SANDSTONE
Mittlerer Keuper (Arnstadt)	0	0	0	134	214.0	207.0	79.8	79.5	MARL	0	0	0	134	214.0	207.0	79.8	79.5	MARL
Mittlerer Keuper (Weser)	0	0	0	112	224.5	214.0	79.5	79.0	GYPSUM	0	0	0	112	224.5	214.0	79.5	79.0	GYPSUM
Mittlerer Keuper (Stuttgart)	0	0	0	10	226.0	224.5	79.0	74.0	SANDSTONE	0	0	0	8	226.0	224.5	79.0	78.0	SANDSTONE
Mittlerer Keuper (Grabfeld)	0	0	0	140	232.5	226.0	10.0	0.0	GYPSUM	0	0	0	141	232.5	226.0	78.0	75.0	GYPSUM
Unterer Keuper (Erfurt)	0	75	75	0	235.0	232.5	-	-	SANDSTONE	0	13	13	33	235.0	232.5	75.0	74.0	SANDSTONE
Oberer Muschelkalk	75	133	58	0	238.5	235.0	-	-	LIMEmarly	13	76	63	0	238.5	235.0	-	-	LIMEmarly
Mittlerer Muschelkalk	133	210	77	0	240.0	238.5	-	-	DOLOMITE	76	156	80	0	240.0	238.5	-	-	DOLOMITE
Unterer Muschelkalk	210	320	110	0	243.0	240.0	-	-	LIMEmarly	156	266	110	0	243.0	240.0	-	-	LIMEmarly
Oberer Buntsandstein (Röt)	320	480	160	0	244.5	243.0	-	-	LIME&EVAP	266	424	158	0	244.5	243.0	-	-	LIME&EVAP
Solling	480	493	13	0	245.0	244.5	-	-	SANDshaly	424	435	11	0	245.0	244.5	-	-	SANDshaly
Hardegsen	493	530	37	0	247.0	245.0	-	-	SANDshaly	435	463	28	0	247.0	245.0	-	-	SANDshaly
Dethfurt	530	565	35	0	247.5	247.0	-	-	SANDshaly	463	511	48	0	247.5	247.0	-	-	SANDshaly
Volpriehausen	565	658	93	0	248.5	247.5	-	-	SANDshaly	511	606	95	0	248.5	247.5	-	-	SANDshaly
Bernburg	658	807	149	0	250.0	248.5	-	-	SAND&SHALE	606	746	140	0	250.0	248.5	-	-	SAND&SHALE
Calvörde	807	947	140	0	251.0	250.0	-	-	SAND&SHALE	746	896	150	0	251.0	250.0	-	-	SAND&SHALE
Zechstein	947	1267	320	0	258.0	251.0	-	-	EVAPORITE	896	1196	300	0	258.0	251.0	-	-	EVAPORITE
-	-	-	-	-	-	258.0	-	-	-	-	-	-	-	-	258.0	-	-	-

Layer	virtual well M									virtual well N								
	top [m]	base [m]	thickness [m]	eroded [m]	depo. from [Ma]	depo. to [Ma]	eroded from [Ma]	eroded to [Ma]	lithology	top [m]	base [m]	thickness [m]	eroded [m]	depo. from [Ma]	depo. to [Ma]	eroded from [Ma]	eroded to [Ma]	lithology
Tertiär	0	0	0	80	41.0	33.0	33.0	10.0	Sandcongl	0	0	0	80	41.0	33.0	33.0	10.0	Sandcongl
Oberes Campan	0	0	0	0	73.0	41.0	-	-	none	0	0	0	0	73.0	41.0	-	-	none
höhere Oberkreide	0	0	0	0	89.0	73.0	-	-	none	0	0	0	0	89.0	73.0	-	-	none
tiefere Oberkreide (Turon)	0	0	0	65	93.5	89.0	87.0	86.0	LIMESTONE	0	0	0	65	93.5	89.0	87.0	86.0	LIMESTONE
tiefere Oberkreide (Cenoman)	0	0	0	35	99.0	93.5	86.0	85.0	LIMEmarly	0	0	0	35	99.0	93.5	86.0	85.0	LIMEmarly
höhere Unterkreide (Alb)	0	0	0	250	112.2	99.0	85.0	84.0	SANDSTONE	0	0	0	250	112.2	99.0	85.0	84.0	SANDSTONE
höhere Unterkreide (Apt)	0	0	0	150	121.0	112.2	84.0	83.5	SANDSTONE	0	0	0	150	121.0	112.2	84.0	83.5	SANDSTONE
tiefere Unterkreide	0	0	0	100	142.0	121.0	83.5	83.2	SANDSTONE	0	0	0	100	142.0	121.0	83.5	83.2	SANDSTONE
Oberer Jura (Malm)	0	0	0	600	154.0	142.0	83.2	82.0	LIMEmarly	0	0	0	200	154.0	142.0	83.2	82.0	LIMEmarly
Mittlerer Jura (Dogger)	0	0	0	600	177.0	154.0	82.0	81.5	SHALE&LIME	0	0	0	350	177.0	154.0	82.0	81.5	SHALE&LIME
Unterer Jura (Lias)	0	0	0	300	200.0	177.0	81.5	80.0	MARL	0	0	0	200	200.0	177.0	81.5	80.0	MARL
Oberer Keuper (Exter)	0	0	0	53	207.0	200.0	80.0	79.8	SANDSTONE	0	0	0	53	207.0	200.0	80.0	79.8	SANDSTONE
Mittlerer Keuper (Arnstadt)	0	0	0	134	214.0	207.0	79.8	79.5	MARL	0	0	0	134	214.0	207.0	79.8	79.5	MARL
Mittlerer Keuper (Weser)	0	0	0	112	224.5	214.0	79.5	79.0	GYPSUM	0	0	0	112	224.5	214.0	79.5	79.0	GYPSUM
Mittlerer Keuper (Stuttgart)	0	0	0	8	226.0	224.5	79.0	78.0	SANDSTONE	0	0	0	8	226.0	224.5	79.0	78.0	SANDSTONE
Mittlerer Keuper (Grabfeld)	0	0	0	141	232.5	226.0	78.0	76.0	GYPSUM	0	0	0	141	232.5	226.0	78.0	75.0	GYPSUM
Unterer Keuper (Erfurt)	0	1	1	47	235.0	232.5	76.0	74.0	SANDSTONE	0	38	38	6	235.0	232.5	75.0	74.0	SANDSTONE
Oberer Muschelkalk	1	65	64	0	238.5	235.0	-	-	LIMEmarly	38	100	62	0	238.5	235.0	-	-	LIMEmarly
Mittlerer Muschelkalk	65	138	73	0	240.0	238.5	-	-	DOLOMITE	100	173	73	0	240.0	238.5	-	-	DOLOMITE
Unterer Muschelkalk	138	247	109	0	243.0	240.0	-	-	LIMEmarly	173	280	107	0	243.0	240.0	-	-	LIMEmarly
Oberer Buntsandstein (Röt)	247	406	159	0	244.5	243.0	-	-	LIME&EVAP	280	450	170	0	244.5	243.0	-	-	LIME&EVAP
Solling	406	417	11	0	245.0	244.5	-	-	SANDshaly	450	456	6	0	245.0	244.5	-	-	SANDshaly
Hardegsen	417	457	40	0	247.0	245.0	-	-	SANDshaly	456	493	37	0	247.0	245.0	-	-	SANDshaly
Dethfurt	457	490	33	0	247.5	247.0	-	-	SANDshaly	493	526	33	0	247.5	247.0	-	-	SANDshaly
Volpriehausen	490	592	102	0	248.5	247.5	-	-	SANDshaly	526	628	102	0	248.5	247.5	-	-	SANDshaly
Bernburg	592	718	126	0	250.0	248.5	-	-	SAND&SHALE	628	770	142	0	250.0	248.5	-	-	SAND&SHALE
Calvörde	718	883	165	0	251.0	250.0	-	-	SAND&SHALE	770	922	152	0	251.0	250.0	-	-	SAND&SHALE
Zechstein	883	1300	417	0	258.0	251.0	-	-	EVAPORITE	922	1300	378	0	258.0	251.0	-	-	EVAPORITE
-	-	-	-	-	-	258.0	-	-	-	-	-	-	-	-	258.0	-	-	-

	virtual well O									virtual well P								
Layer	top [m]	base [m]	thickness [m]	eroded [m]	depo. from [Ma]	depo. to [Ma]	eroded from [Ma]	eroded to [Ma]	lithology	top [m]	base [m]	thickness [m]	eroded [m]	depo. from [Ma]	depo. to [Ma]	eroded from [Ma]	eroded to [Ma]	lithology
Tertiär	0	0	0	80	41.0	33.0	33.0	10.0	Sandcongl	0	0	0	80	41.0	33.0	33.0	10.0	Sandcongl
Oberes Campan	0	0	0	0	73.0	41.0	-	-	none	0	0	0	0	73.0	41.0	-	-	none
höhere Oberkreide	0	0	0	0	89.0	73.0	-	-	none	0	0	0	0	89.0	73.0	-	-	none
tiefere Oberkreide (Turon)	0	0	0	65	93.5	89.0	87.0	86.0	LIMESTONE	0	0	0	65	93.5	89.0	87.0	86.0	LIMESTONE
tiefere Oberkreide (Cenoman)	0	0	0	35	99.0	93.5	86.0	85.0	LIMEmarly	0	0	0	35	99.0	93.5	86.0	85.0	LIMEmarly
höhere Unterkreide (Alb)	0	0	0	250	112.2	99.0	85.0	84.0	SANDSTONE	0	0	0	250	112.2	99.0	85.0	84.0	SANDSTONE
höhere Unterkreide (Apt)	0	0	0	150	121.0	112.2	84.0	83.5	SANDSTONE	0	0	0	150	121.0	112.2	84.0	83.5	SANDSTONE
tiefere Unterkreide	0	0	0	100	142.0	121.0	83.5	83.2	SANDSTONE	0	0	0	100	142.0	121.0	83.5	83.2	SANDSTONE
Oberer Jura (Malm)	0	0	0	400	154.0	142.0	83.2	82.0	LIMEmarly	0	0	0	400	154.0	142.0	83.2	82.0	LIMEmarly
Mittlerer Jura (Dogger)	0	0	0	400	177.0	154.0	82.0	81.5	SHALE&LIME	0	0	0	300	177.0	154.0	82.0	81.5	SHALE&LIME
Unterer Jura (Lias)	0	0	0	50	200.0	177.0	81.5	80.0	MARL	0	0	0	400	200.0	177.0	81.5	80.0	MARL
Oberer Keuper (Exter)	0	0	0	53	207.0	200.0	80.0	79.8	SANDSTONE	0	0	0	53	207.0	200.0	80.0	79.8	SANDSTONE
Mittlerer Keuper (Arnstadt)	0	0	0	134	214.0	207.0	79.8	79.5	MARL	0	0	0	134	214.0	207.0	79.8	79.5	MARL
Mittlerer Keuper (Weser)	0	0	0	112	224.5	214.0	79.5	79.0	GYPSUM	0	0	0	112	224.5	214.0	79.5	79.0	GYPSUM
Mittlerer Keuper (Stuttgart)	0	0	0	10	226.0	224.5	79.0	78.8	SANDSTONE	0	0	0	10	226.0	224.5	79.0	78.8	SANDSTONE
Mittlerer Keuper (Grabfeld)	0	0	0	140	232.5	226.0	78.8	78.5	GYPSUM	0	0	0	140	232.5	226.0	78.8	78.5	GYPSUM
Unterer Keuper (Erfurt)	0	0	0	50	235.0	232.5	78.5	78.0	SANDSTONE	0	0	0	50	235.0	232.5	78.5	78.0	SANDSTONE
Oberer Muschelkalk	0	0	0	60	238.5	235.0	78.0	77.7	LIMEmarly	0	0	0	60	238.5	235.0	78.0	77.7	LIMEmarly
Mittlerer Muschelkalk	0	0	0	75	240.0	238.5	77.7	77.5	DOLOMITE	0	0	0	75	240.0	238.5	77.7	77.5	DOLOMITE
Unterer Muschelkalk	0	0	0	110	243.0	240.0	77.5	77.2	LIMEmarly	0	0	0	110	243.0	240.0	77.5	77.2	LIMEmarly
Oberer Buntsandstein (Röt)	0	0	0	160	244.5	243.0	77.2	76.5	LIME&EVAP	0	0	0	160	244.5	243.0	77.2	76.5	LIME&EVAP
Solling	0	0	0	30	245.0	244.5	76.5	76.3	SANDshaly	0	0	0	30	245.0	244.5	76.5	76.3	SANDshaly
Hardegsen	0	0	0	40	247.0	245.0	76.3	76.0	SANDshaly	0	0	0	40	247.0	245.0	76.3	76.0	SANDshaly
Dethfurt	0	0	0	30	247.5	247.0	76.0	75.9	SANDshaly	0	0	0	30	247.5	247.0	76.0	75.9	SANDshaly
Volpriehausen	0	0	0	80	248.5	247.5	75.9	75.7	SANDshaly	0	0	0	80	248.5	247.5	75.9	75.7	SANDshaly
Bernburg	0	0	0	100	250.0	248.5	75.7	75.0	SAND&SHALE	0	0	0	100	250.0	248.5	75.7	75.0	SAND&SHALE
Calvörde	0	0	0	100	251.0	250.0	75.0	73.0	SAND&SHALE	0	0	0	100	251.0	250.0	75.0	73.0	SAND&SHALE
Zechstein	0	20	20	100	258.0	251.0	10.0	0.0	SHALE&SAND	0	20	20	100	258.0	251.0	10.0	0.0	SHALE&SAND
-	-	-	-	-	-	258.0	-	-	-	-	-	-	-	-	258.0	-	-	-

Layer	virtual well Q								
	top [m]	base [m]	thickness [m]	eroded [m]	depo. from [Ma]	depo. to [Ma]	eroded from [Ma]	eroded to [Ma]	lithology
Tertiär	0	0	0	80	41.0	33.0	33.0	10.0	Sandcongl
Oberes Campan	0	0	0	0	73.0	41.0	-	-	none
höhere Oberkreide	0	0	0	0	89.0	73.0	-	-	none
tiefere Oberkreide (Turon)	0	0	0	65	93.5	89.0	87.0	86.0	LIMESTONE
tiefere Oberkreide (Cenoman)	0	0	0	35	99.0	93.5	86.0	85.0	LIMEmarly
höhere Unterkreide (Alb)	0	0	0	250	112.2	99.0	85.0	84.0	SANDSTONE
höhere Unterkreide (Apt)	0	0	0	150	121.0	112.2	84.0	83.5	SANDSTONE
tiefere Unterkreide	0	0	0	100	142.0	121.0	83.5	83.2	SANDSTONE
Oberer Jura (Malm)	0	0	0	400	154.0	142.0	83.2	82.0	LIMEmarly
Mittlerer Jura (Dogger)	0	0	0	400	177.0	154.0	82.0	81.5	SHALE&LIME
Unterer Jura (Lias)	0	0	0	400	200.0	177.0	81.5	80.0	MARL
Oberer Keuper (Exter)	0	0	0	53	207.0	200.0	80.0	79.8	SANDSTONE
Mittlerer Keuper (Arnstadt)	0	0	0	134	214.0	207.0	79.8	79.5	MARL
Mittlerer Keuper (Weser)	0	0	0	112	224.5	214.0	79.5	79.0	GYPSUM
Mittlerer Keuper (Stuttgart)	0	0	0	8	226.0	224.5	79.0	78.8	SANDSTONE
Mittlerer Keuper (Grabfeld)	0	0	0	141	232.5	226.0	78.8	78.5	GYPSUM
Unterer Keuper (Erfurt)	0	0	0	48	235.0	232.5	78.5	78.0	SANDSTONE
Oberer Muschelkalk	0	0	0	64	238.5	235.0	78.0	77.7	LIMEmarly
Mittlerer Muschelkalk	0	0	0	73	240.0	238.5	77.7	77.5	DOLOMITE
Unterer Muschelkalk	0	0	0	109	243.0	240.0	77.5	77.2	LIMEmarly
Oberer Buntsandstein (Röt)	0	0	0	159	244.5	243.0	77.2	76.5	LIME&EVAP
Solling	0	0	0	11	245.0	244.5	76.5	76.3	SANDshaly
Hardegsen	0	0	0	40	247.0	245.0	76.3	76.0	SANDshaly
Dethfurt	0	0	0	33	247.5	247.0	76.0	75.9	SANDshaly
Volpriehausen	0	0	0	102	248.5	247.5	10.0	0.0	SANDshaly
Bernburg	0	120	120	0	250.0	248.5	-	-	SAND&SHALE
Calvörde	120	270	150	0	251.0	250.0	-	-	SAND&SHALE
Zechstein	270	570	300	0	258.0	251.0	-	-	EVAPORITE
Rotliegend	570	830	260	0	300.0	258.0	-	-	SAND&SHALE
Ilfelder Rhyolith	830	1130	300	0	304.0	300.0	-	-	Andesite (igneous)
Rotliegend	1130	1440	310	0	306.0	304.0	-	-	SANDcongl
-	-	-	-	-	-	306.0	-	-	-

10. II.3. Petrography and texture

Table A 5: Borehole, depth, porosity, permeability, formation, facies type and texture of the analyzed Buntsandstein samples (sorting: 2 – moderately, 3 – moderately well, 4 – well, 5 – very well; roundness: 1 – angular, 2 – subangular, 3 – subrounded, 4 – rounded, 5 – well rounded).

thin section	borehole	borehole number	depth	porosity [%]	permeability [mD]	formation	facies type	mean grain size [mm]	sorting	mean roundness	grain contacts
Fh13 - 4	Fh13-63	9	408,4	-	-	smH	sandflat	0,2	3,5	3,0	point-contacts > long-contacts
Fh13 - 5	Fh13-63	9	410,2	4,8	0,1	smH	sandflat	0,3	3,0	2,5	point-contacts > long-contacts
Fh13 - 7	Fh13-63	9	410,9	13,0	3,7	smH	sandflat	0,2	3,5	2,5	long-contacts > concave-convex
Fh13 - 8	Fh13-63	9	411,2	13,9	0,1	smH	sandflat	0,2	4,0	3,0	long-contacts > > concave-convex
Fh13 - 11	Fh13-63	9	417,4	4,7	0,2	smH	eolian	0,6	4,0	3,5	point-contacts > long-contacts
Fh13 - 12	Fh13-63	9	419,2	4,9	0,1	smH	sandflat	0,4	3,5	2,5	point-contacts > > long-contacts
Fh13 - 13	Fh13-63	9	425,0	8,2	93,9	smH	eolian	0,5	3,0	3,5	long-contacts > point-contacts
Fh13 - 15	Fh13-63	9	425,9	11,1	11,1	smH	sandflat	0,3	4,0	3,5	long-contacts > concave-convex
Fh13 - 21	Fh13-63	9	440,7	16,0	0,3	smH	sandflat	0,2	4,0	3,0	point-contacts > long-contacts
Fh13 - 24	Fh13-63	9	442,6	19,0	225,6	smH	sandflat	0,2	3,0	3,5	point-contacts > > long-contacts
Fh13 - 27	Fh13-63	9	445,9	15,0	1,8	smH	sandflat	0,3	2,5	3,5	long-contacts > point-contacts > concave-convex
Fh13 - 28	Fh13-63	9	446,9	-	-	smH	eolian	0,4	2,5	3,5	point-contacts > > long-contacts
FH13 - 30	Fh13-63	9	449,7	14,1	1,1	smH	sandflat	0,2	3,5	3,5	point-contacts > long-contacts
Fh13 - 41	Fh13-63	9	467,0	17,5	7,8	smD	sandflat	0,2	3,5	3,5	long-contacts > concave-convex
Fh13 - 42	Fh13-63	9	467,2	15,6	1,1	smD	sandflat	0,2	3,5	2,5	long-contacts > concave-convex > point-contacts
FH13 - 46	Fh13-63	9	470,2	17,0	17,0	smD	sandflat	0,3	4,0	2,5	point-contacts > long-contacts
Fh13 - 47	Fh13-63	9	470,5	12,4	0,0	smD	sandflat	0,2	4,5	2,5	long-contacts > > point-contacts
Fh13 - 50	Fh13-63	9	471,9	21,3	59,2	smD	sandflat	0,3	3,5	2,5	point-contacts > long-contacts
Fh13 - 51	Fh13-63	9	472,5	18,8	37,7	smD	sandflat	0,3	3,0	3,5	point-contacts > long-contacts
Fh13 - 52	Fh13-63	9	473,0	17,6	71,5	smD	sandflat	0,3	3,0	2,5	point-contacts > > long-contacts
Fh13 - 88	Fh13-63	9	477,1	-	-	smD	eolian	0,8	2,5	4,5	point-contacts > long-contacts > sutured-contact > concave-convex
Fh13 - 57	Fh13-63	9	478,4	8,9	29,5	smD	eolian	0,9	3,5	4,5	point-contacts > > long-contacts > concave-convex
Fh13 - 59	Fh13-63	9	480,3	15,9	9,7	smD	sandflat	0,3	3,5	2,5	long-contacts > concave-convex
Fh13 - 60	Fh13-63	9	480,6	16,6	1,2	smD	sandflat	0,3	4,5	2,5	point-contacts > long-contacts > concave-convex
Fh13 - 64	Fh13-63	9	485,4	13,7	0,2	smV	sandflat	0,2	3,5	2,5	long-contacts > point-contacts
Fh13 - 70	Fh13-63	9	494,8	5,7	0,1	smV	sandflat	0,4	2,5	3,5	point-contacts > long-contacts > concave-convex
Fh13 - 78	Fh13-63	9	502,2	9,6	0,1	smV	sandflat	0,4	3,0	3,5	point-contacts > > long-contacts > concave-convex
Fh13 – 79	Fh13-63	9	505,3	11,3	5,2	smV	sandflat	0,3	2,5	3,5	point-contacts > long-contacts
Fh13 - 82	Fh13-63	9	507,7	8,7	5,1	smV	sandflat	0,5	2,5	3,5	long-contacts > point-contacts
Fh13 - 84	Fh13-63	9	508,7	18,2	0,4	smV	sandflat	0,2	3,5	2,5	point-contacts > long-contacts
Fh13 - 85	Fh13-63	9	508,9	12,8	0,1	smV	sandflat	0,2	4,5	3,0	long-contacts > point-contacts
Fh13 - 93	Fh13-63	9	513,5	17,0	1,7	smV	eolian	0,5	3,5	3,5	point-contacts > > long-contacts
Fh13 - 96	Fh13-63	9	517,6	-	-	smV	sandflat	0,2	3,5	2,5	point-contacts > > long-contacts
Fh13 - 97	Fh13-63	9	518,0	-	-	smV	sandflat	0,2	3,5	2,5	point-contacts > long-contacts
Fh13 - 110	Fh13-63	9	528,5	13,9	1,1	smV	sandflat	0,2	3,5	2,5	point-contacts > long-contacts > concave-convex
Fh13 -134	Fh13-63	9	548,0	-	-	smV	sandflat	0,3	2,5	2,5	long-contacts > point-contacts
Fh13 - 140	Fh13-63	9	553,5	-	-	smV	sandflat	0,1	3,5	2,5	long-contacts > point-contacts
Fh13 - 158	Fh13-63	9	577,9	-	-	smV	sandflat	0,4	2,5	3,5	point-contacts > > long-contacts > concave-convex
Fh13 - 170	Fh13-63	9	476,7	17,2	141,4	smD	eolian	-	-	-	-
Fh13 - 171	Fh13-63	9	579,0	9,9	0,4	smD	eolian	-	-	-	-
Fh13 - 35	Fh13-63	9	-	-	-	-	sandflat	0,2	4,0	2,5	long-contacts > concave-convex
Gü1 - 2	Gü1-64	10	564,8	15,0	72,1	smS	fluvial	0,3	3,5	2,5	long-contacts > point-contacts > > concave-convex

thin section	borehole	borehole number	depth	porosity [%]	permeability [mD]	formation	facies type	mean grain size [mm]	sorting	mean roundness	grain contacts
Gü1 - 4	Gü1-64	10	565,2	16,5	235,1	smS	fluvial	0,2	4,0	2,5	long-contacts > > concave-convex > point-contacts
Gü1 - 6	Gü1-64	10	566,7	15,7	151,0	smS	fluvial	0,2	3,5	2,5	concave-convex > long-contacts > point-contacts
Gü1 - 11	Gü1-64	10	575,5	16,4	118,6	smH	sandflat	0,2	4,5	3,5	long-contacts > point-contacts > concave-convex
Gü1 - 13	Gü1-64	10	576,4	14,2	311,1	smH	sandflat	0,3	3,5	3,5	long-contacts > point-contacts > concave-convex
Gü1 - 15	Gü1-64	10	577,0	14,9	21,9	smH	sandflat	0,2	3,0	2,5	long-contacts > concave-convex > point-contacts
Gü1 - 16	Gü1-64	10	577,4	11,9	32,4	smH	sandflat	0,3	2,5	4,5	long-contacts > point-contacts > concave-convex
Gü1 - 18	Gü1-64	10	578,1	0,5	0,0	smH	sandflat	-	-	-	-
Gü1 - 20	Gü1-64	10	579,4	8,6	7,2	smH	sandflat	0,2	3,5	3,5	long-contacts > concave-convex > point-contacts
Gü1 - 22	Gü1-64	10	580,7	5,6	1,3	smH	sandflat	0,3	3,5	3,5	long-contacts > point-contacts > concave-convex
Gü1 - 25	Gü1-64	10	582,6	9,9	14,4	smH	sandflat	0,3	4,0	2,5	long-contacts > concave-convex > point-contacts > sutured-contact
Gü1 - 26	Gü1-64	10	582,9	-	-	smH	sandflat	-	-	-	-
Gü1 - 28	Gü1-64	10	583,3	9,4	10,2	smH	sandflat	0,2	4,0	4,5	long-contacts > point-contacts > concave-convex
La35 - 2	La35-70	7	402,4	15,8	20,3	smS	fluvial	0,2	4,5	2,5	long-contacts > point-contacts
La35 - 3	La35-70	7	404,0	12,4	21,3	smS	fluvial	0,2	3,5	2,5	long-contacts > point-contacts
La35 - 4	La35-70	7	404,4	9,3	-	smS	fluvial	0,3	1,5	3,5	point-contacts > long-contacts
La35 - 7	La35-70	7	405,9	15,2	30,4	smS	fluvial	0,3	3,0	3,5	point-contacts > long-contacts > concave-convex
La35 - 10	La35-70	7	407,6	14,0	4,8	smS	fluvial	0,2	3,5	3,5	long-contacts > point-contacts
La35 - 11	La35-70	7	408,1	10,6	4,1	smS	fluvial	0,2	3,5	3,0	long-contacts > point-contacts
La35 - 12	La35-70	7	408,8	11,5	5,1	smS	fluvial	0,3	2,5	3,5	long-contacts > point-contacts
La35 - 13	La35-70	7	409,6	13,3	18,2	smH	sandflat	0,3	3,0	3,5	point-contacts > long-contacts
La35 - 15	La35-70	7	410,4	16,6	59,8	smH	sandflat	0,3	3,5	3,5	long-contacts > point-contacts > concave-convex
La35 - 16	La35-70	7	410,8	9,5	5,4	smH	sandflat	0,3	3,5	3,5	point-contacts > long-contacts
La35 - 19	La35-70	7	412,4	17,4	0,3	smH	sandflat	0,1	4,5	3,5	long-contacts > point-contacts
La35 - 23	La35-70	7	414,6	11,6	0,0	smH	sandflat	-	3,0	2,5	-
La35 - 29	La35-70	7	418,8	14,0	1,2	smH	sandflat	0,2	3,0	4,5	point-contacts > long-contacts
La35 - 31	La35-70	7	419,8	23,5	2,6	smH	sandflat	0,2	4,5	4,0	point-contacts > long-contacts > concave-convex
La35 - 34	La35-70	7	421,2	21,5	0,9	smH	sandflat	0,2	3,5	4,0	long-contacts > point-contacts
RKS4 - 5	Rks4-69	4	434,7	1,9	0,1	smS	fluvial	0,3	3,5	3,5	point-contacts > > long-contacts > concave-convex
RKS4 - 7	Rks4-69	4	435,2	3,0	0,8	smS	fluvial	0,2	3,0	3,5	point-contacts > > long-contacts > concave-convex
RKS4 - 19	Rks4-69	4	441,9	-	-	smH	sandflat	0,2	3,5	2,5	point-contacts > long-contacts
RKS4 - 23	Rks4-69	4	444,2	19,8	0,5	smH	sandflat	0,1	4,0	1,0	point-contacts > long-contacts
RKS4 - 27	Rks4-69	4	450,0	13,0	0,1	smH	sandflat	0,1	3,5	3,5	long-contacts > point-contacts
Te - 2	Te1-69	6	447,7	2,6	-	smH	sandflat	0,2	3,0	3,0	point-contacts > long-contacts > concave-convex
Te - 3	Te1-69	6	448,1	-	-	smH	sandflat	0,1	2,5	2,5	point-contacts > long-contacts > concave-convex
Te - 7	Te1-69	6	451,5	14,5	-	smH	sandflat	0,1	4,0	2,5	long-contacts > point-contacts > concave-convex
Te - 11	Te1-69	6	453,7	-	-	smH	sandflat	0,2	2,5	3,5	long-contacts > point-contacts > concave-convex
Te - 16	Te1-69	6	455,6	-	-	smH	sandflat	0,2	2,0	3,0	point-contacts > long-contacts > concave-convex
Te - 18	Te1-69	6	457,2	-	-	smH	sandflat	0,1	2,5	3,5	point-contacts > long-contacts > concave-convex
Te - 22	Te1-69	6	461,4	-	-	smH	eolian	0,4	3,5	3,5	point-contacts > > long-contacts > concave-convex
Te - 26	Te1-69	6	463,2	-	-	smH	sandflat	0,1	4,0	2,5	long-contacts > point-contacts > concave-convex
Te - 29	Te1-69	6	465,2	6,0	-	smH	sandflat	0,2	3,5	3,5	-
RKS2 - 1	RKS2-83	3	466,6	21,7	33,1	smH	sandflat	0,2	4,5	3,5	point-contacts > long-contacts
RKS2 - 2	RKS2-83	3	472,9	13,5	39,5	smH	sandflat	0,2	3,5	4,0	point-contacts > long-contacts
RKS2 - 3	RKS2-83	3	483,1	5,2	1,6	smH	eolian	0,7	4,0	4,5	concave-convex > long-contacts(> sutured-contact) > point-contacts
RKS2 - 4	RKS2-83	3	492,0	9,4	0,4	smD	lacustrine	0,1	3,5	2,0	long-contacts > point-contacts > concave-convex
RKS2 - 5	RKS2-83	3	503,2	8,3	0,4	smD	sandflat	0,3	2,5	3,5	long-contacts > concave-convex > sutured-contacts
RKS2 - 6	RKS2-83	3	509,3	10,4	109,0	smD	sandflat	0,2	2,5	3,5	long-contacts > point-contacts > concave-convex
RKS2 - 7	RKS2-83	3	517,1	26,6	310,0	smD	eolian	0,2	3,0	4,5	long-contacts > point-contacts > concave-convex
RKS2 - 8	RKS2-83	3	530,4	5,7	0,5	smV	eolian	0,5	3,0	4,5	long-contacts > point-contacts > concave-convex
RKS2 - 9	RKS2-83	3	554,2	15,5	220,0	smV	sandflat	0,3	2,5	3,5	long-contacts > point-contacts > concave-convex
RKS2 - 10	RKS2-83	3	572,5	13,6	4,9	smV	sandflat	0,2	2,5	2,5	long-contacts > point-contacts

thin section	borehole	borehole number	depth	porosity [%]	permeability [mD]	formation	facies type	mean grain size [mm]	sorting	mean roundness	grain contacts
RKS2 - 11	RKS2-83	3	590,3	12,8	5,8	smV	sandflat	0,1	3,5	3,5	long-contacts > point-contacts > concave-convex
RKS2 - 12	RKS2-83	3	608,3	14,8	4,0	smV	sandflat	0,3	2,0	4,0	long-contacts > concave-convex > point-contacts
RKS2 - 13	RKS2-83	3	621,9	16,2	2,6	smV	sandflat	0,2	3,5	2,5	long-contacts > point-contacts > concave-convex
RKS2 - 14	RKS2-83	3	623,0	13,3	11,5	smV	eolian	0,6	4,5	4,5	long-contacts > point-contacts > concave-convex
RKS2 - 15	RKS2-83	3	634,9	17,2	5,0	suB	lacustrine	0,1	4,0	2,5	-
RKS2 - 16	RKS2-83	3	660,5	15,0	4,0	suB	lacustrine	0,2	3,5	3,0	-
RKS2 - 17	RKS2-83	3	672,6	14,4	1,3	suB	lacustrine	0,1	3,5	3,0	long-contacts > point-contacts
RKS2 - 18	RKS2-83	3	683,1	12,1	0,3	suB	lacustrine	0,1	4,0	2,5	long-contacts > point-contacts
RKS2 - 19	RKS2-83	3	715,2	11,6	0,1	suB	lacustrine	0,1	4,5	2,5	long-contacts > > point-contacts
RKS2 - 20	RKS2-83	3	718,6	13,3	0,1	suB	lacustrine	0,1	4,5	2,5	long-contacts > point-contacts > concave-convex
RKS2 - 21	RKS2-83	3	732,4	17,7	0,2	suB	lacustrine	0,1	4,5	3,0	(long-contacts > point-contacts)
RKS2 - 22	RKS2-83	3	744,8	10,8	0,1	suB	lacustrine	0,1	4,5	2,5	long-contacts > point-contacts > concave-convex
RKS2 - 23	RKS2-83	3	788,1	1,4	0,1	suC	sandflat	0,3	4,0	3,5	point-contacts > long-contacts > concave-convex
RKS2 - 24	RKS2-83	3	826,6	8,8	0,1	suC	sandflat	0,1	4,5	1,5	long-contacts > point-contacts
RKS2 - 25	RKS2-83	3	845,3	5,1	3,0	suC	sandflat	0,2	3,0	2,0	long-contacts > point-contacts
RKS2 - 26	RKS2-83	3	893,3	11,8	0,1	suC	lacustrine	0,1	4,5	1,5	point-contacts > long-contacts
RKS2 - 27	RKS2-83	3	908,0	10,8	0,1	suC	lacustrine	0,1	4,5	1,0	long-contacts > point-contacts
RKS2 - 31	RKS2-83	3	441,3	4,9	0,2	smS	fluvial	0,2	2,5	3,5	point-contacts > concave-convex > long-contacts
RKS2 - 32	RKS2-83	3	448,8	-	-	smS	fluvial	0,3	3,5	3,5	point-contacts > long-contacts
RKS2 - 33	RKS2-83	3	481,4	-	-	smH	eolian	0,3	2,0	4,0	point-contacts > long-contacts > concave-convex
RKS2 - 34	RKS2-83	3	503,5	21,3	200,0	smD	eolian	0,2	2,0	4,0	point-contacts > long-contacts > concave-convex
RKS2 - 35	RKS2-83	3	570,1	14,5	56,0	smV	eolian	0,5	4,0	4,5	long-contacts > point-contacts > concave-convex
RKS2 - 36	RKS2-83	3	609,0	-	-	smV	eolian	0,4	3,5	3,5	long-contacts > concave-convex > point-contacts
RKS2 - 37	RKS2-83	3	614,5	-	-	smV	eolian	0,4	4,0	3,5	point-contacts > long-contacts > concave-convex
Ballst - 22	Ballst1-63	8	502,0	15,6	247,2	smS	fluvial	0,2	4,0	1,0	long-contacts > point-contacts > concave-convex
Ballst - 23	Ballst1-63	8	518,7	17,1	16,4	smS	fluvial	0,1	4,5	2,0	long-contacts > concave-convex > point-contacts
Ballst - 24	Ballst1-63	8	525,8	21,7	595,4	sm?	eolian	0,3	3,0	3,0	long-contacts > concave-convex > point-contacts
Ballst - 25	Ballst1-63	8	547,6	15,6	56,8	sm?	sandflat	0,2	4,0	2,0	long-contacts > concave-convex > point-contacts
Ballst - 26	Ballst1-63	8	553,3	12,8	33,8	sm?	eolian	0,2	2,5	2,5	long-contacts > concave-convex > point-contacts
Ballst - 27	Ballst1-63	8	596,8	-	-	sm?	eolian	0,3	1,5	3,0	long-contacts > point-contacts > concave-convex
Ballst - 28	Ballst1-63	8	600,6	18,8	185,1	sm?	eolian	0,3	3,0	3,0	long-contacts > concave-convex > point-contacts
Ballst - 29	Ballst1-63	8	621,4	9,0	79,1	sm?	eolian	0,3	3,5	4,0	long-contacts > concave-convex > point-contacts
Ballst - 30	Ballst1-63	8	638,8	15,7	10,2	sm?	sandflat	0,2	4,5	3,0	long-contacts > point-contacts > concave-convex
Ballst - 31	Ballst1-63	8	672,4	15,6	133,2	sm?	sandflat	0,2	3,5	3,0	long-contacts > point-contacts > concave-convex
Ballst - 32	Ballst1-63	8	688,3	15,8	59,4	sm?	sandflat	0,2	4,5	2,5	long-contacts > concave-convex > point-contacts
Ballst - 1	Ballst1-63	8	692,4	17,7	1,4	sm?	sandflat	0,1	4,5	4,0	long-contacts > concave-convex > point-contacts
Ballst - 2	Ballst1-63	8	695,5	19,2	23,9	sm?	sandflat	0,2	4,5	3,0	long-contacts > point-contacts > concave-convex
Ballst - 3	Ballst1-63	8	703,0	12,1	1,2	sm?	sandflat	0,2	3,0	3,5	long-contacts > concave-convex > point-contacts
Ballst - 4	Ballst1-63	8	713,0	11,0	37,0	sm?	sandflat	0,3	3,0	3,0	long-contacts > concave-convex > point-contacts
Ballst - 5	Ballst1-63	8	717,5	4,7	1,8	sm?	sandflat	0,3	2,5	3,0	long-contacts > point-contacts > concave-convex
Ballst - 6	Ballst1-63	8	724,5	10,8	6,2	sm?	sandflat	0,2	3,0	3,0	long-contacts > concave-convex > point-contacts
Ballst - 7	Ballst1-63	8	729,4	16,9	58,6	sm?	lacustrine	0,3	2,5	2,0	long-contacts > concave-convex > point-contacts
Ballst - 8	Ballst1-63	8	741,6	9,7	0,3	suB	lacustrine	0,2	4,5	3,5	long-contacts > concave-convex > point-contacts
Ballst - 9	Ballst1-63	8	750,5	8,7	0,3	suB	lacustrine	0,2	3,5	3,5	long-contacts > point-contacts > concave-convex
Ballst - 10	Ballst1-63	8	784,3	17,0	2,9	suB	lacustrine	0,2	3,0	3,0	long-contacts > concave-convex > point-contacts
Ballst - 11	Ballst1-63	8	809,1	5,9	0,1	suB	lacustrine	0,3	4,5	2,5	long-contacts > point-contacts > concave-convex
Ballst - 12	Ballst1-63	8	843,4	11,9	0,1	suB	lacustrine	0,1	4,5	3,0	long-contacts > concave-convex > point-contacts
Ballst - 13	Ballst1-63	8	850,5	9,4	0,6	suB	lacustrine	0,1	3,5	2,0	long-contacts > concave-convex > point-contacts
Ballst - 14	Ballst1-63	8	867,2	6,8	6,5	suC	lacustrine	0,2	4,0	3,0	long-contacts > point-contacts > concave-convex
Ballst - 15	Ballst1-63	8	906,4	7,2	0,2	suC	lacustrine	0,3	2,5	4,0	long-contacts > point-contacts > concave-convex
Ballst - 16	Ballst1-63	8	953,8	14,9	18,1	suC	lacustrine	0,3	4,0	3,0	long-contacts > point-contacts > concave-convex
Ballst - 17	Ballst1-63	8	979,5	6,7	0,0	suC	lacustrine	0,1	3,5	3,0	long-contacts > concave-convex > point-contacts
Ballst - 18	Ballst1-63	8	1011,9	10,6	0,1	suC	lacustrine	0,1	3,5	2,0	long-contacts > concave-convex > point-contacts

thin section	borehole	borehole number	depth	porosity [%]	permeability [mD]	formation	facies type	mean grain size [mm]	sorting	mean roundness	grain contacts
Ballst - 19	Ballst1-63	8	1036,4	7,2	0,1	suC	lacustrine	0,1	3,5	2,0	long-contacts > concave-convex > point-contacts
Ag - 1 (p1)	Ag3-87	5	803,70	-	0,6	smV	sandflat	-	-	-	-
Ag - 2 (p2)	Ag3-87	5	807,00	-	3,8	smV	sandflat	-	-	-	-
Ag - 3 (p3)	Ag3-87	5	810,50	10,0	1,3	smV	sandflat	-	-	-	-
Ag - 4 (p4)	Ag3-87	5	811,10	23,8	101,5	smV	sandflat	-	-	-	-
Ag - 5 (p5)	Ag3-87	5	813,50	14,9	10,6	smV	sandflat	-	-	-	-
Ag - 6 (p6)	Ag3-87	5	817,50	19,2	127,4	smV	sandflat	-	-	-	-
Ag - 7 (p7)	Ag3-87	5	819,70	16,4	4,2	smV	sandflat	-	-	-	-
Ag - 8 (p8)	Ag3-87	5	821,30	17,1	30,7	smV	sandflat	-	-	-	-
Ag - 9 (p9)	Ag3-87	5	824,20	10,6	4,1	smV	sandflat	-	-	-	-
Ag - 10 (p10)	Ag3-87	5	826,10	14,1	35,8	smV	sandflat	-	-	-	-
Ag - 11 (p11)	Ag3-87	5	828,50	12,9	204,2	smV	sandflat	-	-	-	-
Ag - 12 (p12)	Ag3-87	5	829,30	5,5	0,2	smV	sandflat	-	-	-	-
Ag - 13 (p13)	Ag3-87	5	827,40	15,9	408,5	smV	sandflat	-	-	-	-
Ag - 14 (p14)	Ag3-87	5	805,10	16,6	1,5	smV	sandflat	-	-	-	-
Ge - 1	Ge1-61	1	147,50	22,7	1193,5	smS	fluvial	-	-	-	-
Ge - 2	Ge1-61	1	148,50	17,7	409,0	smS	fluvial	-	-	-	-
Ge - 3	Ge1-61	1	153	18,1	211,2	smS	fluvial	-	-	-	-
Ge - 4	Ge1-61	1	158	21,3	1740,2	smS	fluvial	-	-	-	-
Ge - 5	Ge1-61	1	161	22,8	1616,0	smS	fluvial	-	-	-	-
Bi - 1	Bi1-61	2	14,50	23,3	95,1	smV?	sandflat?	-	-	-	-
Bi - 2	Bi1-61	2	17,10	21,4	600,3	smV?	sandflat?	-	-	-	-
Bi - 3	Bi1-61	2	26,90	19,8	523,8	smV?	sandflat?	-	-	-	-
Bi - 4	Bi1-61	2	36,80	17,9	153,6	smV?	sandflat?	-	-	-	-
Bi - 5	Bi1-61	2	41,00	22,8	603,2	smV?	sandflat?	-	-	-	-
Bi - 6	Bi1-61	2	44,00	17,5	141,5	smV?	sandflat?	-	-	-	-
Bi - 7	Bi1-61	2	67,80	16,9	31,5	smD?	sandflat?	-	-	-	-
Bi - 8	Bi1-61	2	85,00	12,4	29,9	smD?	sandflat?	-	-	-	-
Bi - 9	Bi1-61	2	96,00	9,4	1,3	smD?	sandflat?	-	-	-	-
Bi - 10	Bi1-61	2	127,80	10,2	22,8	smV	sandflat?	-	-	-	-
Bi - 11	Bi1-61	2	134,10	16,8	3,6	smV	sandflat?	-	-	-	-
Bi - 12	Bi1-61	2	141,50	22,1	-	smV	sandflat?	-	-	-	-
Bi - 13	Bi1-61	2	147,50	-	26,2	smV	sandflat?	-	-	-	-
Bi - 14	Bi1-61	2	162,00	-	-	smV	sandflat?	-	-	-	-
Hartschwinden 1	Outcrop	-	0,0	13,6	0,1	smV	sandflat	-	-	-	-
Hartschwinden 2	Outcrop	-	0,0	19,3	32,4	smV	sandflat	-	-	-	-
Werraufer 1	Outcrop	-	0,0	20,2	3,6	suC	sandflat?	-	-	-	-
Werraufer 2	Outcrop	-	0,0	18,5	0,8	suC	sandflat?	-	-	-	-
Vacha 1	Outcrop	-	0,0	10,6	55,6	smV	fluvial?	-	-	-	-
Vacha 2	Outcrop	-	0,0	5,7	0,2	smV	fluvial?	-	-	-	-
Ludwigstein 1	Outcrop	-	0,0	7,8	1,5	smS	fluvial	-	-	-	-
Ludwigstein 2	Outcrop	-	0,0	14,0	38,4	smS	fluvial	-	-	-	-
Hanstein 1	Outcrop	-	0,0	24,6	511,1	smS	fluvial	-	-	-	-
Hanstein 2	Outcrop	-	0,0	16,0	115,5	smS	fluvial	-	-	-	-
Brehme 1 (Br-1)	Outcrop	-	0,0	28,9	1671,4	smS	fluvial	-	-	-	-
Brehme 2 (Br-2)	Outcrop	-	0,0	32,7	2676,1	smS	fluvial	-	-	-	-
Brehme 3 (Br-3)	Outcrop	-	0,0	30,8	3634,0	smS	fluvial	-	-	-	-
Heiligenstadt 2	Outcrop	-	0,0	15,4	53,7	smV	sandflat	-	-	-	-

Table A 6: Detrital composition of the Buntsandstein samples (point-counted).

thin section	detrital quartz				detrital feldspar			rock fragments			detrital clay			mica	oids	heavy minerals	opaque
	qz mono	qz poly	chert	quartz (total)	alkali feldspar	plagioclase	feldspar (total)	magmatic	sedimentary	lithic fragments (total)	iron oxide	matrix	detrital clay (total)				
Fh13 - 4	37,7	12,3	0,3	50,3	17,3	0,0	17,3	0,3	0,0	0,3	0,7	5,7	6,3	0,0	0,0	0,0	0,0
Fh13 - 5	28,7	24,7	0,3	53,7	9,7	0,0	9,7	0,0	2,7	2,7	0,3	0,0	0,3	0,3	0,0	0,0	0,0
Fh13 - 7	42,3	7,0	0,0	49,3	11,7	0,0	11,7	0,0	1,0	1,0	21,3	0,0	21,3	0,3	0,0	0,7	0,0
Fh13 - 8	40,3	5,7	0,0	46,0	11,0	0,0	11,0	0,0	0,7	0,7	21,3	12,3	33,7	2,0	0,0	0,0	0,0
Fh13 - 11	39,3	25,0	0,0	64,3	5,3	0,0	5,3	0,0	1,0	1,0	0,0	0,0	0,0	0,3	0,0	0,0	0,0
Fh13 - 12	30,3	17,3	0,0	47,7	11,3	0,0	11,3	0,3	0,0	0,3	4,3	5,7	10,0	0,3	0,0	0,0	0,0
Fh13 - 13	34,0	23,0	0,0	57,0	5,7	0,0	5,7	0,0	0,0	0,0	3,7	0,3	4,0	0,3	0,0	0,0	0,0
Fh13 - 15	41,3	16,0	0,0	57,3	15,0	0,0	15,0	0,0	0,0	0,0	9,0	6,3	15,3	0,3	0,0	0,0	0,0
Fh13 - 21	42,7	7,0	0,0	49,7	15,3	0,0	15,3	0,0	0,0	0,0	0,3	7,7	8,0	0,3	0,0	0,0	0,0
Fh13 - 24	35,3	22,7	0,0	58,0	12,7	0,0	12,7	1,7	1,0	2,7	3,3	0,0	3,3	0,0	0,0	0,0	0,0
Fh13 - 27	45,7	18,0	0,0	63,7	10,7	0,3	11,0	0,7	0,3	1,0	4,3	1,0	5,3	2,0	0,0	0,0	0,0
Fh13 - 28	39,7	26,3	0,3	66,3	8,7	0,0	8,7	0,3	0,0	0,3	5,7	0,0	5,7	0,0	0,0	0,0	0,0
FH13 - 30	32,7	14,3	0,0	47,0	16,0	0,7	16,7	0,3	0,0	0,3	11,3	0,3	11,7	0,3	0,0	0,3	0,0
Fh13 - 41	31,0	7,7	0,0	38,7	22,3	0,3	22,7	0,0	0,3	0,3	1,0	0,7	1,7	0,3	0,0	0,3	0,0
Fh13 - 42	40,0	10,0	0,0	50,0	20,7	0,0	20,7	0,0	2,7	2,7	3,0	7,3	10,3	0,3	0,0	0,0	0,0
FH13 - 46	27,0	8,0	0,0	35,0	17,3	0,0	17,3	0,0	1,7	1,7	25,0	0,0	25,0	0,0	0,0	0,0	0,0
Fh13 - 47	40,7	6,7	0,0	47,3	17,7	0,3	18,0	0,7	1,7	2,3	7,7	8,0	15,7	1,0	0,0	0,7	0,0
Fh13 - 50	29,0	7,0	0,0	36,0	18,3	0,0	18,3	0,0	1,0	1,0	13,7	0,0	13,7	0,0	0,0	0,3	0,0
Fh13 - 51	28,0	8,3	0,0	36,3	27,7	0,0	27,7	0,7	0,0	0,7	5,0	0,3	5,3	0,0	0,0	0,0	0,0
Fh13 - 52	32,1	19,0	0,0	51,0	15,2	0,0	15,2	1,0	0,0	1,0	8,6	0,0	8,6	0,3	0,0	0,0	0,1
Fh13 - 88	28,7	44,0	0,3	73,0	6,0	0,3	6,3	0,7	1,3	2,0	5,7	3,7	9,3	0,3	0,0	0,0	0,0
Fh13 - 57	29,7	28,3	0,0	58,0	8,3	0,0	8,3	1,3	1,3	2,7	4,3	0,0	4,3	0,0	0,0	0,0	0,0
Fh13 - 59	31,0	14,7	0,0	45,7	21,3	0,0	21,3	0,0	0,3	0,3	7,7	0,7	8,3	0,0	0,0	0,0	0,0
Fh13 - 60	38,0	15,3	0,0	53,3	18,0	0,0	18,0	0,7	0,3	1,0	7,0	0,7	7,7	0,0	0,0	0,0	0,0
Fh13 - 64	39,3	6,0	0,0	45,3	16,0	0,3	16,3	1,0	2,3	3,3	7,7	3,3	11,0	0,7	0,0	0,0	0,0
Fh13 - 70	27,3	18,3	0,0	45,7	15,3	0,0	15,3	0,0	0,3	0,3	14,7	0,0	14,7	0,3	0,0	0,0	0,0
Fh13 - 78	36,8	14,1	0,0	50,9	15,5	0,0	15,5	0,0	1,0	1,0	12,0	0,0	12,0	0,0	0,0	0,3	0,0
Fh13 – 79	33,7	12,0	0,0	45,7	22,3	0,0	22,3	0,0	2,3	2,3	7,7	3,3	11,0	1,3	0,0	0,0	0,0
Fh13 - 82	30,7	17,7	0,0	48,3	18,7	0,0	18,7	0,0	0,0	0,0	7,0	16,0	23,0	4,3	0,0	0,0	0,0
Fh13 - 84	35,3	2,3	0,0	37,7	21,0	0,0	21,0	0,0	2,7	2,7	15,0	0,0	15,0	0,0	0,0	0,0	0,0
Fh13 - 85	34,0	9,0	0,0	43,0	23,7	0,0	23,7	0,0	1,3	1,3	2,0	0,0	2,0	0,0	0,0	0,0	0,0
Fh13 - 93	26,9	17,3	0,0	44,2	16,7	0,0	16,7	1,7	0,0	1,7	0,0	10,2	10,2	0,7	0,0	0,3	0,0
Fh13 - 96	33,0	7,7	0,0	40,7	23,7	0,0	23,7	0,0	2,0	2,0	3,3	0,0	3,3	0,0	0,0	0,0	0,0
Fh13 - 97	37,7	6,7	0,0	44,3	22,3	0,0	22,3	0,0	2,0	2,0	0,3	0,7	1,0	1,3	0,0	0,0	0,0
Fh13 - 110	27,3	6,7	0,0	34,0	22,7	0,0	22,7	0,0	0,3	0,3	0,0	0,0	0,0	0,3	0,0	0,0	0,0
Fh13 -134	33,3	12,3	0,3	46,0	24,3	0,0	24,3	2,0	1,0	3,0	7,7	1,0	8,7	0,3	0,0	0,0	0,0
Fh13 - 140	38,0	4,7	0,3	43,0	26,0	1,7	27,7	0,0	0,3	0,3	3,0	5,3	8,3	2,0	0,0	0,0	0,0
Fh13 - 158	20,7	2,0	0,0	22,7	7,7	0,3	8,0	0,3	1,7	2,0	0,7	57,7	58,3	6,3	0,0	0,0	0,0
Fh13 - 170	29,3	24,3	0,0	53,7	14,7	0,0	14,7	1,0	0,0	1,0	9,0	0,0	9,0	0,0	0,0	0,0	0,0
Fh13 - 171	30,7	20,0	0,7	51,3	17,0	0,7	17,7	1,0	0,7	1,7	0,0	3,3	3,3	0,0	0,0	1,0	0,0
Fh13 - 35	50,3	10,0	0,0	60,3	22,3	0,7	23,0	0,3	0,0	0,3	2,3	0,0	2,3	0,3	0,0	0,0	0,0
Gü1 - 2	45,7	10,0	1,0	56,7	10,7	0,0	10,7	-	-	8,0	0,0	2,7	2,7	1,0	0,0	0,3	0,3
Gü1 - 4	48,0	6,0	0,3	54,3	13,7	0,3	14,0	-	-	6,0	0,0	2,3	2,3	1,0	0,0	0,7	0,0
Gü1 - 6	43,7	9,0	0,0	52,7	10,3	0,0	10,3	-	-	7,0	0,0	0,3	0,3	0,7	0,0	2,7	0,7
Gü1 - 11	46,0	13,3	0,3	59,7	14,3	0,0	14,3	0,33	0,0	0,3	0,0	0,0	0,0	0,0	0,0	0,0	0,0
Gü1 - 13	38,3	11,3	0,0	49,7	12,3	0,0	12,3	-	-	1,7	0,0	0,0	0,0	0,0	0,0	0,0	0,3
Gü1 - 15	43,3	10,3	0,3	54,0	17,0	0,3	17,3	1,0	0,0	1,0	0,0	0,0	0,0	1,3	0,0	0,0	0,0
Gü1 - 16	45,3	11,7	0,7	57,7	16,0	0,0	16,0	-	-	3,0	0,0	0,3	0,3	0,3	0,0	0,0	0,3

thin section	detrital quartz				detrital feldspar			rock fragments			detrital clay			mica	ooids	heavy minerals	opaque
	qz mono	qz poly	chert	quartz (total)	alkali feldspar	plagioclase	feldspar (total)	magmatic	sedimentary	lithic fragments (total)	iron oxide	matrix	detrital clay (total)				
Gü1 - 18	37,3	27,7	0,3	65,3	4,7	0,0	4,7	0,0	0,0	0,0	0,0	0,0	0,0	0,3	0,0	0,0	0,0
Gü1 - 20	40,3	7,3	0,0	47,7	18,3	0,0	18,3	-	-	2,7	0,0	0,7	0,7	1,3	0,0	0,0	0,0
Gü1 - 22	49,3	12,3	0,0	61,7	10,3	0,0	10,3	1,0	0,0	1,0	0,0	0,0	0,0	0,0	0,0	0,0	0,0
Gü1 - 25	45,7	8,7	0,0	54,3	17,0	0,0	17,0	-	-	2,7	0,0	1,7	1,7	0,7	0,0	0,0	0,0
Gü1 - 26	-	-	-	-	-	-	-	-	-	-	-	-	-	-	-	-	-
Gü1 - 28	48,0	9,7	0,0	57,7	13,3	0,0	13,3	0,0	0,3	0,3	0,0	0,0	0,0	0,0	0,0	0,0	0,0
La35 - 2	47,0	11,0	0,0	58,0	10,7	0,3	11,0	1,0	0,0	1,0	0,0	0,0	0,0	7,3	0,0	0,0	0,0
La35 - 3	46,7	12,0	0,0	58,7	8,0	0,0	8,0	1,3	0,0	1,3	0,0	3,0	3,0	1,7	0,0	0,0	0,0
La35 - 4	36,0	17,0	0,0	53,0	10,0	0,0	10,0	1,7	0,0	1,7	0,0	0,3	0,3	0,3	0,0	0,0	0,0
La35 - 7	35,0	17,7	0,0	52,7	19,7	0,0	19,7	0,0	0,7	0,7	0,0	0,0	0,0	0,0	0,0	0,0	0,0
La35 - 10	46,0	14,7	0,0	60,7	15,3	0,3	15,7	0,0	3,0	3,0	0,0	0,0	0,0	0,0	0,0	0,3	0,0
La35 - 11	48,3	8,0	0,0	56,3	5,7	0,0	5,7	-	-	0,0	0,0	8,0	8,0	0,7	0,0	1,3	0,7
La35 - 12	38,7	15,0	0,0	53,7	19,3	0,0	19,3	-	-	1,3	0,0	0,0	0,0	0,0	0,0	0,3	0,0
La35 - 13	33,7	13,0	0,7	47,3	16,0	0,3	16,3	-	-	3,7	0,0	3,3	3,3	1,0	0,0	0,3	0,0
La35 - 15	36,0	7,7	0,3	44,0	16,3	0,0	16,3	-	-	5,3	0,0	0,0	0,0	0,3	0,0	0,0	0,0
La35 - 16	41,0	19,3	0,7	61,0	10,3	0,3	10,7	0,0	1,0	1,0	0,0	0,0	0,0	0,0	0,0	0,0	0,0
La35 - 19	39,0	5,3	0,3	44,7	15,0	0,0	15,0	-	-	3,3	0,0	7,0	7,0	1,7	0,0	3,0	0,0
La35 - 23	36,7	5,3	0,0	42,0	14,7	0,0	14,7	-	-	5,0	0,0	9,3	9,3	6,0	0,0	0,3	0,0
La35 - 29	33,7	15,0	0,0	48,7	16,0	0,0	16,0	0,0	2,0	2,0	1,7	0,0	1,7	0,3	0,0	0,0	0,0
La35 - 31	36,7	14,0	0,0	50,7	15,3	0,0	15,3	0,0	0,3	0,3	3,3	0,0	3,3	0,0	0,0	0,0	0,0
La35 - 34	34,0	11,3	0,0	45,3	17,7	0,3	18,0	-	-	2,0	0,0	6,0	6,0	2,0	0,0	0,0	0,0
RKS4 - 5	52,3	10,3	0,0	62,7	1,0	0,0	1,0	0,0	0,0	0,0	0,0	0,0	0,0	0,0	0,0	0,0	0,0
RKS4 - 7	58,7	11,0	0,0	69,7	1,0	0,0	1,0	0,0	0,0	0,0	0,0	0,3	0,3	0,0	0,0	0,0	0,0
RKS4 - 19	44,0	11,3	0,0	55,3	12,7	0,7	13,3	0,3	0,7	1,0	3,3	0,0	3,3	1,0	0,0	0,0	0,0
RKS4 - 23	43,0	7,3	0,0	50,3	9,3	1,3	10,7	1,3	0,0	1,3	8,3	0,0	8,3	1,7	0,0	0,0	0,0
RKS4 - 27	46,3	7,0	0,0	53,3	7,7	1,7	9,3	0,7	0,0	0,7	0,0	0,0	0,0	3,7	0,0	0,0	0,0
Te - 2	56,7	9,3	0,0	66,0	5,3	0,0	5,3	0,0	0,0	0,0	0,0	0,0	0,0	0,0	0,0	0,0	0,0
Te - 3	32,3	4,7	0,0	37,0	5,0	0,3	5,3	0,0	0,0	0,0	1,0	44,7	45,7	8,0	0,0	0,0	0,0
Te - 7	53,3	11,7	0,0	65,0	9,0	0,0	9,0	0,0	0,0	0,0	7,0	1,3	8,3	0,0	0,0	0,0	0,0
Te - 11	49,7	8,3	0,0	58,0	9,3	0,0	9,3	0,3	0,3	0,7	6,7	8,7	15,3	0,7	0,0	0,0	0,0
Te - 16	35,7	9,0	0,3	45,0	9,0	0,3	9,3	1,0	4,0	5,0	3,0	19,3	22,3	2,7	0,0	0,0	0,0
Te - 18	47,3	10,7	0,0	58,0	8,7	0,0	8,7	0,3	1,0	1,3	9,0	0,7	9,7	0,7	0,0	0,0	0,0
Te - 22	43,7	21,0	0,7	65,3	3,7	0,0	3,7	0,0	2,0	2,0	1,7	1,3	3,0	0,0	0,0	0,0	0,0
Te - 26	44,0	7,0	0,0	51,0	9,3	0,7	10,0	1,3	1,3	2,7	9,7	0,7	10,3	4,7	0,0	0,0	0,0
Te - 29	47,0	12,7	0,0	59,7	12,7	0,7	13,3	0,3	0,0	0,3	0,0	0,7	0,7	1,0	0,0	0,0	0,0
RKS2 - 1	36,7	8,3	0,0	45,0	26,3	0,0	26,3	0,7	0,0	0,7	5,7	0,0	5,7	1,3	0,0	0,0	0,0
RKS2 - 2	35,3	20,0	0,0	55,3	16,0	0,0	16,0	0,0	0,0	0,0	6,7	0,0	6,7	0,0	0,0	0,0	0,0
RKS2 - 3	29,7	39,3	0,0	69,0	1,0	0,0	1,0	0,0	0,0	0,0	0,0	0,0	0,0	0,0	0,0	0,0	0,0
RKS2 - 4	41,0	9,3	0,0	50,3	32,0	0,3	32,3	1,0	0,0	1,0	0,0	0,0	0,0	1,0	0,0	0,0	0,0
RKS2 - 5	36,3	20,7	0,0	57,0	22,0	0,0	22,0	1,3	0,0	1,3	10,0	0,0	10,0	0,0	0,0	0,0	0,0
RKS2 - 6	27,0	16,7	0,0	43,7	28,3	0,7	29,0	0,3	0,0	0,3	2,7	0,0	2,7	1,3	0,0	0,0	0,0
RKS2 - 7	44,3	16,7	0,0	61,0	17,0	0,3	17,3	1,0	0,0	1,0	0,0	0,0	0,0	0,0	0,0	0,0	0,0
RKS2 - 8	31,7	31,0	0,0	62,7	10,0	0,0	10,0	2,0	0,0	2,0	7,0	0,0	7,0	0,0	0,0	0,0	0,0
RKS2 - 9	34,0	23,0	0,0	57,0	19,3	0,0	19,3	1,3	2,3	3,7	1,7	0,0	1,7	0,3	0,0	0,0	0,0
RKS2 - 10	36,7	13,7	0,0	50,3	20,0	0,3	20,3	0,0	0,0	0,0	19,7	0,0	19,7	0,3	0,0	0,0	0,0
RKS2 - 11	34,7	22,3	0,0	57,0	17,3	0,0	17,3	1,3	0,0	1,3	12,3	0,0	12,3	0,0	0,0	0,0	0,0
RKS2 - 12	33,7	25,7	0,3	59,7	18,3	0,3	18,7	3,0	0,0	3,0	6,3	0,0	6,3	0,0	0,0	0,0	0,0
RKS2 - 13	41,3	10,3	0,0	51,7	28,3	0,3	28,7	1,7	0,0	1,7	0,3	0,0	0,3	0,3	0,0	0,0	0,0
RKS2 - 14	28,3	38,7	0,7	67,7	8,3	0,0	8,3	0,0	0,0	0,0	0,0	0,0	0,0	0,0	0,0	0,0	0,0
RKS2 - 15	38,3	8,3	0,3	47,0	36,7	0,0	36,7	0,3	0,0	0,3	0,0	0,0	0,0	0,0	0,0	0,0	0,0

thin section	detrital quartz				detrital feldspar			rock fragments			detrital clay			mica	ooids	heavy minerals	opaque
	qz mono	qz poly	chert	quartz (total)	alkali feldspar	plagioclase	feldspar (total)	magmatic	sedimentary	lithic fragments (total)	iron oxide	matrix	detrital clay (total)				
RKS2 - 16	40,7	10,3	0,7	51,7	29,7	0,7	30,3	0,7	0,0	0,7	0,0	0,0	0,0	3,0	0,0	0,0	0,0
RKS2 - 17	29,7	9,3	0,3	39,3	33,0	0,3	33,3	2,3	0,0	2,3	0,0	0,0	0,0	1,3	0,0	0,7	0,0
RKS2 - 18	40,3	7,3	0,0	47,7	27,3	0,3	27,7	0,3	0,0	0,3	3,3	0,0	3,3	1,3	0,0	0,0	0,0
RKS2 - 19	31,3	7,7	0,0	39,0	30,7	0,0	30,7	2,0	0,0	2,0	13,0	0,0	13,0	2,7	0,0	0,0	0,0
RKS2 - 20	33,7	11,7	0,0	45,3	37,0	0,0	37,0	1,0	0,0	1,0	2,7	0,0	2,7	3,0	0,0	0,0	0,0
RKS2 - 21	29,0	10,0	0,3	39,3	36,3	0,0	36,3	1,7	0,0	1,7	0,0	0,0	0,0	4,7	0,0	0,0	0,0
RKS2 - 22	28,3	12,3	0,0	40,7	29,0	0,0	29,0	0,3	0,0	0,3	9,3	0,0	9,3	2,7	0,0	0,0	0,0
RKS2 - 23	28,0	12,7	0,0	40,7	19,7	0,7	20,3	0,7	0,0	0,7	2,0	0,0	2,0	0,3	0,0	0,0	0,0
RKS2 - 24	47,3	2,7	0,3	50,3	15,3	0,7	16,0	0,0	0,0	0,0	19,0	0,0	19,0	1,3	0,0	0,0	0,0
RKS2 - 25	42,3	5,7	0,0	48,0	15,7	0,0	15,7	0,0	0,0	0,0	0,0	0,0	0,0	2,3	0,0	0,3	0,0
RKS2 - 26	50,7	1,0	0,0	51,7	16,7	0,3	17,0	0,0	0,0	0,0	0,0	0,0	0,0	2,0	0,0	1,7	0,0
RKS2 - 27	52,0	2,7	0,0	54,7	20,7	1,3	22,0	0,0	0,0	0,0	0,0	0,0	0,0	1,3	0,0	2,7	0,0
RKS2 - 31	40,7	24,3	0,0	65,0	8,7	0,0	8,7	0,0	0,0	0,0	0,0	0,0	0,0	0,0	0,0	0,0	0,0
RKS2 - 32	38,3	15,3	0,0	53,7	16,7	0,0	16,7	0,0	0,0	0,0	3,0	0,0	3,0	0,0	0,0	0,0	0,0
RKS2 - 33	31,0	39,0	0,0	70,0	5,3	0,3	5,7	0,3	0,0	0,3	0,0	0,0	0,0	0,0	0,0	0,0	0,0
RKS2 - 34	35,0	26,0	0,7	61,7	16,7	0,3	17,0	0,3	0,0	0,3	0,0	0,0	0,0	0,0	0,0	0,0	0,0
RKS2 - 35	29,7	28,3	0,7	58,7	9,7	0,7	10,3	1,3	1,0	2,3	0,0	0,0	0,0	0,3	0,0	0,0	0,0
RKS2 - 36	25,7	28,3	0,3	54,3	13,0	0,0	13,0	3,0	0,3	3,3	3,7	0,0	3,7	0,0	0,0	0,0	0,0
RKS2 - 37	20,7	34,3	0,0	55,0	12,7	0,3	13,0	3,0	0,0	3,0	2,3	0,0	2,3	0,0	0,0	0,0	0,0
Ballst - 22	43,7	9,3	0,0	53,0	17,0	0,0	17,0	0,0	0,0	0,0	0,0	2,0	2,0	1,0	0,0	0,0	0,0
Ballst - 23	32,3	5,3	0,0	37,7	24,3	0,0	24,3	0,3	0,0	0,3	10,0	0,0	10,0	2,3	0,0	0,0	0,0
Ballst - 24	37,7	22,3	0,0	60,0	14,0	0,0	14,0	0,7	0,0	0,7	0,0	0,7	0,7	0,3	0,0	0,0	0,0
Ballst - 25	37,0	18,7	0,0	55,7	18,3	0,0	18,3	0,0	0,0	0,0	7,0	0,0	7,0	1,0	0,0	0,0	0,0
Ballst - 26	39,3	23,3	0,0	62,7	18,0	0,0	18,0	0,0	0,0	0,0	0,3	0,0	0,3	0,0	0,0	0,0	0,0
Ballst - 27	29,0	31,3	0,0	60,3	19,0	0,3	19,3	0,3	0,7	1,0	6,7	0,7	7,3	1,3	0,0	0,3	0,0
Ballst - 28	29,0	27,0	0,0	56,0	14,5	0,0	14,5	0,0	0,0	0,0	0,5	0,0	0,5	0,5	0,0	0,0	0,0
Ballst - 29	33,3	27,3	0,0	60,7	5,7	0,0	5,7	0,3	0,0	0,3	0,0	0,0	0,0	0,0	0,0	0,0	0,0
Ballst - 30	37,7	16,7	0,0	54,3	26,7	0,0	26,7	0,3	0,0	0,3	1,7	0,0	1,7	0,0	0,0	0,0	0,0
Ballst - 31	36,7	13,3	0,0	50,0	27,7	0,0	27,7	0,0	0,0	0,0	0,3	0,0	0,3	0,0	0,0	0,0	0,0
Ballst - 32	37,7	14,0	0,0	51,7	28,0	0,0	28,0	0,0	0,0	0,0	0,7	0,0	0,7	0,0	0,0	0,0	0,0
Ballst - 1	39,0	2,3	0,0	41,3	32,7	0,0	32,7	0,0	0,0	0,0	6,7	0,0	6,7	0,0	0,0	0,0	0,0
Ballst - 2	52,3	1,3	0,0	53,7	26,3	0,0	26,3	0,0	0,0	0,0	1,0	0,0	1,0	0,0	0,0	0,0	0,0
Ballst - 3	47,3	6,3	0,0	53,7	26,3	0,0	26,3	0,0	0,0	0,0	16,0	0,0	16,0	0,0	0,0	0,0	0,0
Ballst - 4	36,0	14,7	0,0	50,7	21,0	0,0	21,0	0,0	0,0	0,0	0,0	0,0	0,0	0,3	0,0	0,0	0,0
Ballst - 5	36,7	28,0	0,0	64,7	7,7	0,0	7,7	0,0	0,0	0,0	0,0	0,0	0,0	1,0	0,0	0,0	0,0
Ballst - 6	55,3	10,0	0,0	65,3	20,0	0,0	20,0	0,3	0,0	0,3	0,0	0,0	0,0	0,7	0,0	0,0	0,0
Ballst - 7	29,7	20,3	0,0	50,0	27,0	0,0	27,0	0,3	0,0	0,3	1,3	0,0	1,3	0,0	0,0	0,0	0,0
Ballst - 8	25,7	5,0	0,0	30,7	20,3	0,0	20,3	0,0	0,0	0,0	0,7	0,0	0,7	0,0	26,3	0,0	0,0
Ballst - 9	24,3	7,3	0,0	31,7	23,7	0,0	23,7	0,3	0,0	0,3	1,7	0,0	1,7	0,0	7,0	0,0	0,0
Ballst - 10	37,0	6,7	0,0	43,7	21,7	0,0	21,7	0,7	0,0	0,7	5,0	0,0	5,0	3,3	0,0	0,0	0,0
Ballst - 11	29,0	9,7	0,0	38,7	11,0	0,3	11,3	0,3	0,0	0,3	0,0	0,0	0,0	0,0	19,7	0,0	0,0
Ballst - 12	48,0	5,3	0,0	53,3	21,7	0,0	21,7	0,0	0,0	0,0	3,0	0,0	3,0	7,0	0,0	2,0	0,0
Ballst - 13	40,7	9,7	0,0	50,3	19,7	0,0	19,7	0,0	0,0	0,0	9,0	0,0	9,0	13,0	0,0	0,0	0,0
Ballst - 14	35,3	6,0	0,0	41,3	15,0	0,3	15,3	0,0	1,3	1,3	0,7	0,0	0,7	9,0	0,7	0,0	0,0
Ballst - 15	40,3	13,3	0,3	54,0	20,3	0,0	20,3	1,7	0,0	1,7	4,7	0,0	4,7	1,0	0,0	0,0	0,0
Ballst - 16	33,0	13,0	0,0	46,0	23,0	0,0	23,0	1,0	0,0	1,0	2,0	0,0	2,0	0,0	0,7	0,0	0,0
Ballst - 17	31,0	11,3	0,0	42,3	16,7	0,7	17,3	0,0	0,0	0,0	2,0	0,0	2,0	3,3	1,7	0,0	0,0
Ballst - 18	56,7	6,0	0,0	62,7	16,0	0,0	16,0	0,7	0,0	0,7	1,3	0,0	1,3	4,0	0,0	5,0	0,0
Ballst - 19	56,7	3,7	0,0	60,3	15,3	0,0	15,3	0,0	0,0	0,0	0,3	0,0	0,3	5,0	0,0	8,7	0,0

Table A 7: Authigenic minerals and porosity in the Buntsandstein samples (point-counted).

thin section	illite				kaolinite	blocky cements							porosity			intergranular volume (IGV)
	cutanes	radial overgrowth	meshwork	illite (total)		quartz	feldspar	gypsum	anhydrite	carbonate	salt	blocky cements (total)	intragranular	intergranular	porosity (total)	
Fh13 - 4	3,0	0,0	8,7	11,7	0,0	1,3	0,0	0,0	0,0	0,0	0,0	1,3	0,3	12,3	12,7	13,7
Fh13 - 5	0,0	0,0	0,0	0,0	0,0	5,0	0,0	0,0	15,0	13,0	0,0	33,0	0,0	0,3	0,3	33,3
Fh13 - 7	2,0	1,7	0,7	4,3	0,0	0,0	0,0	3,0	0,0	1,3	0,0	4,3	2,0	5,0	7,0	9,3
Fh13 - 8	3,3	0,7	1,0	5,0	0,0	0,0	0,0	0,0	1,0	0,0	0,0	1,0	0,0	0,7	0,7	1,7
Fh13 - 11	1,7	0,0	0,0	1,7	0,0	7,3	0,0	0,0	0,0	1,7	16,7	25,7	0,7	1,0	1,7	26,7
Fh13 - 12	0,3	0,0	0,0	0,3	0,0	9,3	0,7	0,3	0,7	2,7	14,0	27,7	1,3	1,0	2,3	28,7
Fh13 - 13	0,3	0,0	0,0	0,3	0,0	7,7	0,0	17,3	0,0	0,0	0,0	25,0	0,0	7,7	7,7	32,7
Fh13 - 15	1,0	2,0	3,7	6,7	0,0	1,0	0,0	0,0	0,0	0,0	0,0	1,0	0,3	4,0	4,3	5,0
Fh13 - 21	8,0	1,0	8,0	17,0	0,0	0,0	0,0	0,0	1,7	2,0	0,0	3,7	0,0	6,0	6,0	9,7
Fh13 - 24	1,3	0,7	1,7	3,7	0,0	7,0	0,0	0,0	0,0	0,0	0,0	7,0	0,0	12,7	12,7	19,7
Fh13 - 27	2,3	0,0	4,0	6,3	0,0	0,3	0,0	0,0	0,0	0,0	0,0	0,3	0,3	10,0	10,3	10,3
Fh13 - 28	1,3	0,3	1,3	3,0	0,0	0,3	0,0	1,7	0,3	10,0	0,0	12,3	0,7	3,0	3,7	15,3
Fh13 - 30	6,7	0,0	9,7	16,4	0,0	0,7	0,0	0,0	0,3	4,3	0,0	5,3	0,7	1,3	2,0	6,7
Fh13 - 41	3,7	0,0	8,7	12,4	0,0	4,0	1,3	0,3	0,0	0,0	0,0	5,7	5,3	12,7	18,0	18,3
Fh13 - 42	2,7	0,0	7,0	9,7	0,0	1,3	1,0	0,0	0,0	0,0	0,0	2,3	0,7	3,3	4,0	5,7
Fh13 - 46	1,3	0,0	0,0	1,3	0,0	4,0	1,7	0,0	0,0	0,3	0,0	6,0	3,3	10,3	13,7	16,3
Fh13 - 47	7,3	0,0	5,7	13,0	0,0	0,3	0,0	0,0	0,0	0,0	0,0	0,3	0,3	1,3	1,7	1,7
Fh13 - 50	0,3	0,0	2,0	2,3	0,0	8,0	1,3	0,0	0,0	0,0	8,7	18,0	2,3	8,0	10,3	26,0
Fh13 - 51	1,0	0,0	3,0	4,0	0,0	6,3	2,0	0,0	0,0	0,0	0,3	8,7	2,3	15,0	17,3	23,7
Fh13 - 52	0,3	0,0	3,0	3,3	0,0	2,4	1,0	0,0	0,0	0,0	0,0	3,5	3,1	13,8	16,9	17,2
Fh13 - 88	0,0	0,0	0,7	0,7	0,0	0,0	0,0	0,0	0,0	0,0	2,7	2,7	0,7	5,0	5,7	7,7
Fh13 - 57	0,3	0,0	0,0	0,3	0,0	8,0	0,0	11,3	0,7	0,7	0,0	20,7	0,7	5,0	5,7	25,7
Fh13 - 59	1,3	9,0	3,7	14,0	0,0	4,7	0,3	0,0	0,0	0,0	0,0	5,0	0,7	4,7	5,3	9,7
Fh13 - 60	0,7	6,0	3,3	10,0	0,0	3,3	0,0	0,0	0,0	0,0	0,0	3,3	1,3	5,3	6,7	8,7
Fh13 - 64	7,3	4,7	6,7	18,7	0,0	0,3	0,0	0,0	0,0	0,0	0,0	0,3	2,3	2,0	4,3	2,3
Fh13 - 70	1,0	0,0	0,0	1,0	0,0	0,0	0,0	9,0	4,0	0,7	0,0	13,7	3,0	6,0	9,0	19,7
Fh13 - 78	0,0	0,0	0,7	0,7	0,0	6,9	0,7	0,3	0,3	0,0	4,5	12,7	1,7	5,2	6,9	17,9
Fh13 – 79	2,3	2,7	3,3	8,3	0,0	0,3	0,7	7,3	0,0	0,0	0,0	8,3	0,0	0,7	0,7	9,0
Fh13 - 82	2,7	0,3	1,0	4,0	0,0	0,0	0,0	0,7	0,0	1,0	0,0	1,7	0,0	0,0	0,0	1,7
Fh13 - 84	1,0	0,0	0,0	1,0	0,0	5,0	2,0	0,7	0,7	0,0	0,0	8,3	7,0	7,3	14,3	15,7
Fh13 - 85	1,0	1,3	0,0	2,3	0,0	2,7	3,0	9,7	0,0	2,0	0,0	17,3	2,3	8,0	10,3	25,3
Fh13 - 93	0,3	0,0	0,0	0,3	0,0	0,0	0,0	16,3	5,1	1,4	0,0	22,8	0,3	2,7	3,1	25,5
Fh13 - 96	0,3	0,0	0,0	0,3	0,0	6,7	2,7	7,3	0,7	0,3	0,0	17,7	3,7	8,7	12,3	26,3
Fh13 - 97	0,3	0,0	0,0	0,3	0,0	6,3	0,3	0,0	2,7	5,7	0,0	15,0	6,7	7,0	13,7	22,0
Fh13 - 110	1,0	0,0	0,3	1,3	0,0	0,3	0,7	1,7	6,3	12,3	0,0	21,3	4,0	16,0	20,0	37,3
Fh13 -134	1,7	0,0	0,0	1,7	0,0	1,0	1,7	0,0	0,0	1,0	0,0	3,7	0,0	12,3	12,3	16,0
Fh13 - 140	2,0	0,0	0,0	2,0	0,0	3,3	1,0	0,0	0,0	0,3	0,0	4,7	3,3	8,7	12,0	13,3
Fh13 - 158	2,7	0,0	0,0	2,7	0,0	0,0	0,0	0,0	0,0	0,0	0,0	0,0	0,0	0,0	0,0	0,0
Fh13 - 170	0,0	0,7	0,0	0,7	0,0	3,3	0,0	1,0	0,0	1,3	0,0	5,7	0,3	15,0	15,3	20,7
Fh13 - 171	4,3	1,0	0,0	5,3	0,0	0,0	0,0	2,0	0,0	11,7	0,0	13,7	0,3	5,7	6,0	19,3
Fh13 - 35	1,3	0,3	2,3	4,0	0,0	4,0	0,0	0,0	0,0	0,0	0,0	4,0	0,0	5,7	5,7	9,7
Gü1 - 2	8,3	0,0	0,0	8,3	0,0	5,3	0,0	0,0	0,0	0,7	0,0	6,0	0,0	6,0	6,0	12,0
Gü1 - 4	3,0	0,0	1,7	4,7	2,0	4,3	0,0	0,0	0,0	2,0	0,0	6,3	0,0	8,7	8,7	15,0
Gü1 - 6	2,0	0,0	0,0	2,0	1,3	4,0	0,0	0,0	0,3	5,0	0,0	9,3	0,3	12,7	13,0	22,0
Gü1 - 11	3,3	0,0	0,0	3,3	0,7	2,7	0,3	0,0	0,0	2,3	0,0	5,3	0,7	15,7	16,3	21,0
Gü1 - 13	5,3	0,0	0,0	5,3	0,0	13,7	0,0	0,0	0,0	0,3	0,0	14,0	1,3	15,3	16,7	29,3
Gü1 - 15	3,0	1,3	0,0	4,3	2,7	8,7	0,0	0,0	0,0	2,0	0,0	10,7	0,0	8,7	8,7	19,3
Gü1 - 16	2,3	0,0	0,0	2,3	1,0	4,7	0,0	4,7	0,0	3,3	0,0	12,7	0,7	5,7	6,3	18,3

thin section	illite				kaolinite	blocky cements							porosity			intergranular volume (IGV)
	cutanes	radial overgrowth	meshwork	illite (total)		quartz	feldspar	gypsum	anhydrite	carbonate	salt	blocky cements (total)	intragranular	intergranular	porosity (total)	
Gü1 - 18	0,0	0,0	0,0	0,0	1,7	0,7	0,0	0,0	25,0	0,0	0,0	25,7	0,0	2,3	2,3	28,0
Gü1 - 20	4,3	0,0	0,0	4,3	0,3	3,7	0,0	7,3	0,0	9,0	0,0	20,0	0,0	4,7	4,7	24,7
Gü1 - 22	1,3	0,0	0,0	1,3	0,0	6,3	0,0	0,0	0,0	15,0	1,7	23,0	0,0	2,7	2,7	25,7
Gü1 - 25	4,0	0,0	0,0	4,0	1,0	5,7	0,0	3,7	0,0	3,3	0,0	12,7	1,3	4,7	6,0	17,3
Gü1 - 26	-	-	-	-	-	-	-	-	-	-	-	-	-	-	-	-
Gü1 - 28	2,0	0,0	0,0	2,0	1,7	9,7	0,0	8,0	0,0	3,3	0,0	21,0	1,0	3,0	4,0	24,0
La35 - 2	13,0	2,0	1,7	16,7	0,0	0,0	0,0	0,0	0,7	0,3	0,0	1,0	0,0	5,0	5,0	6,0
La35 - 3	3,0	0,0	0,0	3,0	0,0	2,7	0,0	0,0	3,3	9,7	0,0	15,7	1,3	7,3	8,6	23,0
La35 - 4	2,3	0,0	0,0	2,3	0,0	12,0	0,0	0,0	3,3	10,3	0,0	25,7	1,0	5,7	6,7	31,3
La35 - 7	4,0	0,0	0,0	4,0	0,0	5,3	0,0	0,0	1,0	8,3	0,0	14,7	2,0	6,3	8,3	21,0
La35 - 10	6,7	0,0	0,0	6,7	0,0	6,3	0,0	0,0	0,0	1,3	0,0	7,7	0,0	6,0	6,0	13,7
La35 - 11	12,0	2,3	0,0	14,3	0,0	0,3	0,0	0,0	0,3	10,3	0,0	11,0	0,0	2,0	2,0	13,0
La35 - 12	5,7	0,0	0,0	5,7	0,0	5,7	0,0	0,0	0,0	4,7	0,0	10,3	2,3	7,0	9,3	17,3
La35 - 13	6,7	0,0	0,0	6,7	0,0	11,0	0,0	0,0	1,0	1,0	0,0	13,0	3,0	5,3	8,3	18,3
La35 - 15	10,3	0,0	0,0	10,3	0,0	14,3	0,0	0,0	0,3	2,7	0,0	17,3	0,0	6,3	6,3	23,7
La35 - 16	2,0	0,0	0,0	2,0	0,0	9,3	1,0	0,0	0,0	6,7	0,0	17,0	3,3	5,0	8,3	22,0
La35 - 19	8,7	4,7	0,0	13,3	0,0	1,3	0,0	0,0	0,3	4,0	0,0	5,7	1,0	5,3	6,3	11,0
La35 - 23	11,0	0,0	0,0	11,0	0,0	0,3	0,0	0,0	2,3	6,7	0,0	9,3	0,0	2,3	2,3	11,7
La35 - 29	0,7	0,3	1,3	2,3	0,0	18,0	0,3	0,0	2,3	2,7	0,0	23,3	1,7	4,0	5,7	27,3
La35 - 31	1,7	1,7	2,3	5,7	0,0	11,0	0,0	0,0	1,0	0,0	0,0	12,0	3,7	9,0	12,7	21,0
La35 - 34	11,0	3,0	2,7	16,7	0,0	2,0	0,0	0,0	0,7	1,3	0,0	4,0	0,0	6,0	6,0	10,0
RKS4 - 5	0,7	0,0	0,0	0,7	0,0	0,0	0,0	0,0	15,0	20,3	0,0	35,3	0,0	0,3	0,3	35,7
RKS4 - 7	0,7	0,0	0,0	0,7	0,0	0,7	0,0	0,7	26,3	0,7	0,0	28,3	0,0	0,0	0,0	28,3
RKS4 - 19	4,7	0,0	0,0	4,7	0,3	5,3	0,0	6,0	0,7	0,0	0,0	12,0	0,0	9,0	9,0	21,0
RKS4 - 23	1,3	1,0	1,0	3,7	1,3	4,3	0,7	0,0	0,0	0,0	0,0	5,0	0,0	17,7	17,7	22,7
RKS4 - 27	8,7	0,0	0,0	8,7	1,3	2,3	0,0	0,0	0,0	0,7	0,0	3,0	0,0	20,0	20,0	23,0
Te - 2	0,0	0,0	0,0	0,0	0,0	11,3	0,0	2,3	12,0	1,7	0,0	27,3	0,0	1,3	1,3	28,7
Te - 3	0,7	0,0	3,0	3,7	0,0	0,3	0,0	0,0	0,0	0,0	0,0	0,3	0,0	0,0	0,0	0,3
Te - 7	5,0	1,3	1,3	7,7	0,0	3,3	0,0	0,0	0,3	0,0	0,0	3,7	0,0	6,3	6,3	10,0
Te - 11	2,7	0,0	0,0	2,7	0,0	2,3	0,0	0,0	1,3	0,3	0,0	4,0	0,0	9,3	9,3	13,3
Te - 16	0,7	0,0	0,0	0,7	0,0	7,7	0,0	0,0	0,7	0,3	0,0	8,7	0,0	6,3	6,3	15,0
Te - 18	2,0	2,0	1,7	5,7	0,0	5,7	0,0	0,3	1,0	0,3	0,0	7,3	2,3	6,3	8,7	13,7
Te - 22	1,0	0,0	0,0	1,0	0,0	11,0	0,0	2,0	9,7	0,0	0,0	22,7	0,0	2,3	2,3	25,0
Te - 26	3,7	3,3	6,3	13,3	0,0	3,3	0,0	0,0	0,0	1,7	0,0	5,0	0,0	3,0	3,0	8,0
Te - 29	4,0	6,0	7,0	18,0	0,0	3,7	0,0	0,0	0,0	1,0	0,0	4,7	0,0	2,3	2,3	7,0
RKS2 - 1	0,7	1,7	0,7	3,0	1,7	3,3	0,0	4,3	0,0	0,0	0,0	7,7	1,3	7,3	8,7	15,0
RKS2 - 2	0,0	0,3	0,0	0,3	0,0	5,3	0,0	8,7	0,0	0,0	0,0	14,0	0,3	7,3	7,7	21,3
RKS2 - 3	1,3	0,0	0,0	1,3	0,0	1,0	0,0	26,0	0,0	0,0	0,0	27,0	0,0	1,7	1,7	28,7
RKS2 - 4	1,7	0,0	0,7	2,3	1,3	0,7	0,0	0,7	0,0	0,0	0,0	1,3	2,0	8,3	10,3	9,7
RKS2 - 5	0,3	0,0	0,0	0,3	0,0	0,0	0,0	6,7	0,0	0,0	0,0	6,7	0,3	2,3	2,7	9,0
RKS2 - 6	0,0	0,0	0,0	0,0	0,0	5,7	0,7	3,0	0,0	0,3	0,0	9,7	2,0	11,3	13,3	21,0
RKS2 - 7	2,3	0,0	0,7	3,0	0,7	0,7	0,0	0,0	0,0	0,0	0,0	0,7	3,0	13,3	16,3	14,0
RKS2 - 8	0,3	0,0	0,0	0,3	0,0	0,7	0,0	15,0	0,3	0,0	0,0	16,0	0,7	1,3	2,0	17,3
RKS2 - 9	0,7	0,0	0,0	0,7	0,0	5,7	0,0	0,3	0,0	2,0	5,3	13,3	0,7	3,3	4,0	16,7
RKS2 - 10	0,3	0,0	0,0	0,3	0,0	0,0	0,0	0,0	0,0	0,3	0,0	0,3	1,7	7,0	8,7	7,3
RKS2 - 11	1,0	0,0	0,0	1,0	0,0	0,0	0,0	0,3	0,0	0,0	0,0	0,3	1,7	9,0	10,7	9,3
RKS2 - 12	1,0	0,7	0,0	1,7	0,0	0,3	0,0	0,0	0,0	0,0	0,0	0,3	3,7	6,7	10,3	7,0
RKS2 - 13	1,0	0,0	0,0	1,0	0,0	1,0	0,3	0,0	0,0	2,7	0,0	4,0	0,7	11,7	12,3	15,7
RKS2 - 14	2,0	0,7	0,0	2,7	0,0	0,0	0,0	8,7	0,0	0,0	0,0	8,7	0,3	12,3	12,7	21,0
RKS2 - 15	0,0	0,0	0,0	0,0	0,0	3,7	0,3	0,0	0,3	2,7	0,0	7,0	4,3	4,7	9,0	11,7

thin section	illite				kaolinite	blocky cements							porosity			intergranular volume (IGV)
	cutanes	radial overgrowth	meshwork	illite (total)		quartz	feldspar	gypsum	anhydrite	carbonate	salt	blocky cements (total)	intragranular	intergranular	porosity (total)	
RKS2 - 16	0,3	0,0	0,0	0,3	0,0	2,7	0,0	0,0	0,3	2,7	0,0	5,7	2,0	6,3	8,3	12,0
RKS2 - 17	0,3	0,0	0,3	0,7	0,0	2,7	1,0	0,0	1,0	6,3	0,0	11,0	4,7	6,7	11,3	17,7
RKS2 - 18	0,3	0,0	0,0	0,3	0,0	2,7	0,0	0,0	0,3	6,0	0,0	9,0	0,7	9,7	10,3	18,7
RKS2 - 19	0,0	0,0	0,0	0,0	0,7	1,3	0,0	0,0	0,3	0,0	0,0	1,7	2,0	8,3	10,3	10,0
RKS2 - 20	0,0	0,0	0,0	0,0	0,0	0,7	0,0	0,0	0,3	1,3	0,0	2,3	1,7	7,0	8,7	9,3
RKS2 - 21	0,0	0,0	0,0	0,0	0,0	3,3	0,0	0,0	2,7	4,7	0,0	10,7	2,0	5,3	7,3	16,0
RKS2 - 22	0,7	0,0	0,0	0,7	0,0	3,3	0,0	0,3	4,0	2,0	0,0	9,7	3,0	4,7	7,7	14,3
RKS2 - 23	0,0	0,0	0,0	0,0	0,3	3,7	0,0	0,0	23,7	8,0	0,0	35,3	0,3	0,0	0,3	35,3
RKS2 - 24	0,7	0,3	0,0	1,0	0,7	0,0	0,0	0,0	0,3	0,3	0,0	0,7	0,7	10,3	11,0	11,0
RKS2 - 25	9,0	0,0	0,0	9,0	0,3	1,0	0,0	0,0	5,0	11,3	0,0	17,3	1,0	6,0	7,0	23,3
RKS2 - 26	2,0	0,0	0,0	2,0	0,0	1,0	0,0	0,0	0,0	9,0	1,3	11,3	0,3	14,0	14,3	25,3
RKS2 - 27	1,0	1,3	0,3	2,7	0,0	4,3	0,0	0,0	0,3	0,0	0,0	4,7	0,0	12,0	12,0	16,7
RKS2 - 31	3,0	0,0	4,7	7,7	0,0	0,0	0,0	0,7	15,0	1,3	0,0	17,0	0,0	1,7	1,7	18,7
RKS2 - 32	0,7	0,0	0,0	0,7	0,0	11,3	0,0	6,3	0,0	0,0	0,0	17,7	0,0	8,3	8,3	26,0
RKS2 - 33	0,3	0,0	1,0	1,3	0,0	0,3	0,0	10,7	0,0	9,7	0,0	20,7	0,0	2,0	2,0	22,7
RKS2 - 34	2,7	0,0	0,0	2,7	1,0	0,0	0,0	2,0	0,0	0,0	0,0	2,0	0,3	15,0	15,3	17,0
RKS2 - 35	0,3	0,0	0,0	0,3	0,0	1,7	0,0	11,7	0,0	5,3	0,0	18,7	0,0	9,3	9,3	28,0
RKS2 - 36	0,7	0,0	0,0	0,7	0,0	3,3	1,0	0,0	0,0	0,0	0,0	4,3	2,0	18,7	20,7	23,0
RKS2 - 37	2,0	0,0	0,0	2,0	0,0	4,0	0,0	0,0	0,0	0,0	0,0	4,0	0,7	20,0	20,7	24,0
Ballst - 22	0,3	0,7	0,0	1,0	0,0	8,7	0,7	4,0	0,0	0,7	0,0	14,0	0,0	12,0	12,0	26,0
Ballst - 23	1,0	1,3	0,0	2,3	0,0	7,7	0,3	2,3	0,0	1,3	1,0	12,7	0,3	10,0	10,3	22,7
Ballst - 24	1,7	1,3	0,0	3,0	0,0	11,0	0,0	0,0	0,0	0,7	0,3	12,0	0,0	9,3	9,3	21,3
Ballst - 25	0,3	0,3	0,0	0,7	0,0	6,7	0,3	1,7	0,0	0,0	0,0	8,7	0,3	8,3	8,7	17,0
Ballst - 26	5,3	1,7	0,0	7,0	0,0	0,7	0,0	1,3	0,0	0,0	0,0	2,0	0,0	10,0	10,0	12,0
Ballst - 27	4,0	0,0	0,0	4,0	0,0	0,3	0,0	0,0	0,0	0,3	0,0	0,7	0,0	5,7	5,7	6,3
Ballst - 28	0,5	0,0	0,0	0,5	0,0	4,5	1,0	8,0	0,0	3,0	0,0	16,5	1,0	10,5	11,5	27,0
Ballst - 29	0,0	0,0	0,0	0,0	0,0	7,0	0,0	0,3	3,7	17,3	0,0	28,3	0,0	5,0	5,0	33,3
Ballst - 30	0,7	0,0	0,0	0,7	0,0	1,3	1,0	0,3	0,3	0,7	0,0	3,7	1,3	11,3	12,7	15,0
Ballst - 31	0,0	0,0	0,0	0,0	0,0	4,3	0,3	0,0	4,3	0,7	0,0	9,7	0,7	11,7	12,3	21,3
Ballst - 32	0,0	0,0	0,0	0,0	0,0	3,7	0,0	0,0	5,7	1,7	0,0	11,0	0,7	8,0	8,7	19,0
Ballst - 1	0,3	0,0	0,0	0,3	0,0	0,7	0,7	0,0	0,0	0,7	0,0	2,0	3,3	13,7	17,0	15,7
Ballst - 2	1,0	0,0	0,0	1,0	0,0	4,0	0,0	0,0	0,0	0,0	0,0	4,0	1,7	12,3	14,0	16,3
Ballst - 3	0,0	1,0	0,0	1,0	0,0	0,0	0,0	0,0	0,0	0,0	0,0	0,0	0,0	3,0	3,0	3,0
Ballst - 4	0,0	0,0	0,0	0,0	0,0	9,0	0,0	0,0	0,7	7,7	0,0	17,3	0,0	10,7	10,7	28,0
Ballst - 5	2,3	0,0	0,0	2,3	0,0	0,0	0,0	0,0	0,3	24,0	0,0	24,3	0,0	0,0	0,0	24,3
Ballst - 6	6,7	0,0	0,3	7,0	0,0	0,0	0,0	0,0	0,0	0,0	0,0	0,0	0,0	6,7	6,7	6,7
Ballst - 7	0,7	0,0	1,7	2,3	0,0	7,0	0,7	0,0	0,0	0,0	0,0	7,7	0,7	10,7	11,3	18,3
Ballst - 8	0,0	0,0	0,0	0,0	0,0	6,7	1,0	0,0	1,0	13,0	0,0	21,7	0,0	0,3	0,3	22,0
Ballst - 9	0,7	0,0	0,0	0,7	0,0	20,3	0,7	0,0	0,7	10,7	0,0	32,3	0,0	2,7	2,7	35,0
Ballst - 10	0,7	0,0	0,7	1,3	0,0	2,0	0,3	0,3	0,0	2,3	0,0	5,0	1,0	18,3	19,3	23,3
Ballst - 11	0,3	0,0	0,0	0,3	0,0	4,0	0,0	0,3	1,7	23,3	0,0	29,3	0,3	0,0	0,3	29,3
Ballst - 12	0,7	0,3	0,0	1,0	0,0	2,7	0,7	0,0	0,0	0,3	0,0	3,7	0,3	8,0	8,3	11,7
Ballst - 13	0,7	0,3	0,0	1,0	0,0	1,3	0,3	0,0	0,0	0,0	0,0	1,7	0,3	5,0	5,3	6,7
Ballst - 14	0,7	0,0	0,0	0,7	0,0	2,3	0,3	0,0	0,0	25,7	0,0	28,3	0,0	2,7	2,7	31,0
Ballst - 15	0,0	0,0	0,0	0,0	0,0	16,7	0,0	0,0	1,0	0,0	0,0	17,7	0,0	0,7	0,7	18,3
Ballst - 16	0,3	0,7	0,3	1,3	0,0	7,3	0,0	3,0	3,7	5,0	0,0	19,0	1,3	5,7	7,0	24,7
Ballst - 17	0,7	0,0	0,0	0,7	0,0	1,7	0,0	0,0	0,0	29,7	0,0	31,3	0,3	1,0	1,3	32,3
Ballst - 18	0,0	0,0	0,0	0,0	0,0	4,0	0,0	0,0	0,0	0,7	0,0	4,7	1,0	4,7	5,7	9,3
Ballst - 19	1,7	0,0	0,0	1,7	0,0	2,3	0,0	0,0	0,3	1,7	0,0	4,3	0,3	4,0	4,3	8,3

Table A 8: Normalized quartz, feldspar and lithic fragments content accordingly to McBride (1963) and compaction calculation accordingly to Lundegard (1992) for the Buntsandstein samples.

thin section	normalized QFL content accordingly to McBride (1963)			compaction calculation accordingly to Lundegard (1992)						
	quartz	feldspar	lithic fragments	P_i	intergranular porosity	blocky cements	intergranular volume	copl	cepl	icompact
Fh13 - 4	74,0	25,5	0,5	40,0	12,3	1,3	13,7	30,5	0,9	1,0
Fh13 - 5	81,3	14,6	4,0	40,0	0,3	33,0	33,3	10,0	29,7	0,3
Fh13 - 7	79,6	18,8	1,6	40,0	5,0	4,3	9,3	33,8	2,9	0,9
Fh13 - 8	79,8	19,1	1,2	40,0	0,7	1,0	1,7	39,0	0,6	1,0
Fh13 - 11	91,0	7,5	1,4	40,0	1,0	25,7	26,7	18,2	21,0	0,5
Fh13 - 12	80,3	19,1	0,6	40,0	1,0	27,7	28,7	15,9	23,3	0,4
Fh13 - 13	91,0	9,0	0,0	40,0	7,7	25,0	32,7	10,9	22,3	0,3
Fh13 - 15	79,3	20,7	0,0	40,0	4,0	1,0	5,0	36,8	0,6	1,0
Fh13 - 21	76,4	23,6	0,0	40,0	6,0	3,7	9,7	33,6	2,4	0,9
Fh13 - 24	79,1	17,3	3,6	40,0	12,7	7,0	19,7	25,3	5,2	0,8
Fh13 - 27	84,1	14,5	1,3	40,0	10,0	0,3	10,3	33,1	0,2	1,0
Fh13 - 28	88,0	11,6	0,4	40,0	3,0	12,3	15,3	29,2	8,7	0,8
FH13 - 30	73,4	26,0	0,5	40,0	1,3	5,3	6,7	35,7	3,4	0,9
Fh13 - 41	62,7	36,8	0,5	40,0	12,7	5,7	18,3	26,5	4,2	0,9
Fh13 - 42	68,2	28,2	3,6	40,0	3,3	2,3	5,7	36,4	1,5	1,0
FH13 - 46	64,8	32,1	3,1	40,0	10,3	6,0	16,3	28,3	4,3	0,9
Fh13 - 47	70,0	26,6	3,4	40,0	1,3	0,3	1,7	39,0	0,2	1,0
Fh13 - 50	65,1	33,1	1,8	40,0	8,0	18,0	26,0	18,9	14,6	0,6
Fh13 - 51	56,2	42,8	1,0	40,0	15,0	8,7	23,7	21,4	6,8	0,8
Fh13 - 52	75,9	22,6	1,5	40,0	13,8	3,5	17,2	27,5	2,5	0,9
Fh13 - 88	89,8	7,8	2,5	40,0	5,0	2,7	7,7	35,0	1,8	1,0
Fh13 - 57	84,1	12,1	3,9	40,0	5,0	20,7	25,7	19,3	16,7	0,5
Fh13 - 59	67,8	31,7	0,5	40,0	4,7	5,0	9,7	33,6	3,3	0,9
Fh13 - 60	73,7	24,9	1,4	40,0	5,3	3,3	8,7	34,3	2,2	0,9
Fh13 - 64	69,7	25,1	5,1	40,0	2,0	0,3	2,3	38,6	0,2	1,0
Fh13 - 70	74,5	25,0	0,5	40,0	6,0	13,7	19,7	25,3	10,2	0,7
Fh13 - 78	75,5	23,0	1,5	40,0	5,2	12,7	17,9	26,9	9,3	0,7
Fh13 – 79	64,9	31,8	3,3	40,0	0,7	8,3	9,0	34,1	5,5	0,9
Fh13 - 82	72,1	27,9	0,0	40,0	0,0	1,7	1,7	39,0	1,0	1,0
Fh13 - 84	61,4	34,2	4,3	40,0	7,3	8,3	15,7	28,9	5,9	0,8
Fh13 - 85	63,2	34,8	2,0	40,0	8,0	17,3	25,3	19,6	13,9	0,6
Fh13 - 93	70,7	26,6	2,7	40,0	2,7	22,8	25,5	19,4	18,4	0,5
Fh13 - 96	61,3	35,7	3,0	40,0	8,7	17,7	26,3	18,5	14,4	0,6
Fh13 - 97	64,6	32,5	2,9	40,0	7,0	15,0	22,0	23,1	11,5	0,7
Fh13 - 110	59,6	39,8	0,6	40,0	16,0	21,3	37,3	4,3	20,4	0,2
Fh13 -134	62,7	33,2	4,1	40,0	12,3	3,7	16,0	28,6	2,6	0,9
Fh13 - 140	60,6	39,0	0,5	40,0	8,7	4,7	13,3	30,8	3,2	0,9
Fh13 - 158	69,4	24,5	6,1	40,0	0,0	0,0	0,0	40,0	0,0	1,0
Fh13 - 170	77,4	21,2	1,4	40,0	15,0	5,7	20,7	24,4	4,3	0,9
Fh13 - 171	72,6	25,0	2,4	40,0	5,7	13,7	19,3	25,6	10,2	0,7
Fh13 - 35	72,1	27,5	0,4	40,0	5,7	4,0	9,7	33,6	2,7	0,9
Gü1 - 2	75,2	14,2	10,6	40,0	6,0	6,0	12,0	31,8	4,1	0,9
Gü1 - 4	73,1	18,8	8,1	40,0	8,7	6,3	15,0	29,4	4,5	0,9
Gü1 - 6	75,2	14,8	10,0	40,0	12,7	9,3	22,0	23,1	7,2	0,8
Gü1 - 11	80,3	19,3	0,4	40,0	15,7	5,3	21,0	24,0	4,1	0,9
Gü1 - 13	78,0	19,4	2,6	40,0	15,3	14,0	29,3	15,1	11,9	0,6
Gü1 - 15	74,7	24,0	1,4	40,0	8,7	10,7	19,3	25,6	7,9	0,8

thin section	normalized QFL content accordingly to McBride (1963)			compaction calculation accordingly to Lundegard (1992)						
	quartz	feldspar	lithic fragments	P_i	intergranular porosity	blocky cements	intergranular volume	copl	cepl	icompact
Gü1 - 16	75,2	20,9	3,9	40,0	5,7	12,7	18,3	26,5	9,3	0,7
Gü1 - 18	93,3	6,7	0,0	40,0	2,3	25,7	28,0	16,7	21,4	0,4
Gü1 - 20	69,4	26,7	3,9	40,0	4,7	20,0	24,7	20,4	15,9	0,6
Gü1 - 22	84,5	14,2	1,4	40,0	2,7	23,0	25,7	19,3	18,6	0,5
Gü1 - 25	73,4	23,0	3,6	40,0	4,7	12,7	17,3	27,4	9,2	0,7
Gü1 - 26	-	-	-	-	-	-	-	-	-	-
Gü1 - 28	80,8	18,7	0,5	40,0	3,0	21,0	24,0	21,0	16,6	0,6
La35 - 2	82,9	15,7	1,4	40,0	5,0	1,0	6,0	36,2	0,6	1,0
La35 - 3	86,3	11,8	1,9	40,0	7,3	15,7	23,0	22,1	12,2	0,6
La35 - 4	82,0	15,5	2,6	40,0	5,7	25,7	31,3	12,6	22,4	0,4
La35 - 7	72,1	26,9	0,9	40,0	6,3	14,7	21,0	24,0	11,1	0,7
La35 - 10	76,5	19,7	3,8	40,0	6,0	7,7	13,7	30,5	5,3	0,9
La35 - 11	90,9	9,1	0,0	40,0	2,0	11,0	13,0	31,0	7,6	0,8
La35 - 12	72,2	26,0	1,8	40,0	7,0	10,3	17,3	27,4	7,5	0,8
La35 - 13	70,3	24,3	5,4	40,0	5,3	13,0	18,3	26,5	9,6	0,7
La35 - 15	67,0	24,9	8,1	40,0	6,3	17,3	23,7	21,4	13,6	0,6
La35 - 16	83,9	14,7	1,4	40,0	5,0	17,0	22,0	23,1	13,1	0,6
La35 - 19	70,9	23,8	5,3	40,0	5,3	5,7	11,0	32,6	3,8	0,9
La35 - 23	68,1	23,8	8,1	40,0	2,3	9,3	11,7	32,1	6,3	0,8
La35 - 29	73,0	24,0	3,0	40,0	4,0	23,3	27,3	17,4	19,3	0,5
La35 - 31	76,4	23,1	0,5	40,0	9,0	12,0	21,0	24,0	9,1	0,7
La35 - 34	69,4	27,6	3,1	40,0	6,0	4,0	10,0	33,3	2,7	0,9
RKS4 - 5	98,4	1,6	0,0	40,0	0,3	35,3	35,7	6,7	33,0	0,2
RKS4 - 7	98,6	1,4	0,0	40,0	0,0	28,3	28,3	16,3	23,7	0,4
RKS4 - 19	79,4	19,1	1,4	40,0	9,0	12,0	21,0	24,0	9,1	0,7
RKS4 - 23	80,7	17,1	2,1	40,0	17,7	5,0	22,7	22,4	3,9	0,9
RKS4 - 27	84,2	14,7	1,1	40,0	20,0	3,0	23,0	22,1	2,3	0,9
Te - 2	92,5	7,5	0,0	40,0	1,3	27,3	28,7	15,9	23,0	0,4
Te - 3	87,4	12,6	0,0	40,0	0,0	0,3	0,3	39,8	0,2	1,0
Te - 7	87,8	12,2	0,0	40,0	6,3	3,7	10,0	33,3	2,4	0,9
Te - 11	85,3	13,7	1,0	40,0	9,3	4,0	13,3	30,8	2,8	0,9
Te - 16	75,8	15,7	8,4	40,0	6,3	8,7	15,0	29,4	6,1	0,8
Te - 18	85,3	12,7	2,0	40,0	6,3	7,3	13,7	30,5	5,1	0,9
Te - 22	92,0	5,2	2,8	40,0	2,3	22,7	25,0	20,0	18,1	0,5
Te - 26	80,1	15,7	4,2	40,0	3,0	5,0	8,0	34,8	3,3	0,9
Te - 29	81,4	18,2	0,5	40,0	2,3	4,7	7,0	35,5	3,0	0,9
RKS2 - 1	62,5	36,6	0,9	40,0	7,3	7,7	15,0	29,4	5,4	0,8
RKS2 - 2	77,6	22,4	0,0	40,0	7,3	14,0	21,3	23,7	10,7	0,7
RKS2 - 3	98,6	1,4	0,0	40,0	1,7	27,0	28,7	15,9	22,7	0,4
RKS2 - 4	60,2	38,6	1,2	40,0	8,3	1,3	9,7	33,6	0,9	1,0
RKS2 - 5	71,0	27,4	1,7	40,0	2,3	6,7	9,0	34,1	4,4	0,9
RKS2 - 6	59,8	39,7	0,5	40,0	11,3	9,7	21,0	24,1	7,3	0,8
RKS2 - 7	76,9	21,8	1,3	40,0	13,3	0,7	14,0	30,2	0,5	1,0
RKS2 - 8	83,9	13,4	2,7	40,0	1,3	16,0	17,3	27,4	11,6	0,7
RKS2 - 9	71,3	24,2	4,6	40,0	3,3	13,3	16,7	28,0	9,6	0,7
RKS2 - 10	71,2	28,8	0,0	40,0	7,0	0,3	7,3	35,3	0,2	1,0
RKS2 - 11	75,3	22,9	1,8	40,0	9,0	0,3	9,3	33,8	0,2	1,0
RKS2 - 12	73,4	23,0	3,7	40,0	6,7	0,3	7,0	35,5	0,2	1,0
RKS2 - 13	63,0	35,0	2,0	40,0	11,7	4,0	15,7	28,9	2,8	0,9
RKS2 - 14	89,0	11,0	0,0	40,0	12,3	8,7	21,0	24,1	6,6	0,8

thin section	normalized QFL content accordingly to McBride (1963)			compaction calculation accordingly to Lundegard (1992)						
	quartz	feldspar	lithic fragments	P_i	intergranular porosity	blocky cements	intergranular volume	copl	cepl	icompact
RKS2 - 15	56,0	43,7	0,4	40,0	4,7	7,0	11,7	32,1	4,8	0,9
RKS2 - 16	62,5	36,7	0,8	40,0	6,3	5,7	12,0	31,8	3,9	0,9
RKS2 - 17	52,4	44,4	3,1	40,0	6,7	11,0	17,7	27,1	8,0	0,8
RKS2 - 18	63,0	36,6	0,4	40,0	9,7	9,0	18,7	26,2	6,6	0,8
RKS2 - 19	54,4	42,8	2,8	40,0	8,3	1,7	10,0	33,3	1,1	1,0
RKS2 - 20	54,4	44,4	1,2	40,0	7,0	2,3	9,3	33,8	1,5	1,0
RKS2 - 21	50,9	47,0	2,2	40,0	5,3	10,7	16,0	28,6	7,6	0,8
RKS2 - 22	58,1	41,4	0,5	40,0	4,7	9,7	14,3	30,0	6,8	0,8
RKS2 - 23	65,9	33,0	1,1	40,0	0,0	35,3	35,3	7,2	32,8	0,2
RKS2 - 24	75,9	24,1	0,0	40,0	10,3	0,7	11,0	32,6	0,4	1,0
RKS2 - 25	75,4	24,6	0,0	40,0	6,0	17,3	23,3	21,7	13,6	0,6
RKS2 - 26	75,2	24,8	0,0	40,0	14,0	11,3	25,3	19,6	9,1	0,7
RKS2 - 27	71,3	28,7	0,0	40,0	12,0	4,7	16,7	28,0	3,4	0,9
RKS2 - 31	88,2	11,8	0,0	40,0	1,7	17,0	18,7	26,2	12,5	0,7
RKS2 - 32	76,3	23,7	0,0	40,0	8,3	17,7	26,0	18,9	14,3	0,6
RKS2 - 33	92,1	7,5	0,4	40,0	2,0	20,7	22,7	22,4	16,0	0,6
RKS2 - 34	78,1	21,5	0,4	40,0	15,0	2,0	17,0	27,7	1,4	1,0
RKS2 - 35	82,2	14,5	3,3	40,0	9,3	18,7	28,0	16,7	15,6	0,5
RKS2 - 36	76,9	18,4	4,7	40,0	18,7	4,3	23,0	22,1	3,4	0,9
RKS2 - 37	77,5	18,3	4,2	40,0	20,0	4,0	24,0	21,1	3,2	0,9
Ballst - 22	75,7	24,3	0,0	40,0	12,0	14,0	26,0	18,9	11,4	0,6
Ballst - 23	60,4	39,0	0,5	40,0	10,0	12,7	22,7	22,4	9,8	0,7
Ballst - 24	80,4	18,8	0,9	40,0	9,3	12,0	21,3	23,7	9,2	0,7
Ballst - 25	75,2	24,8	0,0	40,0	8,3	8,7	17,0	27,7	6,3	0,8
Ballst - 26	77,7	22,3	0,0	40,0	10,0	2,0	12,0	31,8	1,4	1,0
Ballst - 27	74,8	24,0	1,2	40,0	5,7	0,7	6,3	35,9	0,4	1,0
Ballst - 28	79,4	20,6	0,0	40,0	10,5	16,5	27,0	17,8	13,6	0,6
Ballst - 29	91,0	8,5	0,5	40,0	5,0	28,3	33,3	10,0	25,5	0,3
Ballst - 30	66,8	32,8	0,4	40,0	11,3	3,7	15,0	29,4	2,6	0,9
Ballst - 31	64,4	35,6	0,0	40,0	11,7	9,7	21,3	23,7	7,4	0,8
Ballst - 32	64,9	35,1	0,0	40,0	8,0	11,0	19,0	25,9	8,1	0,8
Ballst - 1	55,9	44,1	0,0	40,0	13,7	2,0	15,7	28,9	1,4	1,0
Ballst - 2	67,1	32,9	0,0	40,0	12,3	4,0	16,3	28,3	2,9	0,9
Ballst - 3	67,1	32,9	0,0	40,0	3,0	0,0	3,0	38,1	0,0	1,0
Ballst - 4	70,7	29,3	0,0	40,0	10,7	17,3	28,0	16,7	14,4	0,5
Ballst - 5	89,4	10,6	0,0	40,0	0,0	24,3	24,3	20,7	19,3	0,5
Ballst - 6	76,3	23,3	0,4	40,0	6,7	0,0	6,7	35,7	0,0	1,0
Ballst - 7	64,7	34,9	0,4	40,0	10,7	7,7	18,3	26,5	5,6	0,8
Ballst - 8	60,1	39,9	0,0	40,0	0,3	21,7	22,0	23,1	16,7	0,6
Ballst - 9	56,9	42,5	0,6	40,0	2,7	32,3	35,0	7,7	29,8	0,2
Ballst - 10	66,2	32,8	1,0	40,0	18,3	5,0	23,3	21,7	3,9	0,8
Ballst - 11	76,8	22,5	0,7	40,0	0,0	29,3	29,3	15,1	24,9	0,4
Ballst - 12	71,1	28,9	0,0	40,0	8,0	3,7	11,7	32,1	2,5	0,9
Ballst - 13	71,9	28,1	0,0	40,0	5,0	1,7	6,7	35,7	1,1	1,0
Ballst - 14	71,3	26,4	2,3	40,0	2,7	28,3	31,0	13,0	24,6	0,3
Ballst - 15	71,1	26,8	2,2	40,0	0,7	17,7	18,3	26,5	13,0	0,7
Ballst - 16	65,7	32,9	1,4	40,0	5,7	19,0	24,7	20,4	15,1	0,6
Ballst - 17	70,9	29,1	0,0	40,0	1,0	31,3	32,3	11,3	27,8	0,3
Ballst - 18	79,0	20,2	0,8	40,0	4,7	4,7	9,3	33,8	3,1	0,9
Ballst - 19	79,7	20,3	0,0	40,0	4,0	4,3	8,3	34,5	2,8	0,9

Table A 9: Locations and formations of the studied Buntsandstein outcrops.

Outcrop	Formation	Easting	Northing
Rabenschüssel	smS	4472592	5636913
Vollenborn	smV	4395280	5693785
Walpernhain	smV	4496109	5652972
Hartschwinden	smV	4369584	5623857
Werraufer	suC	4373585	5633467
Hachelbich	smS	4428145	5690376
Dermbach-Unteralba	smV	4368030	5624058
Nebra	smH	4470376	5683003
Großwangen	su/smV	4467807	5681503
Die rote Wand / Vacha	smV	4360524	5635037
Am Winterkopf/Militär	smV	4426149	5695677
Hühnerkoppe	smV	4426291	5695794
Mäuserschacht	smV-smD	4427544	5691651
Ortsausg. Sondershausen	smV	4422503	5693611
Witzenhausen	smS	4353328	5692165
Burg Ludwigstein	smS	4354741	5688937
Brehme	smS	4386643	5708227
Burg Hanstein	smS	4356580	5691362
Am Knorrenkopf	smV	4375841	5702407

10. II.4. Microprobe

Table A 10: Backscattered electron image and chemical composition (measured by wavelength-dispersive X-ray spectroscopy) of carbonate cement (Sample Ag-14, Volpriehausen Formation, sandflat facies).

point of measurement	CO_2 (mass%)	MgO (mass%)	CaO (mass%)	SO_3 (mass%)	BaO (mass%)	SrO (mass%)	FeO (mass%)	MnO (mass%)	total (mass%)
1	43,82	20,32	30,02	0,00	0,01	0,00	0,18	0,57	94,93
2	44,57	20,42	30,68	0,00	0,00	0,00	0,51	0,24	96,43
3	45,08	20,28	30,18	0,03	0,00	0,00	0,09	0,78	96,45
4	42,91	18,95	29,63	0,00	0,00	0,00	2,39	0,44	94,32
5	42,08	16,20	29,24	0,00	0,02	0,00	6,53	0,91	94,98
6	39,86	15,67	29,60	0,06	0,00	0,00	7,08	0,98	93,25
7	43,97	17,57	29,82	0,00	0,00	0,00	3,70	0,80	95,86
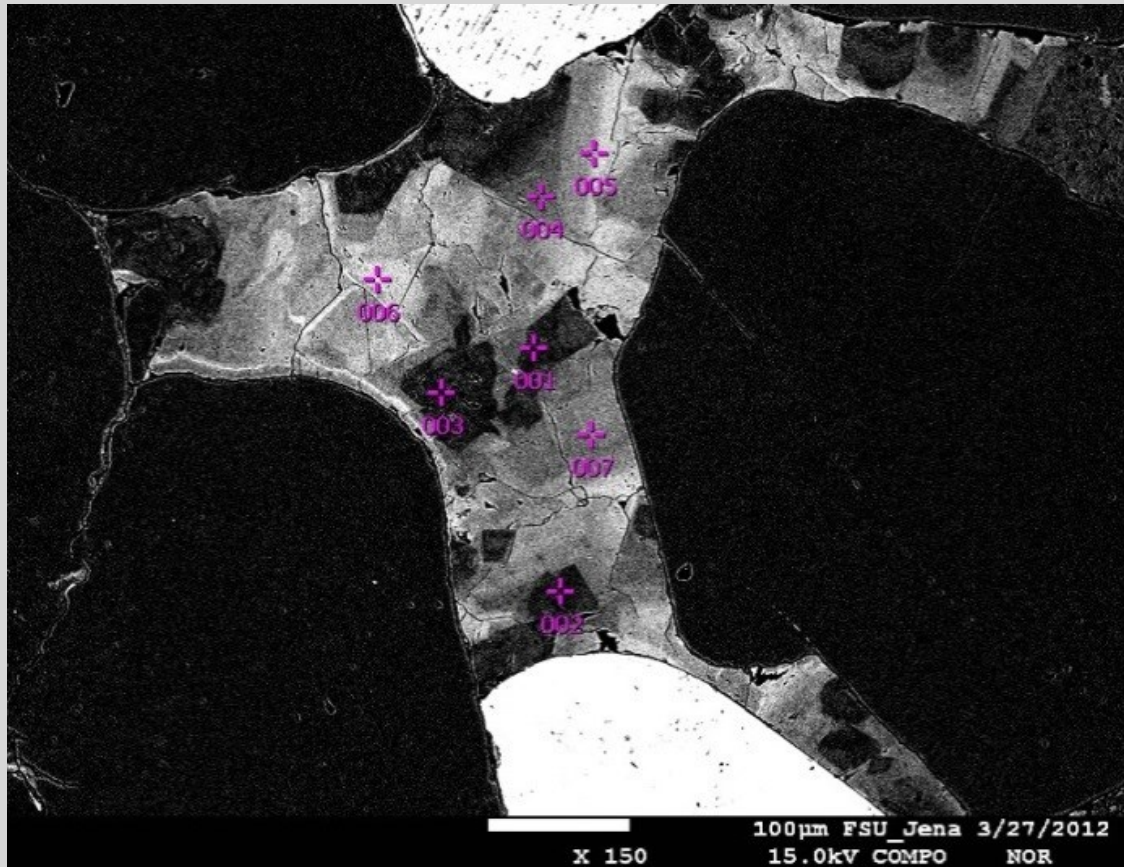
10. II.5. Pore space analysis

Table A 11: Pore space analysis for the Buntsandstein samples. [A]

thin section	borehole	depth [m]	facies	pore amount	pore area [μm²]	porosity (image analysis) [%]	pore density [pores/mm²]	micro-porosity	pore perimeter [μm]	pore perimeter [1/mm]
Fh13 - 5	Fh13-63	410,2	sandflat	87	144310	0,3	1,7	4,5	16525	0,3
Fh13 - 7	Fh13-63	410,9	sandflat	1401	3032633	5,8	26,7	7,2	344857	0,5
Fh13 - 11	Fh13-63	417,4	eolian	554	1324999	2,5	10,5	2,2	141802	2,7
Fh13 - 12	Fh13-63	419,2	sandflat	87	1228596	2,3	1,7	2,6	37197	0,7
Fh13 - 13	Fh13-63	425,0	eolian	995	4295168	8,2	18,9	0,0	391836	7,5
Fh13 - 15	Fh13-63	425,9	sandflat	1530	3180531	6,1	29,1	5,0	443216	8,4
Fh13 - 21	Fh13-63	440,7	sandflat	3008	2871459	5,5	57,2	10,5	511590	9,7
Fh13 - 24	Fh13-63	442,6	sandflat	1995	6023957	11,5	38,0	7,5	718241	13,7
Fh13 - 27	Fh13-63	445,9	sandflat	2308	2259062	4,3	43,9	10,7	441190	8,4
Fh13 - 30	Fh13-63	449,7	sandflat	2522	2902641	5,5	48,0	8,5	509106	9,7
Fh13 - 41	Fh13-63	467,0	sandflat	2660	4716565	9,0	50,6	8,5	712837	13,6
Fh13 - 42	Fh13-63	467,2	sandflat	2014	2999036	5,7	38,3	9,9	482983	8,7
Fh13 - 46	Fh13-63	470,2	sandflat	2384	6237142	11,9	45,4	5,1	779430	14,8
Fh13 - 47	Fh13-63	470,5	sandflat	520	282744	0,5	9,9	11,8	69791	1,3
Fh13 - 50	Fh13-63	471,9	sandflat	2172	4565835	8,7	41,3	12,6	609165	11,6
Fh13 - 51	Fh13-63	472,5	sandflat	2523	8512509	16,2	48,0	2,6	986479	18,8
Fh13 - 52	Fh13-63	473,0	sandflat	2203	5683452	10,8	41,9	6,8	724919	13,8
Fh13 - 57	Fh13-63	478,4	eolian	459	1548371	2,9	8,7	5,9	154824	2,9
Fh13 - 59	Fh13-63	480,3	sandflat	1517	5397404	10,3	28,9	5,7	594720	11,3
Fh13 - 60	Fh13-63	480,6	sandflat	1703	4082266	7,8	32,4	8,8	504294	9,6
Fh13 - 64	Fh13-63	485,4	sandflat	832	773191	1,5	15,8	12,2	141566	2,7
Gü1 - 2	Gü1-64	564,8	fluvial	2417	4245322	7,7	43,8	7,3	613028	11,1
Gü1 - 4	Gü1-64	565,2	fluvial	3022	7593578	14,5	57,5	2,1	928596	17,7
Gü1 - 6	Gü1-64	566,7	fluvial	2643	7860219	15,0	50,3	0,8	883470	16,8
Gü1 - 11	Gü1-64	575,5	sandflat	1367	7418379	14,1	26,0	2,3	678199	12,9
Gü1 - 13	Gü1-64	576,4	sandflat	802	8614481	16,4	15,3	-2,2	503676	9,6
Gü1 - 15	Gü1-64	577,0	sandflat	1491	3184718	6,4	29,9	8,6	460508	9,2
Gü1 - 16	Gü1-64	577,4	sandflat	806	2772736	5,3	15,3	6,6	236720	4,5
Gü1 - 18	Gü1-64	578,1	sandflat	27	549267	1,1	0,5	-0,5	16903	0,3
Gü1 - 20	Gü1-64	579,4	sandflat	1377	2403997	4,6	26,2	4,1	342867	6,5
Gü1 - 22	Gü1-64	580,7	sandflat	475	749702	1,4	9,0	4,2	82902	1,6
Gü1 - 25	Gü1-64	582,6	sandflat	746	2294782	4,4	14,2	5,5	208476	4,0
Gü1 - 28	Gü1-64	583,3	sandflat	984	2103278	4,0	18,7	5,4	222736	4,2
La35 - 2	La35-70	402,4	fluvial	3662	4229693	8,0	69,7	7,8	788806	15,0
La35 - 3	La35-70	404,0	fluvial	1545	2038033	3,9	29,4	8,6	266943	5,1
La35 - 7	La35-70	405,9	fluvial	2128	4270615	8,6	42,6	6,6	579658	11,6
La35 - 10	La35-70	407,6	fluvial	1004	2807655	5,3	19,1	8,6	253754	4,8
La35 - 11	La35-70	408,1	fluvial	446	876261	1,7	8,5	8,9	96451	1,8
La35 - 12	La35-70	408,8	fluvial	1129	2949032	5,6	21,5	5,9	284096	5,4
La35 - 13	La35-70	409,6	sandflat	971	2661975	5,1	18,5	8,2	233616	4,4
La35 - 15a	La35-70	410,4	sandflat	1276	3815447	7,3	24,3	9,3	328167	6,2
La35 - 15b	La35-70	410,4	sandflat	1423	4238244	8,1	27,1	8,5	395597	7,5
La35 - 16a	La35-70	410,8	sandflat	883	3738221	7,1	16,8	2,4	300661	5,7
La35 - 19	La35-70	412,4	sandflat	1676	1576129	3,0	31,9	14,4	203034	3,9
La35 - 23	La35-70	414,6	sandflat	451	606645	1,2	8,6	10,4	69445	1,3
La35 - 24	La35-70	415,5	sandflat	118	231073	0,4	2,2	4,0	35264	0,7
La35 - 29	La35-70	418,8	sandflat	1416	3474891	6,6	26,9	7,4	395112	7,5
La35 - 31	La35-70	419,8	sandflat	3478	7706872	15,4	69,7	8,1	1039352	20,8

thin section	borehole	depth [m]	facies	pore amount	pore area [μm²]	porosity (image analysis) [%]	pore density [pores/mm²]	micro-porosity	pore perimeter [μm]	pore perimeter [1/mm]
La35 - 34	La35-70	421,2	sandflat	1813	2621714	5,0	34,5	16,5	411638	7,8
Rks4 - 5	Rks4-69	434,7	fluvial	38	175013	0,3	0,7	1,5	15809	0,3
Rks4 - 7	Rks4-69	435,2	fluvial	15	229166	0,4	0,3	2,6	6616	0,1
Rks4 - 23	Rks4-69	444,2	sandflat	2769	2302895	4,4	52,7	15,5	462645	8,8
RKS2 - 1	RKS2-83	466,6	sandflat	3096	6450166	12,3	58,9	9,4	892247	17,0
RKS2 - 2	RKS2-83	472,9	sandflat	1295	3047817	5,8	24,6	7,7	363170	6,9
RKS2 - 3	RKS2-83	483,1	eolian	563	854739	1,6	10,7	3,6	130975	2,5
RKS2 - 4	RKS2-83	492,0	lacustrine	3914	3441530	5,2	59,6	4,2	686251	10,4
RKS2 - 5	RKS2-83	503,2	sandflat	592	849363	1,6	11,3	6,7	125830	2,4
RKS2 - 6	RKS2-83	509,3	sandflat	2206	4428385	8,4	42,0	2,0	577660	11,0
RKS2 - 7	RKS2-83	517,1	eolian	2495	8890520	16,9	47,5	9,7	979756	18,6
RKS2 - 8	RKS2-83	530,4	eolian	319	529909	1,0	6,1	4,7	70575	1,3
RKS2 - 9	RKS2-83	554,2	sandflat	1103	1006752	1,9	21,0	13,5	192960	3,7
RKS2 - 10	RKS2-83	572,5	sandflat	2069	4363646	8,3	39,4	5,3	546923	10,4
RKS2 - 11	RKS2-83	590,3	sandflat	1140	2519144	4,8	21,7	8,0	296584	5,6
RKS2 - 12	RKS2-83	608,3	sandflat	1038	2298630	4,4	19,8	10,4	274073	5,2
RKS2 - 13	RKS2-83	621,9	sandflat	3340	3701136	7,0	63,6	9,1	683861	13,0
RKS2 - 14	RKS2-83	623,0	eolian	728	3253371	6,2	13,9	7,1	264271	5,0
RKS2 - 15	RKS2-83	634,9	lacustrine	4724	4965408	9,4	89,9	7,8	938521	17,9
RKS2 - 16	RKS2-83	660,5	lacustrine	3670	3475166	6,6	69,8	8,4	674480	12,8
RKS2 - 17	RKS2-83	672,6	lacustrine	2931	3143871	6,0	55,8	8,5	579264	11,0
RKS2 - 18	RKS2-83	683,1	lacustrine	2682	2304712	4,4	51,0	7,7	468589	8,9
RKS2 - 19	RKS2-83	715,2	lacustrine	1946	1631215	3,1	37,0	8,5	318485	6,1
RKS2 - 20	RKS2-83	718,6	lacustrine	3114	2517731	4,8	59,3	8,5	516241	9,8
RKS2 - 21	RKS2-83	732,4	lacustrine	2630	2076784	4,0	50,1	13,8	433230	8,2
RKS2 - 22	RKS2-83	744,8	lacustrine	1807	1361935	2,6	34,4	8,2	289708	5,5
RKS2 - 23	RKS2-83	788,1	sandflat	199	106539	0,2	3,8	1,2	26024	0,5
RKS2 - 24	RKS2-83	826,6	sandflat	1720	1116549	2,1	32,7	6,6	256454	4,9
RKS2 - 25	RKS2-83	845,3	sandflat	1346	1393700	2,7	25,6	2,4	255141	4,9
RKS2 - 26	RKS2-83	893,3	lacustrine	4733	4193391	8,0	90,1	3,8	840218	16,0
RKS2 - 27	RKS2-83	908,0	lacustrine	4379	3541864	6,7	83,3	4,0	753011	14,3
RKS2 - 31	RKS2-83	441,3	fluvial	426	460020	1,0	9,2	3,9	78325	1,7
RKS2 - 34	RKS2-83	503,5	eolian	2017	6050155	13,0	43,5	8,3	672189	14,5
RKS2 - 35a	RKS2-83	570,1	eolian	2331	3136406	6,8	50,3	7,7	479420	10,3
RKS2 - 35b	RKS2-83	570,1	eolian	973	3021110	6,5	21,0	8,0	324777	7,0
Ballst - 22	Ballst1-63	502,0	fluvial	1833	3651331	7,9	39,5	7,7	464000	10,0
Ballst - 23	Ballst1-63	518,7	fluvial	1678	1347230	2,9	36,2	14,2	297785	6,0
Ballst - 24	Ballst1-63	525,8	eolian	1802	4846728	10,5	38,9	11,2	543136	11,7
Ballst - 25	Ballst1-63	547,6	sandflat	1440	1790938	3,9	31,1	11,7	286761	6,2
Ballst - 26	Ballst1-63	553,3	eolian	1288	1954504	4,2	27,8	8,6	273190	5,9
Ballst - 28	Ballst1-63	600,6	sandflat	3008	4058256	8,8	64,9	10,0	617372	13,3
Ballst - 29	Ballst1-63	621,4	eolian	900	1397750	3,0	19,4	15,8	192717	4,2
Ballst - 30	Ballst1-63	638,8	sandflat	2610	3235327	7,0	56,3	8,7	566861	12,2
Ballst - 31	Ballst1-63	672,4	sandflat	1907	3914129	8,4	41,1	7,2	495888	10,7
Ballst - 32	Ballst1-63	688,3	sandflat	1395	2039254	4,4	30,1	11,4	302705	6,5
Ballst - 1	Ballst1-63	692,4	sandflat	3348	3264945	7,0	72,2	10,6	623260	13,4
Ballst - 2	Ballst1-63	695,5	sandflat	4098	8063398	17,4	88,4	1,8	1175536	25,4
Ballst - 3	Ballst1-63	703,0	sandflat	1547	1724218	3,7	33,4	8,4	321342	6,7
Ballst - 4	Ballst1-63	713,0	sandflat	1326	2889702	6,2	28,6	4,8	353682	7,6
Ballst - 5	Ballst1-63	717,5	sandflat	51	37176	0,1	1,1	4,6	-	0,2
Ballst - 6	Ballst1-63	724,5	sandflat	931	1685190	3,6	20,1	7,1	-	5,1
Ballst - 7	Ballst1-63	729,4	lacustrine	1753	4240998	9,1	37,8	7,8	504434	10,9
Ballst - 8	Ballst1-63	741,6	lacustrine	495	408563	0,9	10,7	8,8	82066	1,8
Ballst - 9	Ballst1-63	750,5	lacustrine	740	782533	1,7	16,0	7,0	136124	2,9

thin section	borehole	depth [m]	facies	pore amount	pore area [µm²]	porosity (image analysis) [%]	pore density [pores/mm²]	micro-porosity	pore perimeter [µm]	pore perimeter [1/mm]
Ballst - 10	Ballst1-63	784,3	lacustrine	1442	1195866	2,6	31,1	14,5	237136	5,1
Ballst - 11	Ballst1-63	809,1	lacustrine	105	50736	0,1	2,3	5,8	13551	0,3
Ballst - 12	Ballst1-63	843,4	lacustrine	451	247450	0,5	9,7	11,3	60613	1,3
Ballst - 13	Ballst1-63	850,5	lacustrine	99	43844	0,1	2,1	9,3	11576	0,2
Ballst - 14	Ballst1-63	867,2	lacustrine	951	571563	1,2	20,5	5,6	134711	2,9
Ballst - 15	Ballst1-63	906,4	lacustrine	675	343597	0,7	14,6	6,4	86990	1,9
Ballst - 16	Ballst1-63	953,8	lacustrine	1699	1614935	3,5	36,6	11,5	321674	6,9
Ballst - 17	Ballst1-63	979,5	lacustrine	224	102688	0,2	4,8	6,5	26625	0,6
Ballst - 18	Ballst1-63	1011,9	lacustrine	893	491277	1,1	19,3	9,5	121229	2,6
Ballst - 19	Ballst1-63	1036,4	lacustrine	449	242530	0,5	9,7	6,6	59225	1,3

Table A 12: Pore space analysis for the Buntsandstein samples (continuation). [B]

thin section	small pores (1-1000 µm)						medium pores (1000-10000 µm)					
	amount	relative amount [%]	area [µm²]	relative area [%]	perimeter [µm]	relative perimeter [%]	amount	relative amount [%]	area [µm²]	relative area [%]	perimeter [µm]	relative perimeter [%]
Fh13 - 5	62	71	22500	16	6408	39	23	26	85864	59	9052	55
Fh13 - 7	957	68	437157	14	117828	34	396	28	987061	33	146855	43
Fh13 - 11	386	70	166188	13	46405	33	145	26	425913	32	57713	41
Fh13 - 12	35	40	15481	1	3879	10	37	43	130826	11	12057	32
Fh13 - 13	499	50	223687	5	60228	15	392	39	1315455	31	170530	44
Fh13 - 15	922	60	401683	13	110911	25	536	35	1630900	51	235627	53
Fh13 - 21	2573	86	1040404	36	297429	58	411	14	911346	32	158324	31
Fh13 - 24	1114	56	510810	8	136639	19	738	37	2492899	41	346721	48
Fh13 - 27	1819	79	770003	34	218277	49	469	20	1162314	51	192709	44
Fh13 - 30	1979	78	811395	28	232510	46	509	20	1300233	45	213028	42
Fh13 - 41	1653	62	794713	17	209589	29	940	35	2639592	56	392987	55
Fh13 - 42	1355	67	611470	20	165131	34	613	30	1624450	54	248699	51
Fh13 - 46	1321	55	625431	10	161675	21	924	39	3054564	49	412610	53
Fh13 - 47	472	91	184816	65	52960	76	48	9	97929	35	16831	24
Fh13 - 50	1269	58	627242	14	159702	26	830	38	2563281	56	340995	56
Fh13 - 51	1358	54	610114	7	165277	17	934	37	3312498	39	445694	45
Fh13 - 52	1163	53	550902	10	144566	20	911	41	2831982	50	395052	54
Fh13 - 57	240	52	122119	8	29935	19	182	40	546678	35	70568	46
Fh13 - 59	683	45	324683	6	86165	14	682	45	2276298	42	295299	50
Fh13 - 60	960	56	450515	11	118865	24	656	39	2009138	49	272848	54
Fh13 - 64	671	81	276491	36	76694	54	152	18	375200	49	55089	39
Gü1 - 2	1441	60	721746	17	181125	30	914	38	2486349	59	350711	57
Gü1 - 4	1791	59	771756	10	208668	22	1055	35	3404139	45	456586	49
Gü1 - 6	1529	58	658112	8	179238	20	946	36	3131792	40	422015	48
Gü1 - 11	575	42	274902	4	71768	11	630	46	2172745	29	289692	43
Gü1 - 13	286	36	141588	2	36382	7	345	43	1156930	13	143915	29
Gü1 - 15	775	52	404330	13	102975	22	664	45	1890886	59	277190	60
Gü1 - 16	374	46	182075	7	37362	16	370	46	1256013	45	125496	53
Gü1 - 18	10	37	4169	1	892	5	6	22	21472	4	2139	13
Gü1 - 20	880	64	404686	17	107667	31	462	34	1323024	55	185615	54

thin section	small pores (1-1000 µm)						medium pores (1000-10000 µm)					
	amount	relative amount [%]	area [µm²]	relative area [%]	perimeter [µm]	relative perimeter [%]	amount	relative amount [%]	area [µm²]	relative area [%]	perimeter [µm]	relative perimeter [%]
Gü1 - 22	294	62	143043	19	29262	35	173	36	439419	59	46517	56
Gü1 - 25	352	47	174695	8	35608	17	342	46	1209069	53	118466	57
Gü1 - 28	520	53	250513	12	51630	23	425	43	1279198	61	133985	60
La35 - 2	2729	75	1203629	28	333765	42	888	24	2121909	50	360407	46
La35 - 3	947	61	461231	23	95272	36	590	38	1455915	71	163912	61
La35 - 7	1254	59	591019	14	155520	27	791	37	2312747	54	318670	55
La35 - 10	478	48	242794	9	49308	19	475	47	1511441	54	151816	60
La35 - 11	240	54	119895	14	24149	25	195	44	550287	63	60015	62
La35 - 12	565	50	274687	9	56774	20	504	45	1593827	54	164952	58
La35 - 13	498	51	249161	9	50680	22	430	44	1235646	46	133183	57
La35 - 15a	558	44	276026	7	56744	17	660	52	2013863	53	211396	64
La35 - 15b	597	42	318216	8	62725	16	732	51	2282514	54	236677	60
La35 - 16a	296	34	154352	4	30539	10	489	55	1574895	42	161073	54
La35 - 19	1252	75	504743	32	100432	49	417	25	981762	62	97416	48
La35 - 23	266	59	133425	22	26021	37	183	41	410995	68	41525	60
La35 - 24	81	69	35255	15	9379	27	31	26	88726	38	15436	44
La35 - 29	745	53	376291	11	91942	23	608	43	1790144	52	223262	57
La35 - 31	2208	63	946648	12	261208	25	1101	32	3602049	47	511195	49
La35 - 34	1277	70	578790	22	156162	38	507	28	1321254	50	201743	49
Rks4 - 5	14	37	8323	5	2002	13	17	45	58352	33	6931	44
Rks4 - 7	5	33	2100	1	585	9	4	27	5854	3	903	14
Rks4 - 23	2249	81	999586	43	269936	58	507	18	1071254	47	175210	38
RKS2 - 1	1696	55	856417	13	215492	24	1297	42	3943979	61	532468	60
RKS2 - 2	717	55	351404	12	88407	24	515	40	1558568	51	196684	54
RKS2 - 3	393	70	176500	21	47907	37	157	28	465249	54	67638	52
RKS2 - 4	3048	78	1409496	41	375162	55	857	22	1897785	55	300045	44
RKS2 - 5	406	69	177173	21	47561	38	176	30	490689	58	66178	53
RKS2 - 6	1172	53	610750	14	146683	25	971	44	2794825	63	359336	62
RKS2 - 7	1005	40	527402	6	127448	13	1277	51	4340465	49	541009	55
RKS2 - 8	187	59	92513	17	22651	32	125	39	331805	63	41441	59
RKS2 - 9	830	75	407673	40	103209	53	270	24	553234	55	86899	45
RKS2 - 10	1220	59	607624	14	151463	28	775	37	2204340	51	294116	54
RKS2 - 11	661	58	332475	13	81001	27	429	38	1300742	52	157788	53
RKS2 - 12	651	63	315105	14	80296	29	342	33	1032573	45	132536	48
RKS2 - 13	2306	69	1106836	30	287513	42	1018	30	2389345	65	375406	55
RKS2 - 14	434	60	200900	6	52659	20	221	30	690764	21	87281	33
RKS2 - 15	3382	72	1587243	32	417212	44	1324	28	3139538	63	498063	53
RKS2 - 16	2739	75	1316427	38	338590	50	924	25	2067029	59	328398	49
RKS2 - 17	2082	71	988697	31	258087	45	833	28	1940365	62	304121	53
RKS2 - 18	2023	75	963059	42	250710	54	657	24	1319664	57	215952	46
RKS2 - 19	1600	82	684282	42	187443	59	331	17	759750	47	114856	36
RKS2 - 20	2523	81	1104534	44	302267	59	580	19	1254942	50	201466	39
RKS2 - 21	2119	81	927589	45	252491	58	508	19	1103900	53	177186	41
RKS2 - 22	1471	81	651959	48	176236	61	333	18	660397	48	109515	38
RKS2 - 23	181	91	67750	64	20013	77	18	9	38789	36	6011	23
RKS2 - 24	1451	84	596190	53	169522	66	268	16	501302	45	85778	33
RKS2 - 25	1016	75	447574	32	121847	48	318	24	779660	56	119616	47
RKS2 - 26	3755	79	1574892	38	441590	53	955	20	2296642	55	367840	44
RKS2 - 27	3517	80	1508809	43	419599	56	852	19	1897145	54	318594	42
RKS2 - 31	335	79	147261	32	40756	52	85	20	224236	49	31600	40
RKS2 - 34	1092	54	546359	9	138403	21	802	40	2396889	40	325687	48
RKS2 - 35a	1649	71	782477	25	202386	42	643	28	1485577	47	225574	47
RKS2 - 35b	549	56	253081	8	67283	21	363	37	1143594	38	156652	48
Ballst - 22	1163	63	560846	15	143466	31	605	33	1753676	48	227063	49

thin section	small pores (1-1000 µm)						medium pores (1000-10000 µm)					
	amount	relative amount [%]	area [µm²]	relative area [%]	perimeter [µm]	relative perimeter [%]	amount	relative amount [%]	area [µm²]	relative area [%]	perimeter [µm]	relative perimeter [%]
Ballst - 23	1320	79	623725	46	171272	58	357	21	712942	53	125688	42
Ballst - 24	1124	62	495782	10	133807	25	566	31	1717040	35	238056	44
Ballst - 25	1006	70	457150	26	118555	41	421	29	1079894	60	151207	53
Ballst - 26	890	69	401660	21	103958	38	374	29	1023769	52	137895	50
Ballst - 28	2158	72	1029366	25	262933	43	805	27	1946004	48	289840	47
Ballst - 29	606	67	267560	19	70925	37	276	31	804853	58	103190	54
Ballst - 30	1783	68	832973	26	218552	39	806	31	2048420	63	315202	56
Ballst - 31	1197	63	557167	14	142296	29	636	33	1961018	50	256752	52
Ballst - 32	929	67	437995	21	112079	37	440	32	1190998	58	160625	53
Ballst - 1	2441	73	1117804	34	295118	47	897	27	2006508	61	315565	51
Ballst - 2	2549	62	1135252	14	307391	26	1392	34	4298709	53	621972	53
Ballst - 3	1102	71	498872	29	139242	43	436	28	1096496	64	169954	53
Ballst - 4	840	63	385395	13	100997	29	428	32	1305989	45	172467	49
Ballst - 5	44	86	20486	55	-	-	7	14	16690	45	-	-
Ballst - 6	509	55	253922	15	-	-	402	43	1118489	66	-	-
Ballst - 7	1104	63	497574	12	132024	26	541	31	1636541	39	218524	43
Ballst - 8	381	77	176743	43	46763	57	114	23	231820	57	35303	43
Ballst - 9	553	75	245567	31	64188	47	183	25	483961	62	67666	50
Ballst - 10	1103	76	536859	45	134380	57	339	24	659007	55	102756	43
Ballst - 11	96	91	36528	72	10863	80	9	9	14207	28	2688	20
Ballst - 12	408	90	169256	68	47098	78	43	10	78194	32	13515	22
Ballst - 13	96	97	39109	89	10752	93	3	3	4735	11	824	7
Ballst - 14	835	88	340858	60	95152	71	116	12	230705	40	39558	29
Ballst - 15	625	93	239530	70	69394	80	50	7	104067	30	17596	20
Ballst - 16	1319	78	576425	36	158746	49	369	22	854668	53	147869	46
Ballst - 17	209	93	78835	77	22391	84	15	7	23853	23	4235	16
Ballst - 18	792	89	316709	64	89710	74	101	11	174568	36	31520	26
Ballst - 19	404	90	175887	73	47397	80	45	10	66643	27	11828	20

Table A 13: Pore space analysis for the Buntsandstein samples (continuation). [C]

thin section	large pores (10000-50000 µm)						very large pores (>50000 µm)					
	amount	relative amount [%]	area [µm²]	relative area [%]	perimeter [µm]	relative perimeter [%]	amount	relative amount [%]	area [µm²]	relative area [%]	perimeter [µm]	relative perimeter [%]
Fh13 - 5	2	2	35946	25	1065	6	0	0	0	0	0	0
Fh13 - 7	43	3	943943	31	63318	18	5	0	664472	22	16857	5
Fh13 - 11	20	4	382586	29	26110	18	3	1	350312	26	11574	8
Fh13 - 12	9	10	161034	13	6150	17	6	7	921256	75	15110	41
Fh13 - 13	96	10	1868546	44	128127	33	8	1	887480	21	32950	8
Fh13 - 15	72	5	1147948	36	96678	22	0	0	0	0	0	0
Fh13 - 21	18	1	404949	14	32072	6	6	0	514760	18	23765	5
Fh13 - 24	141	7	2860481	47	225734	31	2	0	159767	3	9148	1
Fh13 - 27	20	1	326745	14	30204	7	0	0	0	0	0	0
Fh13 - 30	32	1	659418	23	55422	11	2	0	131595	5	8146	2

thin section	large pores (10000-50000 µm)						very large pores (>50000 µm)					
	amount	relative amount [%]	area [µm²]	relative area [%]	perimeter [µm]	relative perimeter [%]	amount	relative amount [%]	area [µm²]	relative area [%]	perimeter [µm]	relative perimeter [%]
Fh13 - 41	64	2	1099952	23	99232	14	3	0	182308	4	11028	2
Fh13 - 42	46	2	763116	25	69153	14	0	0	0	0	0	0
Fh13 - 46	135	6	2282798	37	186588	24	4	0	274349	4	18558	2
Fh13 - 47	0	0	0	0	0	0	0	0	0	0	0	0
Fh13 - 50	72	3	1313769	29	105394	17	1	0	61544	1	3074	1
Fh13 - 51	221	9	3861218	45	333415	34	10	0	728679	9	42093	4
Fh13 - 52	127	6	2177771	38	181788	25	2	0	122797	2	3514	0
Fh13 - 57	35	8	765936	49	49363	32	2	0	113638	7	4958	3
Fh13 - 59	148	10	2578397	48	199416	34	4	0	218026	4	13841	2
Fh13 - 60	86	5	1512090	37	109255	22	1	0	110523	3	3326	1
Fh13 - 64	9	1	121501	16	9783	7	0	0	0	0	0	0
Gü1 - 2	60	2	923110	22	74753	12	2	0	114117	3	6440	1
Gü1 - 4	171	6	3121246	41	245306	26	5	0	296437	4	18037	2
Gü1 - 6	159	6	3168905	40	238933	27	9	0	901410	11	43284	5
Gü1 - 11	140	10	2582076	35	211369	31	22	2	2388656	32	105370	16
Gü1 - 13	132	16	2795497	32	173726	34	39	5	4520466	52	149653	30
Gü1 - 15	52	3	889502	28	80344	17	0	0	0	0	0	0
Gü1 - 16	60	7	1228234	44	69886	30	2	0	106414	4	3975	2
Gü1 - 18	7	26	160393	29	6792	40	4	15	363232	66	7079	42
Gü1 - 20	34	2	535844	22	43172	13	1	0	140443	6	6413	2
Gü1 - 22	8	2	167241	22	7123	9	0	0	0	0	0	0
Gü1 - 25	52	7	911018	40	54402	26	0	0	0	0	0	0
Gü1 - 28	39	4	573567	27	37121	17	0	0	0	0	0	0
La35 - 2	42	1	700225	17	80270	10	3	0	203930	5	14364	2
La35 - 3	8	1	120887	6	7759	3	0	0	0	0	0	0
La35 - 7	82	4	1281226	30	101368	17	1	0	85623	2	4101	1
La35 - 10	49	5	943769	34	47896	19	2	0	109651	4	4733	2
La35 - 11	10	2	141788	16	9727	10	1	0	64290	7	2560	3
La35 - 12	58	5	964963	33	57816	20	2	0	115556	4	4554	2
La35 - 13	39	4	810823	30	40168	17	4	0	366345	14	9585	4
La35 - 15a	55	4	847316	22	51201	16	3	0	678241	18	8825	3
La35 - 15b	91	6	1471402	35	88924	22	3	0	166113	4	7271	2
La35 - 16a	93	11	1708843	46	97810	33	5	1	300130	8	11238	4
La35 - 19	7	0	89624	6	5186	3	0	0	0	0	0	0
La35 - 23	1	0	12162	2	695	1	1	0	50062	8	1204	2
La35 - 24	6	5	107091	46	10449	30	0	0	0	0	0	0
La35 - 29	58	4	1005489	29	66047	17	5	0	302968	9	13861	4
La35 - 31	167	5	3024417	39	259504	25	2	0	133757	2	7446	1
La35 - 34	26	1	440302	17	40895	10	3	0	281367	11	12838	3
Rks4 - 5	7	18	108338	62	6877	43	0	0	0	0	0	0
Rks4 - 7	4	27	66971	29	2330	35	2	13	154241	67	2798	42
Rks4 - 23	13	0	232056	10	17499	4	0	0	0	0	0	0
RKS2 - 1	103	3	1649771	26	144287	16	0	0	0	0	0	0
RKS2 - 2	63	5	1137846	37	78079	21	0	0	0	0	0	0
RKS2 - 3	13	2	212991	25	15431	12	0	0	0	0	0	0
RKS2 - 4	9	0	134250	4	11044	2	0	0	0	0	0	0
RKS2 - 5	10	2	181501	21	12091	10	0	0	0	0	0	0
RKS2 - 6	62	3	939483	21	69611	12	1	0	83327	2	2030	0
RKS2 - 7	207	8	3649636	41	288979	29	6	0	373018	4	22320	2
RKS2 - 8	7	2	105592	20	6482	9	0	0	0	0	0	0
RKS2 - 9	3	0	45846	5	2851	1	0	0	0	0	0	0
RKS2 - 10	72	3	1316315	30	89922	16	2	0	235367	5	11422	2
RKS2 - 11	48	4	773904	31	53299	18	2	0	112023	4	4495	2
RKS2 - 12	44	4	841749	37	56039	20	1	0	109202	5	5202	2

thin section	large pores (10000-50000 μm)						very large pores (>50000 μm)					
	amount	relative amount [%]	area [μm²]	relative area [%]	perimeter [μm]	relative perimeter [%]	amount	relative amount [%]	area [μm²]	relative area [%]	perimeter [μm]	relative perimeter [%]
RKS2 - 13	16	0	204956	6	20942	3	0	0	0	0	0	0
RKS2 - 14	66	9	1528793	47	96182	36	7	1	832914	26	28150	11
RKS2 - 15	18	0	238628	5	23246	2	0	0	0	0	0	0
RKS2 - 16	7	0	91711	3	7493	1	0	0	0	0	0	0
RKS2 - 17	16	1	214809	7	17055	3	0	0	0	0	0	0
RKS2 - 18	2	0	21989	1	1927	0	0	0	0	0	0	0
RKS2 - 19	15	1	187183	11	16186	5	0	0	0	0	0	0
RKS2 - 20	11	0	158255	6	12508	2	0	0	0	0	0	0
RKS2 - 21	3	0	45295	2	3552	1	0	0	0	0	0	0
RKS2 - 22	3	0	49579	4	3957	1	0	0	0	0	0	0
RKS2 - 23	0	0	0	0	0	0	0	0	0	0	0	0
RKS2 - 24	1	0	19058	2	1154	0	0	0	0	0	0	0
RKS2 - 25	12	1	166466	12	13677	5	0	0	0	0	0	0
RKS2 - 26	23	0	321857	8	30788	4	0	0	0	0	0	0
RKS2 - 27	10	0	135910	4	14818	2	0	0	0	0	0	0
RKS2 - 31	6	1	88523	19	5969	8	0	0	0	0	0	0
RKS2 - 34	114	6	2258330	37	167490	25	9	0	848576	14	40609	6
RKS2 - 35a	36	2	673616	21	43068	9	3	0	194737	6	8392	2
RKS2 - 35b	54	6	1054115	35	76479	24	7	1	570320	19	24363	8
Ballst - 22	62	3	1165383	32	85135	18	3	0	171425	5	8336	2
Ballst - 23	1	0	10563	1	825	0	0	0	0	0	0	0
Ballst - 24	105	6	2163809	45	149915	28	7	0	470097	10	21358	4
Ballst - 25	11	1	146574	8	11778	4	2	0	107320	6	5222	2
Ballst - 26	21	2	354999	18	23289	9	3	0	174076	9	8047	3
Ballst - 28	39	1	680541	17	47809	8	6	0	402345	10	16790	3
Ballst - 29	17	2	229262	16	16457	9	1	0	96076	7	2146	1
Ballst - 30	21	1	353934	11	33108	6	0	0	0	0	0	0
Ballst - 31	73	4	1345820	34	93995	19	1	0	50123	1	2844	1
Ballst - 32	26	2	410261	20	30000	10	0	0	0	0	0	0
Ballst - 1	10	0	140634	4	12577	2	0	0	0	0	0	0
Ballst - 2	156	4	2575139	32	242730	21	1	0	54298	1	3444	0
Ballst - 3	9	1	128850	7	12146	4	0	0	0	0	0	0
Ballst - 4	56	4	1064963	37	74320	21	2	0	133355	5	5899	2
Ballst - 5	0	0	0	0	-	-	0	0	0	0	-	-
Ballst - 6	20	2	312779	19	-	-	0	0	0	0	-	-
Ballst - 7	106	6	2004325	47	148434	29	2	0	102558	2	5452	1
Ballst - 8	0	0	0	0	0	0	0	0	0	0	0	0
Ballst - 9	4	1	53005	7	4271	3	0	0	0	0	0	0
Ballst - 10	0	0	0	0	0	0	0	0	0	0	0	0
Ballst - 11	0	0	0	0	0	0	0	0	0	0	0	0
Ballst - 12	0	0	0	0	0	0	0	0	0	0	0	0
Ballst - 13	0	0	0	0	0	0	0	0	0	0	0	0
Ballst - 14	0	0	0	0	0	0	0	0	0	0	0	0
Ballst - 15	0	0	0	0	0	0	0	0	0	0	0	0
Ballst - 16	11	1	183842	11	15059	5	0	0	0	0	0	0
Ballst - 17	0	0	0	0	0	0	0	0	0	0	0	0
Ballst - 18	0	0	0	0	0	0	0	0	0	0	0	0
Ballst - 19	0	0	0	0	0	0	0	0	0	0	0	0

10. II.6. Mineral surfaces

Table A 14: Measured mineral surface areas in the Buntsandstein samples. Ballst-sample values from Naumann (2013).

thin section	facies	colour	detrital components surface area [%]								authigenic minerals surface area [%]						
			quartz	feldspar	lithic fragment	mica	iron oxide	ooids	heavy minerls	opaque	quartz	feldspar	carbonate	anhydrite	gypsum	illite	kaolinite
RKS2 - 4	lacustrine	grey	57,8	37,2	0,1	0,6	0,1	0,0	0,1	0,0	0,4	0,3	1,8	0,0	0,0	1,2	0,4
RKS2 - 21	lacustrine	grey	31,2	54,2	0,0	4,1	0,1	0,0	1,4	0,0	8,3	0,2	0,2	0,1	0,1	0,1	0,0
Ballst - 9	lacustrine	grey	3,9	31,6	0,0	0,6	5,7	10,9	0,0	0,5	18,9	0,0	24,0	0,0	0,0	3,9	0,0
RKS2 -27	lacustrine	grey	57,4	39,2	0,0	0,1	0,9	0,0	0,0	1,5	0,0	0,4	0,0	0,0	0,0	0,5	0,0
Rks2 - 26	lacustrine	grey	51,5	41,6	0,3	2,1	1,4	0,0	0,2	0,0	0,1	0,0	0,6	0,4	0,5	0,5	0,8
Ballst - 18	lacustrine	red	16,2	22,3	0,0	2,3	25,1	0,0	0,0	2,2	16,0	0,0	0,0	15,9	0,0	0,0	0,0
RKS2 - 13	sandflat	grey	46,8	46,9	0,0	0,8	1,3	0,0	0,0	0,0	2,7	0,0	0,8	0,0	0,0	0,7	0,0
Gü1 - 15	sandflat	grey	45,8	18,2	1,1	0,3	0,0	0,0	0,0	0,9	21,6	0,6	0,1	0,0	0,0	8,3	3,1
Ballst - 30	sandflat	grey	37,3	22,3	0,4	2,0	13,1	0,0	0,1	0,3	15,5	0,0	0,3	6,2	0,0	2,5	0,0
RKS2 - 2	sandflat	red	15,5	9,1	0,0	0,1	56,9	0,0	0,0	0,0	15,0	0,0	2,4	0,0	0,4	0,6	0,0
RKS2 - 6	sandflat	red	29,3	21,2	0,0	0,8	35,1	0,0	0,0	0,0	12,3	1,3	0,0	0,0	0,0	0,0	0,0
Ballst - 3	sandflat	red	28,6	14,4	0,5	1,1	41,7	0,0	1,0	0,3	11,6	0,0	0,0	0,0	0,0	0,8	0,0
Gü1 - 4	fluvial	grey	51,9	19,2	1,4	0,1	0,2	0,0	0,0	0,0	22,7	1,3	0,8	0,0	0,0	1,4	0,9
Gü1 - 6	fluvial	grey	44,6	23,3	1,6	3,7	0,0	0,0	0,2	0,1	23,2	1,3	0,0	0,0	0,0	1,2	0,8
La35 - 7	fluvial	grey	41,6	30,0	0,0	0,6	0,3	0,0	0,0	0,1	19,0	0,4	0,0	0,0	0,0	8,0	0,0
La35 - 10	fluvial	grey	49,0	26,3	0,7	0,0	0,0	0,0	0,0	0,0	15,0	2,0	0,0	0,0	0,0	6,9	0,0
Ballst - 22	fluvial	grey	33,9	32,5	2,2	0,8	0,3	0,0	0,6	1,0	26,5	0,0	0,8	0,0	0,0	1,4	0,0
Ballst - 23	fluvial	red	13,3	14,6	0,9	2,1	43,4	0,0	1,0	2,4	21,1	0,0	0,0	0,0	0,0	1,2	0,0
RKS2 - 3	eolian	grey	48,3	7,3	0,0	0,0	0,0	0,0	0,0	0,0	0,0	0,0	0,0	0,0	21,2	23,3	0,0
Fh13 - 13	eolian	grey	32,2	11,6	0,0	0,2	6,8	0,0	0,0	0,0	35,7	1,8	0,0	0,0	11,7	0,0	0,0
Ballst - 24	eolian	grey	42,0	21,1	0,6	6,6	0,5	0,0	0,1	0,4	18,6	0,0	0,0	0,0	0,0	10,1	0,0
RKS2 - 36	eolian	red	8,0	15,3	0,0	0,0	61,8	0,0	0,0	0,0	13,3	1,5	0,0	0,0	0,0	0,1	0,0
Fh13 - 28	eolian	red	58,6	15,0	0,0	2,4	22,4	0,0	0,0	0,0	0,7	0,0	0,0	0,0	0,9	0,0	0,0
Ballst - 28	eolian	red	26,8	25,8	0,5	1,2	24,2	0,0	0,0	0,4	17,2	0,0	1,5	2,1	0,0	0,3	0,0

Selbständigkeitserklärung A86

Hiermit erkläre ich, dass ich die vorliegende Arbeit selbständig und unter Anwendung der gegeben Hilfsmittel und Quellen verfasst habe.

Jena,……………………….. --

Daniel Beyer